MARTIN MARIETTA ENERGY SYSTEMS LIBRARIES

3 4456 0420016 6

ORNL-6869

ornl

OAK RIDGE NATIONAL LABORATORY

MARTIN MARIETTA

Durability of Polymer Matrix Composites for Automotive Structural Applications: A State-of-the-Art Review

J. M. Corum
W. A. Simpson, Jr.
C. T. Sun
R. Talreja
Y. J. Weitsman

OAK RIDGE NATIONAL LABORATORY
CENTRAL RESEARCH LIBRARY
CIRCULATION SECTION
4500N ROOM 175
LIBRARY LOAN COPY
DO NOT TRANSFER TO ANOTHER PERSON
If you want someone else to see this report, send in name with report and the library will arrange a loan.

MANAGED BY
MARTIN MARIETTA ENERGY SYSTEMS, INC.
FOR THE UNITED STATES
DEPARTMENT OF ENERGY

This report has been reproduced directly from the best available copy.

Available to DOE and DOE contractors from the Office of Scientific and Technical Information, P.O. Box 62, Oak Ridge, TN 37831; prices available from (615) 576-8401, FTS 626-8401.

Available to the public from the National Technical Information Service, U.S. Department of Commerce, 5285 Port Royal Rd., Springfield, VA 22161.

This report was prepared as an account of work sponsored by an agency of the United States Government. Neither the United States Government nor any agency thereof, nor any of their employees, makes any warranty, express or implied, or assumes any legal liability or responsibility for the accuracy, completeness, or usefulness of any information, apparatus, product, or process disclosed, or represents that its use would not infringe privately owned rights. Reference herein to any specific commercial product, process, or service by trade name, trademark, manufacturer, or otherwise, does not necessarily constitute or imply its endorsement, recommendation, or favoring by the United States Government or any agency thereof. The views and opinions of authors expressed herein do not necessarily state or reflect those of the United States Government or any agency thereof.

131
bines previous
on of DOE
32.15 and .16.
ner editions are
lete.

U. S. DEPARTMENT OF ENERGY
RECOMMENDATIONS FOR THE ANNOUNCEMENT AND DISTRIBUTION OF DEPARTMENT OF ENERGY (DOE) SCIENTIFIC AND TECHNICAL INFORMATION (STI)

(See instructions on reverse side. Use plain bond paper if additional space is needed for explanations.)

1910-1400
OMB Burden
Disclosure
Statement on
reverse side

RT I *(DOE, DOE Contractors, Grantees, and Awardees complete)*

. Product/Report Data

. (Award) Contract No. DE-AC05-84OR21400

. Title Durability of Polymer Matrix Composites for Automotive Structural Applications - A State of the Art Review

. Product/Report Description

☒ a. Report *(Complete all that apply)*
(1) ☒ Print ☐ Nonprint *(specify)*
(2) ☐ Quarterly ☐ Semiannual ☐ Annual ☐ Final
☒ Topical ☐ Phase I ☐ Phase II
☐ Other *(specify)*

Dates covered _____ thru _____

☐ b. Conference/Meeting/Presentation *(Complete all that apply)*
(1) ☐ Print ☐ Nonprint *(specify)*
☐ Published proceedings
☐ Other *(specify)*

(2) Conference Title *(no abbreviations)*

Location *(city/state/country)*

Date(s) *(m/d/y)* __/__/__ thru *(m/d/y)* __/__/__
Sponsor

☐ c. Software—Additional forms are required. Follow instructions on the back of this form.
☐ d. Other *(Provide complete description)*

B. Patent Information

Yes No
☐ ☒ Is any new equipment, process, or material disclosed?
If yes, identify page numbers

☐ ☒ Has an invention disclosure been submitted?
If yes, identify the disclosure number and to whom it was submitted. Disclosure number
Submitted to

☐ ☒ Are there patent-related objections to the release of this STI product? If so, state the objections.

C. Contact *(Person knowledgeable of content)*
Name
Phone
Position
Organization

ART II *(DOE/DOE Contractors complete/or as instructed by DOE contracting officer)*

A. DOE Identifiers

1. Product/Report Nos. ORNL-6869

2. Funding Office(s) *(NOTE: Essential data)* EE 51 02 00 0

B. Copies for Transmittal to AD-21 (OSTI)
(STI must be of sufficient quality for microfilming/copying.)

☐ 1. One for classified processing
☐ 2. *(number)* for standard classified distribution
☒ 3. Two unclassified for processing
☐ 4. *(number)* for program unclassified distribution
☒ 5. UC/C Category UC-1425 and 1500
☐ 6. Additional instructions/explanations

(Do not identify Sigma categories for Nuclear Weapons Data reports, and do not provide additional instructions that are inconsistent with C below.)

C. Recommendation *("X" at least one)*

☒ 1. Program/Standard Announcement/Distribution
(Available to U.S. and foreign public)

☐ 2. Classified *(Standard Announcement only)*
☐ 3. Special Handling *(Legal basis must be noted below.)*
☐ a. Unclassified Controlled Nuclear Information (UCNI)
☐ b. Export Control/ITAR/EAR
☐ c. Temporary hold pending patent review
☐ d. Translations of copyrighted material
☐ e. Small Business Innovation Research (SBIR)
☐ f. Commercializable information
☐ (1) Proprietary
☐ (2) Protected CRADA information
Release date __/__/__
☐ (3) Other *(explain)*

☐ 4. Program Directed Special Handling *(copy attached)*

D. Releasing Official

A. Patent Clearance *("X" one)*
☐ Has been submitted for DOE patent clearance
☒ DOE patent clearance has been granted

B. Released by
(Name) D.R. Hamrin
(Signature) D R Hamrin / JJ
(Phone) (615) 574-6752
(Date) July 27, 1995

ORNL-6869
Dist. Category UC-1425,-1500

Engineering Technology Division

DURABILITY OF POLYMER MATRIX COMPOSITES FOR AUTOMOTIVE STRUCTURAL APPLICATIONS: A STATE-OF-THE-ART REVIEW

J. M. Corum
W. A. Simpson, Jr.
C. T. Sun
R. Talreja
Y. J. Weitsman

Date Published—

Prepared by the
OAK RIDGE NATIONAL LABORATORY
Oak Ridge, Tennessee 37831-6285
managed by
LOCKHEED MARTIN ENERGY SYSTEMS, INC.
for the
U.S. DEPARTMENT OF ENERGY
under contract DE-AC05-84OR21400

MARTIN MARIETTA ENERGY SYSTEMS LIBRARIES
3 4456 0420016 6

CONTENTS

	Page
LIST OF FIGURES	v
LIST OF TABLES	ix
LIST OF ACRONYMS	xi
PREFACE	xiii
ABSTRACT	xv
1. INTRODUCTION—AN OVERVIEW	1
REFERENCES	2
2. BACKGROUND	3
2.1 DURABILITY ISSUES	3
2.2 MATERIALS OF INTEREST	3
2.3 CHARACTERISTICS OF CSM COMPOSITES	4
REFERENCES	15
3. FATIGUE OF COMPOSITE MATERIALS	17
3.1 INTRODUCTION	17
3.2 FATIGUE LIFE DIAGRAMS	17
3.3 FATIGUE DATA ANALYSIS	23
3.4 SHORT FIBER COMPOSITES	36
3.5 CONTINUOUS STRAND MAT COMPOSITES	46
3.6 MODELS FOR LIFE PREDICTION	49
3.7 CONCLUDING REMARKS	50
REFERENCES	50
4. CREEP IN POLYMERIC COMPOSITES	53
4.1 INTRODUCTION	53
4.2 BASIC CONSIDERATIONS	53
4.3 MODELS FOR CREEP	58
4.4 EXPERIMENTAL CHARACTERIZATION OF CREEP RESPONSE	66
4.5 CONCLUDING REMARKS	69
REFERENCES	69
5. IMPACT RESPONSE AND DAMAGE IN COMPOSITE PLATES	73
5.1 INTRODUCTION	73
5.2 CONTACT BEHAVIOR	73
5.3 IMPACT TESTING METHODS	78
5.4 IMPACT RESPONSE	80
5.5 LOW-VELOCITY IMPACT DAMAGE	86
5.6 RESIDUAL PROPERTIES AFTER IMPACT DAMAGE	99
REFERENCES	101
6. ENVIRONMENTAL EFFECTS IN POLYMERIC COMPOSITES	107
6.1 INTRODUCTION	107
6.2 SORPTION PROCESSES	108
6.3 MOISTURE-INDUCED SWELLING, TEMPERATURE DEPENDENCE, AND TIME SCALES	121
6.4 FLUID EFFECTS ON MECHANICAL RESPONSE AND MECHANICAL PROPERTIES	122
6.5 CONCLUDING REMARKS	128
REFERENCES	128
7. ULTRASONIC TECHNIQUES FOR NONDESTRUCTIVE EVALUATION OF COMPOSITES	139
7.1 INTRODUCTION	139

7.2 LINEAR TECHNIQUES 141
7.3 NONLINEAR TECHNIQUES 158
REFERENCES 161
8. CONCLUSIONS AND RECOMMENDATIONS 171
8.1 DAMAGE AND FAILURE MECHANISM DETERMINATION 171
8.2 FATIGUE 171
8.3 CREEP 172
8.4 IMPACT 173
8.5 ENVIRONMENTAL EFFECTS 174

LIST OF FIGURES

Figure		Page
1.1	Automobile front structure built of PMCs	1
2.1	Plaque of SRIM isocyanurate reinforced with swirl CSM	4
2.2	Room-temperature tensile stress-strain behavior	6
2.3	Room-temperature fatigue test results	7
2.4	Residual tensile strength remaining after prior fatigue cycles	8
2.5	Modulus retention after prior fatigue cycles	9
2.6	Typical room-temperature creep strain response at stress of 14.5 ksi	10
2.7	Creep strain recovery for specimen that had previously accumulated 0.105% creep strain at 16.2 ksi	10
2.8	Creep/recovery tests of 90° specimen loaded first to 80% then to 60% of its average UTS	11
2.9	Comparison of creep curves at room temperature and 250°F (in air at 50% RH)	11
2.10	Weight gain vs square-root of time for specimens soaked in eight different automotive fluids at room temperature	13
2.11	Fluid effects on strength and stiffness (modulus of elasticity) for specimens soaked for 1080 h	14
2.12	C-scan amplitude images of failed tensile specimen (left) and virgin specimen (right)	15
3.1	Fatigue life diagram of unidirectional composite loaded in cyclic tension parallel to fibers	18
3.2	Mechanism of fiber failure in Region I	19
3.3	Mechanism of fiber-bridged matrix cracking in Region II	20
3.4	Mechanism of matrix cracking between fibers in Region III	21
3.5	Trends in fatigue life diagram induced by fiber stiffness and matrix ductility	22
3.6	Matrix flow at crack tip that causes crack-tip blunting, increased crack plane separation, and fiber failure	23
3.7	Fatigue life diagram of glass-epoxy under loading parallel to fibers	24
3.8	Fatigue life diagram of ultra-high modulus graphite-epoxy under loading parallel to fibers	24
3.9	Fatigue life diagram of high modulus graphite-epoxy under loading parallel to fibers	25
3.10	Fatigue life diagram of lower modulus graphite-epoxy under loading parallel to fibers	25
3.11	Fatigue life diagram for unidirectional composites under loading inclined to fibers	26
3.12	Fatigue life diagram of unidirectional glass-epoxy under loading inclined to fibers	27
3.13	Variation of fatigue limit with inclination angle, θ	27
3.14	Comparison of fatigue damage mechanisms in unidirectional and angle-ply laminates	29
3.15	Variation of fatigue limit of angle-ply laminate of glass-epoxy	30
3.16	Development of damage in $(0, 90_2)_s$ laminate of graphite-epoxy reflected as Stages I, II, and III in modulus reduction curve	31
3.17	Development of transverse crack density and modulus under fatigue of $(0, 90_2)_s$ graphite-epoxy laminate	31
3.18	X-ray radiograph showing transverse cracks (horizontal lines), longitudinal cracks (vertical lines), and local delaminations (shadowlike zones) in $(0, 90_2)_s$ graphite-epoxy laminate under fatigue, Stage II	32
3.19	Fatigue life diagram for cross-ply laminate of graphite-epoxy	33

3.20 Development of damage in composite laminates 34
3.21 Fatigue data of three graphite-epoxy composites 34
3.22 Change in longitudinal Young's modulus of woven fabric composite and cross-ply laminate of graphite-epoxy under fatigue 35
3.23 Stress amplitude vs cycles for polyester-resin reinforced with chopped strand mats of glass indicating onset of debonding and cracking under cyclic loading with zero mean stress 36
3.24 Strain to failure of polyester resin with polypropylene maleate adipate flexibilizer and of its composites with chopped strand mats and with fabric 37
3.25 Microcracking in short fiber reinforced SMC-R50 composite 38
3.26 Specimen of short fiber composite with sampling line of length l parallel to axial direction 39
3.27 Cumulative distribution function $F_c(c)$ and density function $f_c(c)$ of crack length at various cycles with maximum stress of 60% of ultimate tensile stress for short fiber SMC-R50 composite 40
3.28 Cumulative distribution function $G_\theta(\theta)$ and density function $g_\theta(\theta)$ of crack orientation at various cycles with maximum stress of 60% of ultimate tensile stress for short fiber SMC-R50 composite 41
3.29 Change in longitudinal Young's modulus of short fiber SMC-R50 composite under fatigue at maximum stress of 60% of the ultimate tensile stress 42
3.30 Schematic of crack zone in fiber avoidance mode of crack growth 43
3.31 Fatigue crack growth data for unreinforced and injection-molded fiber-reinforced polysulfone 44
3.32 Fatigue crack growth data for unreinforced and injection-molded fiber-reinforced nylon 66 44
3.33 S-N data for unnotched polysulfone in unreinforced and various injected-molded fiber-reinforced conditions 45
3.34 Schematic of relationship between fatigue crack growth and S-N behavior of injection-molded fiber-reinforced composites 46
3.35 Fatigue crack growth data for unfilled resin 47
3.36 Fatigue crack growth data for resin with 10% by weight filler 47
3.37 Fatigue crack growth data for resin with 20% by weight filler 48
3.38 Fatigue crack growth data for resin with 30% by weight filler 48
3.39 Comparison of fatigue crack growth data for unfilled resin and for resin with 40% by weight filler 49
4.1 Temperature dependence of creep compliance of PEEK 54
4.2 Temperature dependence of transverse creep compliance of APC-2 unidirectional laminate at 15.22 MPa 55
4.3 Modulus diagram for PMMA showing the glassy regime, the glass-rubber transition, rubbery regime, and regime of viscous flow 56
4.4 Influence of cross-linking on contour of modulus diagram for polyisoprene 56
4.5 Aging effects on creep response of polymers 57
4.6 Transverse tensile compliance-stress-time relationship of typical APC-2 composite laminate 57
4.7 Nonlinearly enhanced creep of unplasticized poly (vinyl chloride) in tension 61
4.8 Creep strains for FM-73 adhesive at various levels of uniaxial stress and data scatterbands 62
4.9 Stress and temperature dependence of creep rupture lifetime for AgCl, aluminum, and Plexiglas 65
4.10 Schematic of strain response of composite to constant loading rates 66
4.11 (*a*) Mechanical conditioning history as (*b*) sequence of creep-recovery periods 68
5.1 Schematic diagram for indentation test setup 74
5.2 Loading, unloading, and reloading curves 75

5.3 Loading curve for $[0/45/0/-45/0]_{2s}$ graphite-epoxy laminate with 12.7-mm spherical indentor 76
5.4 Unloading curves for $[0/45/0/-45/0]_{2s}$ graphite-epoxy laminate with 12.7-mm spherical indentor 77
5.5 Relation between α_0 and α_m ($s_p = 0.094$, $\alpha_p = 0.0167$ mm) 77
5.6 Schematic gas-gun impact setup 78
5.7 Drop-weight tower impact tester 79
5.8 Schematic pendulum-type impact tester 79
5.9 Cantilever-type impact tester 80
5.10 Finite element mesh and stress output locations 81
5.11 Transverse normal stress distribution in $[0_5/90_5/0_5]$ layup 82
5.12 Transducer response histories from experimental and finite element results up to 800 μm 83
5.13 Two-degrees-of-freedom spring-mass model for impact 84
5.14. Nomenclature of damage modes 88
5.15 X-ray radiograph of an impact damage in $[0_3/A/90_6/0_3]$ graphite-epoxy laminate 88
5.16 Young's modulus vs thickness change after impact in SMC-R50 composite 90
5.17 Residual ultimate stress vs thickness change after impact in SMC-1250 composite 90
5.18 Comparison of delamination caused by impact load and static load 91
5.19 Crack length vs impact velocity for $[90_5/0_5/90_5]$ laminate (Type Ia specimen) under drop-weight impact 94
5.20 Schematic double-plate model for delaminated plate 95
5.21 Prediction of delamination front for $[0_3/A/90_6/0_3]$ for maximum impact force of 1000 N (A-FM1000 adhesive film) 96
5.22 Damage in 24-ply AS4/BMI quasi-isotropic laminate subjected to impact of 7/8-in. steel ball at 21 m/s 97
5.23 Damage in 24-ply AS4/PEEK quasi-isotropic laminate subjected to impact of 7/8-in. steel ball at 29 m/s 98
5.24 Fiber breakage in fabric composite 98
5.25 Effect of specimen size on impact residual strength (A-S/4617 composite) 99
5.26 Effect of impactor size on degree of damage at constant damage area 100
5.27 Delamination growth contours for $[(0/90)_s/D/90_{14}/0_{14}]$ cross-ply 101
6.1 Moisture distribution profiles predicted by Fick's Law at various values of nondimensional time t* 109
6.2 Total weight gain $M(t)/M(\infty)$ vs $\sqrt{t^*}$ according to Fick's Law, with locations where departures from straight lines exceed 1% 110
6.3 "Non-Fickian" or "anomalous" sorption and desorption curves compared with Fickian type curves 111
6.4 Schematic curves representing four categories of recorded non-Fickian weight-gain sorption data in polymers and polymeric composites 111
6.5 Recorded concentration values with distribution profiles predicted by Fick's Law 117
6.6 Three-phase oxidation system and excess O_2 distribution in the oxide 119
6.7 Schematic drawing of moisture-induced fiber/matrix interfacial cracks 121
6.8 Creep compliance S_{xx}, as recorded at various temperatures and RHs, for $[\pm 45]_{2s}$ AS/3502 composite specimens 122
6.9 "Master curves" for the transverse compliance S_T, as inferred from data for S_{xx} shown in Fig. 6.8, for AS/3502 composite 123
6.10 Combined shift factor obtained from samples exposed at various temperatures 123
6.11 "Two-stage" creep under extended exposure to environment 124
6.12 A semilogarithmic plot of load P vs failure time t_f in static fatigue tests of glass/polyester composites in sea water 125
7.1 Through-transmission ultrasonic C-scan image (amplitude) of piece of urethane swirl mat composite showing molding mark 144

7.2 Through-transmission ultrasonic C-scan image (velocity) of piece of urethane swirl mat composite showing molding mark 144
7.3 Through-transmission ultrasonic C-scan image (amplitude) of piece of urethane swirl mat composite showing fiber-poor region 145
7.4 Pulse-echo ultrasonic C-scan image (amplitude) of piece of urethane swirl mat composite showing detection of impact damage (near center) and mold mark (10 o'clock position) 146
7.5 Pulse-echo ultrasonic C-scan image (velocity) of piece of urethane swirl mat composite showing detection of impact damage (arrow, near center) and mold mark (brightest indication, near 10 o'clock position) 146
7.6 Variation in longitudinal wave velocity as function of radius in S2 glass-epoxy flywheel subject to spin-induced fatigue 147
7.7 C-scan results at two different gains on S2 glass-epoxy flywheel showing detection of critical radius for matrix cracking 149
7.8 Transfer curve of S2 glass-epoxy composite before (solid curve) and after (dashed curve) application of 2.1% uniaxial strain 150
7.9 Polar backscattering results on quasi-isotropic (transversely isotropic) glass-epoxy composite that has been subjected to fatigue 151
7.10 Diagram showing transducer configuration for excitation and detection of Lamb waves and distortions produced in specimen by two classes of waves 153
7.11 Dispersion curves for symmetric Lamb wave modes in alumina 153
7.12 Dispersion curves for antisymmetric Lamb wave modes in alumina 154
7.13 Experimentally obtained spectrum of Lamb wave modes in alumina coupon 154
7.14 Double-transmission method for generating and detecting Lamb waves in composite laminates 155
7.15 Spectrum of double-transmitted wave in graphite-epoxy composite showing excitation of Lamb wave near 1.5 MHz 156
7.16 Spectral content of 5-MHz transducer used in Lamb wave studies in graphite-epoxy composite 156
7.17 Lamb wave C-scan map of graphite-epoxy composite panel showing image of two simulated impact damage areas 157

LIST OF TABLES

Table		Page
2.1	Room-temperature tensile properties of reference isocyanurate composite	7
6.1	Types of sorption data for various materials and exposures	112
7.1	Elastic constant results	142
7.2	Attenuation (dB)	148

LIST OF ACRONYMS

ACC	Automotive Composites Consortium
CAI	compression after impact
C.O.V.	coefficient of variation
CSM	continuous strand mat
DDB	diodobutane
DOE	Department of Energy
LED	light-emitting diode
LVDT	linear variable differential transformer
NDE	nondestructive evaluation
ORNL	Oak Ridge National Laboratory
PMC	polymer matrix composite
R&D	research and development
RH	relative humidity
RVE	representative volume element
SMC	sheet molding compound
SRIM	structural reaction injection molding
USCAR	United States Council for Automotive Research
UTS	ultimate tensile strength
TBE	S-Tetrabromethane
2-D	two-dimensional
3-D	three-dimensional

PREFACE

This interpretive, state-of-the-art report is the result of one of the initial tasks of the Oak Ridge National Laboratory (ORNL) Durability of Lightweight Composite Structures Project. This project, which is sponsored by the U.S. Department of Energy's (DOE's) Lightweight Materials Program, is focused on resolving the durability issues associated with the use of polymeric composites in automotive structural applications. The DOE Program Manager for the project is S. Diamond of the Office of Transportation Materials.

The objective of this report is to provide an authoritative treatment of the current status of the key durability issues—the effects of cyclic loadings, creep, automotive fluid environments, and low-energy impacts. The report also addresses the state-of-the-art of ultrasonic techniques for nondestructive evaluation of durability-related damage. The work and cooperation of the authors (Ramesh Talreja, Y. Jack Weitsman, C. T. Sun, and W. A. Simpson, Jr.) were, of course, the leading factors contributing to the success of this document. Each is a recognized expert in his respective area.

The Durability of Lightweight Composite Structures Project at ORNL is part of a cooperative effort between DOE and the Automotive Materials Partnership of the United States Council for Automotive Research (USCAR). The Project is being coordinated with the Automotive Composites Consortium (ACC). The specific point of contact within ACC for the project is E. M. Hagerman, while an ad hoc durability group consisting of Hagerman, D. Q. Houston, and S. N. Kakarala provides the overall coordination for ACC. The advice and guidance of these individuals, along with T. J. Dearlove, head of the ACC Materials Group, has been invaluable.

The authors acknowledge with gratitude the assistance of C. C. Southmayd, who edited the report, and R. R. Baxter, who prepared the final manuscript.

J. M. Corum
Oak Ridge National Laboratory

ABSTRACT

A key unanswered question that must be addressed before polymeric composites will be widely used in automotive structural components is their known durability. Major durability issues are the effects that cyclic loadings, creep, automotive fluid environments, and low-energy impacts have on dimensional stability, strength, and stiffness throughout the required life of a composite component. This report reviews the current state of understanding in each of these areas. It also discusses the limited information that exists on one of the prime candidate materials for automotive structural applications—an isocyanurate reinforced with a continuous strand, swirl mat. Because of the key role that nondestructive evaluations must play in understanding damage development and progression, a chapter is included on ultrasonic techniques. A final chapter then gives conclusions and recommendations for research needed to resolve the various durability issues. These recommendations will help provide a sound basis for program planning for the Durability of Lightweight Composite Structures Project sponsored by the U.S. Department of Energy in cooperation with the Automotive Composites Consortium of Chrysler, Ford, and General Motors.

1. INTRODUCTION—AN OVERVIEW

J. M. Corum

Lighter weight, more fuel efficient automobiles of the future will require increased use of lightweight structural materials, such as polymer matrix composites (PMCs). To be acceptable, however, structural composite parts must be produced in high volume at a competitive cost. Liquid molding has the potential to meet these requirements, producing large complicated polymeric composite structural assemblies that achieve a high degree of parts consolidation (Dearlove et al., 1994). Examples of these types of structural components include floor pans, body side frames, cross-members, and front structural members. A schematic of a front structure is shown in Fig. 1.1. This component, which consists of approximately planar isotropic composites for the bulk of the structure, was built as a demonstration project by the Automotive Composites Consortium (ACC), a research and development (R&D) partnership between Chrysler, Ford, and General Motors.

Despite their potential, the use of structural polymeric composites in vehicles has not progressed very rapidly. In part, this is because of the unanswered questions related to the high-volume, low-cost manufacture of components with consistent part-to-part properties and known durability. Answering these questions is a key goal of ACC (Dearlove et al., 1994).

To help resolve the lightweight materials issues, the U. S. Department of Energy (DOE) has entered into a cooperative effort with the Automotive Materials Partnership of the United States Council for Automotive Research (USCAR). In the DOE Lightweight Materials Program those projects in the polymeric composite area are being carried out cooperatively with ACC. One such project, to address the durability issues associated with the application of polymeric composites to automotive structures, was initiated by DOE at Oak Ridge National Laboratory (ORNL) in June 1994. Preparation of this report was one of the initial tasks of the Durability of Lightweight Composite Structures Project.

The objective of the Durability Project is to develop experimentally based, durability driven, design guidelines for automotive composite structures and to demonstrate their applicability to representative lightweight manufacturable automotive structures under representative field loading histories and environments. Key technical issues are the potentially degrading effects that long-term and cyclic loadings, temperature, automotive fluids, aging, and low-energy impacts can have on the dimensional stability, strength,

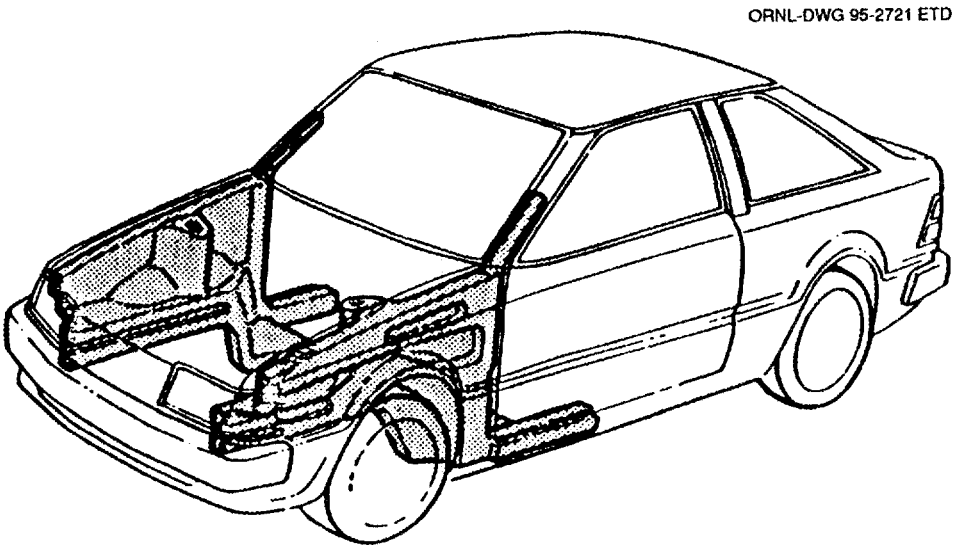

Fig. 1.1. Automobile front structure built of PMCs.

and stiffness of automotive composite structures. Specific objectives of the project are thus to (1) characterize and model the synergistic effects of cyclic and creep loadings, temperature, relevant fluid environments, and multiple low-energy impacts (e.g., tool drops and roadway kickups) on deformation, strength, and stiffness and (2) develop, and validate through subscale component tests, design guidance to assure the long-term (15-year) durability of automotive composite structures.

The early Durability Project strategy has been to (1) perform a series of scoping tests on the reference composite material and (2) enlist the aid of recognized experts in the relevant areas to prepare this state-of-the-art interpretive report. The scoping test results together with the interpretive report findings and recommendations are to then be used as a sound technical basis to develop a comprehensive 5-year program plan for the Durability of Lightweight Composite Structures Project.

The current ACC reference material is a structural reaction injection-molding (SRIM) isocyanurate (polyurethane) reinforced with continuous strand, swirl mat, E glass. The 0.125-in.-thick plaques of this material were supplied by ACC for the preliminary scoping tests. Typical results of these tensile, fatigue, creep, and exposure tests are presented in Chap. 2 as a reference base for considering the reviews and recommendations of the subsequent chapters. Also included in Chap. 2 is a discussion of the limited information on swirl mat composite behavior found in the literature.

Chapter 3, prepared by Ramesh Talreja of the Georgia Institute of Technology, covers fatigue of polymeric composite materials. It makes wide use of "fatigue life" diagrams to better understand and interpret fatigue behavior. Creep in polymeric composites is addressed in Chap. 4, prepared by Y. Jack Weitsman of ORNL and The University of Tennessee/Knoxville. That chapter discusses typical observed behavior and modeling approaches. Chapter 5, by C. T. Sun of Purdue University, discusses impact testing and modeling approaches that have been successfully employed. Chapter 6, prepared also by Weitsman, discusses sorption processes and effects of fluid environments on mechanical properties. Chapter 7, prepared by W. A. Simpson, Jr., of ORNL, reviews ultrasonic techniques for nondestructive evaluation (NDE) of composites. That chapter is included because of the key role that NDE must play in understanding damage development and progression to failure. These five chapters—3 through 7—collectively contain and review hundreds of pertinent references.

The final chapter, Chap. 8, provides conclusions and recommendations drawn from the previous chapters and from discussions with each author. It recommends the general approach in each area—fatigue, creep, impact, environmental effects, and NDE—to be taken in the comprehensive program plan for the Durability of Lightweight Composite Structures Project.

REFERENCE

Dearlove, T. J., et al. 1994. "Development of Standardized Tests for an Automotive Structural Composites Database," pp. 555–66 in *Proceedings of the 10th Annual ASM/ESD Advanced Composites Conference*, ASM International, Materials Park, Ohio.

2. BACKGROUND

J. M. Corum

2.1 DURABILITY ISSUES

An example of a structural composite application in a vehicle was illustrated in Fig. 1.1, where a front structure was depicted. In the large structural parts being considered by ACC, approximately planar isotropic composites will form the bulk of the structure, with engineered fabric patches added as structural demands require. Both adhesive and bolted joints will likely be involved.

Vehicle structures will be subjected to both steady and cyclic loadings. Also, they will be exposed to a variety of environments. Parts could be subjected to temperatures ranging from –40°F to 250°F. In addition to water and salt they could come into contact with a variety of automotive fluids, including windshield washer fluid, battery acid, antifreeze, gasoline, brake fluid, and motor oil. Tool drops and other low-velocity impacts during manufacturing and maintenance, as well as higher velocity impacts from rocks and pebbles kicked up from roadways, could produce invisible damage. These load, temperature, and environmental factors could individually or synergistically have a significant adverse effect on dimensional stability, strength, and stiffness of the composite structure. Since the design of most vehicle structures is stiffness driven, the retention of that stiffness during the 15-year design life is particularly important. Likewise, dimensional stability is important. While the short-term dimensional stability of composites is considered to be typically better than that for metals, it is also more critical due to the inability to deform (reshape) a composite to final tolerances as is currently the practice for sheet metals. Long-term creep could lead to interference of parts, for example, where door, hood, and fender components may be joined to underlying structures. Creep could also lead to an undesired bolt load relaxation in bolted joints.

The goal of the Durability of Lightweight Composite Structures Project at ORNL is to characterize and provide an understanding of the long-term durability of composite structures and to then work with ACC to develop appropriate design allowables and reduction factors to assure that the degrading effects of cyclic and creep loadings, low-energy impacts, and environments are accounted for and that lightweight composite structures in future automobiles have adequate long-term (15-year) durability.

2.2 MATERIALS OF INTEREST

As mentioned in Chap. 1, liquid molding using glass reinforcement is ACC's preferred processing method. The current reference material is an SRIM isocyanurate reinforced with continuous strand, swirl mat, E glass. The ORNL Durability Project is focusing initially on this material. Other promising possibilities, however, include (1) a chopped, directed fiber, glass reinforcement and (2) woven cloth. The chopped fiber reinforcing, which would consist of ~1-in.-long fibers randomly oriented in the plane of the part, is particularly attractive because no preformed mat would be involved; parts could thus be manufactured more economically.

The initial plaques, on which the preliminary scoping data presented in the next section were obtained, were all from a single batch of SRIM isocyanurate reinforced with continuous strand mat (CSM) E glass. Figure 2.1 shows one of the 0.125-in.-thick plaques together with a small piece of the swirl mat reinforcement. The two components of the isocyanurate matrix are an isocyanate and a polyol. With no reinforcing, the tensile strength of the matrix is reported to be 10.2 ksi. The continuous strand swirl mat consists of standard E glass. Strands consisting of several hundred 19-μm-diam (0.0007-in.) monofilaments are used. The filaments have a reported strength of 250 ksi and a modulus of 10×10^6 psi. Sizing (<0.5% by weight) is applied to improve adhesion to the matrix. Binder is applied to hold the mat together (8% by weight). According to the manufacturer, the mat should be transversely isotropic to within 20%.

ORNL-PHOTO 8000-95

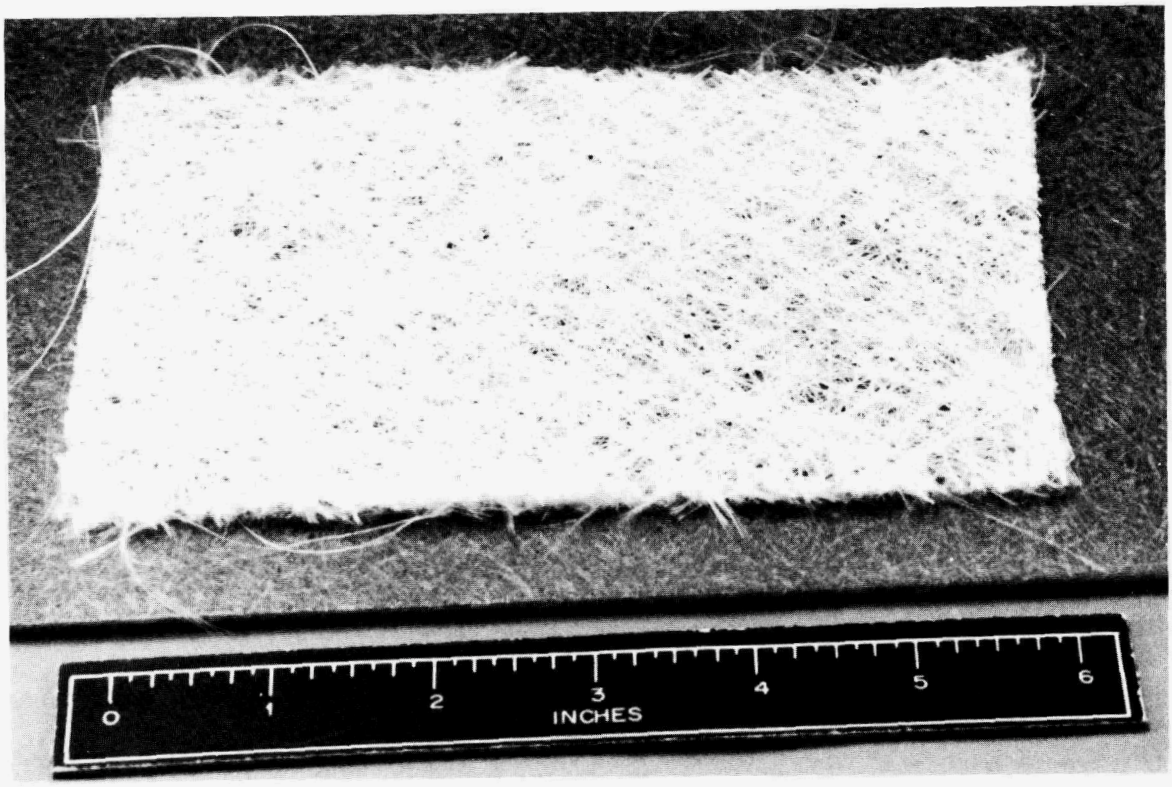

Fig. 2.1. Plaque of SRIM isocyanurate reinforced with swirl CSM. Piece of E-glass mat is also shown.

Five layers of mat were used in the 0.125-in.-thick preliminary isocyanurate plaques. Measurements at The University of Tennessee indicate that the fiber content of the plaques is about 55% by weight.

2.3 CHARACTERISTICS OF CSM COMPOSITES

2.3.1 Literature Information

Although CSM composites have been used for several years, there is a notable dearth of information in the literature on their characteristics and behavior. These composites differ very substantially from other composite materials used to date. Consequently, their response, durability, and failure mechanisms are expected to exhibit characteristics that are unlike those observed in more familiar composite systems.

The literature abounds with information concerning composite laminates, which consist of lay-ups of distinct plies. This architecture results in severe weaknesses in the transverse direction, with ensuing failures by intraply transverse cracking and interply delaminations. The study of these failures dominates current research on composites. To a lesser extent, experience has been gained with sheet molding compound (SMC) composites, which consist of randomly oriented short fibers bound by a polymeric resin. While SMC composites resemble CSM composites more closely, their failures are still affected by fiber pull-outs, and they lack the mechanistic effects caused by the entanglements among the long fibers within the CSM composite. Consequently, while some basic principles governing the performance and modeling of other polymeric composites remain valid for CSM composites, significant differences remain in the details, and a study of these materials demands new and independent approaches.

Two exceptions to the dearth of information on CSM composite behavior are the work led by Stokes at General Electric and by Karger-Kocsis at the University of Kaiserslautern in Germany.

Stokes (1990*a–d*) focused his efforts on understanding and characterizing the inherent small-scale spatial variations in modulus of elasticity and tensile strength in 0.125- to 0.145-in.-thick sheets of Azdel®P100, a polypropylene reinforced with several layers (40%) of random glass mat. By cutting long 1/2-in.-wide tensile test strips from the sheets and measuring the modulus every 1/2 in. along the strips with a 1/2-in. gage length extensometer, he found that the modulus values could vary by a factor of 2 from the 1/2-in. square to the adjacent 1/2-in. square and by a factor of 3 over the 6- by 12-in. plaques. The measurements were made on a single edge of the strips. When measurements were made on both edges, Stokes found that the averages of the two modulus values approached some representative mean for the plaque. Thus he concluded that the material was essentially homogeneous on a sufficiently large scale (a large specimen and a large extensometer measuring strain on the specimen face would give results approaching a mean).

Stokes also measured tensile strength in the long 1/2-in.-wide strips. He found that the failures occurred where the average modulus was low, which also corresponded to areas of low density (fiber-poor areas). Thus, as might be expected, the variations reflect variations in glass density.

Karger-Kocsis and coworkers [Karger-Kocsis (1990, 1991, 1992*a,b*); Karger-Kocsis and Czigany (1993); and Karger-Kocsis and Fejes-Kozma (1994)] have studied glass swirl mat reinforced, reaction-injection molded, polyamides (Nyrim®) and polypropylenes for automotive applications. They have focused primarily on static and dynamic tests of notched specimens (compact tension, Izod, and Charpy). The mat, placed in several layers, was Unifilo U816 from Vetrotex. The polyamide (nylon) with low glass content is, in particular, very transparent. This allowed the failure mode of the mat-reinforced composites to be followed in-situ by light microscopy. The failure surfaces were also studied postmortem by light microscopy and scanning electron microscopy. Simultaneous monitoring of the failure mode by both light microscopy and acoustic emission allowed individual failure events to be related to the acoustic emission signals.

The nylon matrix in the material studied by Karger-Kocsis had a failure strain greater than 50%. This very ductile matrix significantly influenced the failure mechanism. Karger-Kocsis describes the failure events in notched specimens as follows:

1. as crack blunting occurs in the ductile matrix, the fibers debond and strands begin to split up;
2. the very ductile matrix allows the fiber mat network to deform, with further debonding, strand splitting, and matrix voiding ahead of the crack;
3. individual filaments in kinked strands begin to break and pull out; and
4. strands break when the mesh type ductility is exhausted.

Note that in the isocyanurate reference material of ACC, the matrix is brittle rather than ductile; thus the failure events are likely to differ from those observed by Karger-Kocsis.

In studies of specimen size effects, Karger-Kocsis found that fracture mechanics results were independent of specimen size so long as the ligament dimension exceeded some critical value—typically 1/2 in. Below this value, the measured fracture toughness went down because the glass reinforcing acted like chopped, rather than continuous, fibers.

2.3.2 Isocyanurate/CSM Reference Material Behavior

The preliminary ORNL scoping test results presented in this section are for specimens taken from five 25 × 25 × 0.125-in.-thick plaques of the reference isocyanurate material supplied by ACC. The test specimens were all 8 by 1 in. The tensile and fatigue specimens had 2-in.-long tabs on each end. Only a portion of the creep test specimens had tabs.

2.3.2.1 Tensile behavior

Thirty-three room-temperature tensile tests were performed on specimens from the five plaques. The results are shown in Fig. 2.2, where typical (near average) stress-strain curves are shown for the 0° and 90°

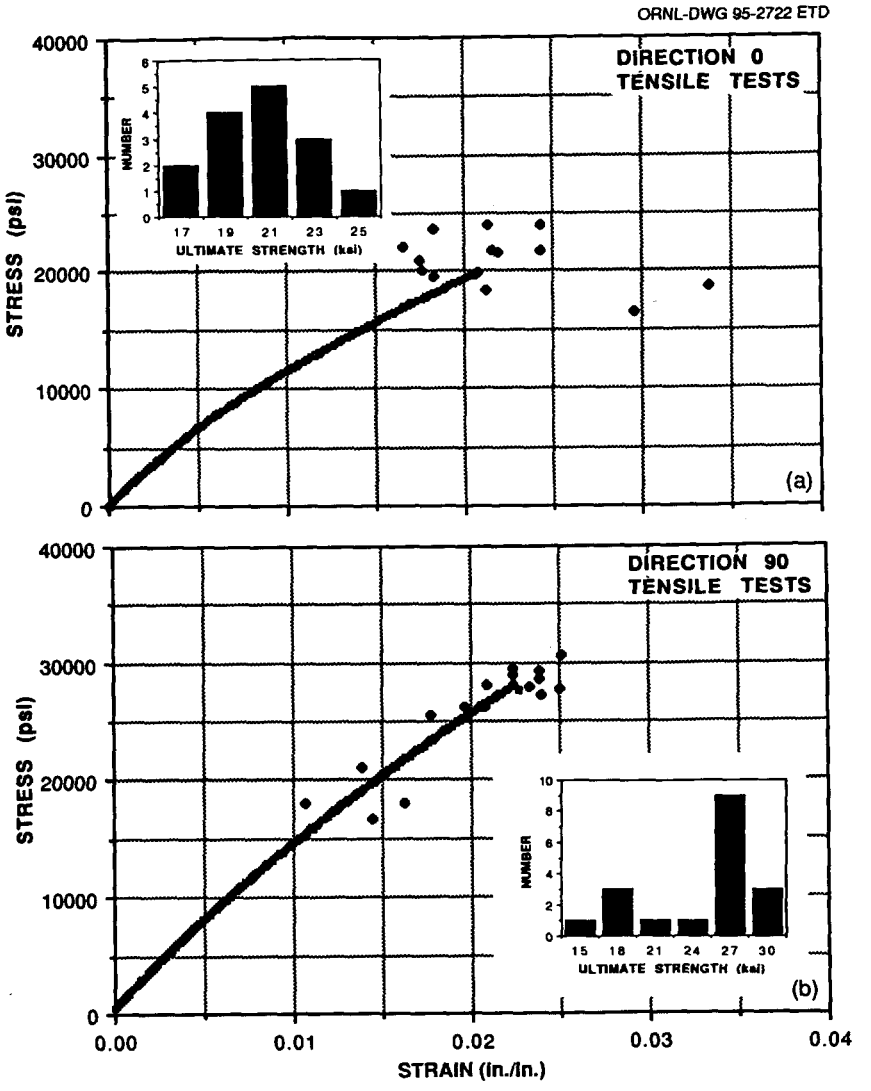

Fig. 2.2. Room-temperature tensile stress-strain behavior: (*a*) 0° direction and (*b*) 90° direction.

plaque directions.* Also shown are the failure points for all of the tests. Insets are histograms showing the distributions of strengths. As can be seen, these particular plaques exhibit some anisotropy, with the 90° direction being strongest. The average measured tensile strength and modulus of elasticity, together with coefficients of variation (C.O.V.), are tabulated in Table 2.1 for the two directions.

The four low points for the 90° direction in Fig. 2.2(*b*) are all from a single plaque, for which the strength in the 90° direction was low and about equal to that in the 0° direction. Strength and modulus values are also tabulated in Table 2.1 with data for that plaque omitted.

2.3.2.2 Fatigue and residual strength

Thirty-eight room-temperature fatigue tests on specimens from the five plaques have been performed. The results are shown in Fig. 2.3. All of the tests were at an R value of 0.1 (ratio of minimum to

*The 0° direction corresponds to the original roll direction of the fiber mat.

Table 2.1. Room-temperature tensile properties of reference isocyanurate composite

	Tensile strength (ksi)		Modulus (10^6 psi)	
	0°	90°	0°	90°
All five plaques				
Average	20.7	25.4	1.34	1.58
C.O.V. (%)	11.1	18.1	7.5	5.1
Four plaques				
Average	21.3	27.4	1.36	1.59
C.O.V. (%)	10.3	9.9	6.6	4.4

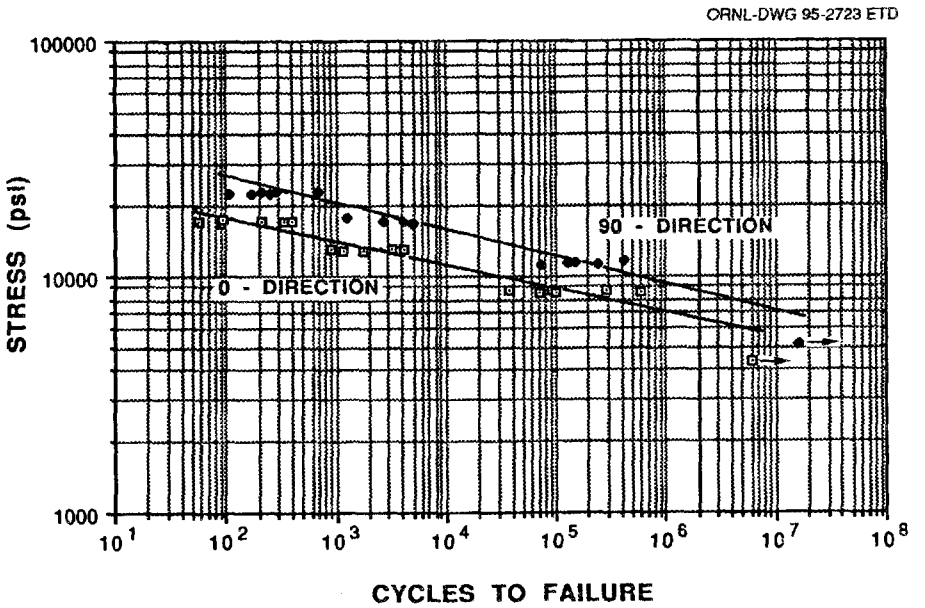

Fig. 2.3. Room-temperature fatigue test results.

maximum stress), and maximum stresses of 80, 60, 40, and 20% of the ultimate tensile strength (UTS) were used. The two run-out points in Fig. 2.3 are at 20% of UTS. These tests were interrupted after having accumulated 6.0 and 16.0 million cycles for the 0° and 90° directions, respectively, and tensile tests to failure were performed. Reductions in UTS were 36% (from 20.7 to 13.3 ksi) for the 0° direction and 55% (from 25.4 to 11.5 ksi) for the 90° direction. Reductions in stiffness were significantly smaller: 11.2% (from 1.34 to 1.19×10^6 psi) for the 0° direction and 10.1% (from 1.58 to 1.42×10^6 psi) for the 90° direction. Dearlove et al. (1994) showed ACC modulus data on this same material system indicating that the modulus decreases linearly throughout a fatigue test with the log of the number of cycles.

Figure 2.4 depicts the results of a more systematic matrix of room-temperature tests to determine the degrading effects that prior fatigue cycles have on residual tensile strength and modulus. In the two plots shown, fatigue tests were interrupted at either 50 or 80% of the expected cyclic life, and the specimens were tensile tested to failure. The data shown in Fig. 2.4(*a*) are for cycling at a maximum stress of 40% of the average UTS, and the points in Fig. 2.4(*b*) are for 60% of UTS. In each plot the tensile data points are shown at N = 0.25. Pure fatigue data points, for the appropriate stress level, are also shown. The curves

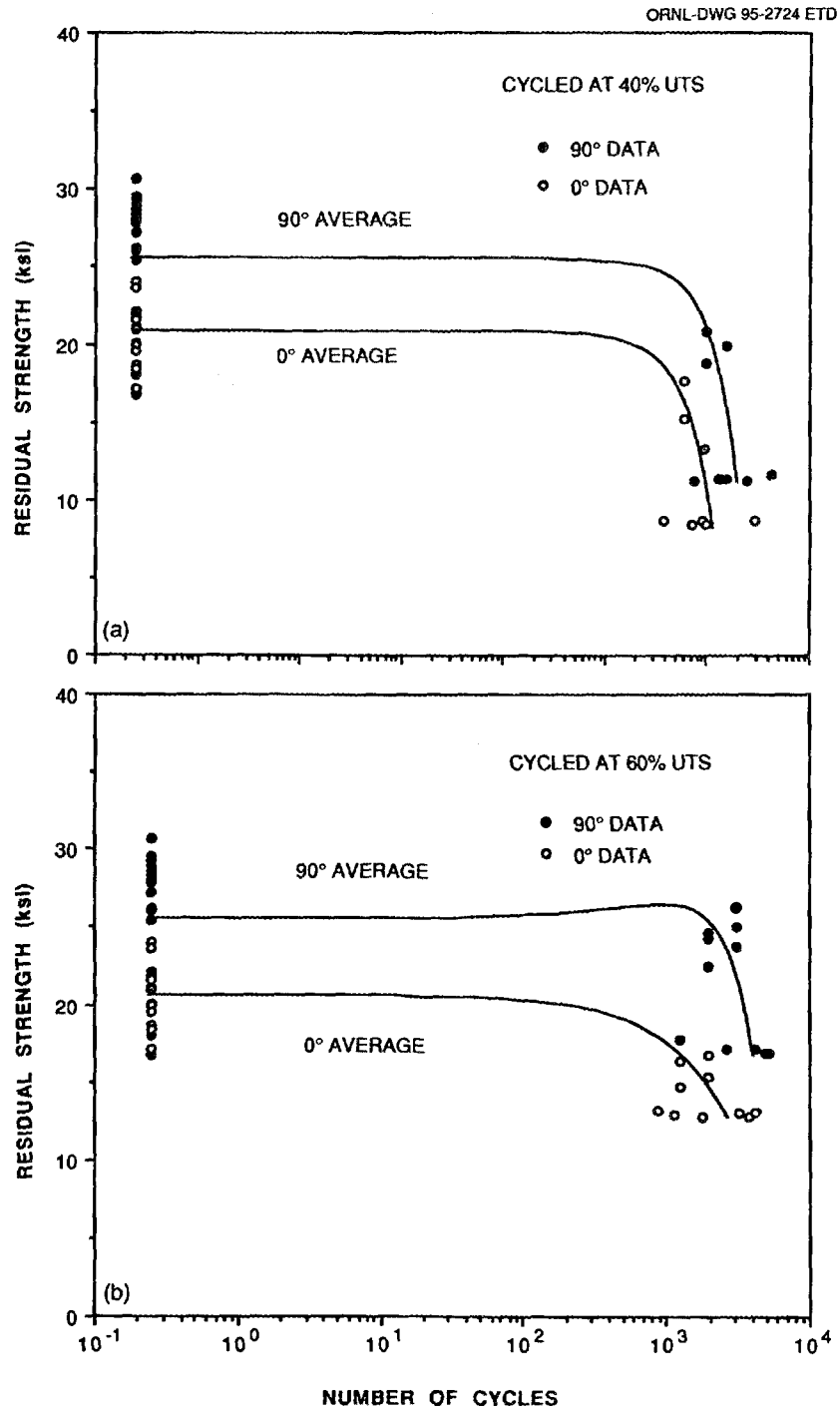

Fig. 2.4. Residual tensile strength remaining after prior fatigue cycles: (*a*) cycled at 40% of UTS and (*b*) cycled at 60% of UTS.

shown are simple binomials fitted to the data. When more data become available and the synergistic effects of other variables are included, plots such as these will help establish reliable design allowables.

Figure 2.5 gives the values of the retained modulus of elasticity measured in the series of tensile failure tests just described. The plots are scaled by the average modulus values from the tensile tests of virgin

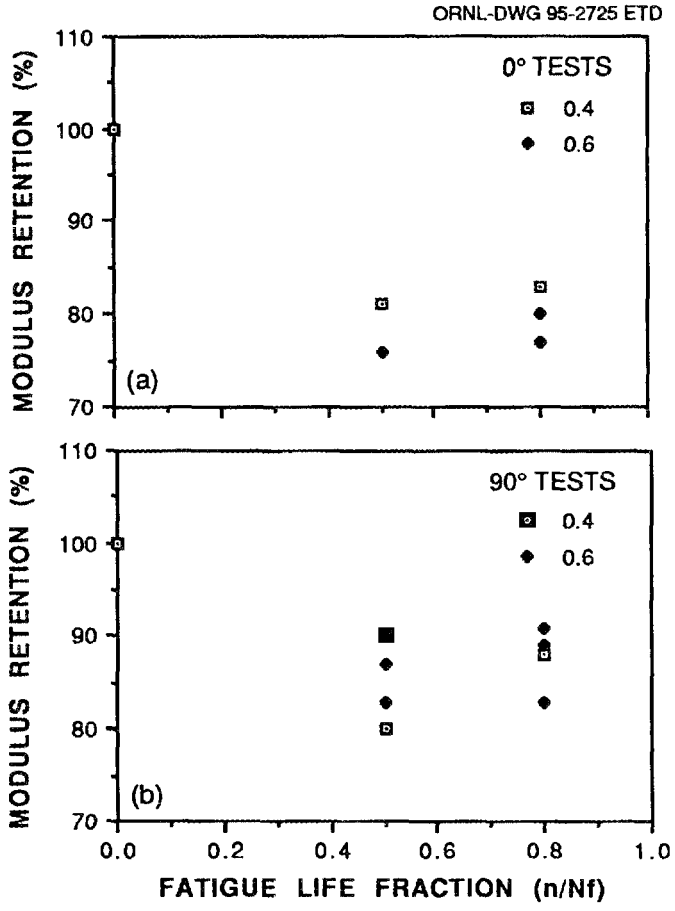

Fig. 2.5. Modulus retention after prior fatigue cycles: (*a*) 0° direction and (*b*) 90° direction.

specimens (Table 2.1). These results indicate that the modulus drops early in the cyclic life. The further loss occurring in the range between 50 and 80% of the fatigue life is negligible.

2.3.2.3 Creep and recovery

Figure 2.6 is a typical room-temperature creep curve, corresponding to a stress level of 14.5 ksi. This response is typical for the higher stress levels at room temperature. The time-dependent straining levels off after a few hundred hours, and the creep curve remains nearly flat. Insufficient data are available to characterize the subsequent creep-rupture, or static-fatigue, behavior. Also the creep response at low stress levels, particularly the linearity of creep with stress, is unknown at present.

Upon unloading, considerable strain recovery occurs with time. This behavior is typified by Fig. 2.7. The response is for a specimen that had previously accumulated an initial strain of 1.149% upon loading to 16.2 ksi and a time-dependent creep strain of 0.105% at 16.2 ksi.

To better understand creep and recovery, a series of exploratory short-term tests has been conducted. In these tests a specimen was loaded to 80% of its ultimate strength for 30 min, then allowed to recover with no load for a minimum of 120 min. Figure 2.8 shows the response. As can be seen, not all of the strain was recovered, and it is postulated that the difference represents irreversible damage. To test this hypothesis, the strain scale was reset to zero, and the specimen was subsequently loaded to a lower level of 60% of UTS for a similar period of creep and recovery. The results are also shown in Fig. 2.8, and they exhibit complete recovery of the creep strain, possibly indicating no additional damage. Although these early tests are too limited to provide firm conclusions, they do illustrate the kinds of tests that will be needed to

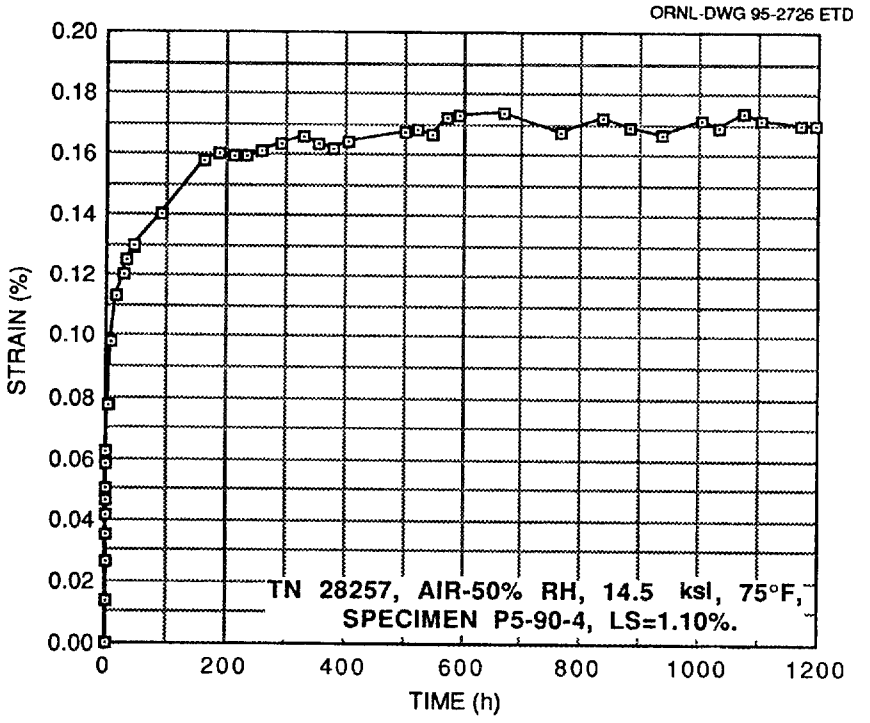

Fig. 2.6. Typical room-temperature creep strain response at stress of 14.5 ksi. Loading strain (not shown) was 1.10%.

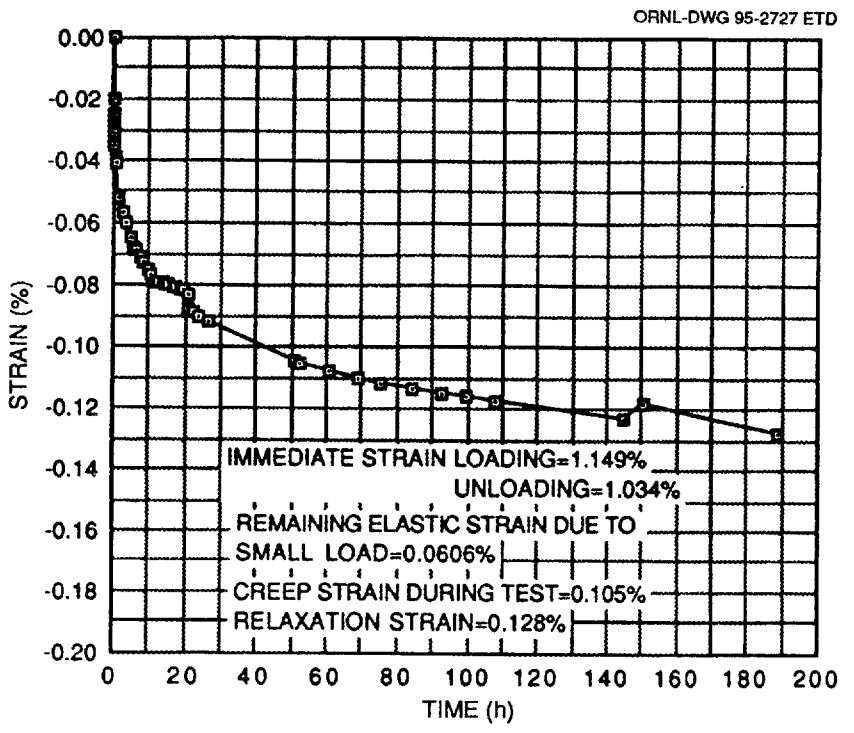

Fig. 2.7. Creep strain recovery for specimen that had previously accumulated 0.105% creep strain at 16.2 ksi.

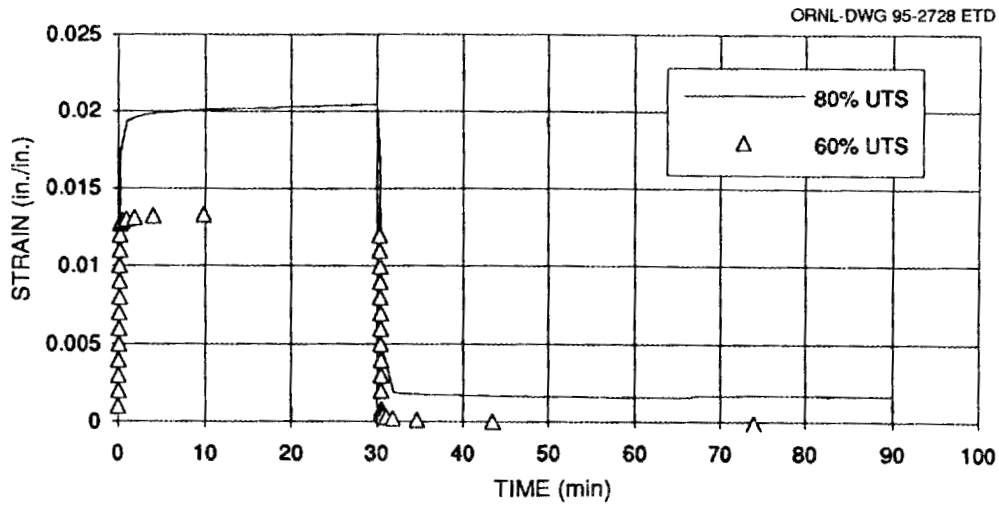

Fig. 2.8. Creep/recovery tests of 90° specimen loaded first to 80% then to 60% of its average UTS.

understand damage. NDE techniques will need to play a central role in quantifying damage at the various phases of loading and unloading.

A few elevated-temperature tests have been performed at 250°F. The results of one of these are shown in Fig. 2.9 and compared to two duplicate room-temperature tests. Considering, especially, that the elevated-temperature test was at a lower stress level than the room-temperature tests, it can be seen that temperature has a very marked effect on creep. The several creep tests that have been performed at 250°F [in air at 50% relative humidity (RH)] all exhibit behavior more typical of thermally activated creep.

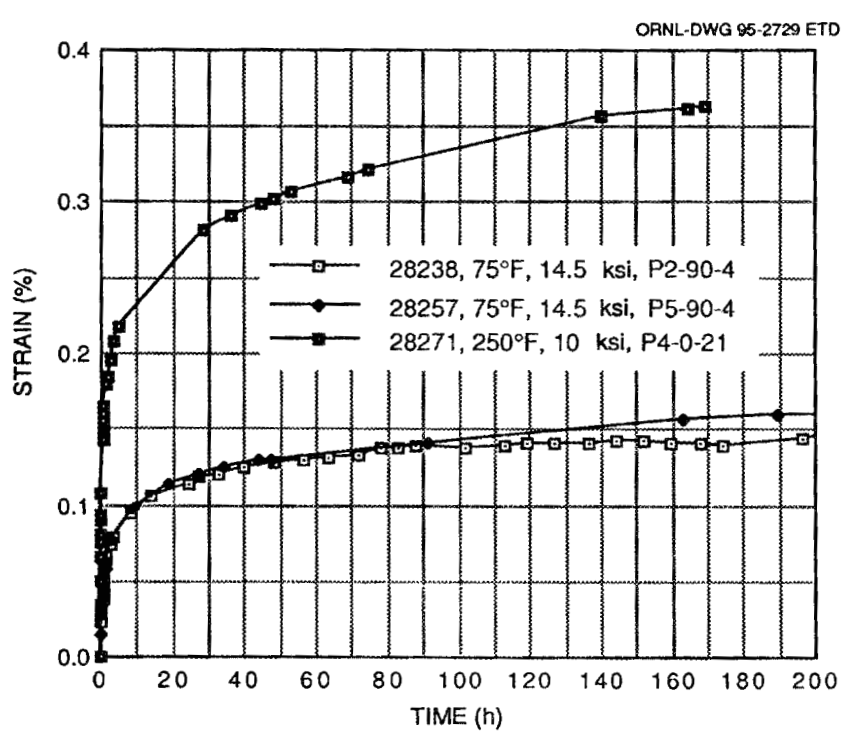

Fig. 2.9. Comparison of creep curves at room temperature and 250°F (in air at 50% RH).

As typified by the curve in Fig. 2.9, the specimens exhibit a period of decreasing creep after loading, followed by a period of creep at nearly constant rate. Failure occurs with little detectable accelerated creep. Figure 2.9 also demonstrates the good reproducibility of creep data collected during two duplicate tests.

2.3.2.4 Fluid Exposure Effects

To gain preliminary insight into the effects of common automotive fluids, tensile specimens have been soaked in one of eight fluids (ten per fluid):

- distilled water,
- saltwater solution (5% NaCl),
- 40% antifreeze (ethylene glycol)/60% water,
- windshield washer fluid (90% methanol),
- used motor oil,
- battery electrolyte (34% sulfuric acid),
- gasoline, and
- brake fluid (glycols).

Two untabbed specimens (one oriented in the 90° direction and one in the 0° direction) were included in each fluid for weight gain (or loss) measurements. Figure 2.10 shows the results for 2600 h of exposure. The data are plotted as a function of the square root of time so that they can be qualitatively compared to the predictions of the common linear Fick's Law for the diffusion of a fluid into a solid (see Chap. 6). Those curves in Fig. 2.10 showing significant weight gain do appear to reflect linear Fickian behavior (compare with Fig. 6.4). At 1080 h, four specimens were removed from each fluid and tensile tested. The relative changes in strength and stiffness from the unexposed specimen average values are depicted in Fig. 2.11. Although four specimens per condition are too few to draw statistically valid conclusions, it appears that battery electrolyte (acid) and brake fluid may have the largest degrading effect on strength. The other fluids degrade the strength by <10%. Antifreeze and windshield washer fluid appear to have the largest effect on stiffness.

Dearlove et al. (1994) reported the ACC data for both stressed and unstressed specimens exposed to water and windshield washer solvent. Both strength and stiffness were presented. The ACC data were for just a 100-h exposure; nonetheless, the reported effect of washer solvent was to reduce strength and stiffness by almost 40%—much larger than the effect shown in Fig. 2.11. These results indicate that larger experimental populations and careful consideration of the fluid ingredients and composite constituents will be required to reliably characterize fluid environment effects. The ACC data for specimens stressed to relatively low stress levels (up to 10% of UTS) during exposure showed that the effect of stress during exposure is small but measurable in both water and washer solvent. Both strength and stiffness were further reduced.

Early creep tests in fluid environments are under way at ORNL. Room-temperature tests at 14.5 ksi in an ethylene glycol/50% water solution and in windshield washer fluid failed in just a few hours.

2.3.2.5 Impact behavior

No controlled impact tests have been performed yet at ORNL on the reference isocyanurate CSM composite. However, Dearlove et al. (1994) presented preliminary ACC drop-weight data on rectangular plaques of an SRIM isocyanurate with 25% (volume) CSM. They found that this material was very easily damaged on impact; very low impact energy levels produced visible damage. However, stiffness decay, which is the most important mechanical property, was relatively insensitive to the presence of the damage. Finally, they reported that the impact damage area, as measured by ultrasonic C-scans, was a near-linear function of impact energy.

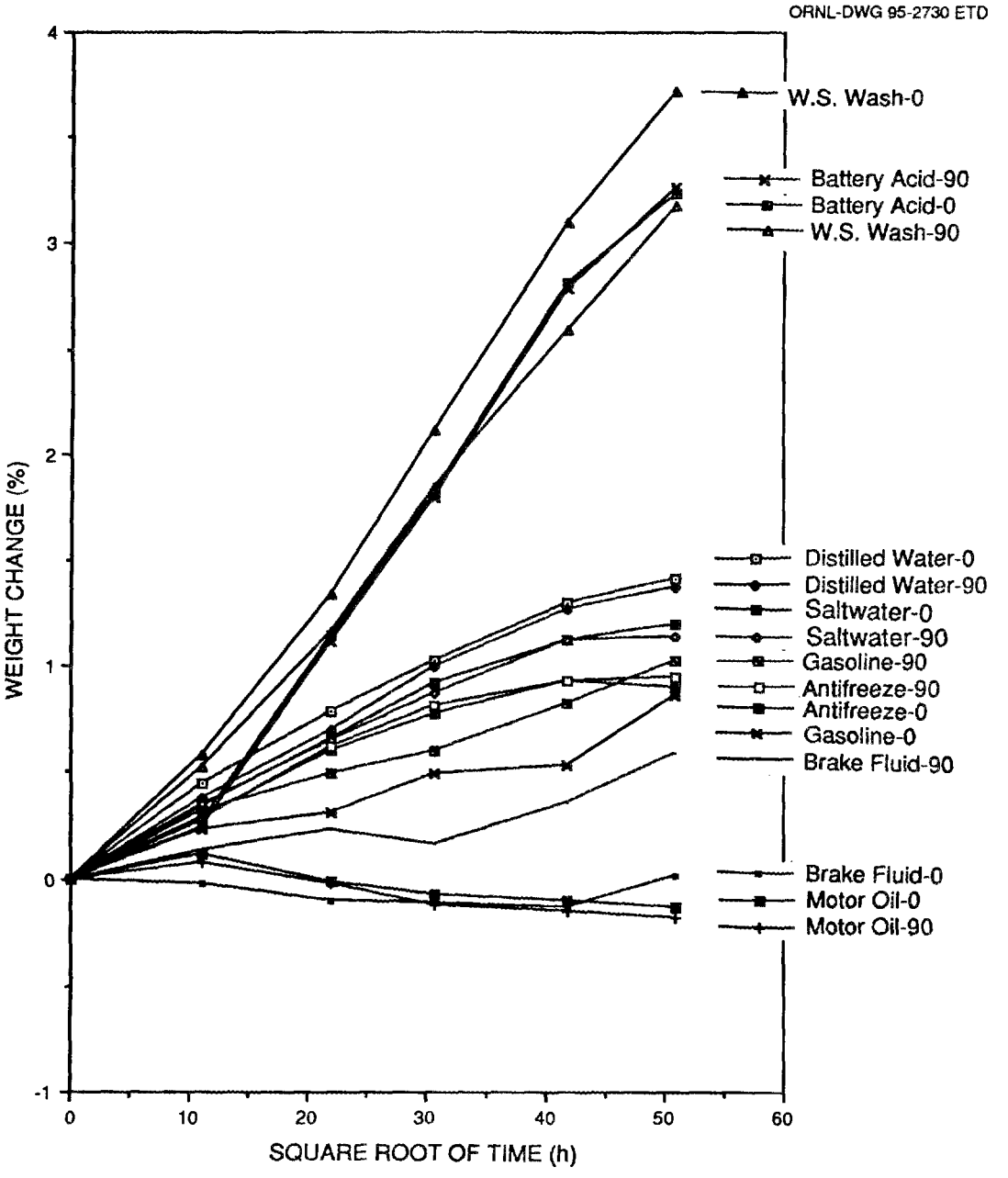

Fig. 2.10. Weight gain vs square-root of time for specimens soaked in eight different automotive fluids at room temperature.

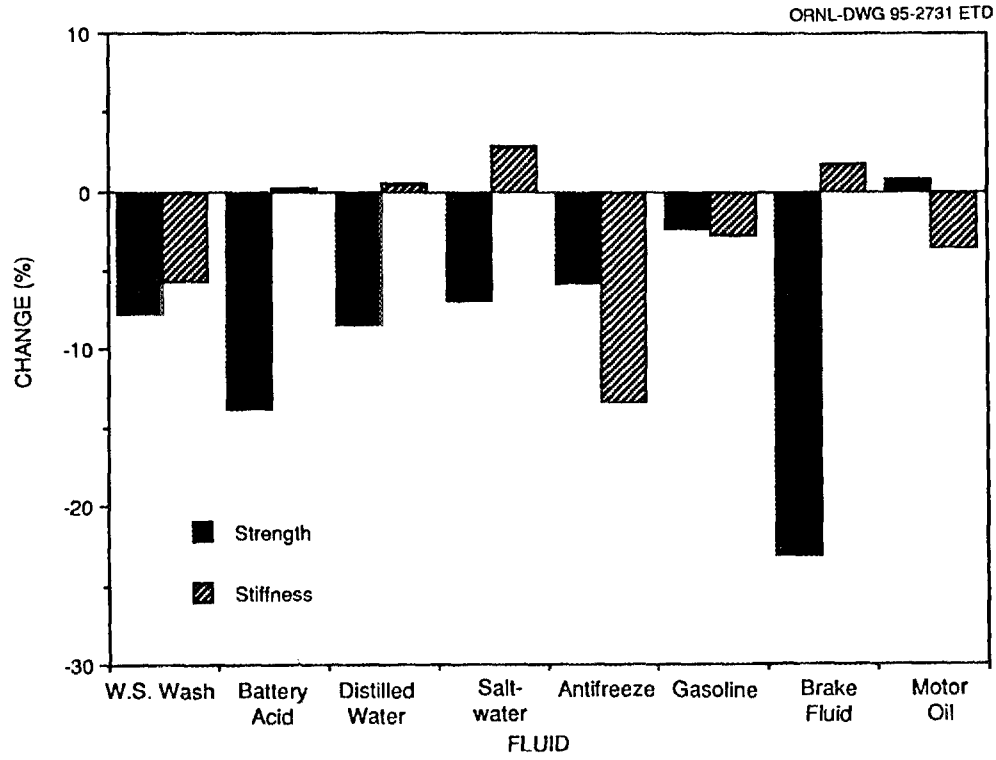

Fig. 2.11. Fluid effects on strength and stiffness (modulus of elasticity) for specimens soaked for 1080 h.

2.3.2.6 Damage detection

The ability to detect and monitor the accumulation of damage is a key requirement. In Chap. 7 of this report, it is shown that ultrasonic C-scans can be used to detect areas of impact damage in the reference isocyanurate CSM composite. Failed tensile and fatigue specimens have also been examined at the Iowa State University's Center for Nondestructive Evaluation using a pulse-echo C-scan at 15 MHz. As typified by Fig. 2.12, which shows images for a failed tensile specimen and a virgin specimen side by side, the distributed damage in failed specimens is very distinct. Specimens from two of the five ORNL plaques were examined, and both amplitude and time-of-flight images showed a significant difference between failed and virgin specimens. While the damage appears relatively uniform over the specimens, close examination of the original color plots indicates the presence of slightly more damage near the failure surface. Also, there is a slight difference between images for tensile and fatigue specimens; the distributed damage appears to be lower in a failed fatigue specimen.

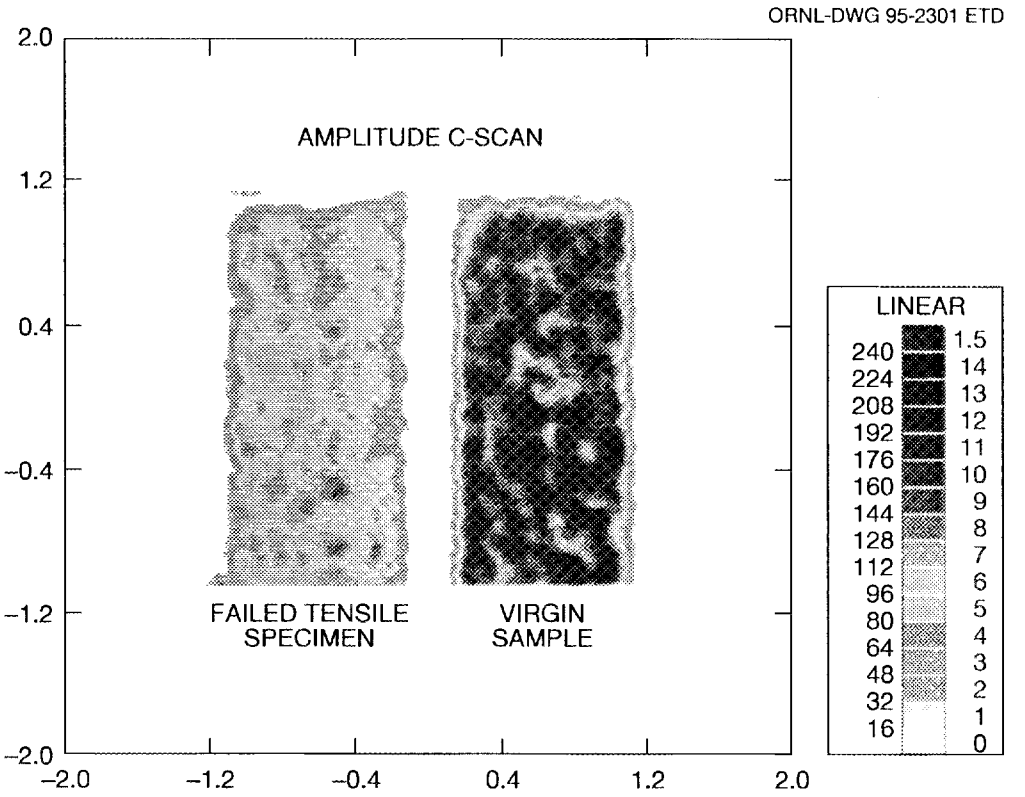

Fig. 2.12. C-scan amplitude images of failed tensile specimen (left) and virgin specimen (right).

REFERENCES

Dearlove, T. J., et al. 1994. "Development of Standardized Tests for an Automotive Structural Composites Database," pp. 555–66 in *Proceedings of the 10th Annual ASM/ESD Advanced Composites Conference*, ASM International Materials Park, Ohio.

Karger-Kocsis, J. 1990. "Dynamic Fracture Mechanics of a RIM Polyamide Block Copolymer Reinforced with Glass Strand Mat," *Polym. Bull.* **24**, 341–48.

Karger-Kocsis, J. 1991. "Environmental Stress Corrosion Behavior of Polyamides and Their Composites with Short Glass Fibers and Glass Swirl Mat," *Polym. Bull.* **26**, 123–30.

Karger-Kocsis, J. 1992*a*. "Fracture and Failure Behavior of Glass Fiber Mat-Reinforced Structural Nylon RIM Composites," *J. Polymer Engineering* **11**(1–2), 153–73.

Karger-Kocsis, J. 1992*b*. "Instrumented Impact Testing of a Glass Swirl Mat-Reinforced Reaction Injection-Molded Polyamide Block Co-polymer (NBC)," *J. Appl. Polym. Sci.* **45**, 1595–1609.

Karger-Kocsis, J., and Czigany, T. 1993. "Fracture Behavior of Glass-Fiber Mat-Reinforced Structural Nylon RIM Composites Studied by Microscopic and Acoustic Emission Techniques," *J. Mater. Sci.* **28**(9), 2438–48.

Karger-Kocsis, J., and Fejes-Kozma, Zs. 1994. "Damage Zone Development and Failure Sequence in Glass Fiber Mat-Reinforced Polypropylene Under Static Loading Conditions," *Mechanics of Composite Materials* **30**(1), 8–13.

Stokes, V. K. 1990*a*. "Random Glass Mat Reinforced Thermoplastic Composites. Part 1: Phenomenology of Tensile Modulus Variations," *Polymer Composites* **11**(1), 32–44.

Stokes, V. K. 1990*b*. "Random Glass Mat Reinforced Thermoplastic Composites. Part II: Analysis of Model Materials," *Polymer Composites* **11**(1), 45–55.

Stokes, V. K. 1990*c*. "Random Glass Mat Reinforced Thermoplastic Composites. Part III: Characterization of the Tensile Modulus," *Polymer Composites* **11**(6), 342–53.

Stokes, V. K., 1990*d*. "Random Glass Mat Reinforced Thermoplastic Composites. Part IV: Characterization of the Tensile Strength," *Polymer Composites* **11**(6), 354–67.

3. FATIGUE OF COMPOSITE MATERIALS

R. Talreja
Georgia Institute of Technology

The mechanisms of damage under cyclic loading of composite materials are of such complexity that a straightforward interpretation of fatigue life data is usually not possible. A logically deduced, systematic conceptual framework for interpretation of composite fatigue data was developed earlier by this author. That framework, in the form of fatigue life diagrams, is described, and its basis is explained. Fatigue life data for long, continuous, fiber-reinforced PMCs are assessed with this framework, and the effects of matrix ductility and fiber stiffness are explained. The role of fiber architecture in affecting fatigue properties is described. The modeling concepts for predicting fatigue life are then discussed, and some progress in this respect is reviewed. The needs for further work, in particular in relation to automotive applications, are outlined.

3.1 INTRODUCTION

Composite materials provide combinations of properties that are generally not achievable with monolithic materials. However, the properties achieved under short-term loading (e.g., stiffness and strength) degrade differently in composites than in monolithic materials under long-term loading. The multiplicity of cracking modes at the microlevel, the local load sharing and transfer among constituents and the coalescence, linkup, and criticality of microfailures create a significant challenge in modeling and predicting the rates of degradation of properties and failure of composites under long-term sustained and cyclic loading conditions. A general theory of fatigue of composite materials is not available and would probably be unreasonable to expect. On the other hand, it is not desirable to generate fatigue data for every configuration as a basis for design. A realistic approach is to search for some characteristic features in the fatigue behavior of a given class of composites and to understand how these are affected by systematic variation of parameters such as constituent properties and geometrical descriptors of microstructure. This approach has led to construction of a conceptual framework for interpretation of the fatigue behavior of a wide class of composite materials, described as fatigue life diagrams (Talreja, 1981). These diagrams do not quantitatively predict fatigue life but provide useful insight for selection of constituents and for developing efficient predictive models. In what follows, a thorough exposition of the fatigue life diagrams will be presented. Certain useful characteristics concerning inherent limits of safe fatigue loads will be described. Modeling approaches proposed in the literature will be critically examined, and gaps and uncertainties in our understanding of composite fatigue behavior will be discussed.

This exposition will be focused on a critical review rather than an exhaustive survey of the literature. (For supplemental information see Boller, 1969; Hahn, 1979; Harris, 1986; and Konur and Matthews, 1989.) Most data examined here will be for typical aerospace composites with polymeric matrices, since the aerospace applications have driven this field in the past. However, some systems developed for automotive applications (e.g., SMCs and other short-fiber composites) will be considered to the extent possible. Finally, the material of interest currently under investigation, the SRIM polymers reinforced with CSM, will be discussed.

3.2 FATIGUE LIFE DIAGRAMS

In analyzing the fatigue behavior of a given material certain basic questions must be addressed: (1) How does the state of the material (expressed in terms of microstructural parameters) change from the initial to the instant when the first maximum load is applied? (2) On reversal of the load to the initial value does the state of the material return to the initial state, and if not, what are the irreversible changes? (3) What are the consequences of these irreversible changes on the state of the material when the previous

maximum load is repeated? (4) What is the critical state of the material causing failure, and how do the progressive (load cycle to load cycle) microstructural changes reach this state?

For monolithic materials such as polymers and metals these questions have been addressed in a large number of studies, and a great deal of progress has been made in devising fatigue-resistant materials as well as in developing methodologies for life prediction. In composites with two distinct constituents and the associated interfacial region, the analysis of fatigue is made difficult by the facts that the fatigue of a constituent material may be significantly affected by the presence of the other constituent and that the interfacial region may entail complicating aspects not present in the fatigue of individual constituents. The difficulty is further enhanced by the simultaneous progression of mechanisms in the constituents and at the interface at differing rates dependent on the level of loading.

In a study directed at PMCs, where these four questions were addressed, a conceptual framework was proposed that facilitated the interpretation of fatigue (Talreja, 1981). The framework is in the form of a fatigue life diagram in which regions of dominant governing mechanisms are identified. For the purpose of this chapter it will be useful to review the concept of a fatigue life diagram. The baseline diagram proposed by Talreja (1981) is for tension-tension loading of unidirectional composites parallel to fibers (Fig. 3.1).

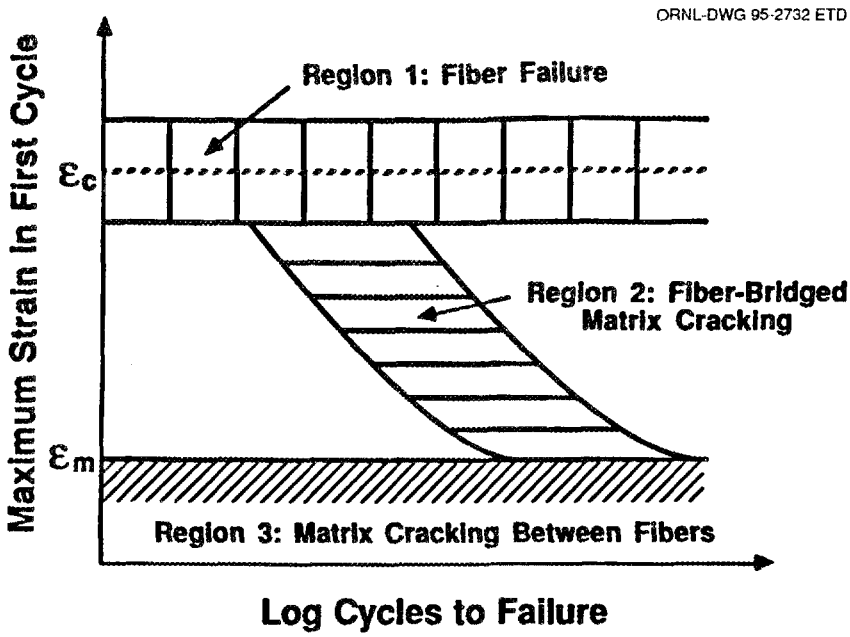

Fig. 3.1. Fatigue life diagram of unidirectional composite loaded in cyclic tension parallel to fibers. *Source*: Reprinted from R. Talreja, *Fatigue of Composite Materials*, Chap. 2 (Fig. 2). ©Technomic Publishing Company, Inc., 1987.

The fatigue life diagram plots the maximum strain attained in the first cycle of a load-controlled fatigue test vs the cycles to failure. The reasons for plotting strain and not stress are as follows.

1. The failure in the first cycle occurs when the composite strain equals the failure strain of fibers, irrespective of the volume fraction of fibers. Thus, one point of the fatigue life diagram can be fixed for a given composite with a given type of fibers.
2. The fatigue limit of a composite is a matrix-governed property (as will be discussed below). Since the matrix undergoes strain-controlled fatigue within the composite, the proper way to indicate the fatigue limit of the composite is in terms of strain.
3. Since the two extremes of the fatigue life are best expressed in terms of strain, there is no compelling reason for not having strain as a variable between these. Additionally, the maximum strain reached in

the first cycle is indicative of the attained state of damage in the composite, which determines its further progression in subsequent cycles.

Let us consider a composite in which the fibers are elastic until failure and the matrix has an elastic limit beyond which it behaves inelastically. To understand the construction of the fatigue life diagram, consider first a load cycle in which the maximum strain achieved is within the scatterband of the composite failure strain (which is also the fiber failure strain). At the maximum load in this cycle a certain number of fibers will be expected to fail (Fig. 3.2). In the regions around the broken fibers the matrix will suffer enhanced stresses causing it to deform further into the inelastic range. On unloading to the initial load the matrix in these regions will not return to its initial state due to irreversibility of the inelastic strain. On reloading to the previous maximum load the stress state in the vicinity of the previously broken fibers will be different from the one that existed at the previous maximum load. Also, due to the extended flow of the matrix at the maximum load, in the vicinity of the previously broken fibers, more fibers than previously will be subjected to enhanced stresses. As a consequence of this, a fiber (or fibers) in the affected zone that did not break previously could break during the load reapplication. This process of fiber failures is highly statistical because (1) the strength of fibers is subject to a large scatter and (2) a match between the renewed stress in a fiber in the affected zone and its strength must be found for fiber failure to occur.

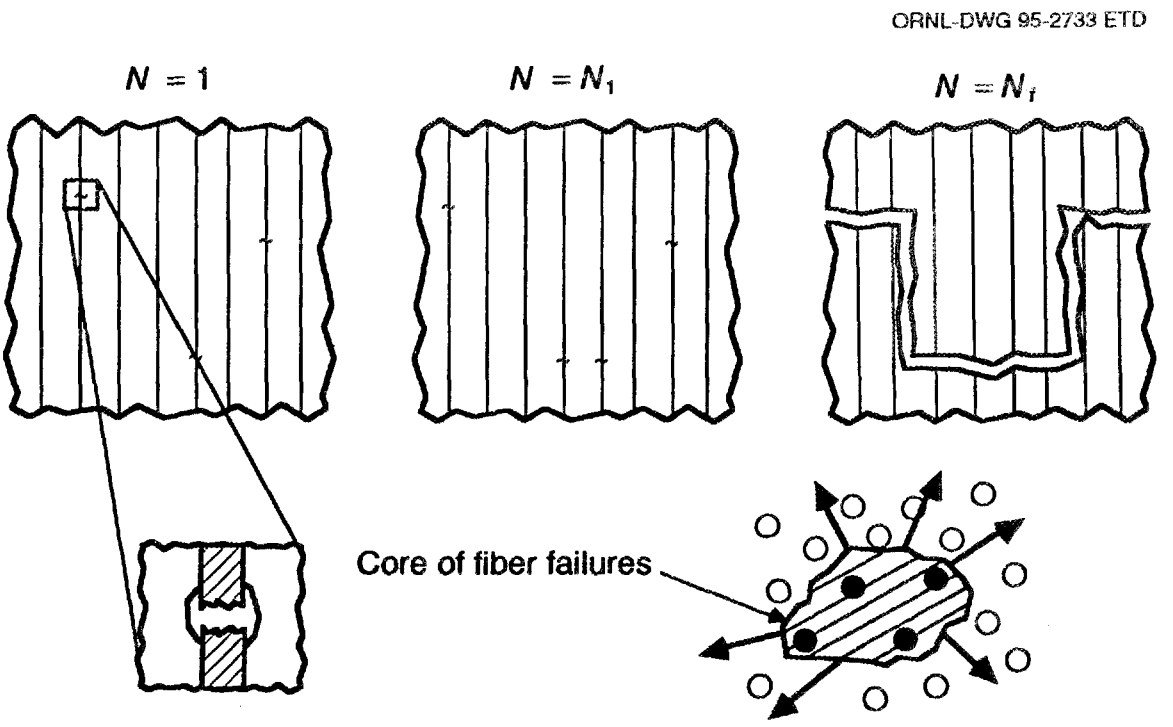

Fig. 3.2. Mechanism of fiber failure in Region I. *Source*: Reprinted with permission of VCH Publishers, Inc.

For the composite failure to occur, a certain number of fibers in an affected zone must fail to form a core of fiber failures connected by the cracked matrix such that the crack front thus formed can grow unstably through the composite (Fig. 3.2). Clearly, the occurrence of composite failure is highly statistical in the sense that a sufficiently large core of fiber failures can form in a few cycles in an affected zone or may take a large number of cycles to form in another affected zone. What is important is the fact that the progressiveness of this process, which may be described by a rate equation, is questionable. In other words the number of cycles to failure associated with this process is a random chance variable. Therefore, in the

fatigue life diagram (Fig. 3.1), the scatterband of composite failure strain is labeled as Region I and is taken to extend over an infinite number of cycles. This implies that if a load cycle that gives the maximum strain within the scatterband of the composite failure strain is repeated, the composite failure may occur at any number of cycles between one and infinity.

Consider next a load cycle that in the first application gives a maximum strain less than the lower limit of the composite failure scatterband (e.g., 5% failure probability value). The number of fiber failures in the first application of such a cycle will be negligible. Assuming that the fibers are brittle and linearly elastic to failure, there would be no change in the deformation of fibers from the first cycle to the next, except that brought about by changes in the matrix behavior. The matrix, on the other hand, undergoes a strain-controlled cycling that would cause fatigue crack initiation and growth in much the same way as in an unreinforced matrix subjected to those cycles. Consequently, the matrix would crack at random sites within the composite volume. When such cracks meet fibers, further growth would depend on how effectively the crack fronts overcome these obstacles. At lower applied loads the matrix cracks would tend to grow around fibers, while at higher applied loads the fibers near the matrix crack fronts would tend to break and would allow the cracks to grow further. When a matrix crack has grown over a distance of a few fiber diameters, its appearance would generally have the features illustrated by Fig. 3.3. Such a crack would be fiber-bridged, more toward the crack tips than in the midregion where fibers would tend to break due to crack plane separation. A bridging fiber would be debonded at the crack planes, as the matrix crack would grow around the fiber by debonding the interface. The cross-sectional view in Fig. 3.3 illustrates how the front of a fiber-bridged matrix crack could appear at various load cycles, indicating the lack of self-similarity in the crack front shape. Also shown in that figure is the unstable (i.e., uncontrolled) growth of the crack at certain load cycles, leading to the final failure.

ORNL-DWG 95-2734 ETD

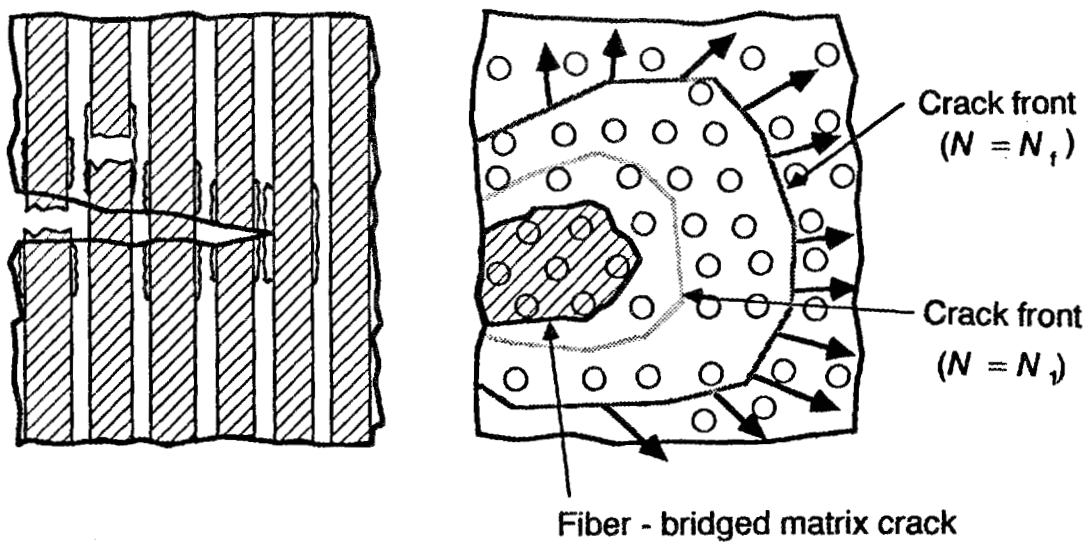

Fig. 3.3. Mechanism of fiber-bridged matrix cracking in Region II. *Source*: Reprinted with permission of VCH Publishers, Inc.

In the fatigue life diagram (Fig. 3.1), Region II represents the manifestation of the fiber-bridged matrix cracking mechanism. The sloping scatterband reflects the fact that as the maximum strain in the first application of a cyclic load is reduced, more cycles would be required to reach failure.

Region III in the fatigue life diagram represents the region in which the final failure is not reached within a "large" number of cycles, typically 10^6 to 10^7 cycles. The maximum strain in this region is too low

to drive the matrix fatigue cracks sufficiently beyond the obstacles provided by the fibers to cause unstable growth of the cracks. The nonpropagating matrix cracks arrested by fibers in this region are illustrated by Fig. 3.4.

ORNL-DWG 95-2735 ETD

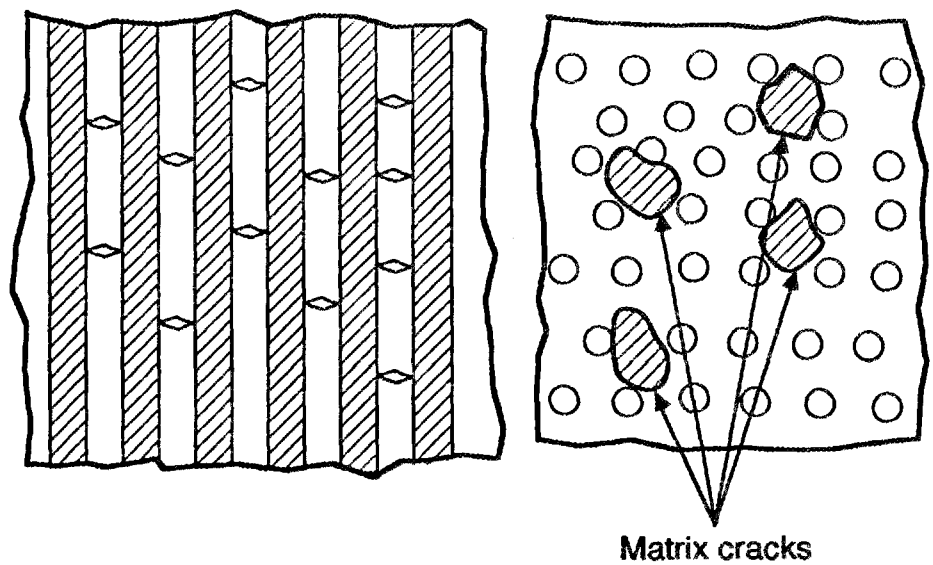

Fig. 3.4. Mechanism of matrix cracking between fibers in Region III. ***Source*****: Reprinted with permission of VCH Publishers, Inc.**

The boundary between Region II and Region III is the fatigue limit of the composite. It can be stated that this limit is bounded from below by the fatigue limit of the matrix material under strain-controlled fatigue, because no fatigue of the composite can be expected if the matrix is not cracked. Thus, if the fibers are of vanishing stiffness, the fatigue limit of the composite will tend to the fatigue limit of the matrix, both values being expressed as strains. With increasing stiffness and volume fraction of fibers, the effectiveness of matrix crack growth suppression by fibers will increase, enhancing the fatigue limit of the composite.

Note that the three-region description of fatigue behavior of unidirectional composites under tension-tension loading parallel to fibers just described is based on the predominant (i.e., governing) mechanisms operating in the regions. Other events would also be occurring alongside these mechanisms but are not considered to have significant effects on fatigue failure. As an example, matrix fatigue cracking would also occur in Region I but is not expected to influence the failure of the composite.

Features in the composite fatigue behavior that can be interpreted with the framework just described are as follows.

1. *Effect of fiber failure strain*—As can be observed from the fatigue life diagram (Fig. 3.1), reducing the composite failure strain by selecting fibers of lower strain to failure would reduce the range of strain over which Region II extends. Indeed, an amazing result can be obtained if the fiber failure strain becomes less than the fatigue limit of the matrix. In that case, Region II vanishes, and the fatigue life diagram consists only of Region I. Thus, the range of the progressive fatigue mechanism can be manipulated and even made to vanish by the fiber failure strain. This effect will be illustrated below by considering actual fatigue data.

2. *Effect of fiber stiffness*—Since Region II of the fatigue life diagram is governed by the fiber-bridged matrix cracking mechanism, the fiber stiffness will have a pronounced effect on this region. Assuming that the rate of growth of the fiber-bridged crack is proportional to some power of the applied strain and that this power (i.e. exponent) is inversely proportional to the fiber stiffness (raised to some

power), it can be seen that Region II will appear as illustrated in Fig. 3.5. Thus, the slope of Region II will be increasingly steeper with increasing fiber stiffness. Also, since the magnitude of the closing pressure on the matrix fatigue cracks depends on the fiber stiffness, their suppression to the nonpropagating state, Region III, is also governed by the fiber stiffness. Therefore, the enhancement of the composite fatigue limit from the matrix fatigue limit occurs as illustrated in Fig. 3.5.

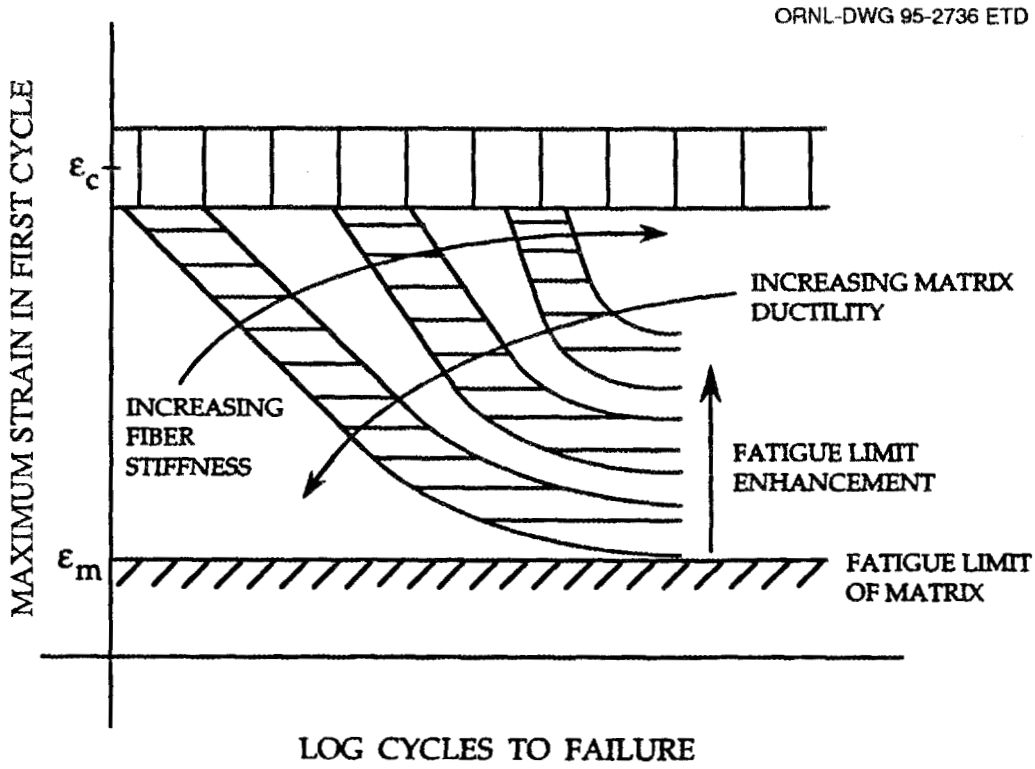

Fig. 3.5. Trends in fatigue life diagram induced by fiber stiffness and matrix ductility.

3. *Effect of matrix ductility*—A ductile matrix will cause plastic zone formation at the matrix crack tips (Fig. 3.6). This will lead to crack-tip blunting and the resulting increase in crack plane separation. The bridging fibers will thus be subjected to increased strain, which will cause earlier failure of fibers than otherwise. These considerations suggest that the trend in Region II of the fatigue life diagram caused by matrix ductility will be as illustrated in Fig. 3.5. This trend and its consequences will be illustrated below by considering actual fatigue data.

As discussed in this chapter, the fatigue life diagram is unaffected by environmental degradation. As discussed later in Sect. 6.4.4, however, environment could play a significant role in the fatigue life diagram structure and the controlling mechanisms. These effects will need to be accounted for in the Durability of Light-Weight Composite Structures Project.

ORNL-DWG 95-2737 ETD

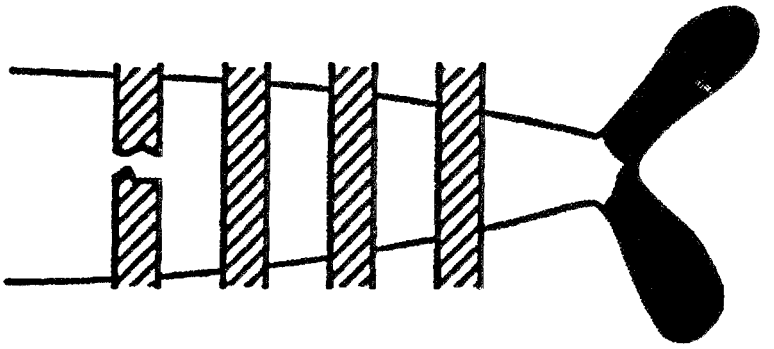

Fig. 3.6. Matrix flow at crack tip that causes crack-tip blunting, increased crack plane separation, and fiber failure.

3.3 FATIGUE DATA ANALYSIS

In the following sections a large number of fatigue data collected from the literature will be analyzed using the fatigue life diagram concept. Tension-tension cyclic loading of unidirectional composites along the fiber direction will be considered first to illustrate the use of the fatigue life diagrams. Effects of constituent properties on the fatigue behavior will thereby be clarified. A treatment of fiber architecture will be conducted by first considering the fatigue behavior under loading inclined to the fiber axis. Various laminate configurations—angle-ply, cross-ply, and combinations of these—will then be treated for further appreciation of the fiber architecture effects. The class of woven fabric composites, which is of particular interest in repair and joining of automotive components, will be considered at the end of this section.

3.3.1 Unidirectional Composites

3.3.1.1 Loading parallel to fibers

To illustrate the significance of fiber stiffness (and the resulting failure strain) on fatigue behavior, data for a glass-epoxy are shown in Fig. 3.7. Note first that fatigue lives for composites of three different volume fractions fall within the same scatterband, while three different and separate scatterbands result when the usual stress-life plots are made (Dharan, 1975). The fatigue limit of neat resin was found by Dharan (1975) to be at 0.6% strain, which is the value set in the fatigue life diagram. Remarkably different behavior is displayed by a graphite-epoxy composite whose strain to failure is only about 0.5%. Assuming that the fatigue limit of epoxy is at least 0.6% strain, the fatigue life diagram takes the shape shown in Fig. 3.8. The sloping scatterband of progressive matrix and interfacial damage disappears, as the fatigue limit of the resin becomes unreachable. Thus, a logical interpretation of the fatigue damage tolerance of ultra-high modulus graphite fiber composites emerges.
Figure 3.9 shows the fatigue life diagram of a high modulus graphite-epoxy composite. The horizontal scatterband (limited by 5% and 95% failure probability levels) is unusually wide here, presumably due to poor quality of fibers and/or composite, and the fatigue limit is once again set at 0.6% for epoxy. The apparent fatigue damage tolerance may now be interpreted differently from the behavior displayed by data in Fig. 3.8.

Data for a lower modulus graphite-epoxy composite are shown plotted in the fatigue life diagram, Fig. 3.10. Note here that the sloping scatterband is further out to the right than that for glass-epoxy composites (Fig. 3.7). This is due to more effective fiber-bridging action by graphite fibers than is possible by the less stiff glass fibers.

ORNL-DWG 95-2738 ETD

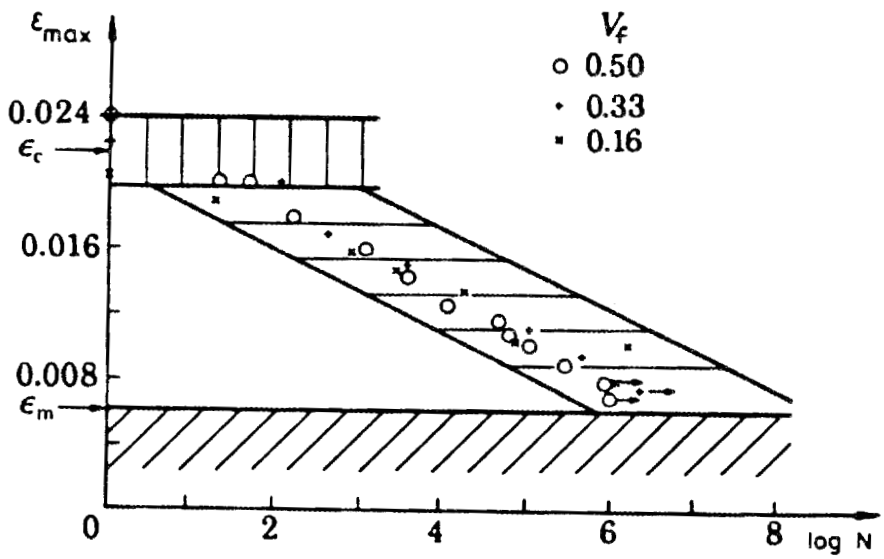

Fig. 3.7. Fatigue life diagram of glass-epoxy under loading parallel to fibers; data from Dharan, 1975. *Source*: Reprinted from R. Talreja, *Fatigue of Composite Materials*, Chap. 2 (Fig. 5). ©Technomic Publishing Company, Inc., 1987.

ORNL-DWG 95-2739 ETD

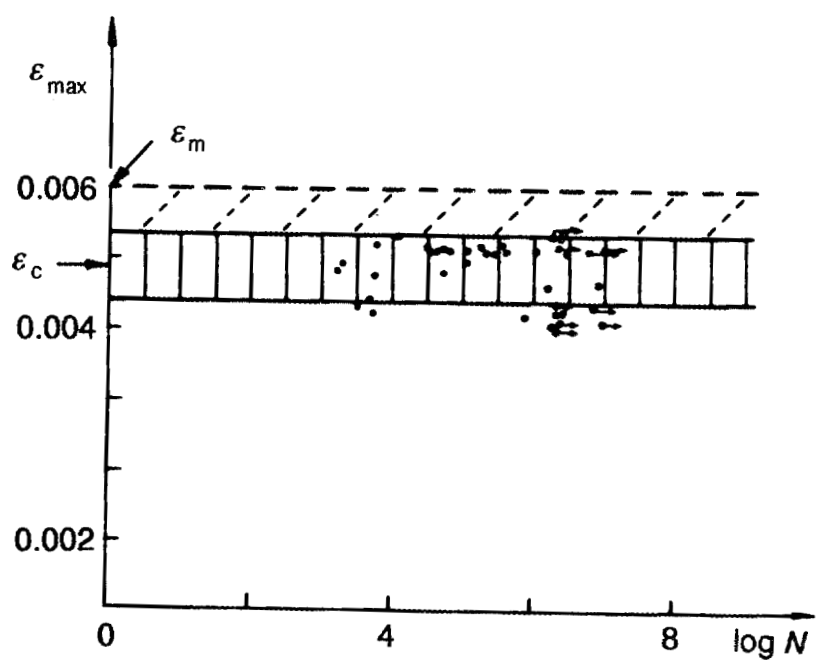

Fig. 3.8. Fatigue life diagram of ultra-high modulus graphite-epoxy under loading parallel to fibers; data from Sturgeon, 1973. *Source*: Reprinted from R. Talreja, *Fatigue of Composite Materials*, Chap. 2 (Fig. 6). ©Technomic Publishing Company, Inc., 1987.

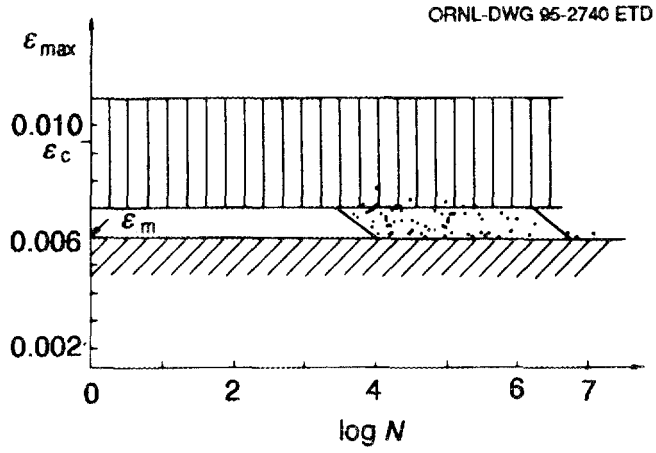

Fig. 3.9. Fatigue life diagram of high modulus graphite-epoxy under loading parallel to fibers; data from Awerbuch and Hahn, 1977. *Source*: Reprinted from R. Talreja, *Fatigue of Composite Materials*, Chap. 2 (Fig. 7). ©Technomic Publishing Company, Inc., 1987.

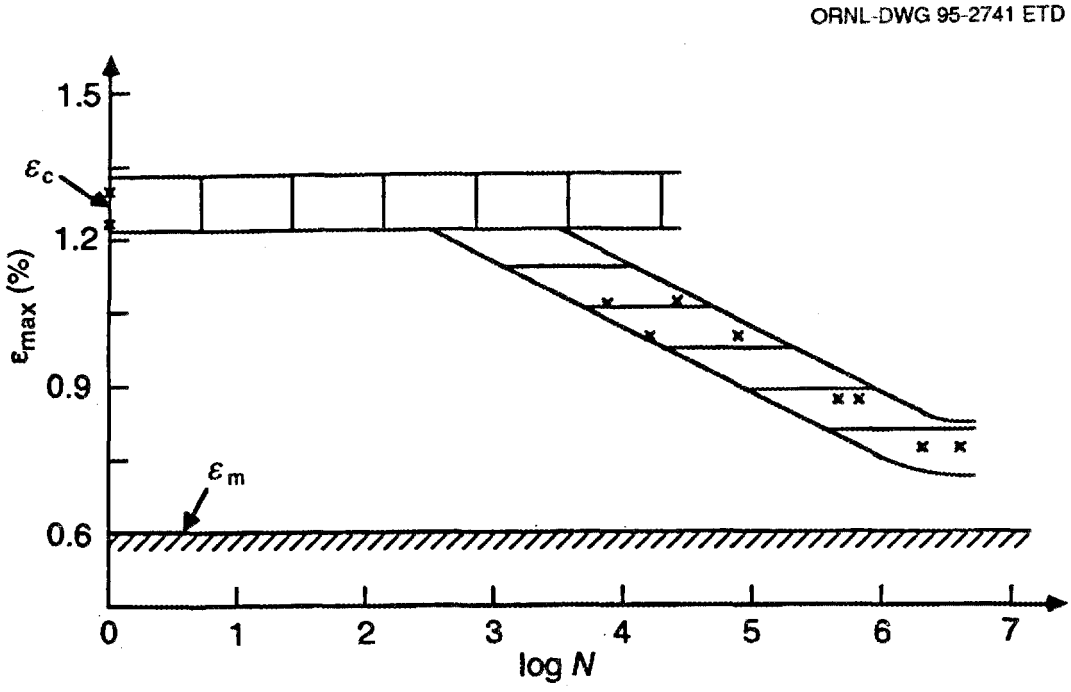

Fig. 3.10. Fatigue life diagram of lower modulus graphite-epoxy under loading parallel to fibers; data from Curtis, 1987. *Source*: Reprinted with permission of Elsevier Science, Inc.

3.3.1.2 Loading inclined to fibers

When loading is not parallel to fibers the fiber/matrix interface is subjected to normal and shear stresses. The interfacial region (interphase) initiates cracks under these stresses that then grow on repeated load application aided by irreversible dissipative processes at crack fronts. The mixed-mode crack growth in interfacial regions becomes the primary progressive fatigue damage mechanism.

The role of fibers under loading inclined to fibers is only significant for small inclination angles (probably <5°). As the inclination angle increases, the normal stress in fibers falls rapidly. At the same

time, normal and shear stresses in the interfacial region increase. The opening-mode contribution to the mixed-mode crack growth also increases with increasing inclination angle. Since the crack growth resistance is expectedly less for opening-mode growth, the threshold strain for crack growth will decrease with increasing inclination angle. Consequently, the fatigue limit will decrease as the inclination angle increases.

The above-mentioned considerations are reflected in the schematic fatigue life diagram, Fig. 3.11. The fatigue life diagram for inclination angle $\theta = 0°$ (i.e., for loading parallel to fibers) is shown in dotted lines as reference. For the inclination angle of more than a few degrees, where fiber failure ceases to be a governing mechanism, the sloping scatterband starts at the static failure strain and ends at the fatigue limit. The horizontal scatterband of fiber failure is lost, and consequently, the mechanism for delaying the progressive damage is also not effective. In the limiting condition of inclination angle, $\theta = 90°$, the opening-mode crack growth, described as transverse fiber debonding, is the predominant mechanism of damage.

ORNL-DWG 95-2742ETD

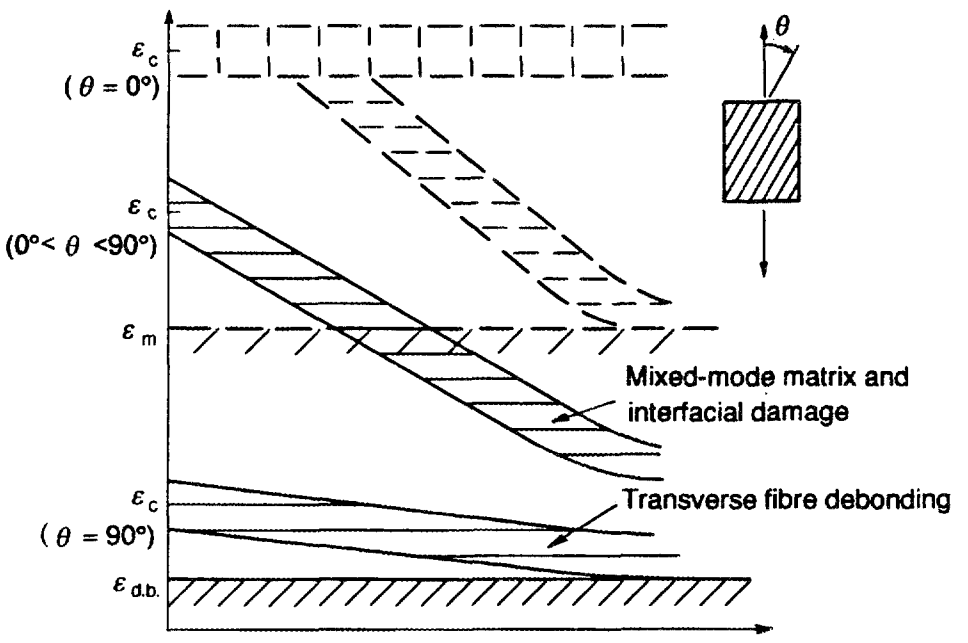

Fig. 3.11. Fatigue life diagram for unidirectional composites under loading inclined to fibers. Dotted-line diagram is for loading parallel to fibers. *Source*: Reprinted with permission of VCH Publishers, Inc.

Test data for a glass-epoxy unidirectional composite subjected to tension-tension fatigue at various inclination angles have been reported by Hashin and Rotem (1973). Their data, reported in terms of the maximum stress, have been replotted with maximum first-cycle strain in Fig. 3.12. The lines drawn through the data points have been started at the static failure strain. The fatigue limit of epoxy, reported by Dharan (1975), is shown as a reference fatigue limit for $\theta = 0°$. The fatigue limit for transverse fiber debonding was reported by Owen and Rose (1970) for various composites of reinforced polyester to be at 0.12% strain. The data for glass-epoxy shown in Fig. 3.12 suggest that this fatigue limit is approximately at the same value.

In Fig. 3.13 the strains at fatigue limits for various inclination angles are plotted. The strain values are taken from the fatigue life diagrams (Fig. 3.12). A smooth curve drawn through the points is made to pass through the reference values at the two extremes, that is, $\theta = 0°$ and $\theta = 90°$, 0.6% and 0.12%, respectively.

ORNL-DWG 95-2743 ETD

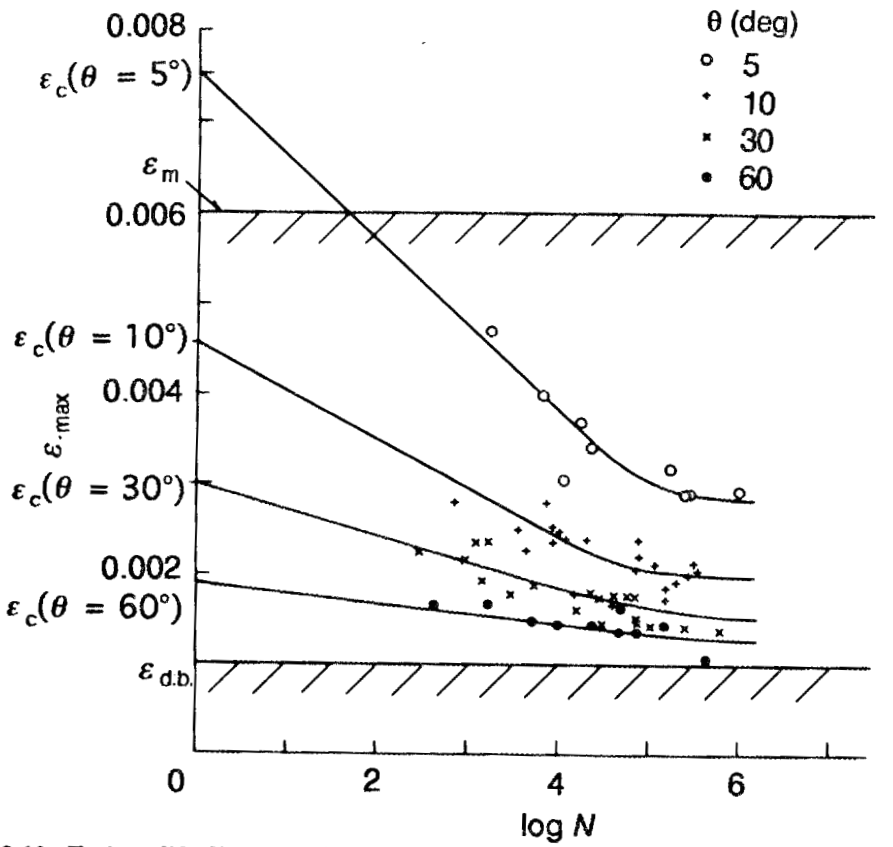

Fig. 3.12. Fatigue life diagram of unidirectional glass-epoxy under loading inclined to fibers; data from Hashin and Rotem, 1973. *Source*: Reprinted from R. Talreja, *Fatigue of Composite Materials*, Chap. 2 (Fig. 11). ©Technomic Publishing Company, Inc., 1987.

ORNL-DWG 95-2744 ETD

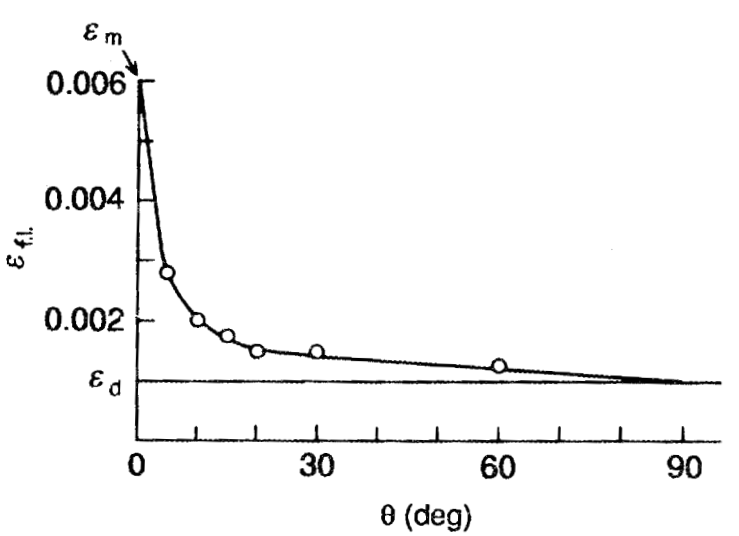

Fig. 3.13. Variation of fatigue limit with inclination angle, θ, based on data of Hashin and Rotem, 1973. *Source*: Reprinted from R. Talreja, *Fatigue of Composite Materials*, Chap. 2 (Fig. 12). ©Technomic Publishing Company, Inc., 1987.

3.3.2 Laminates

A primary motivation for constructing laminates is to achieve a desired combination and distribution of properties. As far as the elastic response is concerned, well-established plate theories exist for making assessment of the stiffness properties. A number of strength criteria have been proposed; although a single criterion has not been found to be universally applicable, sufficient basis exists for evaluation, at least a preliminary one, for selection of laminate configurations. For long-term performance of laminates, in particular under cyclic loads, the situation is far from satisfactory. A selection of laminate configuration on the basis of fatigue performance cannot yet be made. The design approach, instead, has been to select laminate configurations on the basis of stiffness and strength considerations and then to ensure that these properties do not degrade unacceptably under fatigue.

To achieve rational and efficient design procedures for laminates under fatigue the first step is to generate basic understanding of the damage development process. In the following sections this aspect will be reviewed, and the role of damage mechanisms will be interpreted with the aid of fatigue life diagrams. For the sake of clarity and systematic description, laminates of angle-ply and cross-ply types will be considered before discussing more general laminates.

3.3.2.1 Angle-ply laminates

This class of laminates [i.e. ($\pm\theta$) orientation] is widely used in filament-wound structures. It is also suited for systematic studies of the "constraint effect" in laminates. For illustration of this effect, consider the fatigue damage of unidirectional composites under loading inclined to fibers. As discussed previously, the predominant damage mechanism here is the mixed-mode cracking in the fiber/matrix interfacial region. Indeed, failure will occur when a single crack grown from a preexisting flaw reaches a critical size at which stage further growth becomes unstable (see Fig. 3.14*a*). Now consider a unidirectional ply placed in an angle-ply laminate subjected to loading along the symmetry axis (see Fig. 3.14*b*). Under the effect of the stresses in the plane of a ply, mixed-mode cracking will also occur here. However, growth of a crack here will be under constraint of the adjacent ply (or plies), and failure of the laminate will not depend on the length of the crack since the constraining ply (or plies) will locally (i.e., at crack fronts) carry the load shed by the cracking ply. If fibers in a constraining ply sustain the additional load, which acts over a distance from the crack planes (called the shear-lag distance due to the ensuing shear stress at the interface between the plies), more cracks can form further away. This multiple cracking process has been treated by Aveston, Cooper, and Kelly (1971) and since then by many others. In angle-ply laminates loaded along a symmetry axis, the multiple cracking process takes place in plies of both orientations since the plies of one orientation apply constraint to the plies of the other orientation and simultaneously crack under the constraint of plies of that orientation.

Under cyclic tensile loads of a constant amplitude, the multiple cracking process in an angle-ply laminate progresses and causes an increase of the crack number density. If no other damage mechanism is initiated, the multiple intraply cracking process will stop when saturation spacings between cracks in plies of both orientations have been reached. However, the intraply crack fronts can locally debond the ply interfaces if the debond energy is exceeded by the local strain energy release rate. The delaminations thus caused (see Fig. 3.14) can grow under cyclic loads. The stress states in plies in the delamination regions will then change and may cause fiber failures and thereby failure of the laminate. The delaminations can also merge together by growth and cause laminate failure by separating plies from each other sufficiently such that linkage of intralaminar cracks throughout the thickness is achieved.

The process of damage in angle-ply laminates has not been quantitatively analyzed for predicting fatigue life. It can, however, be appreciated, from the description of the damage process given above, that the constraint effect (determined by ply thickness, orientation, and stiffness) governs initiation, progression, and eventual saturation of intraply cracking. The associated local delamination process is also affected by the ply constraint since the surface displacements of the intraply cracks are subject to this constraint. For a given ply material and stacking sequence, the constraint effect can be made to vary by varying the off-axis angle of angle-ply laminates. Fatigue life data for angle-ply laminates of glass-epoxy with the off-axis angle (denoted by θ in Fig. 3.14) of various values between 30° and 60° were reported by Rotem and

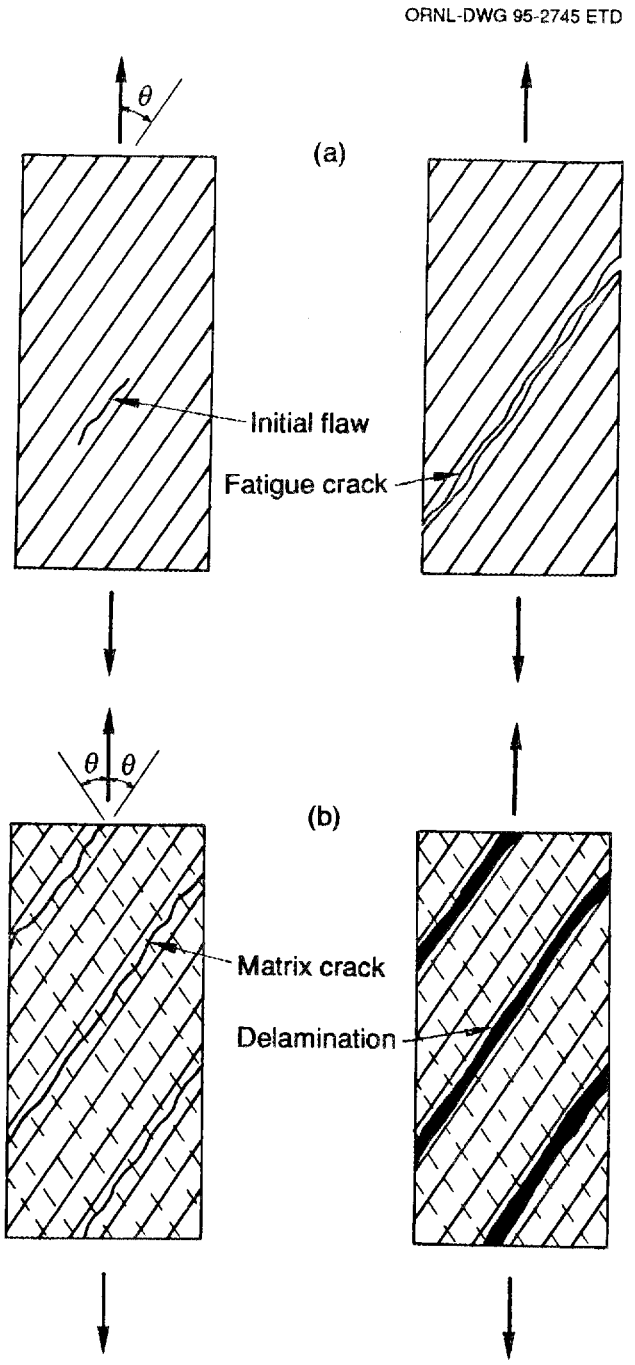

Fig. 3.14. Comparison of fatigue damage mechanisms in unidirectional and angle-ply laminates: (*a*) cracking from initial flaw in unidirectional ply under loading inclined to fibers and (*b*) multiple matrix cracking in one ply of angle-ply laminate under constraint of adjacent ply of opposite orientation. The intraply cracks cause delaminations along crack fronts. *Source*: Reprinted with permission of VCH Publishers, Inc.

Hashin (1976). The fatigue limits taken from their data have been plotted as strains (by dividing their stress by their reported elastic moduli) and are shown in Fig. 3.15. Also shown in the figure are fatigue limit data, connected by a dotted line, for unidirectional composites of the same material under loading inclined to the fibers. Comparison of the two sets of data gives a good illustration of the constraint effect discussed previously. A significant improvement in the fatigue performance due to the constraint effect (or simply the fiber architecture) is thus displayed. (The nature of the variation of the fatigue limit of angle-ply laminates of glass-epoxy, shown in Fig. 3.15, has been found to be slightly different by a recent study, yet to be published. The improvement over unidirectional composites remains at about the same magnitude).

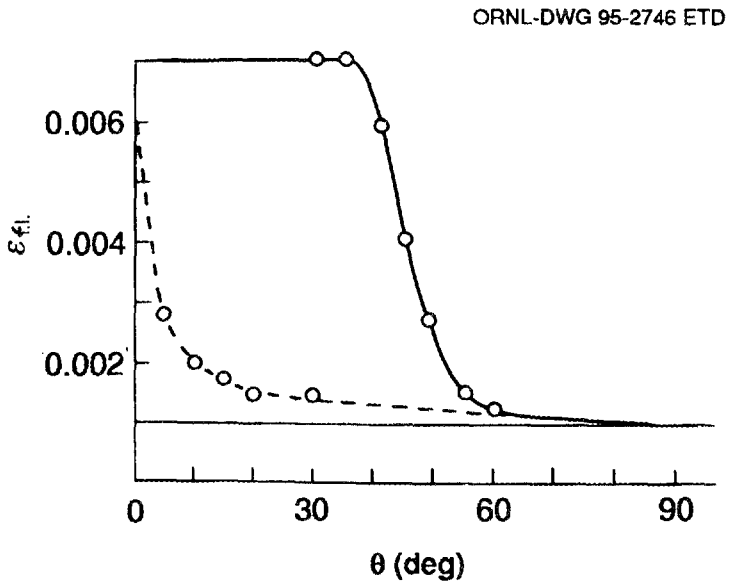

Fig. 3.15. Variation of fatigue limit of angle-ply laminate of glass-epoxy. Fatigue limits are taken from data reported by Rotem and Hashin, 1976. The dotted line reproduces fatigue limit variation for unidirectional composites (Fig. 3.12). *Source*: Reprinted from R. Talreja, *Fatigue of Composite Materials*, Chap. 2 (Fig. 13). ©Technomic Publishing Company, Inc., 1987.

3.3.2.2 Cross-ply laminates

This class of laminates [i.e. (0/90) orientation], although of less practical application than the angle-ply laminates, has been the subject of extensive analytical, numerical and experimental studies. The reason is that the multiple transverse cracking in these laminates is constrained by longitudinal plies that remain uncracked in most cases on loading in the longitudinal direction, while in angle-ply laminates both sets of off-axis plies crack simultaneously. Thus, the multiple transverse cracking can be studied under the constant constraint of the longitudinal plies. The constraint can, however, only be varied by varying the ratio of thickness of the two sets of plies, if the same ply material is used throughout the thickness. The studies related to the cracking behavior of cross-ply laminates have been concerned with three aspects: the initiation of cracking, also called the first-ply failure; the development (i.e., multiplication) of cracking; and the changes (reduction) of stiffness properties due to cracking. A recent state-of-the-art review of this subject is given in Han and Hahn (1989). Most studies reviewed there have treated monotonic tensile stressing of cross-ply laminates along longitudinal plies.

A thorough study of tensile fatigue of cross-ply laminates of graphite-epoxy has been reported by Jamison et al. (1984). The evolution of fatigue damage was described by separating it into three stages, the reflection of which was shown by the modulus reduction curve in Fig. 3.16, where the three stages are marked as I, II, and III. Stage I consists of transverse crack formation that progresses with the cycles

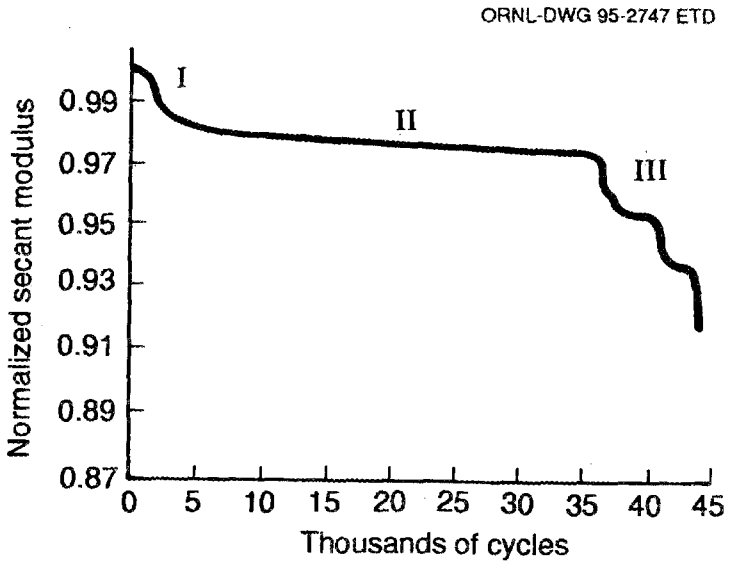

Fig. 3.16. Development of damage in $(0, 90_2)_s$ laminate of graphite-epoxy reflected as Stages I, II, and III in modulus reduction curve. *Source*: Jamison et al., 1984. Reprinted with permission of American Society of Testing and Materials.

applied until a fairly constant spacing between cracks is attained. Figure 3.17 shows the transverse crack density with cycles and the associated reduction in the longitudinal Young's modulus of the laminate. Damage in Stage II is exemplified by an X-ray radiograph shown in Fig. 3.18. The horizontal lines are the transverse cracks in 90° plies, and the vertical lines represent longitudinal cracks between fibers in 0° plies. These cracks initiate in Stage I but are fewer in number and shorter in length. The initiation of these cracks is attributed to the tensile stress normal to fibers resulting from the difference of the Poisson's ratio in the two ply directions. Subsequent to the appearance of the transverse and longitudinal cracks, delaminations of

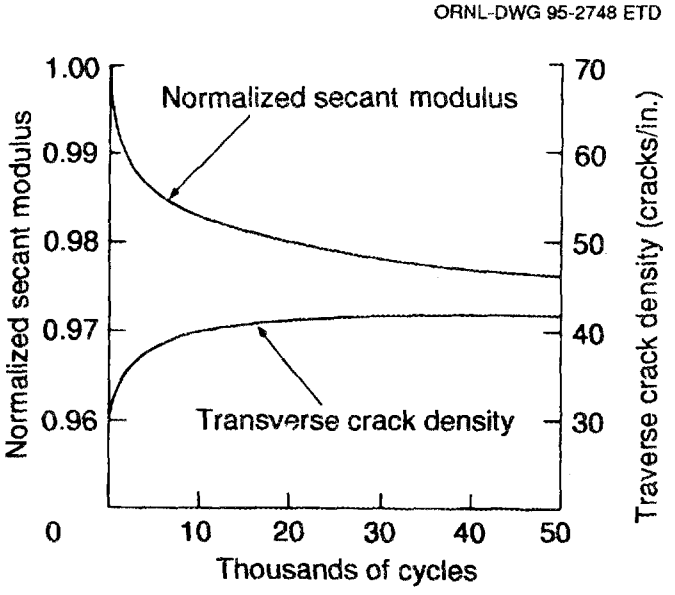

Fig. 3.17. Development of transverse crack density and modulus under fatigue of $(0, 90_2)_s$ graphite-epoxy laminate. *Source*: Jamison et al., 1984. Reprinted with permission of American Society of Testing and Materials.

ORNL-DWG 95-2749 ETD

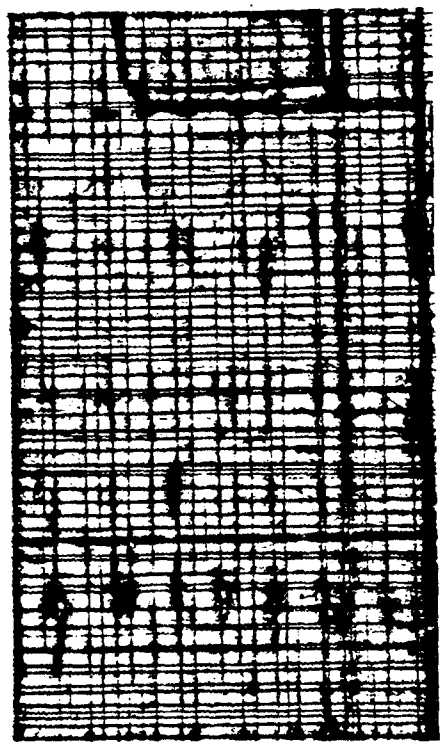

Fig. 3.18. X-ray radiograph showing transverse cracks (horizontal lines), longitudinal cracks (vertical lines), and local delaminations (shadowlike zones) in $(0, 90_2)_s$ graphite-epoxy laminate under fatigue, Stage II. *Source*: Jamison et al., 1984. Reprinted with permission of American Society of Testing and Materials.

roughly elliptical shape were found located around the crossover points of the two sets of cracks. These delaminations appear as shadowlike regions in the X-ray radiographs (e.g., Fig. 3.18). By scanning electron microscopy of sections cut at various places along a delamination it was found that a delamination was formed by diversion of a longitudinal crack into the interlaminar plane. Stage III of damage was found to be dominated by growth and coalescence of the delaminations and fiber failures in the delaminated regions. The delamination growth was primarily in the longitudinal direction. The coalescence of such delaminations formed strips of width equal to the spacing between adjacent longitudinal cracks. Failure of such strips by fiber breakage in them induced the laminate failure.

It may be argued that if the maximum strain attained in the first application of a tensile load on a given cross-ply laminate does not exceed the threshold strain for multiple transverse cracking, subsequent application of the same load will not cause fatigue failure (in, e.g., 10^6 cycles). Thus, the strain to onset of multiple cracking may be taken as a good estimate of the fatigue limit. The static (or one cycle) failure limit is given by the fiber failure strain, which is also the composite failure strain. A fatigue life diagram of a cross-ply laminate will thus have these two strains (i.e., strain to multiple transverse cracking and strain to fiber failure) as the two limits.

Figure 3.19 shows an example of the fatigue life behavior of a cross-ply laminate. The data taken from Grimes (1977) are interpreted on the basis of the fatigue life diagram concept. The fatigue limit is placed at a strain of 0.43%, which was the strain at which the plot of longitudinal stress vs transverse strain showed a proportionality limit indicating onset of (multiple) transverse cracking. A scatterband is placed horizontally about the static failure strain to indicate the presence of the nonprogressive fiber failure

ORNL-DWG 95-2750 ETD

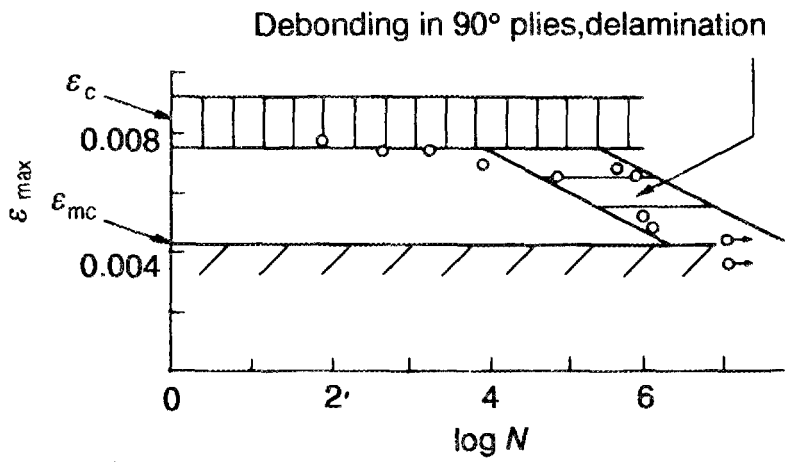

Fig. 3.19. Fatigue life diagram for cross-ply laminate of graphite-epoxy; data from Grimes, 1977. *Source*: Reprinted from R. Talreja, *Fatigue of Composite Materials*, Chap. 2 (Fig. 14). ©Technomic Publishing Company, Inc., 1987.

mechanism discussed above in connection with tensile fatigue of unidirectional composites under loading parallel to fibers. In a cross-ply laminate this mechanism will also exist due to the presence of the 0° plies stressed parallel to fibers.

3.3.2.3 General laminates

Numerous laminate configurations can be obtained by combining the unidirectional, angle-ply, and cross-ply arrangements. A number of these have been studied by various workers. A summary of an extensive range of investigations has been reported by Reifsnider, Henneke, Stinchcomb, and Duke (1983). Figure 3.20 shows the schematic description of the controlling damage mechanisms suggested by them for a wide class of laminates. The initial stage of damage development consists of multiple matrix cracking along fibers in plies inclined to the applied load direction. The nature of this cracking process is as that described above for angle-ply laminates and cross-ply laminates. The saturation of the intraply cracking process in individual plies has been found to lead to a cracking state that is a generic property of the given laminate and is independent of the loading amplitude or in general the path of loading. This state has been called the Characteristic Damage State (CDS) and signifies termination of the initial stage of damage development. Further damage on continued cycling occurs by local debonding of interply bonds at the fronts of the intraply cracks. This causes delamination, which grows in the interlaminar planes and leads to coalescence of adjacent delamination zones and stress enhancement in the separated plies. This enhances fiber breakage and induces instability of the damage developments leading to final failure.

The complexity of the damage development process has not yet allowed a quantitative description of the rates of the process. A pragmatic approach at present is, therefore, to search for trends in the fatigue lives induced by changes of ply orientations from a basic configuration. As an example of this consider three laminate configurations: a unidirectional; $(0, \pm 45)_s$; and $(0, \pm 45, 90)_s$ all of the same graphite-epoxy. Fatigue life data for these laminates obtained under tension-tension loading have been kindly given to the author by Dr. P. T. Curtis of the Royal Aerospace Establishment in the United Kingdom. In Fig. 3.21 the data have been plotted together on axes of the maximum strain in the first cycle and the logarithm of the number of cycles to failure. With data for a unidirectional composite in view, the fatigue life diagram has been drawn. The usual characteristic features of the diagram discussed above are present. It is of interest to see that fatigue lives for $(0, \pm 45)_s$ and $(0, \pm 45, 90)_s$ laminates fall within the lower part of the sloping scatterband of the unidirectional composite. This suggests that at relatively low strains the progressive

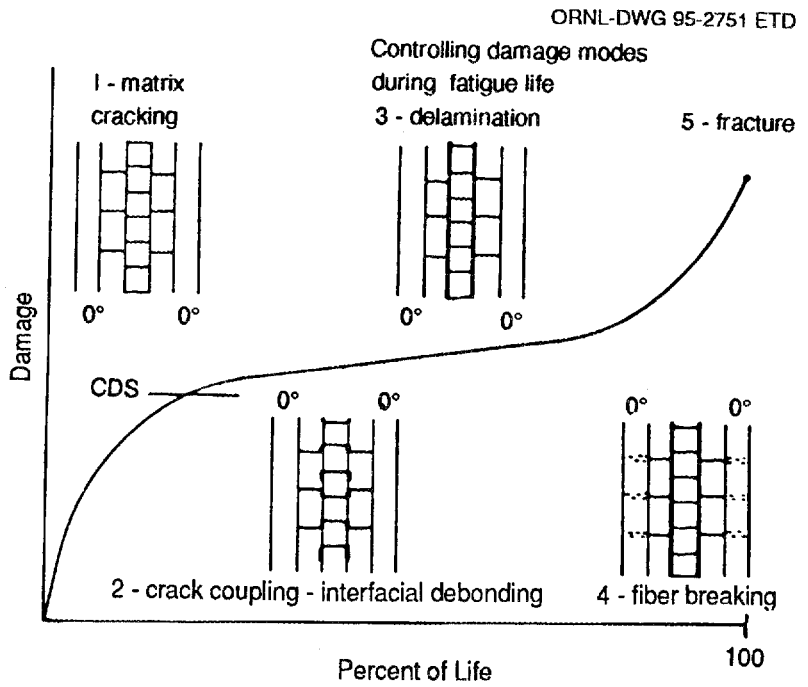

Fig. 3.20. Development of damage in composite laminates. *Source*: Reifsnider et al. (1983). Used with permission of author.

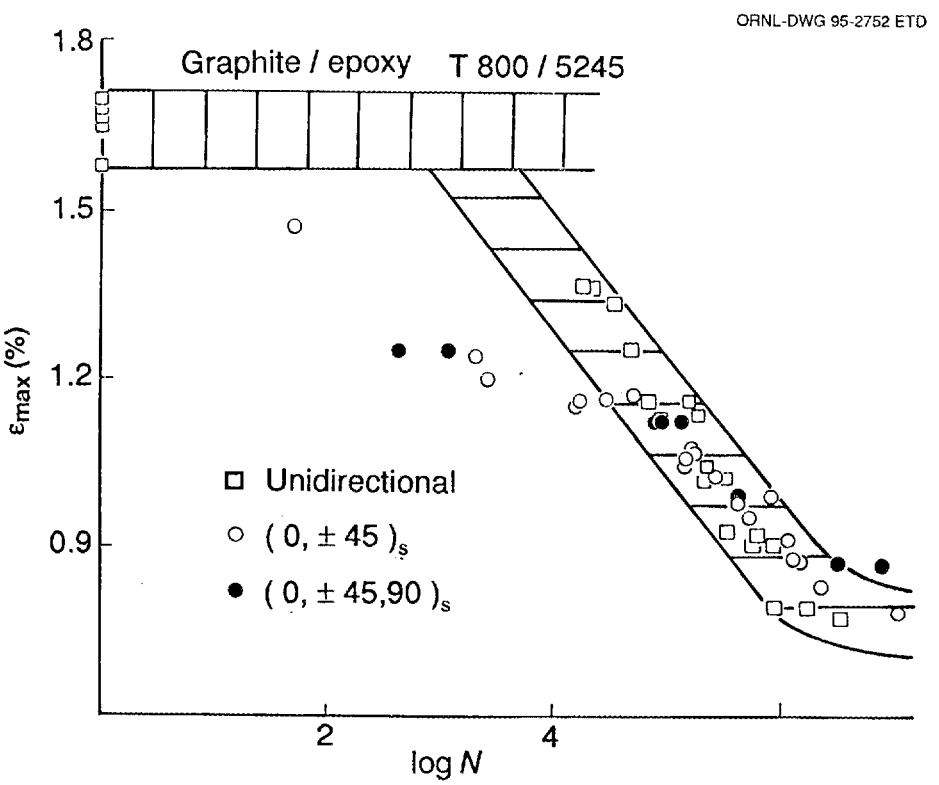

Fig. 3.21. Fatigue data of three graphite-epoxy composites (private communication from P. T. Curtis, Royal Aerospace Establishment, U.K.). The drawn fatigue life diagram is for unidirectional composite only.

damage mechanism of matrix cracking and the associated interfacial failure in unidirectional composites dominates and governs the fatigue life. At higher strains the deviation in fatigue lives of the two laminates from the sloping scatterband of the unidirectional composite may now be interpreted as due to the delamination growth in the laminates causing enhanced stresses in the 0° plies and the consequent lower fatigue lives.

3.3.3 Woven Fabric Composites

Woven fabric composites are a useful class of composites, in particular for structures with large thickness. Little work on fatigue behavior of these composites has, however, been reported. A systematic study has been conducted by Schulte, Reese, and Chou (1987), which will be summarized below.

Schulte, Reese, and Chou (1987) tested an eight-harness satin weave of graphite fibers impregnated by an epoxy resin. Laminates of this material were made by stacking the prepregs and curing them. For comparison, continuous fiber cross-ply laminates of the same material were made. Development of damage in the laminates under tension-tension fatigue was studied by conducting X-ray radiography intermittently during fatigue and by postfailure scanning electron microscopy of the interlaminar regions.

The development of damage in the initial stage showed basically the same features as have been observed in cross-ply laminates. Cracks were found to initiate in the warp (transverse to loading) direction along the fibers. On continued loading longitudinal cracks appeared between fibers in the fill direction in the undulation regions where the fill fibers cross over the warp fibers. The crack densities increased with load cycling, and a uniformly distributed pattern of orthogonal cracks appeared to develop. On further cycling, delaminations were observed confined primarily to the undulation regions. Thus a uniform distribution of delamination areas in the interlaminar planes developed. Toward the end of fatigue life fiber bundles were found to fail in the undulation regions. A progressive weakening of the laminate strength then led to final failure.

Figure 3.22 shows the Young's modulus change with fatigue life for the woven fabric composite. Data for the straight fiber cross-ply laminate are also plotted in the figure for comparison. The differences in the two systems appear beyond about 50% of fatigue life, suggesting that the delaminations at the undulating regions in the woven fabric laminate are responsible for the extra reduction of stiffness.

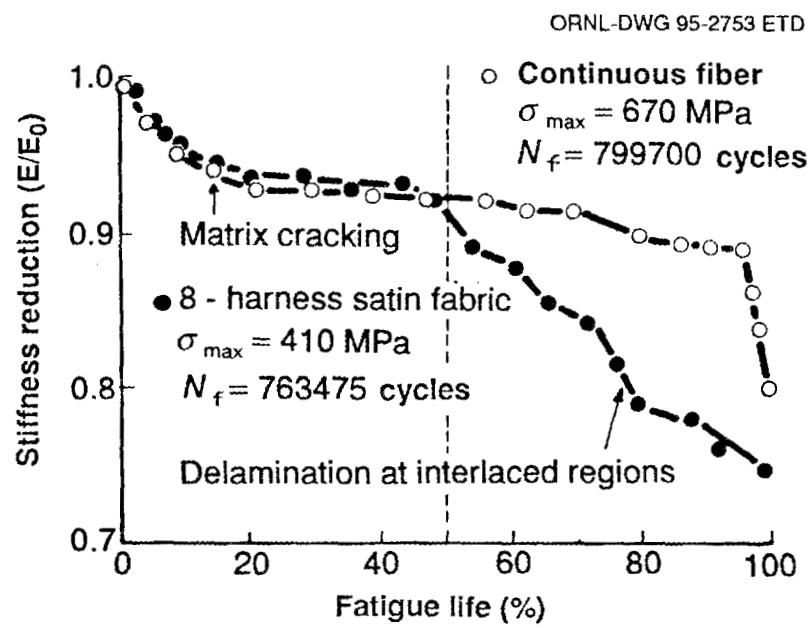

Fig. 3.22. Change in longitudinal Young's modulus of woven fabric composite and cross-ply laminate of graphite-epoxy under fatigue; data from Schulte et al., 1987. *Source*: Adapted with permission of Elsevier Science, Inc.

The fatigue limit of the woven fabric laminate was found at 0.62% strain as against the value of 0.85% for the straight fiber cross-ply laminate. Although the reasons for this difference have not been explored, it is likely that the cause lies in the reduced constraint to transverse cracking provided by the curved fibers in the woven fabric composite.

3.4 SHORT FIBER COMPOSITES

A substantial amount of work on fatigue of chopped-strand mat reinforced polyester was reported by Owen and associates from 1967 to 1979 and has been summarized by Owen (1982). The material consisted of 50-mm glass multifilament strands randomly arranged in a plane and surrounded by a polyester resin. Flat plates of the composite were made with a wet lay-up technique. Fiber strands could be observed by optical microscopy with transmitted light in thin plates. Combining this with observations of polished edges of specimens the mechanisms of debonding and resin cracking were detected. Debonding of strands from the matrix was the first mechanism observed in static as well as fatigue loading. The first group of strands to debond had fiber axes approximately normal to the applied load direction. With increased load level or number of cycles of a maximum load, debonding of strands deviating from the normal to the load axis occurred. The debond cracks extended into resin-rich areas, causing resin cracking that grew with further load cycling. Figure 3.23 shows when debonding, cracking, and separation of the specimen occurred at various stress amplitudes in a cyclic loading with zero mean stress (Owen, Smith, and Dukes, 1969). It is noted that the stress threshold below which no debonding occurs may be usable as a conservative estimate of the fatigue limit.

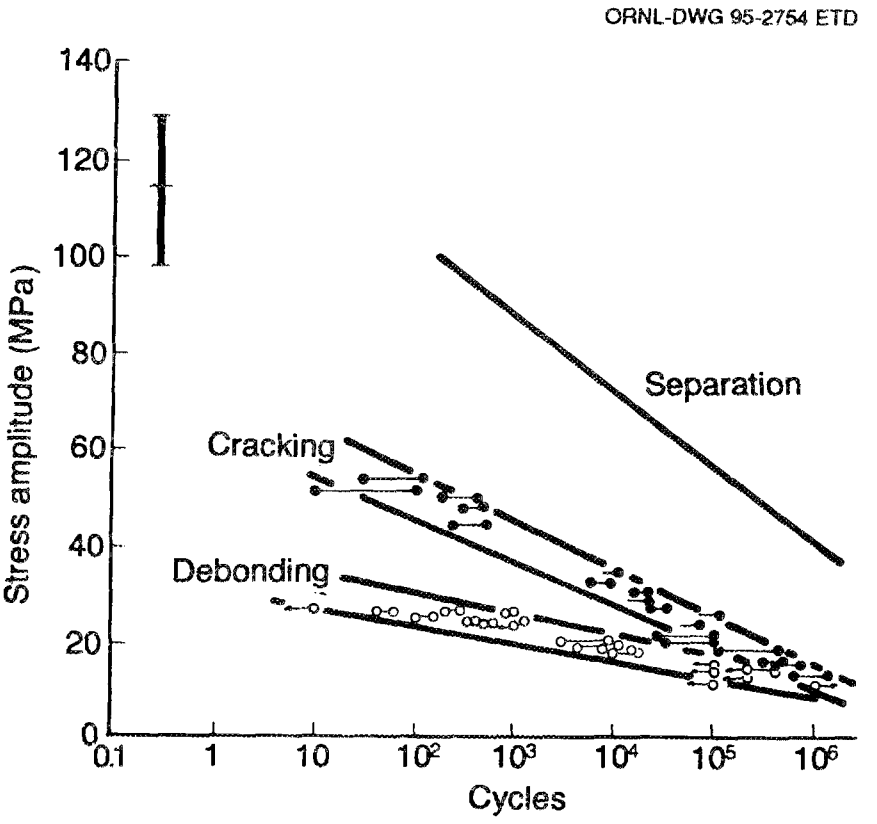

Fig. 3.23. Stress amplitude vs cycles for polyester-resin reinforced with chopped strand mats of glass indicating onset of debonding and cracking under cyclic loading with zero mean stress. *Source*: Owen et al., 1969. Used with permission of the Plastics Institute.

It was thought that improvement in the polyester resin ductility might delay the onset and development of fatigue damage in the reinforced resin. A flexibilizing agent was added to the resin to increase its strain to failure. The static strain to failure of the composite showed, however, only slight improvement (see Fig. 3.24) (Owen and Rose, 1970). The elastic modulus of the resin decreased with increasing flexibilizer content, causing the composite modulus also to decrease. However, it turned out that the strain for onset of debonding remained unaffected at about 0.3% under static loading irrespective of the flexibilizer content. More importantly, the stress-cycle plots for onset of debonding (e.g., that in Fig. 3.23) for all composites tested, with varying contents of flexibilizer in resin, collapsed in a single curve (or band) when strain was plotted instead of stress. Also, the threshold strain for debonding in fatigue, referred to as fatigue limit for transverse fiber debonding, came out to be a fairly constant value of 0.12%.

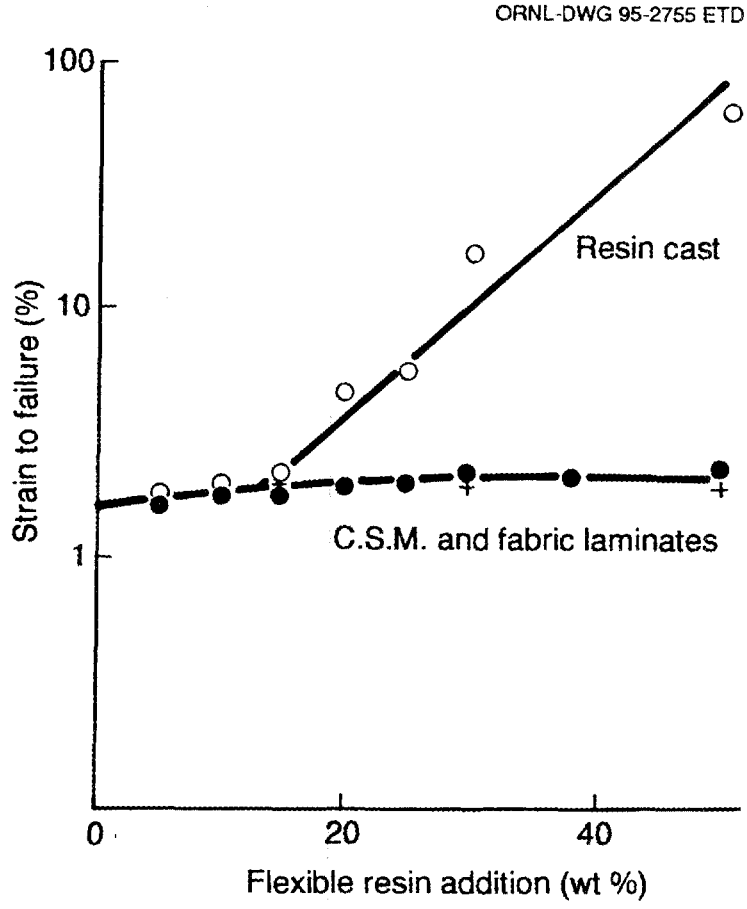

Fig. 3.24. *Strain to failure of polyester resin with polypropylene maleate adipate flexibilizer and of its composites with chopped strand mats and with fabric. Source*: Owen and Rose (1970). Reprinted with special permission of Modern Plastics, © 1970, McGraw-Hill, Inc., New York.

As far as resin cracking is concerned, Owen and Rose (1970) found that no significant delay in its occurrence was observed with the addition of flexibilizer in resin. For high contents of the flexibilizer, however, it was found that cracks appeared at the ends of strands that were aligned with the loading axis slightly before initiation of transverse fiber debonding.

An investigation of fatigue damage in SMCs, was reported by Wang, Chim, and Suemasu (1986) [see also Wang, Suemasu, and Chim (1987)]. The material investigated is denoted as SMC-R50 and consists of chopped glass fibers of length 25.4 mm, calcium carbonate filler, and polyester resin. The fibers are randomly oriented in the plane of the sheet and constitute 50% by weight of the composite. The main

difference from the material of the work described above is that the fibers are about half as long here and are more evenly spread rather than being clumped together as thick strands. The observations of damage were made by taking replicas of the specimen surface periodically during the cyclic tensile loading. The replicas were sputtered and examined in a scanning electron microscope.

Observations showed that in a resin-rich area microcracks formed nearly normal to the loading direction. In a fiber-dominant region with fibers aligned with the loading direction, cracks appeared between fibers, also normal to the loading direction, and were limited in length by the interfiber spacing. Debonding of fiber strands roughly normal to the loading axis was also seen. Typical micrographs showing the cracks are reproduced in Fig. 3.25. All crack types were grouped together for the purpose of statistical descriptions. This was achieved by a crack sampling procedure where cracks intersecting a straight line parallel to the loading axis were counted. The crack size and orientation were represented by the parameters c and θ (see Fig. 3.26). From the sampling statistics, distributions of the two parameters were derived assuming Weibull-type functions. The cumulative distribution function for crack length, denoted $F_c(c)$, and its density function $f_c(c)$ are shown in Fig. 3.27 for a fatigue loading with the maximum stress at 60% of the ultimate tensile stress. For the same loading the cumulative distribution and density functions for crack orientation, $G_\theta(\theta)$ and $g_\theta(\theta)$, respectively, are shown in Fig. 3.28. The main observations of interest concerning

ORNL-PHOTO 8091-95

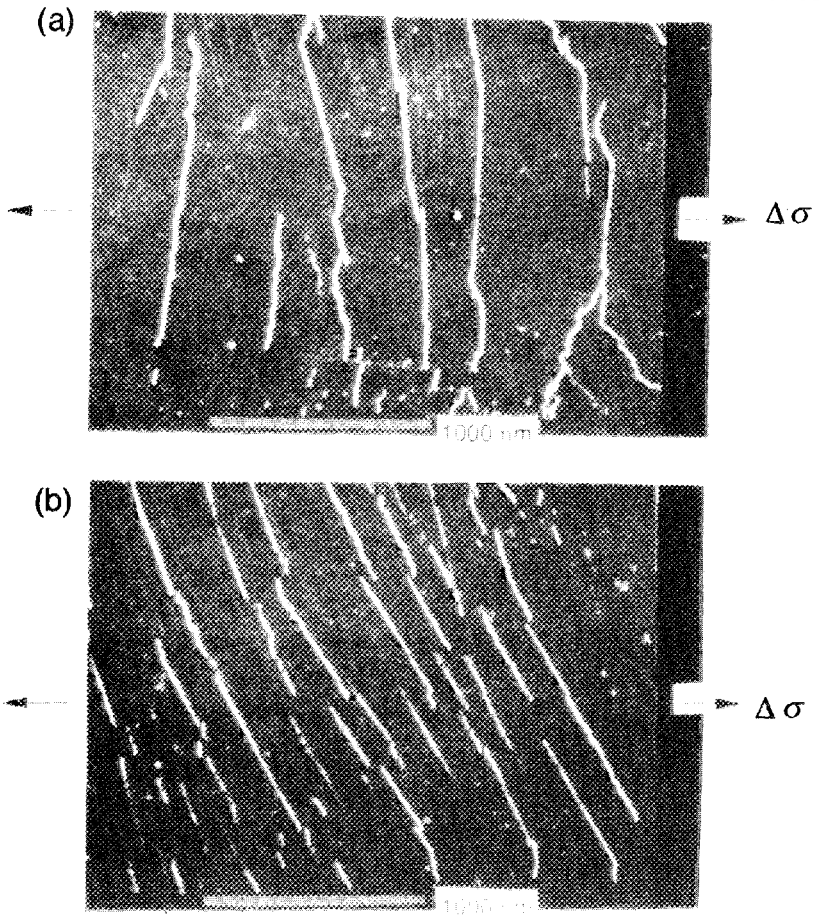

Fig. 3.25. Microcracking in short fiber reinforced SMC-R50 composite: (*a*) cracks in resin-rich region and (*b*) cracks in fiber-dominant region with fibers oriented at angle to loading direction. *Source*: Wang et al., 1987. Reprinted with permission from "Analysis of Fatigue Damage Evolution and Associated Anisotropic Elastic Property Degradation in Random Short-Fiber Composite," *J. Comp. Mats.* 21, 1084–1105 (Fig. 2). ©Technomic Publishing Company, Inc., 1987.

ORNL-DWG 95-2757 ETD

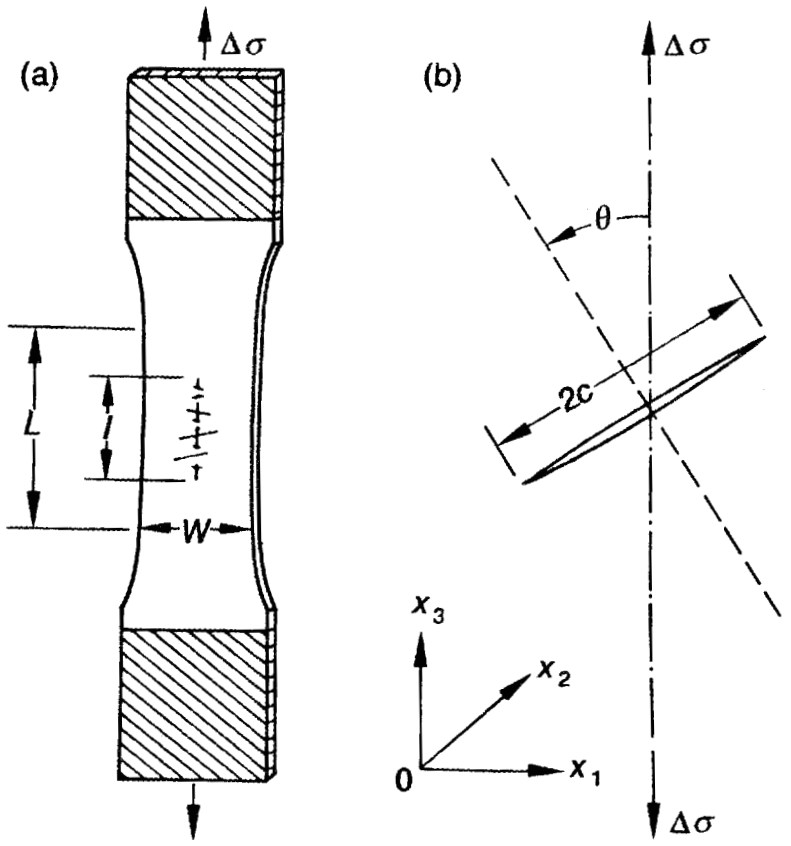

Fig. 3.26. Specimen of short fiber composite with sampling line of length l parallel to axial direction. A crack intersecting the sampling line is described by length 2c and angle θ. *Source*: Wang et al., 1987. Reprinted with permission from "Analysis of Fatigue Damage Evolution and Associated Anisotropic Elastic Property Degradation in Random Short-Fiber Composite," *J. Comp. Mats.* 21, 1084–1105 (Fig. 1). ©Technomic Publishing Company, Inc., 1987.

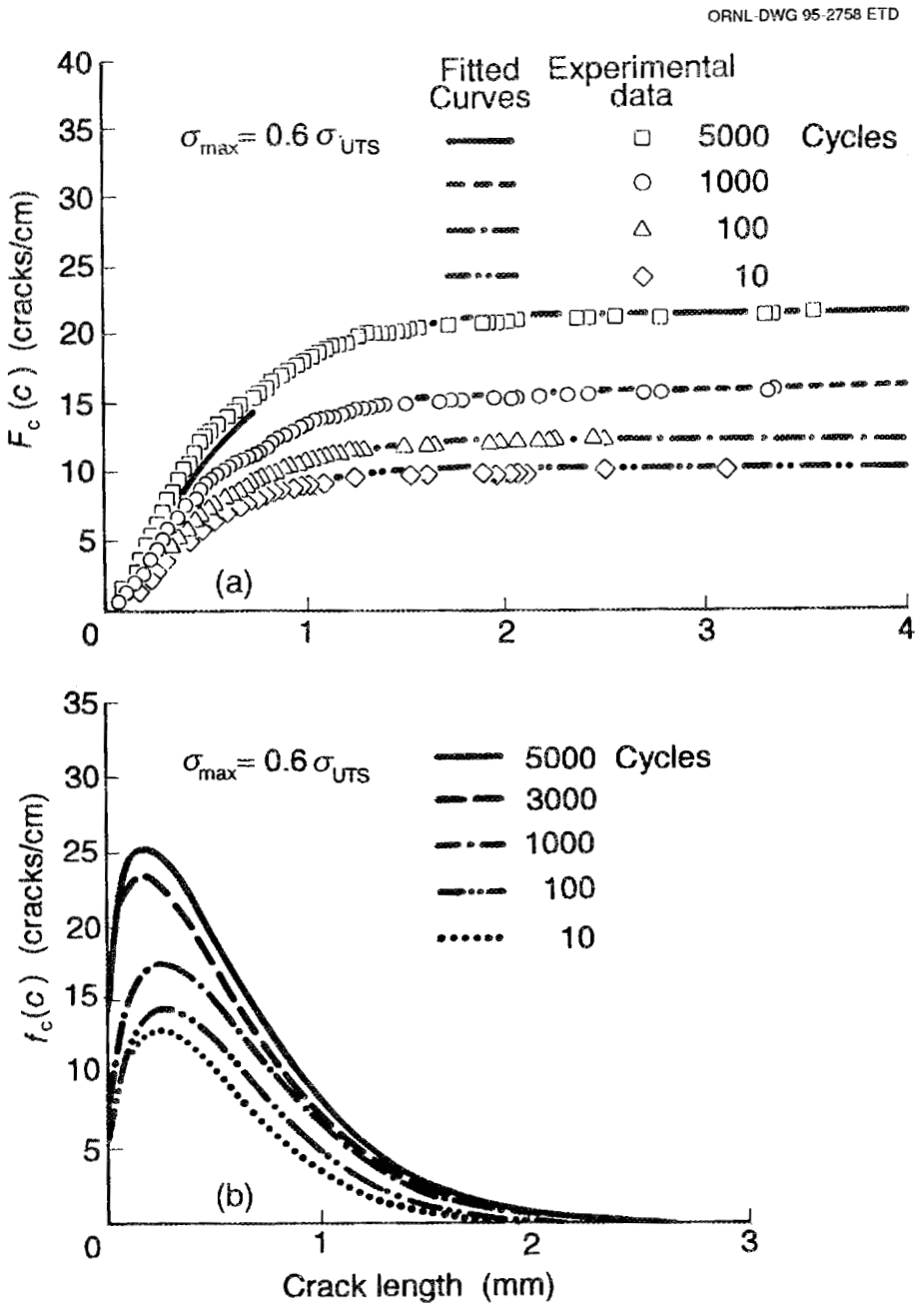

Fig. 3.27. Cumulative distribution function $F_c(c)$ and density function $f_c(c)$ of crack length at various cycles with maximum stress of 60% of ultimate tensile stress for short fiber SMC-R50 composite. *Source*: Wang et al., 1987. Reprinted with permission from "Analysis of Fatigue Damage Evolution and Associated Anisotropic Elastic Property Degradation in Random Short-Fiber Composite," *J. Comp. Mats.* 21, 1084–1105 (Figs. 4 and 5). ©Technomic Publishing Company, Inc., 1987.

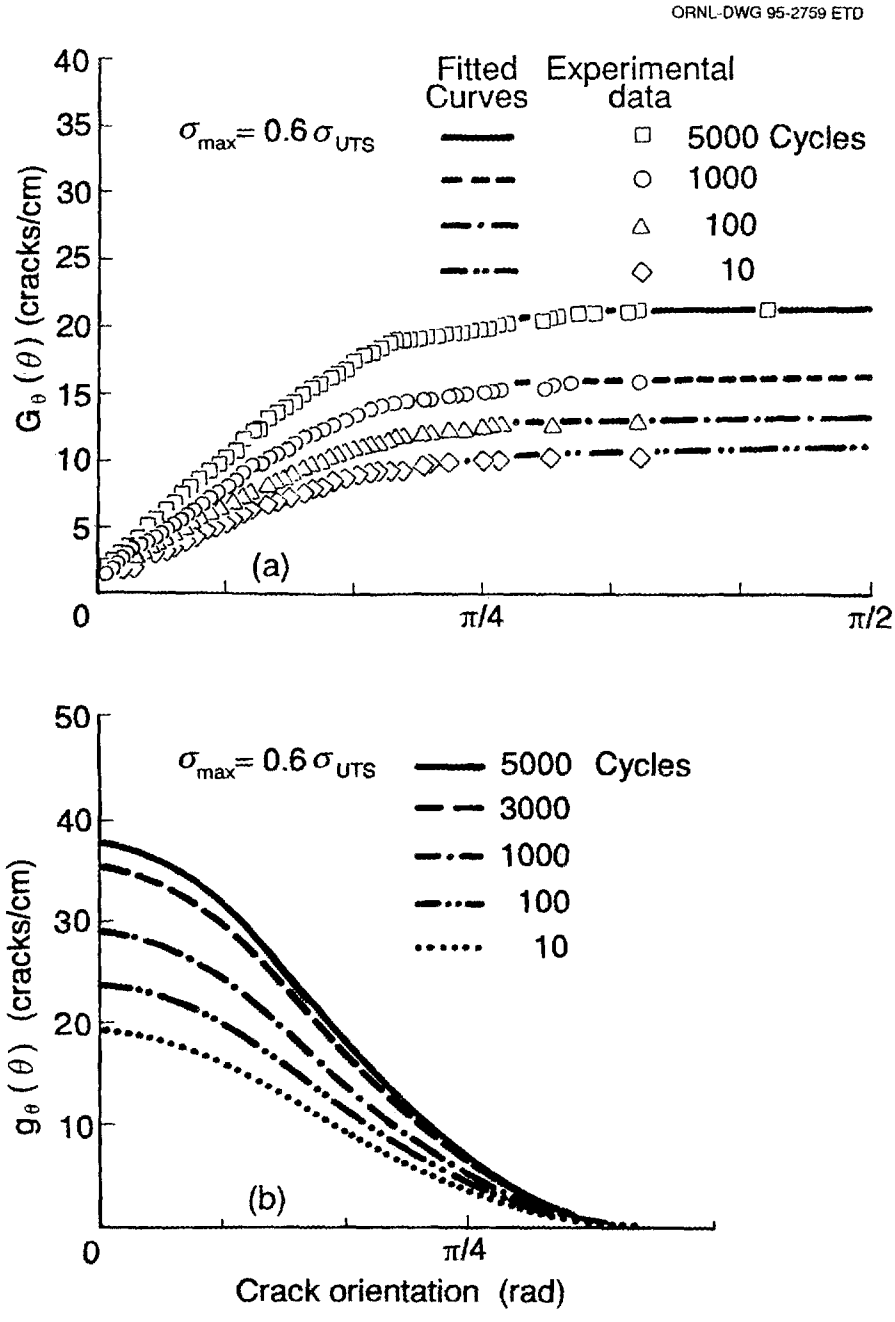

Fig. 3.28. Cumulative distribution function $G_\theta(\theta)$ and density function $g_\theta(\theta)$ of crack orientation at various cycles with maximum stress of 60% of ultimate tensile stress for short fiber SMC-R50 composite. *Source*: Wang et al., 1987. Reprinted with permission from "Analysis of Fatigue Damage Evolution and Associated Anisotropic Elastic Property Degradation in Random Short-Fiber Composite," *J. Comp. Mats.* 21, 1084–1105 (Figs. 9 and 10). ©Technomic Publishing Company, Inc., 1987.

the microcrack geometry are that most cracks remain <1 mm in length during fatigue and that their orientations are mainly within 30° of the normal to the loading direction.

The multitude of microcracks within the volume of an SMC degrade the elastic constants. Figure 3.29 shows the longitudinal Young's modulus vs the number of cycles applied. The predicted curve in the figure is calculated by a "self-consistent estimation scheme," using the measured crack statistics (Wang, Chim, and Suemasu, 1986). The preferential cracking resulting from the applied uniaxial loading leads to anisotropy in the initially isotropic SMC material. This necessitates calculation of more elastic constants than those needed to characterize the virgin state of the materials.

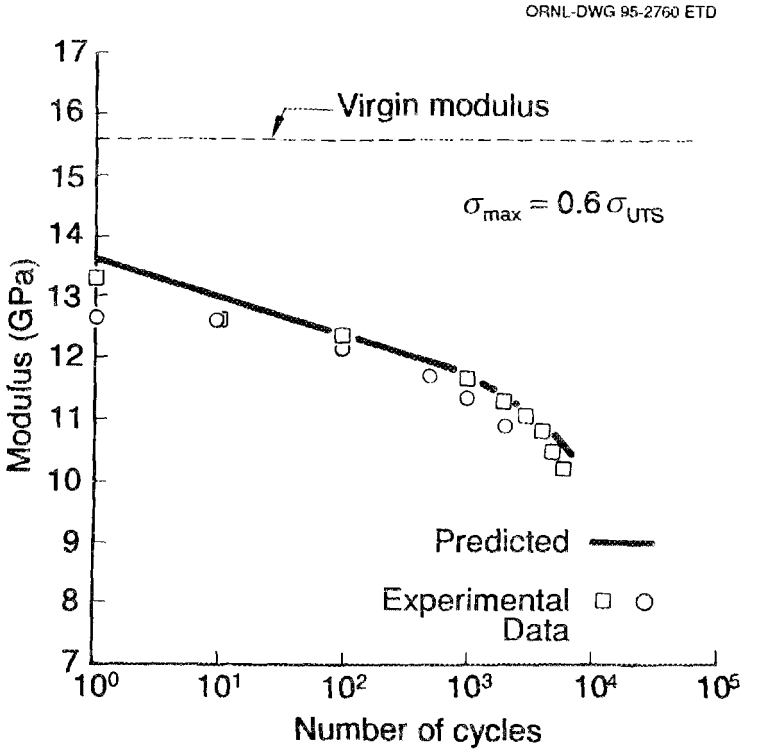

Fig. 3.29. Change in longitudinal Young's modulus of short fiber SMC-R50 composite under fatigue at maximum stress of 60% of the ultimate tensile stress. *Source*: Wang et al., 1987. Reprinted with permission from "Analysis of Fatigue Damage Evolution and Associated Anisotropic Elastic Property Degradation in Random Short-Fiber Composite," *J. Comp. Mats.* 21, 1084–1105 (Fig. 13). ©Technomic Publishing Company, Inc., 1987.

Studies related to fatigue of injection-molded reinforced thermoplastics have been reported by Mandell, Huang, and McGarry (1982) and by Mandell, McGarry, and Li (1985). These authors have studied growth of a precut crack under cyclic tensile loading. The plane of the precut crack was normal to the dominant fiber direction, which was also the direction of loading. The materials tested were commercial injection molding compounds containing 30 to 40% by weight of glass or graphite fibers. The matrix materials were engineering thermoplastics, including semicrystalline Nylon 66, amorphous polycarbonate, polysulfone, amorphous polyamide, and semicrystalline polyphenylene sulfide. The fibers were reported to seldom exceed 1 mm in length and to have typical length of 0.2 mm, giving a typical length-to-diameter aspect ratio of 20.

Optical and scanning electron microscopy were used to study the mode of crack growth; this mode was described as a fiber avoidance mode. Although differences were found from material to material, the dominant feature of the crack growth process was described as a main crack growing in a zigzag pattern that avoided cutting through fibers and instead found local paths of lower resistance along the fibers and between the fibers. Local failure zones were found ahead of the main crack tip. These zones contained

isolated crazes or isolated shear yielding. It was thought that these zones coalesce and merge into the main crack. The schematic in Fig. 3.30 depicts the fiber avoidance mode of crack growth with local failure zones ahead of the crack. The band of width (or height) h about the crack plane is suggested by the authors to be characteristic of the material microstructure and independent of the loading mode. The authors further suggest that only processes within this band govern crack growth (i.e., a plastic zonelike concept).

ORNL-DWG 95-2761 ETD

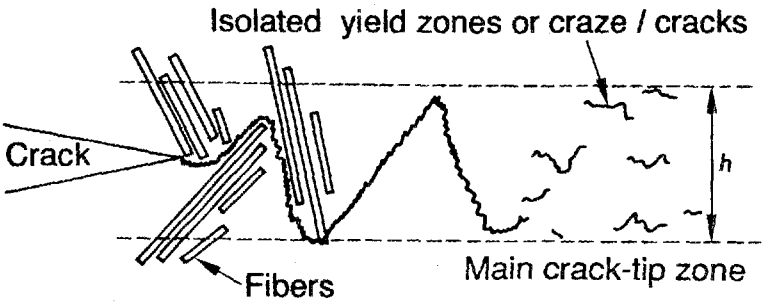

Fig. 3.30. Schematic of crack zone in fiber avoidance mode of crack growth. *Source*: Mandell et al., 1985. Reprinted with permission of American Society of Testing and Materials.

The crack growth rate is taken to be given by the Paris law:

$$\frac{da}{dN} = AK_{max}^{m} \quad , \tag{3.1}$$

where a is the crack length, N is the number of cycles, K is the stress intensity factor, and A and m are constants.

For a zigzagging crack the measurement of crack length is not simple. The zigzag pattern observed on the specimen surface does not necessarily hold through the specimen thickness. The authors give no details concerning this, but it appears that they use the projected length on the extended initial crack plane measured on the specimen surface. In any case, their crack growth data are reproduced in Figs. 3.31 and 3.32. It is noted that the crack growth exponent increases from the value of 4 for unreinforced matrix to 7 (for Nylon 66) or 8 (for polysulfone).

Assuming the Paris law to hold until the critical crack length to failure, the fatigue life can be obtained by integrating Eq. (3.1). The slope of the S-N line on a log-log scale would then be the inverse of the exponent in the Paris law. Figure 3.33 shows the S-N data for unreinforced and reinforced polysulfone with the corresponding slopes indicated. The deviation at high stresses is attributed to general yielding of the materials.

From the work of Mandell, Huang, McGarry, and Li (1982, 1985) summarized above, it may be concluded that for sufficiently small fibers a crack emanating in a resin-rich area may grow under cyclic loading, avoiding fibers in its path by zigzagging around them, until a critical size is attained beyond which further growth is unstable and failure results. The question remains as to what role the fibers play other than being in the way of a growing matrix crack and thereby slowing down its rate of growth. Based on some fracture toughness considerations, Mandell, McGarry, and Li (1985) suggest that the ultimate tensile strength (UTS) of a composite, determined by the fiber strength, geometry and volume fraction, determines also the fatigue strength. The schematic of the relationship between fatigue crack growth and fatigue life, suggested by Mandell, McGarry, and Li. (1985), is reproduced in Fig. 3.34.

The difficulties related to characterization of fatigue crack growth data in composites are illustrated by a systemic investigation on composites with spherical fillers reported by Gadkaree and Salee (1983). They studied fatigue crack growth in cantilever beam specimens of a thermoplastic Bisphenol A-terephalate/isophthalate copolyester, filled with a fly-ash filler with mean diameter of 20 μm. Standard fracture mechanics techniques of compliance calibration of crack length were used. Tests were carried out with composites containing 10, 20, 30, and 40% by weight of filler. The crack growth data for unfilled resin are

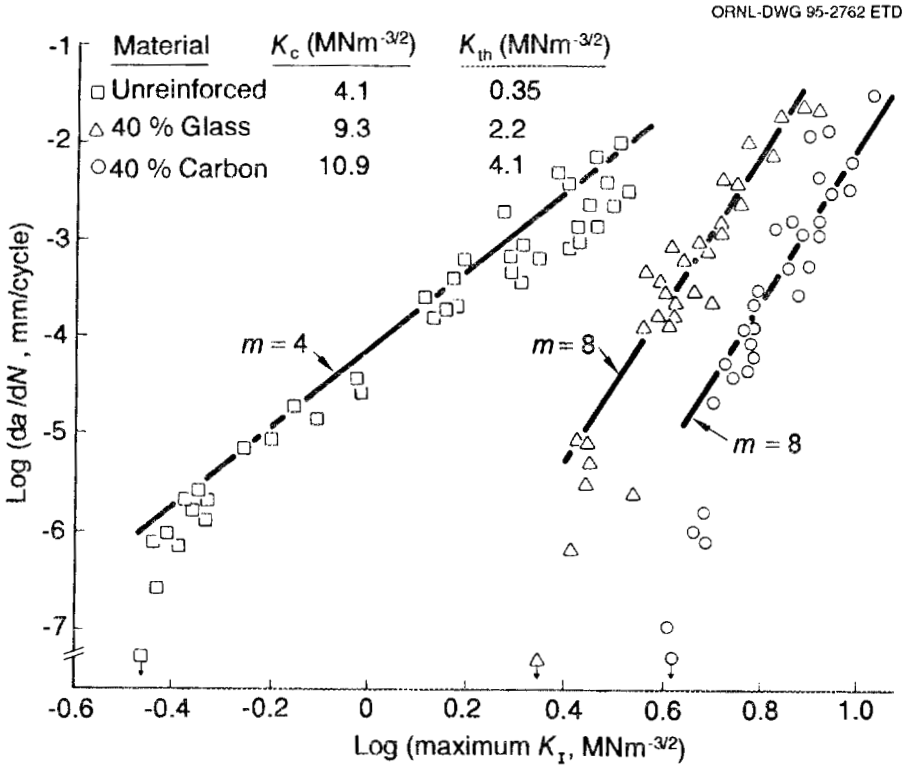

Fig. 3.31. Fatigue crack growth data for unreinforced and injection-molded fiber-reinforced polysulfone. *Source*: Mandell et al., 1985. Reprinted with permission of American Society of Testing and Materials.

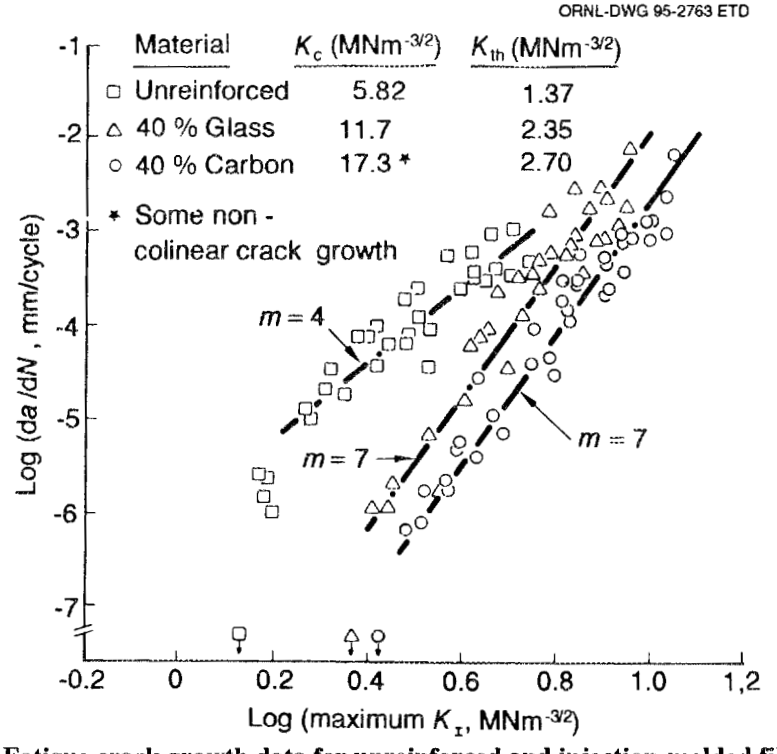

Fig. 3.32. Fatigue crack growth data for unreinforced and injection-molded fiber-reinforced nylon 66. *Source*: Mandell et al., 1985. Reprinted with permission of American Society of Testing and Materials.

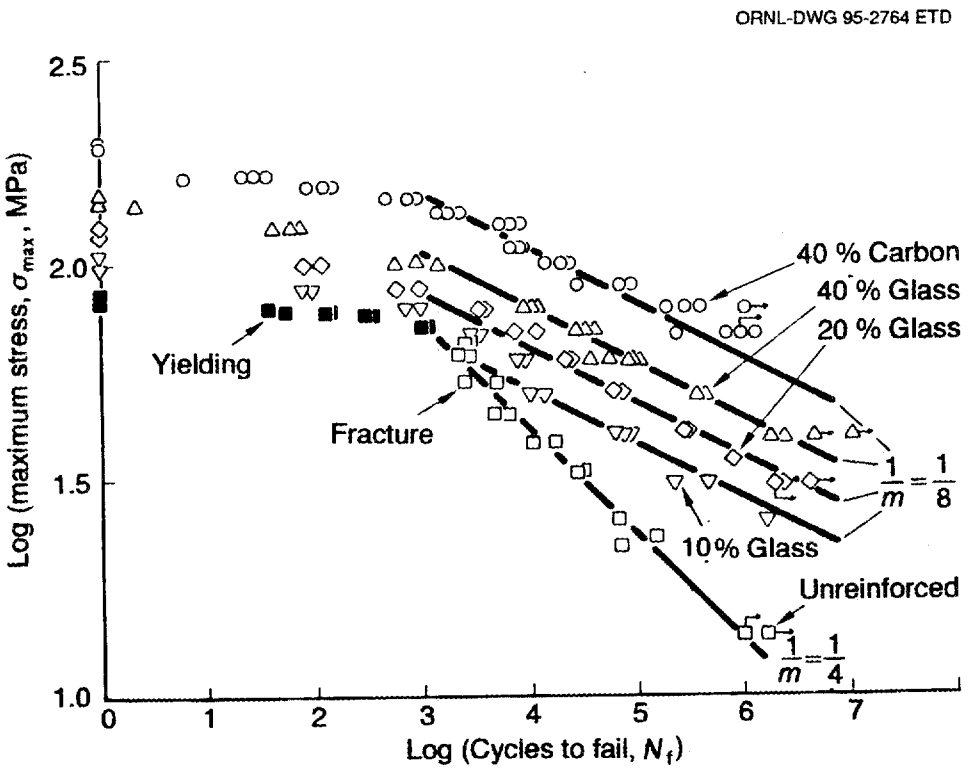

Fig. 3.33. S-N data for unnotched polysulfone in unreinforced and various injected-molded fiber-reinforced conditions. *Source*: Mandell et al., 1985. Reprinted with permission of American Society of Testing and Materials.

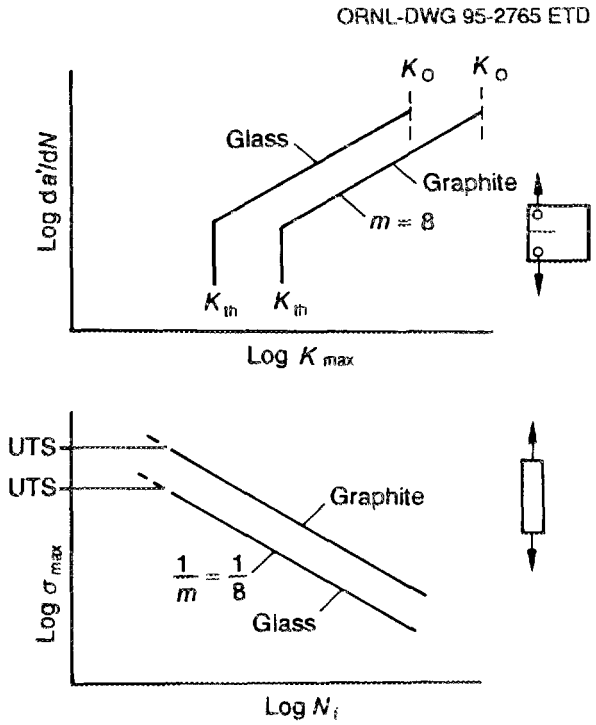

Fig. 3.34. Schematic of relationship between fatigue crack growth and S-N behavior of injection-molded fiber-reinforced composites. *Source*: Mandell et al., 1985. Reprinted with permission of American Society of Testing and Materials.

shown in Fig. 3.35, and the Paris law constants derived from best-fit are also indicated. Note that the exponent value is fairly close to the value of 4 generally reported for polymers. The data for a composite with 10% by weight of filler are shown in Fig. 3.36. The exponent here takes the value 8.78, which is not far from the values of 7 and 8 found by Mandell et al. (1985) for their injection-molded composites. The data for composites with 20 and 30% by weight of filler are shown next in Figs. 3.37 and 3.38. The data here fail to be characterized by the Paris law. Finally a comparison of the data for unfilled resin and the composite with 40% by weight of filler is shown in Fig. 3.39. Once again, the composite data show lower growth rates but cannot by described by the Paris law. Apparently, there are certain mean interfiber or interparticle spacings below which crack growth becomes erratic and cannot be described by the stress intensity parameter.

3.5 CONTINUOUS STRAND MAT COMPOSITES

CSM composites are of interest to the automotive industry because of the inexpensive processing that can be achieved with this class of materials. The reinforcement is swirled mats of glass fibers randomly arranged in a two-dimensional configuration, and sheets of the material are made by the SRIM process. This particular fiber architecture has been decided on the basis of considerations of processing. The challenge now is to determine if the performance requirements can be met and how a safe and reliable design may be achieved with these materials. For this we must understand how the mechanisms of damage operate at the microlevel and how the overall properties are affected by these mechanisms.

To appreciate the nature of the problem, consider the simpler case of swirl mat composite *without damage*. For this case, assuming that the microstructure remains stationary (i.e., the volume fraction and orientation distribution of fibers do not change), it is not clear at what length scale averaging of the microstructure should be done to arrive at the "global" properties. Recently, Stokes (1990*a,b,c,d*) in a four-part study of a 40% random glass mat polypropylene composite found that the tensile modulus varied by a factor of 2 over a 12.7-mm (1/2-in.) distance and the variation of this property over a plaque of 150 × 305 mm (6 × 12 in.) was by a factor of 3. Changing the gage length from 12.7 mm would expectedly

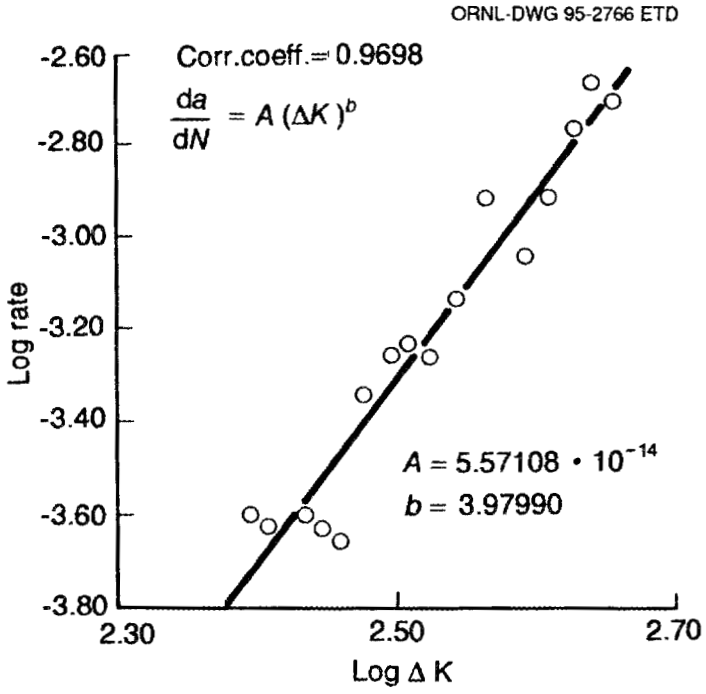

Fig. 3.35. Fatigue crack growth data for unfilled resin. ***Source*****: Gadkaree and Salee, 1983. Reprinted with permission of Society of Plastics Engineers.**

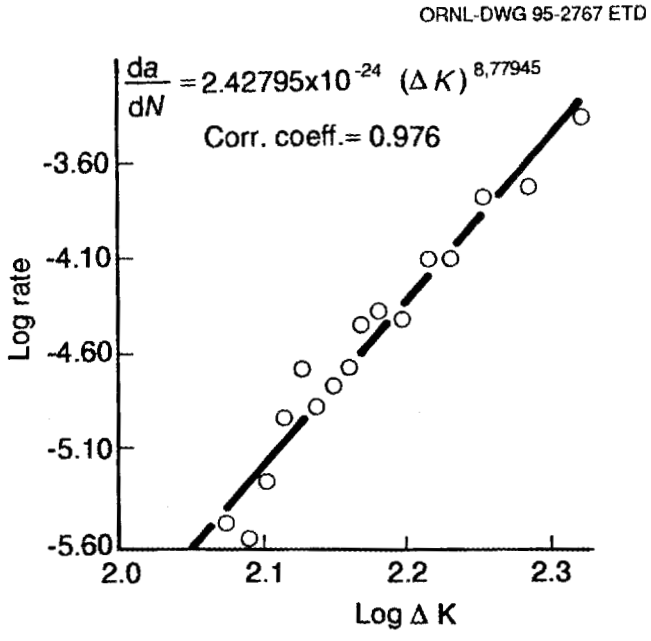

Fig. 3.36. Fatigue crack growth data for resin with 10% by weight filler. ***Source*****: Gadkaree and Salee, 1983. Reprinted with permission of Society of Plastics Engineers.**

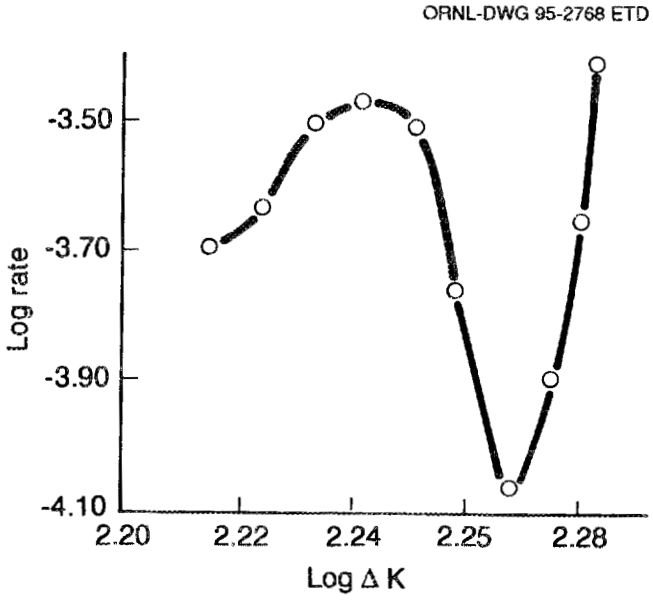

Fig. 3.37. Fatigue crack growth data for resin with 20% by weight filler. *Source*: Gadkaree and Salee, 1983. Reprinted with permission of Society of Plastics Engineers.

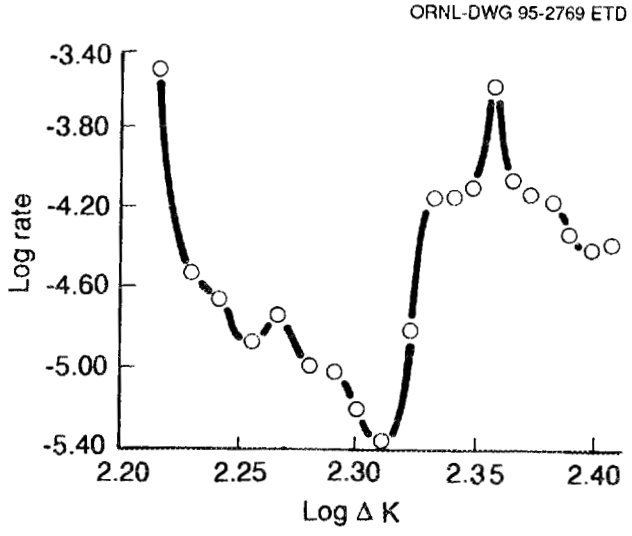

Fig. 3.38. Fatigue crack growth data for resin with 30% by weight filler. *Source*: Gadkaree and Salee, 1983. Reprinted with permission of Society of Plastics Engineers.

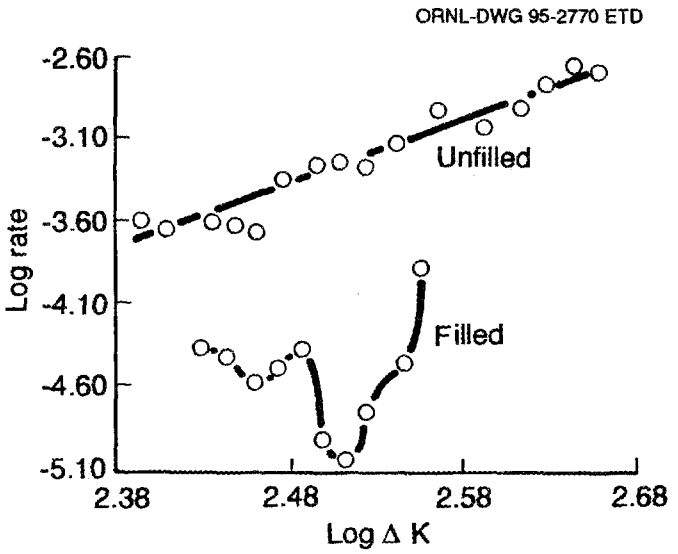

Fig. 3.39. Comparison of fatigue crack growth data for unfilled resin and for resin with 40% by weight filler. *Source*: Gadkaree and Salee, 1983. Reprinted with permission of Society of Plastics Engineers.

also affect this variation. The question is: what is the size of a representative volume element (RVE) within which the fiber distribution may be regarded as statistically homogeneous? Even harder questions arise when damage initiates and evolves under cyclic loading: what is the scale at which statistical descriptors of damage (e.g., crack density) should be described and how do local damage mechanisms affect the RVE size? Only through revisiting the basic concepts in association with systematic studies of microstructural damage—its initiation and evolution—can we hope to answer these fundamental questions. Then, the basis for developing models to describe stiffness and strength degradation in long-term loading could be provided and a methodology for life prediction developed.

3.6 MODELS FOR LIFE PREDICTION

Any approach to fatigue life prediction should be preferably based on the understanding of the governing mechanisms of fatigue failure. The conceptual framework discussed above aids in clarifying the relative roles of these mechanisms and the associated ranges of operation. To quantitatively model the development of the mechanisms, appropriate mechanics of deformation and failure must be applied. However, the fatigue life diagram can be used to guide such efforts. In the following a discussion of the possible modeling approaches will be made, keeping the fatigue life diagrams just discussed as a background.

3.6.1 Region I

As discussed, Region I of the fatigue life diagram is governed by a stochastic fiber failure process in composites where the matrix material is brittle (e.g., a nontoughened epoxy). A model for this phenomenon is difficult to construct due to insufficient understanding of the governing parameters of the stochastic process. An approach to such modeling belongs to the field of first-passage problems (see, e.g., Crandall et al., 1966). It may be recalled that this region exists primarily in uniaxial loading parallel to fibers in brittle matrix composites and vanishes for ductile matrix composites in this loading mode and for off-axis loading in all composites.

3.6.2 Region II

The underlying mechanism in this region is fiber-bridged matrix cracking. The essential parameters that should be included in any model of this mechanism are the matrix plasticity (or viscoplasticity at high

temperatures), the fiber elastic moduli and strength, the fiber/matrix interfacial characteristics related to debonding, and the residual stress state. Most previous efforts directed at modeling of the fiber-bridged matrix cracking have been motivated by the behavior of ceramic matrix composites (Marshall et al., 1985; Budiansky et al., 1986; and McCartney, 1987). There are significant differences between ceramic matrix composites and polymer matrix composites with regard to the matrix deformation, in particular the cyclic deformation and the interfacial debonding.

3.6.3 Region III

This region is of interest for design of components for applications where fatigue damage cannot be tolerated. The boundary of this region with Region II provides the fatigue limit beyond which failure can occur in what is considered to be a finite life. The strain values for the fatigue limit of the systems discussed above are in the range of 0.1 to 0.6%. These low values suggest the need to investigate the means of improving this property. This can conceivably be achieved if models are developed for the mechanism in Region III. As discussed above, this mechanism appears to be matrix cracking prevented by fibers growing to an unstable state. The fatigue limit of the matrix material would thus be the lower bound to the fatigue limit of the composite. The fiber stiffness is a possible means of improving the composite fatigue limit, as discussed above.

3.7 CONCLUDING REMARKS

This exposition has reviewed the fatigue behavior of PMCs with reinforcement in the form of long, continuous fibers in unidirectional and laminated configurations, as woven fabrics, and as short fibers. A systematic scheme based on the underlying mechanisms of damage, which takes the form of fatigue life diagrams, has been described for a consistent interpretation of the fatigue data. The effects of fiber stiffness, matrix ductility, and fiber architecture have been clarified and illustrated by interpreting fatigue data in accordance with the fatigue life diagrams. For each region of the fatigue life diagram for the basic configuration of a unidirectional composite, modeling concepts have been discussed. For short fiber composites, the fracture-mechanics-based approach to fatigue has been discussed and scrutinized, and limitations of this approach have been noted. For composites of interest in automotive applications, namely with CSMs of swirled fibers, the need to clarify the issues related to the relationship between local and global properties has been discussed. It is expected that most methods applicable to homogeneous materials and to materials with oriented microstructures such as laminates would not apply to composites with swirl mat reinforcement.

REFERENCES

Aveston, J., Cooper, G. A., and Kelly, A. 1971. *Conference on the Properties of Fibre Composites, National Physical Laboratory*, IPC Science and Technology Press, Guildford, Surrey, pp. 15–26.

Awerbuch, J., and Hahn, H. T. 1977. *Fatigue of Filamentary Composite Materials*, ASTM. STP **636**, American Society for Testing and Materials, Philadelphia, pp. 248–66.

Boller, K. H. 1969. *Composite Materials: Testing and Design*, ASTM STP **460**, American Society for Testing and Materials, Philadelphia, pp. 217–35.

Budiansky, B., Hutchinson, J. W., and Evans, A. G. 1986. *J. Mech. Phys. Solids* **34**, 167.

Crandall, S. H., Chandiramani, K. L., and Cook, R. G. 1966. *J. App. Mech.* **33**, 532.

Curtis, P. T. 1987. *Proceedings of Sixth International Conference on Composite Materials and Second European Conference on Composite Materials*, Vol. 4, Elsevier Applied Science, London and New York, p. 4-54–4.64.

Dharan, C. K. H. 1975. *Fatigue of Composite Materials*, ASTM STP **569**, American Society for Testing and Materials, Philadelphia, pp. 171–88.

Gadkaree, K. P., and Salee, G. 1983. *Polymer Composites* **4**, 19.

Grimes, G. C. 1977. *Composite Materials: Testing and Design*, ASTM STP **617**, American Society for Testing and Materials, Philadelphia, pp. 106–19.

Hahn, H. T. 1979. *Composite Materials: Testing and Design*, ASTM STP **674**, ed. S. W. Tsai, American Society for Testing and Materials, Philadelphia, pp. 383–417.

Han, Y.-M., and Hahn, H. T. 1989. *Ply Cracking in Composite Laminates*, CMTC-8937, Composite Manufacturing Technology Center, University Park, Pennsylvania.

Harris, B. 1986. *Engineering Composite Materials*, Institute of Metals, London.
Hashin, Z., and Rotem, A. (1973) *J. Comp. Mats.* **7**, 448.

Jamison, R. D., et al. 1984. *Effects of Defects in Composite Materials*, ASTM STP **836**, American Society for Testing and Materials, Philadelphia, pp. 21–55.

Konur, O., and Matthews, F. L. 1989. *Composites* **20**, p. 317.

Mandell, J. F., Huang, D. D., and McGarry, F. J. 1982. *Short Fiber Reinforced Composite Materials*, ASTM STP **772**, ed. B. A. Sanders, American Society for Testing and Materials, Philadelphia, pp. 3–32.

Mandell, J. F., McGarry, F. J., and Li, C. G. 1985. *High Modulus Fiber Composites in Ground Transportation and High Volume Application*, ASTM STP **873**, ed. D. W. Wilson, American Society for Testing and Materials, Philadelphia, pp. 36–50.

Marshall, D. B., Cox, B. N., and Evans, A. G. 1985. *Acta. Metall.* **33**, 2013.

McCartney, L. N. 1987. *Proc. R. Soc. Lond.* **A409**, 329.

Owen, M. J., Smith, T. R., and Dukes, R. 1969. *Plast. Poly.* **37**, 227.

Owen, M. J., and Rose, R. G. 1970. *Mod. Plast.* **47**, 130.

Owen, M. J. 1974. *Composite Materials Vol. 5, Fatigue and Fracture*, ed. L. J. Broutman, Academic Press, New York, pp. 341–69.

Owen, M. J. 1982. *Short Fiber Reinforced Composite Materials*, ASTM STP **772**, ed. B. A. Sanders, American Society for Testing and Materials, Philadelphia, pp. 64–84.

Reifsnider, K. L. 1983. *Mechanics of Composite Materials, Recent Advances*, ed. Z. Hashin and C. T. Herakovich, Pergamon, New York, pp. 399–420.

Rotem, A., and Hashin, Z. 1976. *AIAA J.* **14**, 868.

Schulte, K., Reese, E., and Chou, T.-W. 1987. *Sixth International Conference on Composite Materials, Second European Conference on Composite Materialism*, Vol. 4, ed. F. L. Matthews, N. C. R. Buskell, J. M. Hodgkinson, and J. Morton, Elsevier, London, pp. 89–99.

Stinchcomb, W. W., and Reifsnider, K. L. 1979. *Fatigue Mechanisms*, ASTM STP **675**, ed. J. T. Fong, American Society for Testing and Materials, Philadelphia, pp. 762–87.

Stokes, V. K. 1990. *Polymer Composites* (*a*) **11**, 32; (*b*)**11**, 45; (*c*)**11**, 342; (*d*)**11**, 354.

Sturgeon, J. B. 1973. *Proceedings of the 28th Annual Technical Conference of the Society of the Plastics Industry*, pp. 12–13.

Talreja, R. 1981. *Proc. R. Soc. Lond.* **A378**, 461.

Wang, S. S., Chim, E. S. M., and Suemasu, H. 1986. *J. Appl. Mech.* **53**, 339.

Wang, S. S., Suemasu, H., and Chim. E. S. M. 1987. *J. Comp. Mats.* **21**, 1084.

4. CREEP IN POLYMERIC COMPOSITES

Y. Jack Weitsman

4.1 INTRODUCTION

The creep response of polymeric composites compounds the inherent time-dependent behavior of the polymeric phase, the temporal behavior of certain fibers (such as glass), and the highly complex damage mechanisms that arise due to fiber-matrix debonds, interlayer delaminations, and diffuse microcracking. Since all the latter damage mechanisms are also time-dependent and occur conjointly with polymeric creep, it is extremely difficult to separate out the individual contributions of molecular creep processes and time-dependent, damage mechanisms to recorded, overall creep data.

The creep and relaxation response of polymers within the linear range of behavior was modeled with a high degree of success by linear viscoelasticity theory. However, in spite of steady (but slow) progress over the last 30 years, the understanding and modeling of the nonlinear behavior of polymers is still the subject of ongoing research and is riddled with controversy. Furthermore, only tentative progress has been achieved in the modeling of damage in composite materials, even upon assuming linear-brittle behavior. The major hurdle, which impedes meaningful progress in the latter endeavor, seems to be an inherent inability to establish physically meaningful damage evolution relations.

Beyond the linear range of behavior, progress in the understanding and modeling of creep in polymeric composites seems to be hindered as much by the absence of a comprehensive data base as by inadequacies and controversies in the mathematical and basic mechanics and thermodynamics formulations.

Among the very few reviews on the subject are two earlier articles (Halpin, 1968; Schapery, 1968) and three more recent ones (Suvorova, 1985; Dillard, 1991; Schapery, 1992). It is interesting to note that time-dependent behavior is addressed in only two of the several current textbooks on composites (Christensen, 1979; Gibson, 1994).

The majority of works to date on creep in polymeric composites pertain to laminates that consist of plies reinforced by unidirectional fibers, with much of the remainder devoted to particulate reinforcement. Very little information is available on SMCs, which consist of resin and chopped fibers, and very scant data are known for swirl mat composites.

4.2 BASIC CONSIDERATIONS

The thermomechanical response of polymers is understood in terms of and correlated with their molecular architecture. Polymers consist of long-chain molecules whose "backbones" are held together by strong chemical bonds. The individual long chains are joined by much weaker bonds to form the bulk polymeric matter. In addition, most polymers contain side groups made of shorter molecular segments. Unlike crystalline structures (as in metals) the polymeric molecules are not arrayed in orderly fashions and are therefore not tightly packed, thereby containing "free volume," which is devoid of matter.

Polymer chains may be cross-linked to each other by chemical agents to form thermosets or may be interconnected to each other by physical entanglement to form thermoplastics. In either case, polymers exhibit creep under sustained mechanical loads, though more substantial creep occurs in thermoplastics than in thermosets.

The underlying creep mechanisms in polymers differ from those in metals. While metal creep is dominated by dislocation motions and events at intercrystalline boundaries, the creep of polymers is controlled by configurational changes in the long-chain molecules and by motions of the side groups. In the case of thermoplastics, creep is enhanced by the relative slippage between neighboring molecules.

In all circumstances creep is greatly accelerated by temperature. The main causes for the above acceleration are a thermally induced increase in the free volume, which affords more space for molecular motions, accompanied by a rise in the agitational energy for molecular vibrations and relative motions.

A most dramatic increase in the creep response of polymers occurs around the "glass transition temperature," T_g, where the weak intermolecular bonds break down or the physical entanglements among adjacent long-chain molecules loosen up, freeing the bulk polymer to sustain large configurational changes under relatively small loads. Less significant transitions (denoted as "β" and "γ" transitions, in contrast with the spectacular "α" transition at T_g) occur at temperatures below T_g, when sufficient increments in the free volume allow less restricted motions of the side groups.

Typical isothermal creep data at various levels of temperature are shown in Figs. 4.1 and 4.2 for PEEK resin and for a uniaxially reinforced graphite/PEEK composite loaded transversely to the fiber direction, respectively. The data are represented as creep compliance, which is the time-dependent creep strain divided by the constant applied stress. Note the sixfold increase in the strains, recorded 200 min after load application, at 188°C when compared with the those at 25°C in Fig. 4.1 and a corresponding threefold increase in Fig. 4.2.

The inverse of creep is given by relaxation. Namely, while creep refers to time-dependent strains under applied stress, relaxation refers to stresses due to prescribed strains. Typical plots demonstrating the

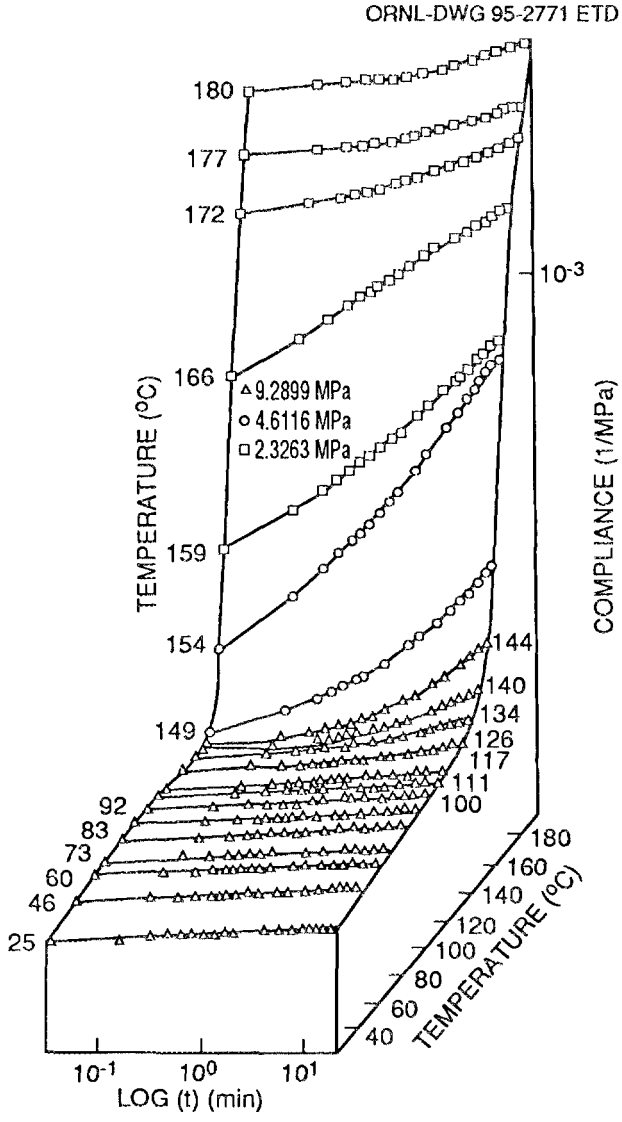

Fig. 4.1. Temperature dependence of creep compliance of PEEK. ***Source*****: Xiao, 1987, p. 83. Adapted with permission of the Free University–Brussels.**

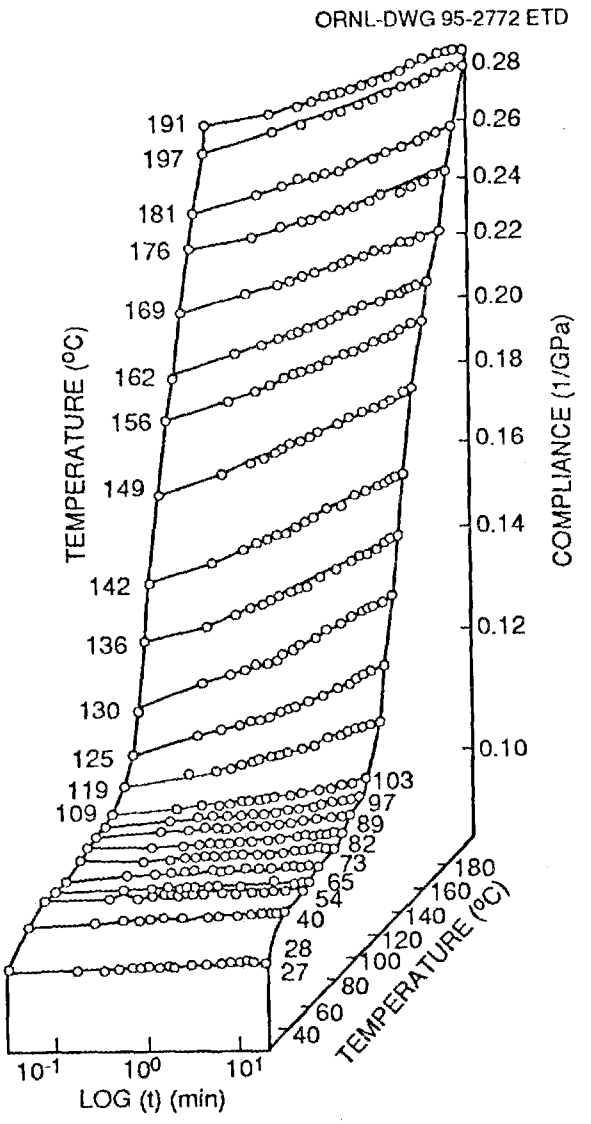

Fig. 4.2. Temperature dependence of transverse creep compliance of APC-2 unidirectional laminate at 15.22 MPa. *Source*: Xiao, 1987, p. 109. Adapted with permission of Free University–Brussels.

effects of temperature on relaxation are shown in Fig. 4.3. Here, the relaxation modulus that is plotted is the time-dependent stress divided by the constant applied strain. The family of curves plotted in that figure exhibit the temporal dependence of the relaxation behavior. The effects of the degree of cross-linking on the relaxation modulus are shown in Fig. 4.4. Both Figs. 4.3 and 4.4 are reproduced from an engineering text (Ashby and Jones, 1986).

As can be seen from Figs. 4.1 to 4.3 the major effect of temperature is to compress the time for creep and relaxation of polymers. This phenomenon, denoted as the "time-temperature analogy," suggests a possibility for accelerated testing of creep behavior. If the foregoing analogy accounts for the entire influence of temperature, it implies that the time-dependent molecular processes at any specified (fixed) temperature level are identical to those at another temperature level, provided one speeds up or slows down the time-recording mechanism. Such behavior is denoted as a thermorheologically simple response, and the required temperature-dependent adjustment in the time-scale is called the shift-factor function, denoted by $a_T(T)$.

ORNL-DWG 95-2773 ETD

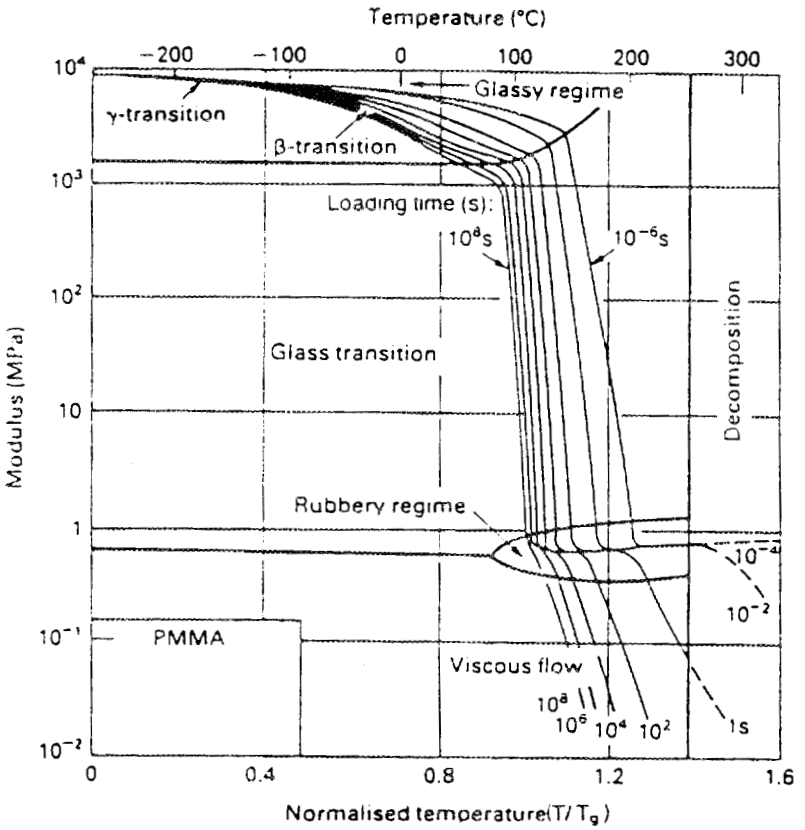

Fig. 4.3. Modulus diagram for PMMA showing the glassy regime, the glass-rubber transition, rubbery regime, and regime of viscous flow. The diagram is typical of linear-amorphous polymers. *Source*: Ashby and Jones, 1986. Reprinted with permission of Butterworth-Heineman, Ltd.

ORNL-DWG 95-2774 ETD

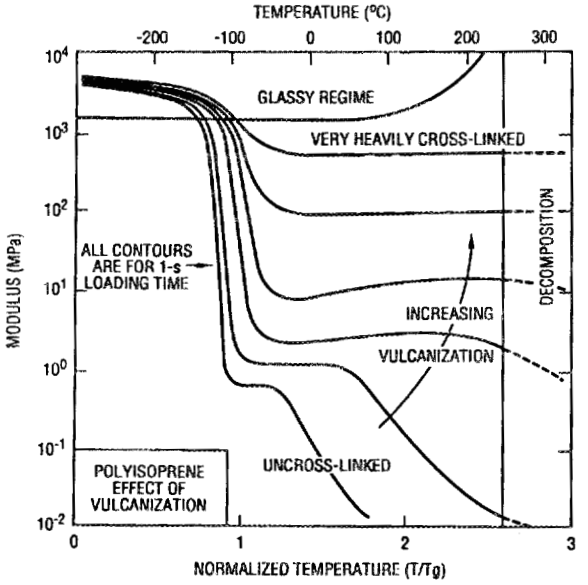

Fig. 4.4. Influence of cross-linking on contour of modulus diagram for polyisoprene. *Source*: Ashby and Jones, 1986. Redrawn with permission of Butterworth-Heineman, Ltd.

However, in most realistic circumstances, temperature tends to cause modulus softening, in addition to the aforementioned acceleration of the time scale for creep. In such cases the behavior is called "thermorheologically complex."

Another important time-dependent phenomenon that occurs in polymers is aging. This phenomenon is attributable to the spontaneous and gradual collapse of the free volume contained within the polymer and tends to restrict molecular motions as the material ages. Consequently, polymers become more brittle with age, and the creep response of freshly manufactured polymers exceeds that of older materials as shown schematically in Fig. 4.5 (Struik, 1978).

As mentioned in Sect. 4.1, at certain stress levels the response of polymers is no longer linear; namely, an increase in stress is accompanied by a disproportionate increase in the time-dependent strains. The threshold levels for the onset of nonlinearity are temperature dependent. This is shown in Fig. 4.6 for an APC-2 (graphite/PEEK) composite (Xiao, 1987).

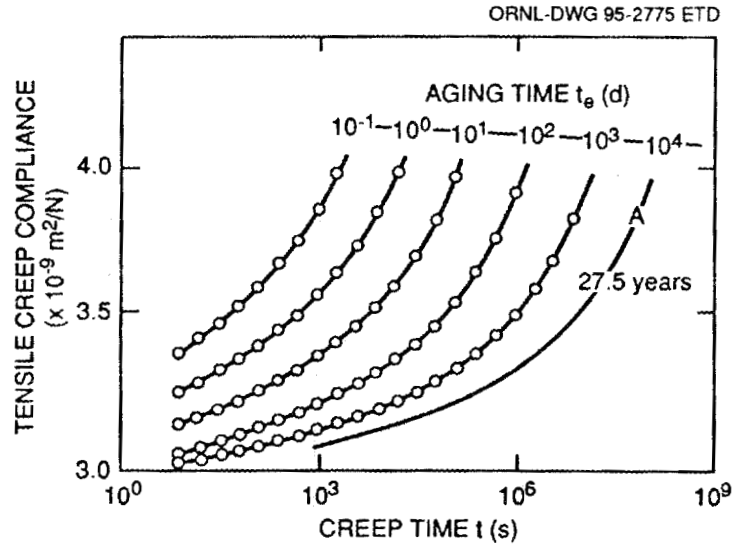

Fig. 4.5. Aging effects on creep response of polymers. *Source*: Struik, 1978, p. 33. Redrawn with author's permission.

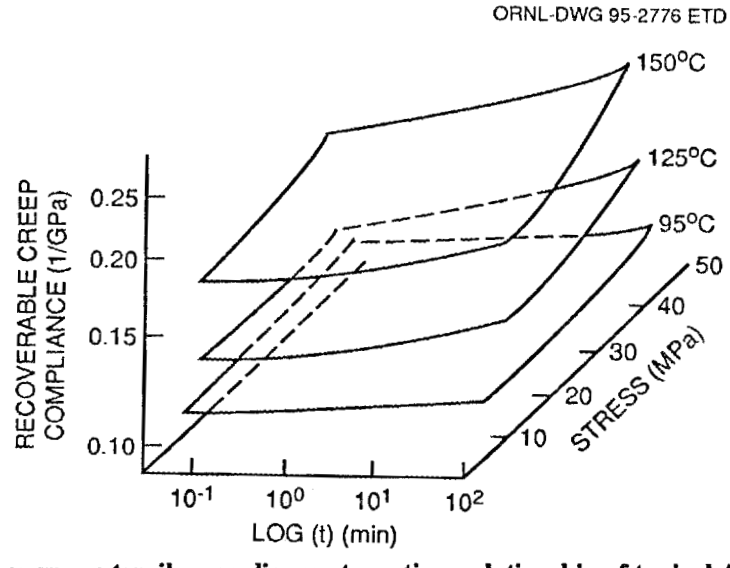

Fig. 4.6. Transverse tensile compliance-stress-time relationship of typical APC-2 composite laminate. *Source*: Xiao, 1987, p. 124. Redrawn with permission of Free University–Brussels.

A major contribution to the time-dependent response of polymeric composites stems from the aforementioned temporal behavior of the polymeric resins. For very stiff and elastic fibers the creep of the composite is controlled by the creep of the polymer. However, in the case of glass and Kevlar fibers (e.g., Charles, 1958*a,b*), which are themselves susceptible to creep, the time-dependent behavior of the composite encompasses the temporal responses of both fibrous and matrix phases. It should be recognized that the fibers would cause spatial nonuniformity in the stress fields within the resin, activating nonlinearity at lower nominal levels of applied stresses.

In addition, as noted in Sect 4.1, the presence of fibers is most likely associated with the existence of a complex internal flaw structure that evolves according to its own time-dependent mechanistic response. Although no comprehensive model exists at the present time to account for the above simultaneously developing processes, it can be shown that, in the least, it is necessary to employ a "rheologically complex" constitutive relation when attempting to relate concurrent time-dependent processes.

4.3 MODELS FOR CREEP

4.3.1 Viscoelasticity—General Background

The fundamental concepts that underlie the models for creep in polymeric composites derive from statistical considerations of configurations of long-chain segments (Billmeyer, 1971; Rudin, 1982; Alkonis and MacKnight, 1983) as well as from nonequilibrium thermodynamics (Prigogine, 1967; deGroot and Mazur, 1984).

The above concepts were recast (Rouse, 1953; Bueche, 1954; Zimm, 1956) into mathematical models that corresponded to the mechanical response of series and parallel assemblages of springs and dash-pots. Subsequently, these models were reestablished from derivations based upon the systematic methodology of continuum mechanics (Biot, 1954, 1958; Schapery, 1964, 1966, 1969). The latter works by Schapery appear to present the most useful linear and nonlinear viscoelastic model to date for a wide range of polymeric materials and polymeric composites.

Another approach, based upon the methodology of continuum mechanics and irreversible thermodynamics, utilizes expansions in multiple and higher order convolution integrals to model nonlinear viscoelastic behavior (Green et al., 1957, 1959, 1960; Noll, 1958). Comprehensive lists of references can be found in viscoelasticity texts (e.g., Findley et al., 1976; Christensen, 1982).

4.3.2 Linear Viscoelasticity

Let $\{I\}$ denote an input history and $R\{I\}$ be the response to that input. Linear behavior is characterized by

$$R\{I_1 + I_2\} = R\{I_1\} + R\{I_2\} \quad , \tag{4.1}$$

and

$$R\{cI\} = cR\{I\} \quad , \quad \text{constant } c \quad . \tag{4.2}$$

Specifically, denote by $D(t)$ the strain-response to a unit-step stress input, namely

$$\varepsilon\{\sigma = H(t)\} = D(t) \quad ; \tag{4.3}$$

and, inversely, let $E(t)$ signify the stress-response to a unit strain input, to wit

$$\sigma\{\varepsilon = H(t)\} = E(t) \quad . \tag{4.4}$$

Then the linear viscoelastic response to general, time-varying strain or stress inputs $\varepsilon = \varepsilon(t)$ or $\sigma = \sigma(t)$ is expressed by the convolution integrals

$$\varepsilon(t) = \int_{-\infty}^{t} D(t - \tau)\dot{\sigma}(\tau)d\tau \quad , \tag{4.5}$$

and

$$\sigma(t) = \int_{-\infty}^{t} E(t - \tau)\dot{\varepsilon}(\tau)d\tau \quad . \tag{4.6}$$

In Eqs. (4.3) to (4.6), t denotes time, and the time-dependent functions D(t) and E(t) are the creep compliance and relaxation modulus, respectively.

As mentioned in Sect. 4.2, "thermorheologically simple" behavior is featured by a temperature-induced compression of the time scale only. If the above time compression is prescribed by a shift-factor function $a_T(T)$, then Eqs. (4.5) and (4.6) should be rewritten in terms of "reduced times" ξ instead of real time t. For the circumstances of fluctuating temperatures, T = T(t), this is accomplished by evaluating the reduced times ξ and ξ' according to

$$\xi = \xi(t) = \int_0^t \frac{d\tilde{t}}{a_T[T(\tilde{t})]} \quad \text{and} \quad \xi' = \xi(\tau) = \int_0^\tau \frac{d\tilde{t}}{a_T[T(\tilde{t})]} \quad , \tag{4.7}$$

and acknowledging the presence of thermal strains $\varepsilon_{th}(t)$.

Altogether, thermorheologically simple viscoelastic behavior under fluctuating temperatures is expressed by

$$\varepsilon(t) - \varepsilon_{th}(t) = \int_{-\infty}^{t} D(\xi - \xi')\dot{\sigma}(\tau)d\tau \quad ; \tag{4.8}$$

and inversely

$$\sigma(t) = \int_{-\infty}^{t} E(\xi - \xi')[\dot{\varepsilon}(\tau) - \dot{\varepsilon}_{th}(\tau)]d\tau \quad . \tag{4.9}$$

In Eqs. (4.8) and (4.9) ε_{th} is the strain due to free thermal expansion. In principle, this strain is also given by a convolution integral involving the history-dependent coefficient of thermal expansion α and the temperature input. However, in most circumstances α does not depend on time, though it may depend on the temperature T.

The creep-compliance and stress-relation functions, D(t) and E(t), are not inverse of each other, but their Carson transforms are, namely

$$\tilde{E}(S)\tilde{D}(S) = 1 \quad . \tag{4.10}$$

[The Carson transform of a function F(t) is defined by $\tilde{F}(S) = S\bar{F}(S)$, where $\bar{F}(S)$ is the Laplace transform of F(t)].

However, for most polymeric materials $E(t) \sim 1/D(t)$ to within an error not exceeding 10%. Improved correlations between E(t) and D(t) are available, without resort to Carson transforms (e.g., Pipkin, 1972).

Although viscoelastic stress analysis is beyond the scope of this review, it is worth mentioning that the "quasi-elastic" approximation, which is based upon an approximate method for Laplace transform inversion (Schapery, 1962, 1965), provides a simple and useful tool to solve a large class of linear

viscoelastic boundary value problems. This method applies to most polymeric materials and circumvents the need to perform Laplace transform inversion that, at least formally, is necessitated by the more general Correspondence Principle approach (Lee, 1955).

According to the quasi-elastic approximation, denote the supposedly known linear elastic solution to a specified boundary value problem with a unit-step input, I_H, by $R_H^e\{I_H, C_{ij}\}$, where C_{ij} are the time-independent elastic moduli; then the solution to the same boundary value problem in linear viscoelasticity is given by $R_H^{v.e.} = R_H^e\{I_H, C_{ij}(t)\}$, where $C_{ij}(t)$ are the corresponding time-dependent moduli.

The solution to fluctuating inputs follows from $R_H^{v.e.}$ by means of superposition integrals akin to those in Eqs. (4.5) and (4.6). Note that the validity of the quasi-elastic approximation is restricted to inputs with limited fluctuations.

The basic concept utilized in the quasi-elastic approximation carries over, under some restrictions, to the viscoelastic characterization of polymeric composites. Accordingly, if an elastic property of a composite P can be related in terms of the elastic properties of the matrix and fibrous phases, P_m and P_f, by an expression

$$P = F(P_m, P_f, \ldots) \ , \tag{4.11}$$

then the corresponding viscoelastic composite quantity is given by

$$P(t) = F(P_m(t), P_f \ , \ldots) \ , \tag{4.12}$$

where $P_m(t)$ denotes the time-dependent property of the matrix.

Equation (4.12) applies only within the linear range and is limited to those cases when the viscoelastic response of the bulk polymer does not differ from its in situ behavior within the composite.

Linear, thermorheologically complex viscoelastic response is expressed by modifying Eqs. (4.5) and (4.6) to read

$$\varepsilon(t) - \varepsilon_{th}(t) = \int_{-\infty}^{t} D(\xi - \xi') \ \frac{d}{d\tau} \left\{ \frac{\sigma(\tau)}{b_T[T(\tau)]} \right\} d\tau \quad , \tag{4.13}$$

and

$$\sigma(t) = \int_{-\infty}^{t} E(\xi - \xi') \ \frac{d}{d\tau} \left\{ \frac{\varepsilon(\tau) - \varepsilon_{th}(\tau)}{g_T[T(\tau)]} \right\} d\tau \quad , \tag{4.14}$$

respectively.

The temperature-dependent functions $b_T(T)$ and $g_T(T)$ are denoted as "vertical-shift" functions.

Significant mathematical simplifications occur for creep compliancxes expressed by a power-law form, namely

$$D(t) = D_0 + D_1 \, t^n \ , \tag{4.15}$$

and to a lesser extent for power-law-like relaxation, such as

$$E(t) = \begin{cases} Et^{-n} \\ E_1 + \dfrac{E_2}{(A + t)^n} \end{cases} \ . \tag{4.16}$$

It turns out that the time-dependent response of most polymeric materials and many polymeric composites can be fit by Eqs. (4.15) and (4.16). In view of the ensuing benefits for subsequent stress analysis and predictions of long-time response, it is advantageous to attempt to fit data into those expressions.

4.3.3 Nonlinear Viscoelasticity

It has already been mentioned that the modeling of nonlinear viscoelastic behavior of polymers and polymeric composites is subject to many current disagreements. While it is commonly agreed that stress enhances the creep compliance of resins, as can be seen from Figs. 4.6–4.8, the controversy focuses on the specific causes.

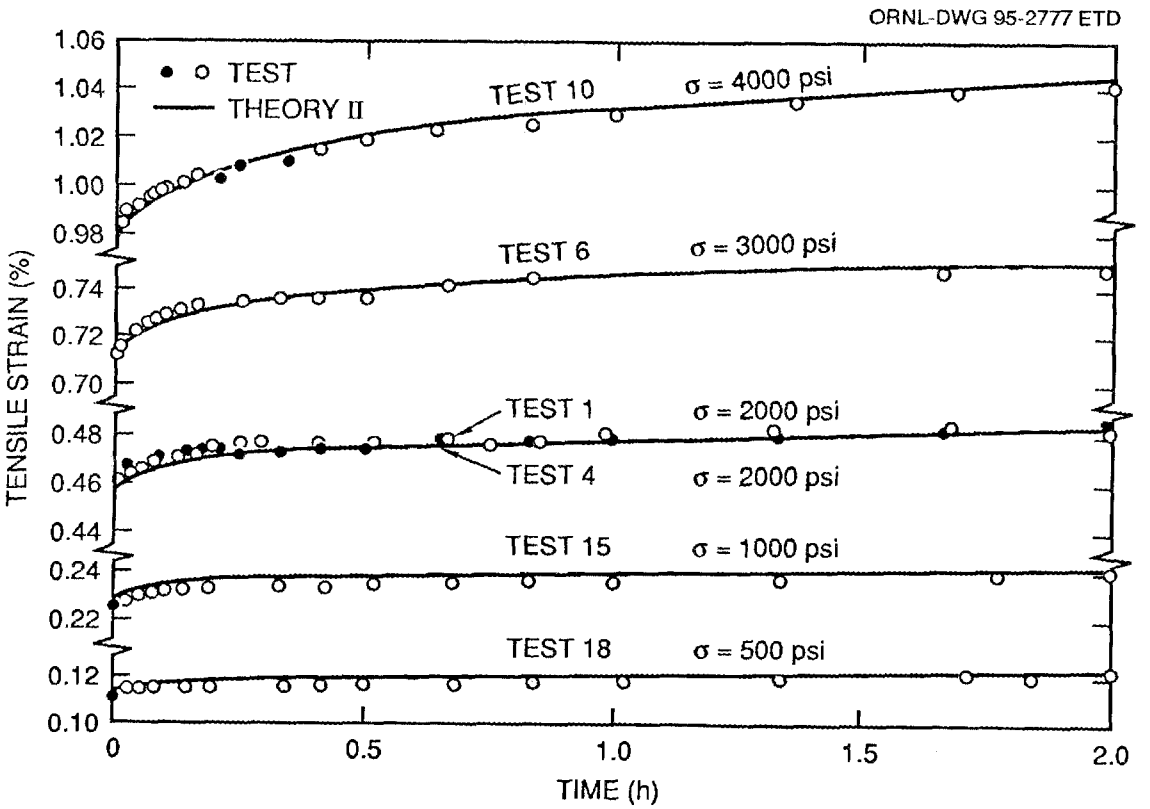

Fig. 4.7. Nonlinearly enhanced creep of unplasticized poly (vinyl chloride) in tension. ***Source:*** **Onaran and Findley, 1965, p. 321. Adapted with permission of Society of Rheology.**

Knauss and Emri (1987) attributed nonlinearity to stress effects on free volume, thereby relating it as a function of the spherical stress σ_{kk}. On the other hand, observations that equivalent degrees of mechanically enhanced aging occurred under uniaxial tensile and compressive stresses led Sternstein (1976) and Myers et al. (1976) to conclude that nonlinearity is driven by shear, rather than dilatational, stresses. It is worthwhile noting that in some cases the nonlinear viscoelastic response of fiber-reinforced composites was successfully related to the octahedral shear stress (Lou and Schapery, 1971; Xiao, 1987).

The nonlinear viscoelastic models of Schapery (1966, 1969) relate the nonlinearity by means of three stress-dependent functions (g_0, g_1, g_2) and a stress-time shift-factor function a_σ. Although these four functions are constrained to depend on mathematically appropriate stress invariants, they contain—in principle—both shear and dilatational stress components.

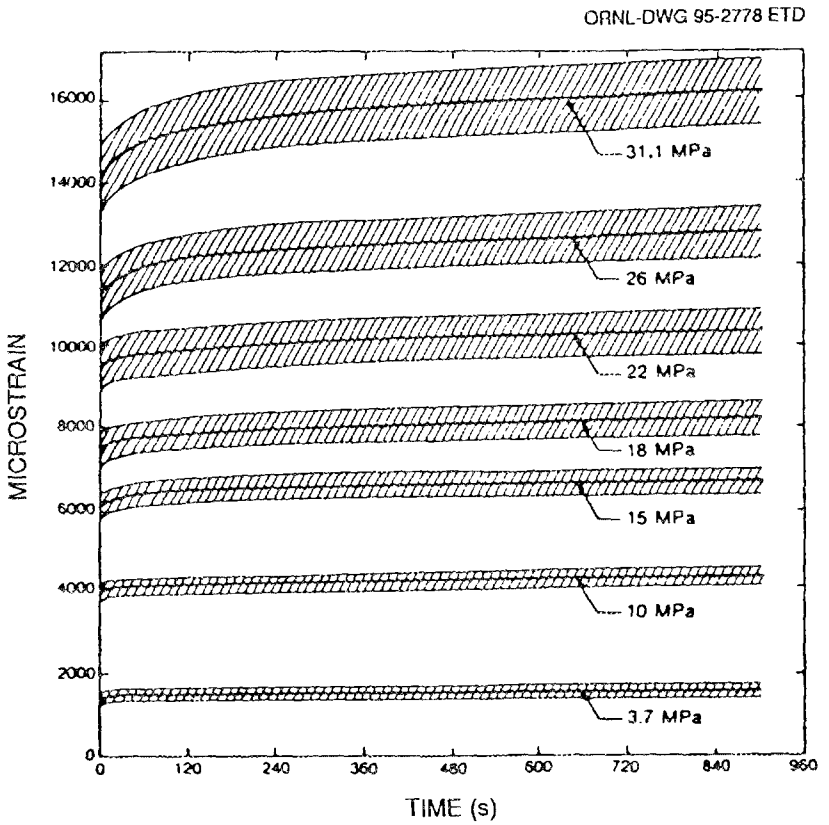

Fig. 4.8. Creep strains for FM-73 adhesive at various levels of uniaxial stress and data scatter-bands. *Source*: Peretz and Weitsman, 1982. Adapted with permission of American Institute of Physics.

Specifically, for the one-dimensional case, Schapery's model (1969) gives

$$\varepsilon = g_0 A(0)\sigma + g_1 \int_0^t \Delta A(\Psi - \Psi') \frac{d(g_2\sigma)}{d\tau} d\tau \quad . \tag{4.17}$$

In Eq. (4.17), $A(0)$ and $\Delta A(\Psi)$ are the initial and transient components of the linear creep compliance, and Ψ is the "reduced" time given by

$$\Psi = \int_0^t \frac{d\tilde{t}}{a_\sigma(\sigma(\tilde{t}))} \quad \text{and} \quad \Psi' = \int_0^\tau \frac{d\tilde{t}}{a_\sigma[\sigma(\tilde{t})]} \quad . \tag{4.18}$$

Nonlinear thermoviscoelastic behavior is expressed upon replacing ε with $\varepsilon - \varepsilon_{th}$ on the left side of Eq. (4.17) and letting $g_i = g_i(\sigma,T)$ instead of $g_i = g_i(\sigma)$ $(i = 0, 1, 2)$ on the right side of Eq. (4.17). In addition, Ψ and Ψ' in Eq. (4.18) should also depend on both stress and temperature, thus

$$\Psi = \int_0^t \frac{d\tilde{t}}{a[\sigma(\tilde{t}), T(\tilde{t})]} \quad \text{and} \quad \Psi' = \int_0^\tau \frac{d\tilde{t}}{a[\sigma(\tilde{t}), T(\tilde{t})]} \quad . \tag{4.19}$$

The form of Eq. (4.17) is constrained by the fact that it predicts complete recovery of strains at sufficiently long times after the removal of external loads. This restriction can be removed by adding the term $g_3 t$ to the right side of Eq. (4.17).

Several specific forms of nonlinear behavior are, in fact, subcases of Eq. (4.17). For instance, Findley and Peterson (1958) employed a power-law creep model with nonlinear coefficients to describe the viscoelastic response of plastic laminates. They utilized

$$\varepsilon(t) = \varepsilon_0 + mt^n \ , \tag{4.20}$$

where $\varepsilon_0 = \varepsilon_0' \ \sinh(\sigma/\sigma_\varepsilon)$, and $m = m' \sinh(\sigma/\sigma_m)$.

Dillard et al. (1982, 1983) employed the form of Eq. (4.20) together with the results of Lou and Schapery (1971) to model the nonlinear viscoelastic response of composite laminates. Since the matrix in these laminates is subjected to combined stresses, the stress dependence of ε_0 and m was expressed through τ_{oct} instead of σ.

Finally, it is worth noting that the nonlinear viscoelastic and thermoviscoelastic response of the FM-73 adhesive was characterized by Peretz and Weitsman (1982, 1983) through combinations of power-law and exponentials functions g_0, g_1, g_2, and a. For the limited ranges of stress and temperature employed in the latter works, it was possible to incorporate the separate effects of those parameters in product forms: namely, $g_1(\sigma,T) = \bar{g}_i(\sigma)\hat{g}_i(T)$ (i = 0, 1, 2, no summation on i), and $a(\sigma,T) = a_\sigma(\sigma)a_T(T)$.

4.3.4 Viscoplasticity

Another approach to the modeling of creep derives from plasticity theory, which was applied initially to metal matrix composites. However, for uniaxially reinforced polymeric composites, Sun and Chen (1989) and Yoon and Sun (1991) developed a simplified single-parameter plasticity model for creep in off-axis unidirectionally reinforced coupons. The model was subsequently extended to laminated plates (Wang, Sun, and Gates, 1990) and to thermal effects (Sun and Wang, 1991). Rate dependence was included by means of an overstress model, as well as through a modified Bodner-Partom model.

The model yielded reasonably good predictions for monotonically increasing loads as well as for residual thermal stresses in APC-2 laminates. However, it should be noted that the above single-parameter model applies only to composites that consist of unidirectionally reinforced plies, since the geometric constraints imposed by such reinforcement are employed at the outset of the formulation.

4.3.5 Fracture, Damage, and Durability

Time-dependent material response gives rise to time-dependent crack growth. The two phenomena were correlated by Schapery (1975*a,b,c*) in the context of linear viscoelasticity theory. Accordingly, the rate of crack growth $\dot{\ell}$ in polymers is related by the expression

$$\Gamma = \frac{1-\nu^2}{2} K_I^2 D\left(\frac{\alpha}{3\dot{\ell}}\right) \ , \tag{4.21}$$

where K_I is the stress intensity factor determined by the external load, D and ν are the creep compliance and Poisson's ratio of the polymer, while α and Γ represent characteristics of the fracture resistance. Specifically, α is the length of the damage zone ahead of the crack tip, and Γ denotes the energy required to tear a ligament of damaged polymeric matter.

For a specified form of creep compliance it is possible to invert Eq. (4.21) and relate the time-dependent crack growth $\dot{\ell} = \dot{\ell}(t)$ to the history of the external load, since $K_I = K_I[\sigma(t)]$.

In particular, for power-law creep $D(t) = D_1 t^n$ [which is the same as Eq. (4.15), but with $D_0 = 0$], it is possible to reduce Eq. (4.21) to read

$$\dot{\ell} = AK_I^q \ , \tag{4.22}$$

where A contains Γ, a, v, and D_1 and q is related to the power of n.

Furthermore, Eq. (4.21) yields an expression for time-to-failure under constant load σ_∞ of the form

$$t_f = B\sigma_\infty^{-q} \ . \tag{4.23}$$

Finally, Eq. (4.21) can also predict time-to-failure under time-varying external loads, resembling a Miner-rule type of relation (Schapery, 1975*c*). [See also Eq. (4.26) below].

The forms of the foregoing results, which were derived for polymeric resins, were assumed to remain valid for fiber-reinforced composites as well (Christensen, 1994; Christensen and Glaser, 1994). For unidirectionally reinforced polymeric composites loaded parallel to the fiber direction, the above forms were extended to incorporate the statistics of static strength and thereby yield probabilistic predictions for durability under applied loads.

Additional considerations of creep rupture times are listed in one of the above-mentioned review articles (Dillard, 1991).

An alternate approach to durability was taken by Zhurkov (1965), where time to failure t_r was derived from fundamental concepts of fracture of interatomic binding forces. These considerations yielded the following expression:

$$t_r = t_0 \exp\left(\frac{U_0 - \gamma\sigma}{kT}\right) \ , \tag{4.24}$$

where t_0 is a characteristic time, U_0 is activation energy for failure, γ accounts for sensitivity to stress, and k is the Bolzman constant. The validity of Eq. (4.24) was demonstrated for several materials, as shown in Fig. 4.9 (after Zhurkov, 1965).

An alternate form of Eq. (4.24) reads

$$\log t_r = A - B\sigma \ , \tag{4.25}$$

which agrees with the form of Eq. (4.23).

As was already noted, in the paragraph following Eq. (4.23), Eq. (4.24) can be employed to predict time-to-failure, t_f, under fluctuating stress and temperature; namely,

$$\int_0^{t_f} \frac{dt}{t_r[\sigma(t),\ T(t)]} = 1 \ . \tag{4.26}$$

It is worth observing that the above time-to-failure (which resembles that of Schapery, 1975*c*) does not distinguish among disparate *sequences* of applied loads.

Equation (4.24) was employed by Chiao et al. (1977) for evaluating the lifetime of unidirectionally reinforced Kevlar 49/epoxy composites under various levels of constant tension and temperature. Thirty replicate tests were conducted at each stress and temperature level, and the time-to-failure data were reduced by means of Weibull statistics. Consequently, Chiao et al. were able to predict times-to-failure within various prescribed levels of reliability.

Among the very few attempts to account for time-dependent damage in viscoelastic materials, it is worth mentioning the model presented by Suvorova (1985) in which the measure of damage was correlated with the amount of nonrecoverable strain, which remains permanently long after the complete removal of

ORNL-DWG 95-2779 ETD

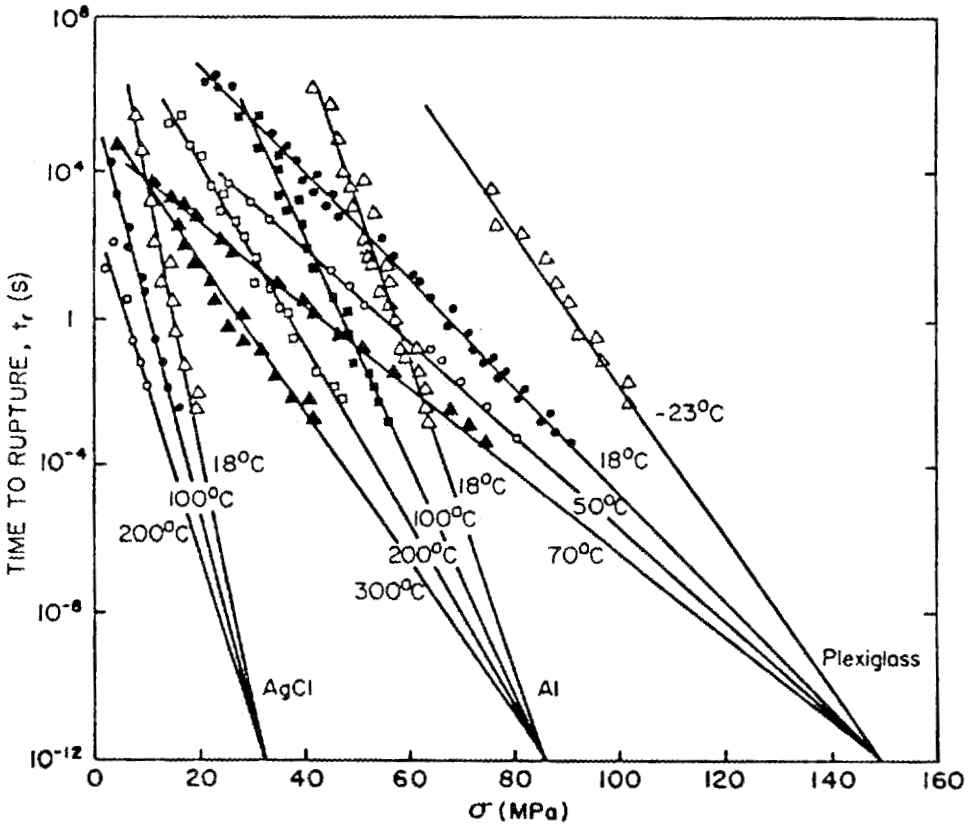

Fig. 4.9. Stress and temperature dependence of creep rupture lifetime for AgCl, aluminum, and Plexiglas. *Source*: Zhurkov, 1965. Adapted with permission of *Int. J. Fract.*

the applied load. Accordingly, Suvorova introduces two creep compliances, L(t) and M(t),* associated with recoverable and nonrecoverable strains, respectively, and modifies Eq. (4.5) to read

$$\varphi[\varepsilon(t)] = \sigma(t) + \int_0^t \left[L(t-\tau)+M(t-\tau)\right]\sigma(\tau)dt \qquad 0 < t < t^* , \tag{4.27}$$

with

$$\varphi[\varepsilon(t)] = \sigma(t) + \int_0^t L(t-\tau)\,\sigma(\tau)dt + \int_0^{t^*} M(t^*-\tau)\,\sigma(\tau)dt \qquad t > t^* . \tag{4.28}$$

In the above equations $\phi[\varepsilon(t)]$ accounts for any time-independent nonlinearity that may occur in the response of the material, and t^* is the time when $\varepsilon(t)$ attains its maximal value under the prescribed load history. The above choice of t^* is based on the assumption that healing does not occur, and thereby all non-recoverable deformation is generated during the stage of increasing strains. In some sense M(t) plays the role of g_3t mentioned in the paragraph that follows Eq. (4.19).

The compliance M(t) is further related to an internal-variable damage parameter w, which admits a time-dependent character. Consequently, Suvorova (1985) establishes systematic expressions for time-to-failure and fatigue life, which she correlates reasonably well with experimental results.

*In fact, L and M are the time-derivatives of creep compliances (i.e., $L=\dot{D}$).

In addition, Suvorova (1985) provides a qualitative explanation for the rate-dependence of the strength of polymeric composites. Accordingly, there is an important interplay between the rate of loading and the time required to propagate cracks within the polymeric phase of the composites due to the visco-elasticity of that phase.

4.4 EXPERIMENTAL CHARACTERIZATION OF CREEP RESPONSE

4.4.1 Preliminary Tests

An important role of preliminary tests is to identify some fundamental features of the creep behavior of the material under consideration. These features include the extent of creep, its statistical scatter, and the range of its linear behavior. Other aspects include the extent of strain recovery upon load removal and sensitivity to temperature and humidity.

Familiarity with the above features provides guidance regarding the choice (or choices) of an appropriate mechanics model for the creep behavior, thereby directing the detailed experimental tasks that are to follow.

Preliminary data on swirl mat composites (refer to Sect. 2.3) suggest that their creep response falls within the typical range of the time-dependent response of polymers as shown in Figs. 4.1 and 4.7, with scatter resembling that shown in Fig. 4.8. However, both creep and recovery data are essential to the selection and development of a creep model.

Another kind of preliminary data, which are useful in determining the range of linear behavior, concerns the recording of strain $\varepsilon(t)$ under various values of constant loading rates; that is, $\sigma(t) = Rt\,H(t)$ with $R = R_1, R_2, R_3 \ldots (R_1 < R_2 < R_3 < \ldots$, say).

It can be shown that plots of $\varepsilon(t)/\sigma(t)$ (or $\log \varepsilon/\sigma$) vs time t (or log t) cluster within the linear range and "fan out" in the nonlinear range, as sketched in Fig. 4.10. The stress corresponding to point B in that figure augurs the onset of nonlinearity.

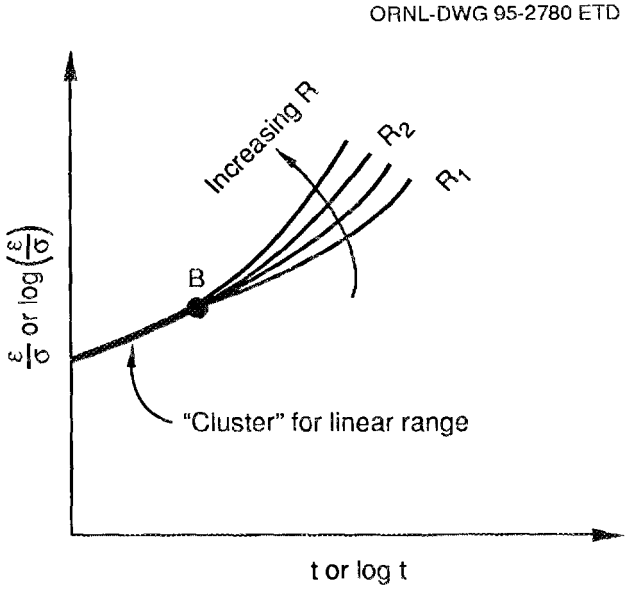

Fig. 4.10. Schematic of strain response of composite to constant loading rates.

4.4.2 Characterization Tests

In view of the fact that creep of the vast majority of polymeric composites fits the power-law form listed in Eq. (15), it is useful to conduct tests that determine the quantities D_0 and D_1 as well as the power n in that equation.

While D_0 can be established directly by taking the limit of $\varepsilon(t)$ as $t \to 0^+$, the values of D_1 and n can be determined by conducting creep and recovery tests. These tests involve the step application, followed by the step removal, of a constant stress; namely,

$$\sigma(t) = \sigma_0[H(t) - H(t - t_1)] \ , \tag{4.29}$$

which results in creep and recovery strains of the form

$$\frac{\varepsilon(t)}{\sigma_0} = D(t) = \begin{cases} D_0 + D_1 t^n & 0 < t < t_1 \\ D_1\left[t^n - (t - t_1)^n\right] & t > t_1 \end{cases} \ . \tag{4.30}$$

Note that only D_1 and n are involved in the recovery range $t > t_1$.

A separation between D_1 and n is obtained by considering the nondimensional lapsed time $\lambda = (t - t_1)/t_1$; thereby the recovery compliance during $t > t_1 (\lambda > 0)$ is given by

$$D(t) = \hat{D}(\lambda) = D_1 t_1^n\left[(\lambda + 1)^n - \lambda^n\right] \cdot \tag{4.31}$$

Consequently, the plot of

$$\log \hat{D}(\lambda) = \log\left(D_1 t_1^n\right) + \log\left[(\lambda + 1)^n - \lambda^n\right], \tag{4.32}$$

vs $\log \lambda$ yields the best value of n and, subsequently, the best value of D_1.

An alternative method to determine D_0, D_1, and n was proposed by Boller (1957). Accordingly, let $\varepsilon(t_1)$, $\varepsilon(t_2)$, and $\varepsilon(t_3)$, denoted by ε_1, ε_2, and ε_3, respectively, be the strains recorded at times $t_1 < t_2 < t_3$, with $t_2 = \sqrt{t_1 t_3}$. Then

$$D_0 = \frac{1}{\sigma_0} \frac{\varepsilon_1\varepsilon_3 - \varepsilon_2^2}{\varepsilon_1 - 2\varepsilon_2 + \varepsilon_3} \ , \quad n = \log\left(\frac{\varepsilon_3 - \varepsilon_2}{\varepsilon_2 - \varepsilon_1}\right) \Big/ \log\left(t_2/t_1\right) \ ,$$

$$\text{and } D_1 = \frac{1}{\sigma_0} \frac{\varepsilon_1 - D_0\sigma_0}{t_1^n} \ . \tag{4.33}$$

For "power-law materials" temperature effects on creep are reflected in a temperature-dependent initial compliance $D_0 = D_0(T)$. In a compressed-time dependence of the creep component, Eq. (4.8) thereby yields

$$D(t;T) = D_0(T) + D_1 \cdot \left[t/a_T(T)\right]^n \ . \tag{4.34}$$

In this case, it can be shown that the right-hand side of Eq. (4.32) will contain the added term

$$-n \log a_T(T) \ . \tag{4.35}$$

This enables the determination of $a_T(T)$ from isothermal creep and recovery data at various levels of temperature T.

For a thermorheologically complex response, the determination of the additional function $b_T(T)$ in Eq. (4.13) requires the performance of sudden temperature-drop tests (Harper and Weitsman, 1985).

Similarly, it can be shown that creep and recovery tests at various levels of constant stress are necessary and sufficient to evaluate the stress dependence of the functions g_0, g_1, g_2, and a_σ in Eqs. (4.17) and (4.18) (Peretz and Weitsman, 1982), while similar isothermal data at various constant levels of temperature, as well as sudden temperature-drop data, are required to determine the temperature-dependence of the above functions (Peretz and Weitsman, 1983).

The mechanical response of polymers exhibits significant statistical scatter, which is further amplified in the case of fiber-reinforced polymeric composites. The data scatter may become so large as to obscure the effects of temperature, moisture, and stress on creep and frustrate any effort at rational characterization. It is therefore useful to separate out the statistical effects due to inherent randomness in the material microstructure from the influences of stress and environment on the creep of polymeric composites. Such a separation is accomplished by subjecting the material to a history of preloading, which tends to regulate its response to subsequent loading. A typical "stress conditioning" history, which was employed for the creep characterization of automotive composites (Jerina et al., 1979), is shown in Fig. 4.11. Typically, the load/unloading sequence suffices for the characterization of creep for times not exceeding the duration of the conditioning history and for stresses below the level of the conditioning stress. It is worth noting that data scatter remains even in conditioned specimens, as may be observed from the scatterbands shown in Fig. 4.8.

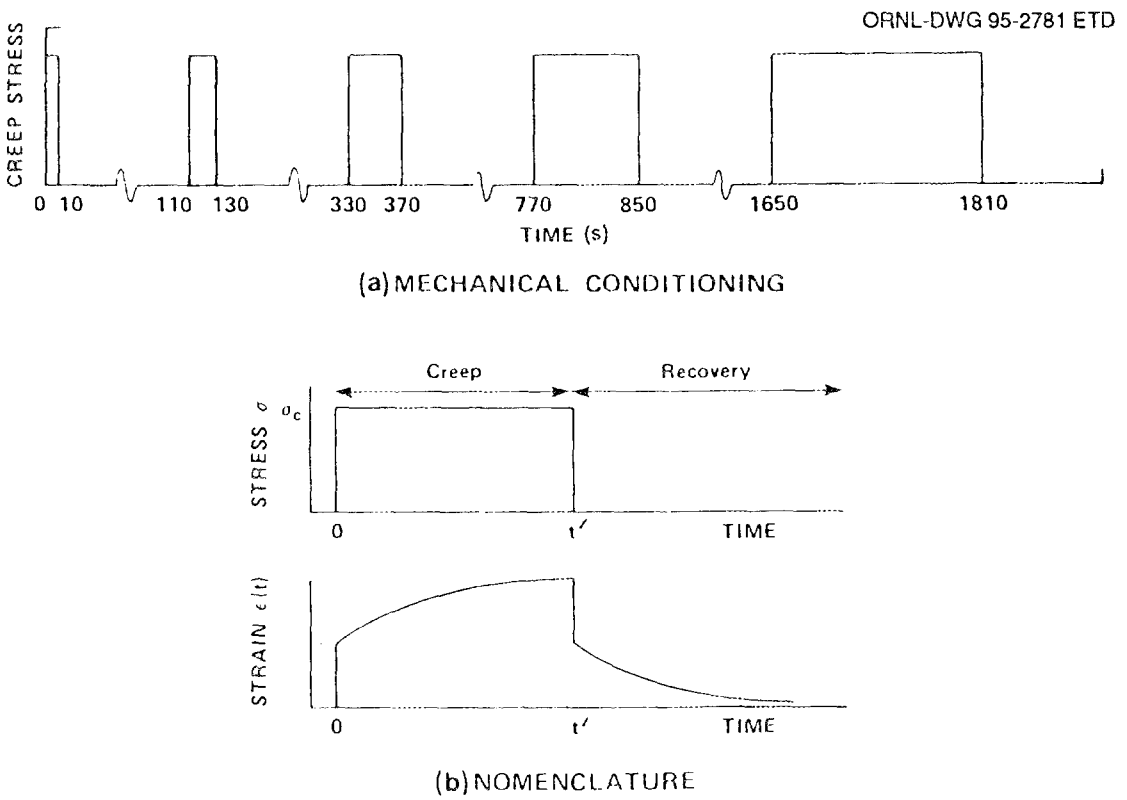

Fig. 4.11. (*a*) Mechanical conditioning history as (*b*) sequence of creep-recovery periods. *Source*: Jerina et al., 1979.

Moisture affects creep of polymers and polymeric resins in manners that are somewhat analogous to those due to temperature. A reasonably detailed exposition of these effects is given in Chap. 6.

4.5 CONCLUDING REMARKS

The experimental evaluation of creep of polymeric composites is essential for the construction of constitutive models of their response. These models may consist of various versions of viscoelasticity and viscoplasticity and were proven to possess reasonable, though limited, predictive capabilities for the deformations that ensue the application of stresses and the imposition of environmental exposures. The validity of those predictions diminishes with increasing stress amplitudes and levels of environmental exposure due to the onset of various time-dependent damage mechanisms, which are not considered by the above theoretical models. In addition, the foregoing mechanisms bring about a substantial increase in the data scatter, which cannot be incorporated within the existing deterministic models.

The circumstances are even less satisfactory concerning predictions of durability, which contain the same degree of uncertainty that exists with regard to fatigue.

Nevertheless, the construction of a rational model on the foundation of a well-conceived data base enables the derivation of expressions that provide at least the appropriate formats for predicting the material response. All such predictions should, of course, be subjected to subsequent verification tests.

REFERENCES

Alkonis, J. J., and MacKnight, W. J. 1983. *Introduction to Polymer Viscoelasticity*, Wiley-Interscience, New York.

Ashby, M. F., and Jones, D. R. H. 1986. *Engineering Materials 2*, Pergamon Press, Oxford, pp. 226–27.

Billmeyer, F. W. 1971. *Textbook of Polymer Science*, 2d. ed., Wiley-Interscience, New York.

Biot, M. A. 1954. "Theory of Stress-Strain Relations in Anisotropic Viscoelasticity and Relaxation Phenomena," *J. Appl. Phys.* **25**(11), 1385–91.

Biot, M. A. 1958. "Linear Thermodynamics and the Mechanics of Solids," *Proceedings of the Third U.S. National Congress of Applied Mechanics*, American Society of Mechanical Engineers.

Boller, K. H. 1957. *Tensile Stress Rupture and Creep Characteristics of Two Glass-Fabric-Base Plastic Laminates*, Forest Products Laboratory, Madison, Wisconsin, 1957.

Bueche, F. 1954. "The Viscoelastic Properties of Plastics," *J. Chem. Phys.* **22**(4), 603–10.

Charles, R. J. 1958*a*. "Static Fatigue of Glass I," *J. Appl. Phys.* **29**(11), 1549–53.

Charles, R. J. 1958*b*. "Static Fatigue of Glass II," *J. Appl. Phys.* **29**(11), 1554–60.

Chiao, C. C., Sherry, R. J., and Hetherington, N. W. 1977. "Experimental Verification of an Accelerated Test for Predicting the Lifetime of Organic Fiber Composites," *J. Compos. Mater.* **11**, 79–91.

Christensen, R. M. 1979. *Mechanics of Composite Materials*, J. Wiley & Sons, New York.

Christensen, R. M. 1982. *Theory of Viscoelasticity*, 2d ed., Academic Press, New York.

Christensen, R. M. 1994. "Heterogeneous Material Mechanics at Various Scales," *Mechanics USA 1994*, ed. A. S. Kobayahi, *Proceedings of the Twelfth U.S. National Congress of Applied Mechanics, 1994 Annual Supplement to Applied Mechanics Review*, AMR **146**, S20–S33.

Christensen, R. M., and Glaser, R. E. 1994. "Life Prediction for Graphite Epoxy Fiber Composites," *Mech. Res. Comm.* **21**(2), 121–30.

Dillard, D. A. 1991. "Viscoelastic Behavior of Laminated Composite Materials," *Fatigue of Composite Materials*, ed. K. L. Reifsnider, Elsevier Applied Science Publishers, Ltd., England, 339–84.

Dillard, D. A., and Brinson, H. F. 1983. "A Numerical Procedure for Predicting Creep and Delayed Failures in Laminated Composites," *Long Term Behavior of Composites*, ed. T. K. O'Brien, ASTM STP **813**, American Society for Testing and Materials, Philadelphia, pp. 23–37.

Dillard, D. A., Morris, D. A., and Brinson, H. F. 1982. "Predicting Viscoelastic Response and Delayed Failures in General Laminated Composites," *Composite Materials: Testing and Design*, 6th Conference, ed. I. M. Daniel, ASTM 787, American Society for Testing and Materials, Philadelphia, pp. 357–70.

Findley, W. N., Lai, J. S., and Onaran, K. 1976. *Creep and Relaxation of Nonlinear Viscoelastic Materials*, North-Holland Publishing Co., Amsterdam.

Findley, W. N., and Peterson, D. B. 1958. "Prediction of Long-Time Creep with Ten-Year Creep Data on Four Plastic Laminates," *Proceedings of the ASTM* **58**, 841–61.

Gibson, R. F. 1994. *Principles of Composite Material Mechanics*, McGraw Hill, New York.

Green, A. E., and Rivlin, R. S. 1957. "The Mechanics of Nonlinear Materials with Memory, Part I," *Archive for Rational Mechanics and Analysis* **1**, 1–21.

Green, A. E., and Rivlin, R. S. 1960. "The Mechanics of Nonlinear Materials with Memory, Part III," *Archive for Rational Mechanics and Analysis* **4**, 387–404.

Green, A. E., Rivlin, R. S., and Spencer, A. J. M. 1959. "The Mechanics of Nonlinear Materials with Memory, Part II," *Archive for Rational Mechanics and Analysis* **3**, 82–90.

deGroot, S. R., and Mazure, P. 1984. *Non-Equilibrium Thermodynamics*, Dover, New York.

Halpin, J. C. 1968. "Introduction to Viscoelasticity," in *Composite Materials Workshop*, ed. Tsai, Halpin, and Pagano, Technomic Publishing Co., Lancaster, Pennsylvania, pp. 87–152.

Harper, B. D., and Weitsman, Y. 1985. "Characterization of Thermorheologically Complex Materials," *Journal of Rheology* **29**(1), 49–68.

Jerina, K. L., Alexander, R. M., and Schapery, R. A. 1979. *Viscoelastic Deformation and Failure Behavior of Automotive Composites*, Texas A & M University, Mechanics and Materials Center Report MM 3979-79-4, November 1979.

Knauss, W. G., and Emri, I. 1987. "Volume Change and the Non-Linear Thermo-Viscoelastic Constitution of Polymers," *Polymer Eng. Sci.* **27**, 86–100.

Lee, E. H. 1955. "Stress Analysis in Viscoelastic Bodies," *Quart. Appl. Math.* **13**, 183–90.

Lou, Y. C., and Schapery, R. A. 1971. "Viscoelastic Characterization of a Nonlinear Fiber-Reinforced Plastic," *J. Comp. Mater.* **5**, 208–34.

Myers, F. A., Cama, F. C., and Sternstein, S. S. 1976. "Mechanically Enhanced Aging of Glassy Polymers," *Annals of the New York Academy of Sciences* **279**, 94–99.

Noll, W. 1958. "A Mathematical Theory of the Mechanical Behavior of Continuous Media," *Archive for Rational Mechanics and Analysis* **2**, 197–226.

Onaran, K., and Findley, W. N. 1965. "Combined Stress Creep Experiments on a Non-linear Viscoelastic Material to Determine the Kernel Functions for a Multiple Integral Representation of Creep," *Transactions of the Society of Rheology* **9**(2), 299–327.

Peretz, D., and Weitsman, Y. 1982. "Nonlinear Viscoelastic Characterization of FM-73 Adhesive," *Journal of Rheology* **26**(3), 245–61.

Peretz, D., and Weitsman, Y. 1983. "The Nonlinear Thermoviscoelastic Characterization of FM-73 Adhesives," *Journal of Rheology* **27**(2), 97–114.

Pipkin, A. C. 1972. *Lectures on Viscoelasticity Theory*, Springer-Verlag, Berlin.

Prigogine, I. 1967. *Thermodynamics of Irreversible Process*, Wiley-Interscience, New York.

Rouse, P. E. 1953. "A Theory of the Linear Viscoelastic Properties of Dilute Solutions of Coiling Polymers," *Journal of Chem. Phys.* **21**(7), 1272–80.

Rudin, A. 1982. *The Elements of Polymer Science and Engineering*, Academic Press, New York.

Schapery, R. A. 1962. "Approximate Methods of Transform Inversion for Viscoelastic Stress Analysis," *Proceedings of the Fourth U.S. National Congress of Applied Mechanics*, pp. 1075–85.

Schapery, R. A. 1964. "Application of Thermodynamics to Thermomechanical, Fracture, and Birefringent Phenomena in Viscoelastic Media," *J. Appl. Phys.* **35**(3), 1451–65.

Schapery, R. A. 1965. "A Method of Viscoelastic Stress Analysis Using Elastic Solutions," *J. Franklin Inst.* **279**(4), 268–89.

Schapery, R. A. 1966. "An Engineering Theory of Nonlinear Viscoelasticity with Applications," *International Journal of Solids and Structures* **2**, 407–25.

Schapery, R. A. 1968. "Stress Analysis of Viscoelastic Composite Materials," *Composite Materials Workshop*, ed. Tsai, Halpin, and Pagano. Technomic Publishing Co., Lancaster, Pennsylvania, pp. 153–92.

Schapery, R. A. 1969. *Further Development of the Thermodynamic Constitutive Theory: Stress Formulation*, Purdue University, Report AA and ES 69-2 (AFML Contract F33615-67-C-1412), Lafayette, Indiana.

Schapery, R. A. 1975*a*. "A Theory of Crack Initiation and Growth in Viscoelastic Media. I. Theoretical Development," *Int. J. Fract.* **11**(1), 141–59.

Schapery, R. A. 1975*b*. "A Theory of Crack Initiation and Growth in Viscoelastic Media. II. Approximate Methods of Analysis," *Int. J. Fract.* **11**(3), 369–88.

Schapery, R. A. 1975*c*. "A Theory of Crack Initiation and Growth in Viscoelastic Media. III. Analysis of Continuous Growth," *Int. J. Fract.* **11**(4), 549–62.

Schapery, R. A. 1992. "On Nonlinear Viscoelastic Constitutived Equations for Composite Materials," *Proceedings of the Seventh International Congress on Experimental Mechanics, Las Vegas, June 8–11, 1992*, pp. 9–21, The Society for Experimental Mechanics, Inc., Bethel, Connecticut.

Sternstein, S. S. 1976. "Homogeneous and Inhomogeneous Properties of Glassy Polymers," *Polymer Preprints* **17**, 136–41.

Struik, L. C. E. 1978. *Physical Aging in Amorphous Polymers and Other Materials*, Elsevier Applied Science Publishers, Ltd., England, p. 33.

Sun, C. T., and Chen, J. L. 1989. "A Simple Flow Rule for Characterizing Nonlinear Behavior of Fiber Composites," *J. Compos. Mater.* **23**(10), 1009–20.

Sun, C. T., and Wang, C. 1991. "Characterization of APC-2 Thermoplastic Composite Under Forming Temperatures," *Proceedings of the Thirty-Sixth International SAMPE Symposium, San Diego, California*, pp. 1602–16.

Suvorova, J. V. 1985. "The Influence of Time and Temperature on the Reinforced Plastic Strength," *Handbook of Composites*, ed. G. C. Sih and A. M. Skudra, Vol. 3, Elsevier Applied Science Publishers, Ltd., England, pp. 177–213.

Wang, C., Sun, C. T., and Gates, T. S. 1990. "Elastic Viscoplastic Behavior of Fiber-Reinforced Thermoplastic Composites," *Proceedings of the Thirty-First AIAA, Structures, Structural Dynamics and Materials Conference, Long Beach, California, April 2–4, 1990*, pp. 578–86.

Xiao, X. 1987. *Viscoelastic Characterization of Thermoplastic Matrix Composites*, Ph.D. Thesis, Free University of Brussels, November 1987.

Yoon, K. J., and Sun, C. T. 1991. "Characterization of Elastic-Viscoplastic Properties of an AS4/PEEK Thermoplastic Composite," *J. Comp. Mater.* **25**(10), 1277–96.

Zhurkov, S. N. 1965. "Kinetic Concept of the Strength of Solids," *Int. J. Fract. Mech.* **1**, 311–23.

Zimm, B. H. 1956. "Dynamics of Polymer Molecules in Dilute Solution: Viscoelasticity, Flow Birefringence and Dielectric Loss," *J. Chem. Phys.* **24**(2), 269–78.

5. IMPACT RESPONSE AND DAMAGE IN COMPOSITE PLATES

C. T. Sun
Purdue University

5.1 INTRODUCTION

Except for braided composites and three-dimensional (3-D) carbon-carbon composites, most composite structures are two-dimensional (2-D) in nature. That is, they are constructed to take stresses in the planar directions, and there are no through-the-thickness fiber reinforcements. Because of this weakness, many "2-D" composite structures are susceptible to impact damage.

In the study of impact of composite structures, most researchers have chosen to consider the generic case involving a flat composite plate subjected to impact of a relatively rigid impactor. Moreover, only transverse impact (impact velocity is perpendicular to the plate) was considered because it represents the most severe impact condition. Even with such a simplified structural configuration and loading condition, the resulting impact response and damage are still extremely complicated. Further simplification of the problem is desirable.

Key impact responses are identified as

- contact force (magnitude and duration),
- wave motion, and
- failure modes and damage area.

For a low-velocity impact, we may assume that the contact time is long compared with the period of the lowest mode of vibration of the target plate and that wave propagation induced by impact can be neglected. In addition, static failure criteria are valid for low-velocity impact.

The assumptions adopted in conjunction with low-velocity impact significantly simplify the analysis of impact problems. Even so, low-velocity impact problems are still largely unsolved, especially impact damage predictions. A large number of papers have investigated different aspects of impact of composites. An excellent literature survey has been provided by Abrate (1991).

The purpose of this chapter is to summarize the methods (both analytical and experimental) that have been successfully employed in the study of impact of composites. In addition, the major results obtained so far are discussed.

5.2 CONTACT BEHAVIOR

The transfer of energy from a moving projectile to a target composite plate is through the contact of the two bodies. The result of such contact is a local deformation (indentation) in the composite that, in turn, gives rise to the contact force plus the global deformation that arises due to the contact force.

To analyze the impact response and damage in the composite plate, the contact behavior must be modeled first. The classical Hertzian contact law between an elastic sphere or cylinder and an elastic half-space has been used by many authors for the study of impact of homogeneous isotropic materials [see Goldsmith (1960)]. Since laminate composite plates are anisotropic and nonhomogeneous in the thickness direction, direct applications of the classical Hertzian contact formula are questionable.

There are two general approaches toward modeling contact behavior. The first approach resorts to performing indentation tests from which the load-indentation relation is established. The second approach relies on the analysis of the contact problem to derive the load-indentation relation. Linear elasticity is assumed. In the following subsections, these two approaches are discussed.

5.2.1 Indentation Test

Contact problems are highly nonlinear mathematically and are very difficult to solve even if the contacting bodies are linearly elastic and geometrically simple. The degree of difficulty increases if damage, such as permanent indentation, is to be considered. For indentors that have irregular shapes, analytical solutions for the contact problem would be prohibited.

To circumvent the aforementioned difficulties, Yang and Sun (1983) first proposed conducting indentation tests to obtain load-indentation curves for loading, unloading, and reloading. Although they used only spherical indentors to test laminates of carbon/epoxy composites, the procedure is suitable for other material systems and indentors of other shapes.

The indentation test setup is shown schematically in Fig. 5.1. The linear variable differential transformer (LVDT) is mounted with a C bracket on the indentor. The displacement measured by the LVDT is the relative displacement between the indentor and the back surface of the specimen, or the indentation. Such a setup allows the specimen to maintain a traction-free back surface as in most impact tests.

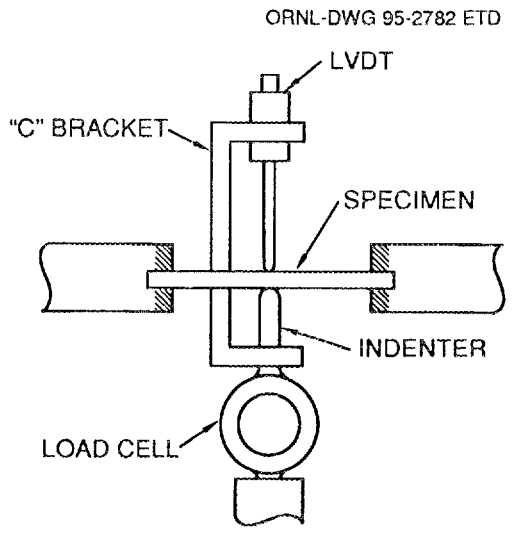

Fig. 5.1. Schematic diagram for indentation test setup.

There are three major parts of the contact force-indentation relation, that is, loading, unloading and reloading segments, as shown in Fig. 5.2. The loading curve can be obtained by monotonic loading. The unloading and reloading curves depend on the maximum contact force (F_m) at which unloading begins. For modeling the unloading behavior, a few unloading curves corresponding to different values of F_m must be generated.

5.2.2 Modeling Contact Behavior

The classical Hertzian contact law between an elastic sphere and elastic half-space is

$$F = k\alpha^{3/2} , \tag{5.1}$$

where F is the contact force, α is indentation, and the contact rigidity k is given by

$$k = \frac{4}{3} R_s^{1/2} \left[\frac{1-\nu_s^2}{E_s} + \frac{1-\nu_t^2}{E_t} \right]^{-1} . \tag{5.2}$$

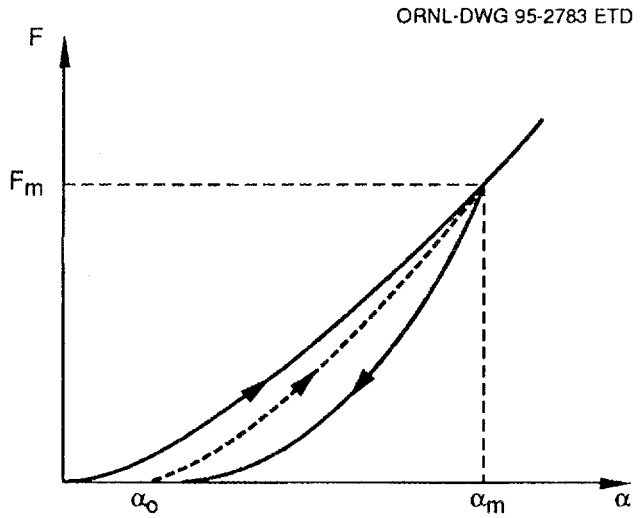

Fig. 5.2. Loading, unloading, and reloading curves.

In Eq. (5.2), R_s is the radius of the sphere, v is Poisson's ratio, E is Young's modulus, and subscripts s and t indicate the sphere and the target, respectively.

A modified contact rigidity for composite materials was proposed by Sun (1977) as

$$k = \frac{4}{3} R_s^{1/2} \left[\frac{1-\nu_s^2}{E_s} + \frac{1}{E_3} \right]^{-1} , \tag{5.3}$$

where E_3 is the transverse modulus of the composite. This expression is not very accurate, especially for high contact forces.

Using indentation test data, Yang and Sun (1983) proposed the following contact models:

- Loading $\quad F = k\alpha^n$, (5.4)
- Unloading $\quad F = F_m \left(\frac{\alpha - \alpha_0}{\alpha_m - \alpha_0} \right)^q$, (5.5)
- Reloading $\quad F = k_I (\alpha - \alpha_0)^p$. (5.6)

For glass-epoxy and graphite-epoxy, they found that n = 1.5, q = 2.5, and p = 1.5 provided a good fit to the data. The permanent indentation α_0 can be written as a function of α_m as

$$\frac{\alpha_0}{\alpha_m} = 1 - \left(\frac{\alpha_{cr}}{\alpha_m} \right)^{2/5} , \qquad \alpha_0 = 0 \quad \text{if} \quad \alpha_m \le \alpha_{cr} . \tag{5.7}$$

The value α_{cr} is to be determined from the test data.

The reloading rigidity k_1 in Eq. (5.6) is determined if the unloading conditions (F_m, α_m and α_0) are specified; that is (for p = 1.5),

$$k_1 = \frac{F_m}{(\alpha_m - \alpha_0)^{1.5}} \quad . \tag{5.8}$$

An alternative expression for the permanent indentation α_0 was proposed by Tan and Sun (1985) as

$$\alpha_0 = s_p(\alpha_m - \alpha_p) \ , \tag{5.9}$$

where s_p and α_p are to be determined from indentation test data. It is interesting to note that α_0 is linearly related to α_m.

Figures 5.3 and 5.4 are typical loading and unloading curves, respectively, for a graphite-epoxy composite laminate indented with a 12.7-mm-diam steel indentor obtained by Tan and Sun (1985). Figure 5.5 is a typical curve for permanent indentation α_0 vs the maximum indentation α_m [see Eq. (5.9)]. The model predictions are excellent.

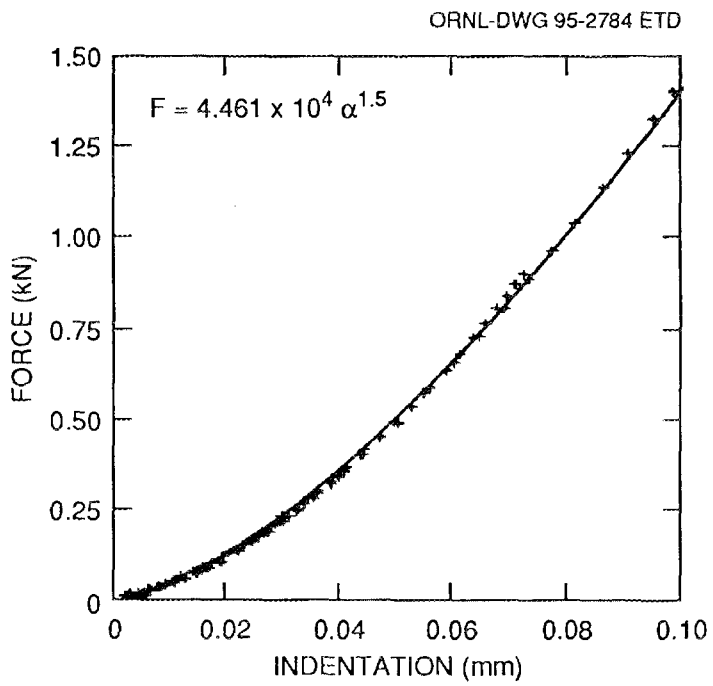

Fig. 5.3. Loading curve for $[0/45/0/-45/0]_{2s}$ graphite-epoxy laminate with 12.7-mm spherical indentor. Solid line is the model fit.

This contact model was used successfully by Gu and Sun (1987*b*) to describe the contact behavior between steel balls and SMC-R50.

5.2.3 Analysis of Contact Problems

Contact problems have attracted the attention of many authors [see Johnson (1987)]. Of relevance to our interest here is the contact between an indentor and a beam, plate, or shell. Many authors [Keer and Miller (1983), Sun and Sankar (1985), Keer and Schonberg (1986), Sankar (1987 and 1989)] have studied the effect of structural deflection on local contact behavior. In general, a flexible structure tends to result in greater contact areas and, consequently, higher contact rigidities.

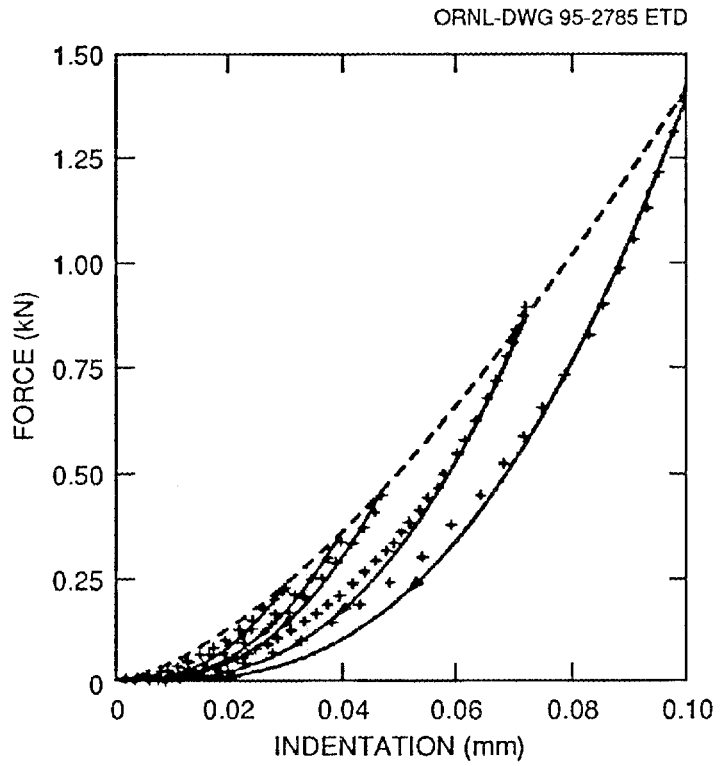

Fig. 5.4. Unloading curves for $[0/45/0/-45/0]_{2s}$ graphite-epoxy laminate with 12.7-mm spherical indentor.

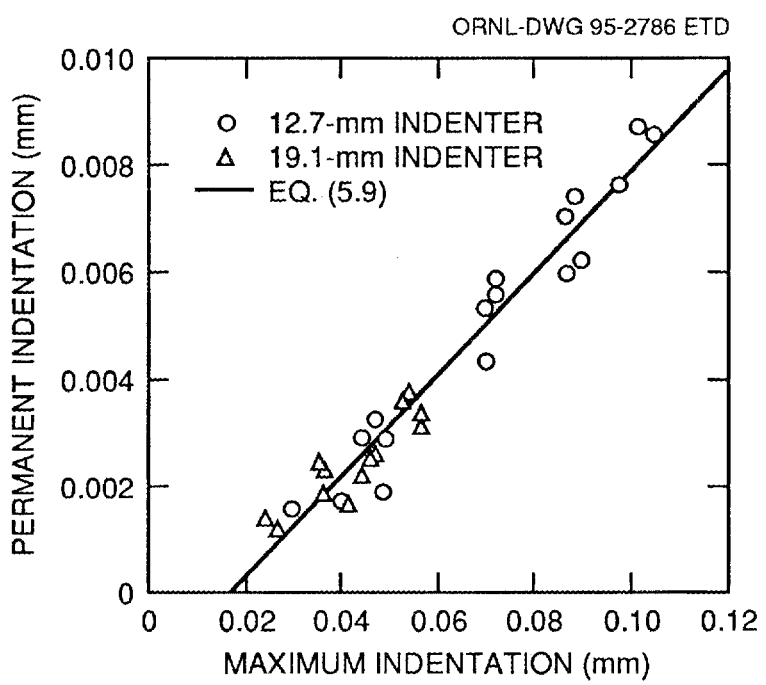

Fig. 5.5. Relation between α_0 and α_m (s_p = 0.094, α_p = 0.0167 mm).

Recently, Wu and Yen (1994) solved the problem of elastic contact between a composite laminate and a rigid sphere using an exact Green's function for the laminate. Their solutions indicate that the contact force is proportional to the transverse modulus of elasticity E_3 of the laminate. The effects of other moduli on the contact force-indentation relation are insignificant. It was also found that change of stacking sequence and span of the composite plate did not influence the contact force-indentation relation. This finding is consistent with the indentation test results obtained by Yang and Sun (1983).

5.3 IMPACT TESTING METHODS

In this section, several commonly used experimental setups for impact testing are presented. Impact velocity as well as contact force measurements are also discussed.

5.3.1 Setups for Impact Testing

Over the years, several basic types of apparatus have been used to generate impact in order to simulate foreign object impact phenomena. They are gas gun, drop-weight tower, pendulum, and cantilever type apparatus.

Generally speaking, the gas-gun system (Fig. 5.6) is usually used to generate high impact speeds with small impactors. In this setup, a high-pressure air tank is used to give the impactor an initial velocity; the impactor then travels along the gun barrel and hits the target. Impact velocity is mostly measured through the use of a velocity measuring system, which consists of two light-emitting diodes (LEDs) and photo sensors. The travel time of the impactor between the two sets of sensors separated at a fixed distance is used to determine the impact velocity.

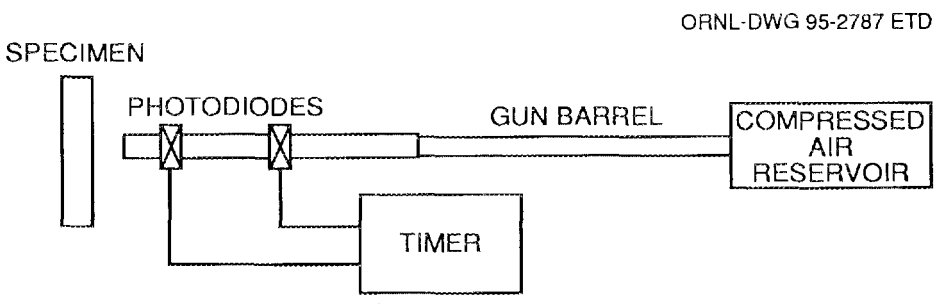

Fig. 5.6. Schematic gas-gun impact setup.

Many of the low-velocity impact tests are conducted with a drop-weight tower (Fig. 5.7). This apparatus allows the use of both small and heavy impactors. However, the velocity generated by this setup is usually within 10 m/s. An indentor (sphere, cylinder, etc.) is mounted under the drop-weight. During the experiment, the drop-weight is lifted to a certain level and then released; the impactor (and the drop-weight) then travels freely and hits the target. Velocity is usually measured by using the initial height of the drop-weight and free fall velocity equation $\left(V = \sqrt{2gh}\right)$. If more accurate impact velocity is sought, the deformation of the target is accounted for when using the velocity equation. Alternatively, the velocity measuring device described above can also be used here. Hodgkinson et al. (1982) used a laser-doppler velocimeter for precise measurement of the impactor during the entire contact event.

The pendulum tester consisting of a steel rod impactor with a string (Fig. 5.8) was also used by some researchers to generate low-velocity impact (Doyle, 1984). A cantilever apparatus shown in Fig. 5.9 was used by Lal (1983).

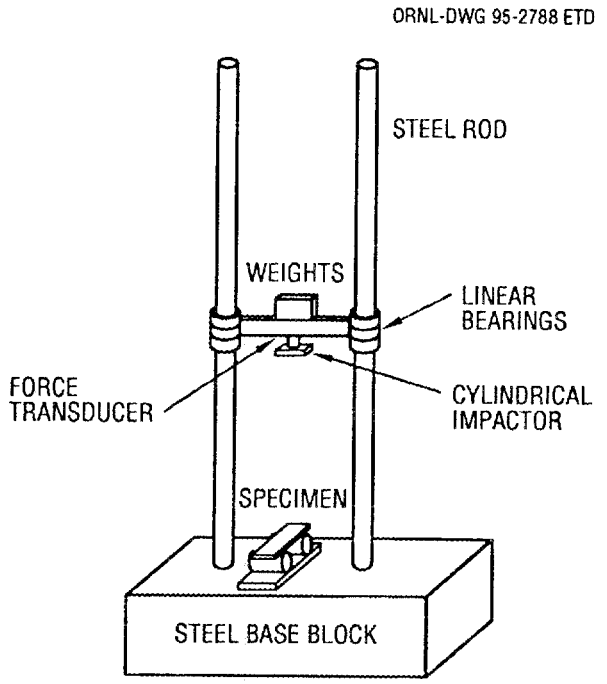

Fig. 5.7. Drop-weight tower impact tester.

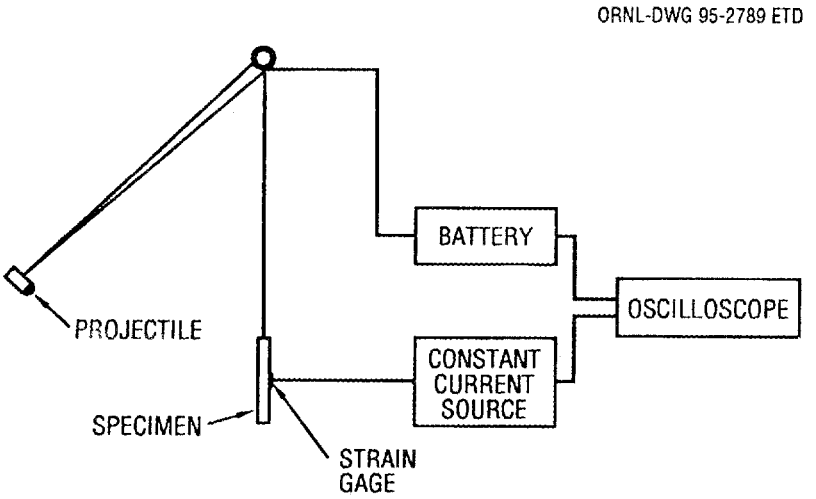

Fig. 5.8. Schematic pendulum-type impact tester.

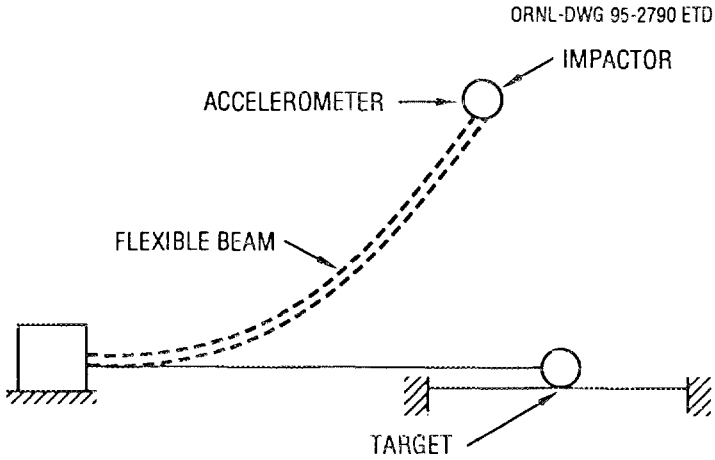

Fig. 5.9. Cantilever-type impact tester.

5.3.2 Contact Force Measurement

One of the most important parameters in impact response is contact force. The contact force history can be measured through a direct or indirect method. With the direct method, the response of the impactor, such as contact force and acceleration, is measured directly on the impactor. This is accomplished by mounting a force transducer (Tan and Sun, 1985) or an accelerometer (Lal, 1983) on the impactor. The signal from the force transducer or the accelerometer is recorded; from this record the contact force history is obtained. The direct method is simple because it does not require complicated structural analysis.

The indirect method measures the response of the target through the use of a strain gauge. Subsequently, structural analysis is performed to extract the contact force history based on the strain history at a certain location. This method was employed by Doyle (1984) and Chang and Sun (1989). The accuracy of the indirect method depends on the accuracy of the structural model and method of analysis. For impact that inflicts appreciable damage, this method is not recommended.

5.4 IMPACT RESPONSE

Motion and stresses in composite plates induced by impact have been investigated by many researchers. In most cases, the target plate was assumed to be elastic, and its elastic properties were not affected by impact damage.

The models used in impact analysis can be categorized as 3-D analysis, 2-D (beam, plate, and shell) analysis, and analysis using simple spring-mass models. Use of the 3-D elasticity model is motivated by the need to know local contact stresses, especially transverse normal stresses and transverse shear stresses over the thickness of the plate. Most 3-D analyses resorted to the use of finite elements (Sun and Liou, 1989; Wu and Chang, 1989; Finn and Springer, 1993) or numerical methods derived from variational formulations (Bogdanovich and Yarve, 1990). In dynamic analysis, the 3-D models are computationally very expensive.

Except for the contact zone, out-of-plane normal stress is negligible, and the plate can be modeled accurately with a shear deformable plate theory, such as the Mindlin/Reissner plate theory. The finite element method has been the most widely used method in dynamic impact analysis (Chen and Sun, 1985; Tan and Sun, 1985; Choi et al., 1991 and 1992). The Rayleigh-Ritz method was employed by a few researchers (Qian and Swanson, 1990; Cairns and Lagace, 1989). In general, contact force as well as stresses outside the contact zone are accurately described by the 2-D model.

The simplest representation of the impact problem is the use of spring-mass models. The assumption on which these models are based is that dynamic deformation of the target composite structure during impact is similar to static deformation. Thus, the stiffness of the structure can be represented by linear springs. These models are suitable for low-velocity impact in which contact time is much longer than the

period of the lowest mode of vibration, and wave propagation in the target structure is not important. Many authors have proposed and used spring-mass models, because of their simplicity, to determine contact force history (Lal, 1983; Caprino, 1984; Shivakumar et al., 1985; Sjoblom et al., 1988).

5.4.1 Effect of Wave Propagation Through the Plate Thickness

The notion that compression waves are reflected by a free surface into tensile waves may lead one to wonder whether wave propagation through the thickness of the plate can be neglected, as in the 2-D models. Since composite plates usually lack through-the-thickness reinforcement, the reflected tensile wave, if it exists, may cause delamination. This question must be answered before proper impact models can be selected.

Joshi and Sun (1985) used a 2-D plane strain model to investigate wave propagation produced by an impact load on a $[0_5/90_5/0_5]$ graphite-epoxy composite laminate. The finite element method was used in the analysis. The contact pressure distribution was assumed to be semicircular, as shown in Fig. 5.10. The time variation of the loading is a half sine function with total contact time of 40 μs.

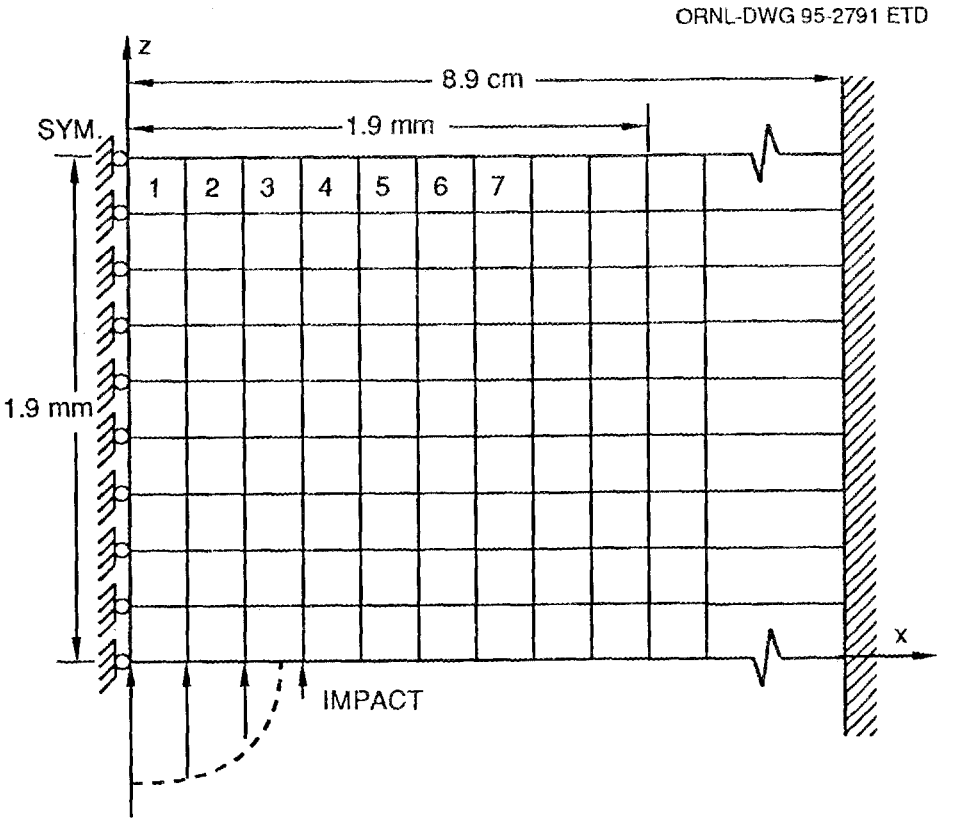

Fig. 5.10. Finite element mesh and stress output locations.

Figure 5.11 shows the transverse normal stress σ_{zz} distributions at time 20 μs at various sections. The numeral labels indicate the locations of the sections shown in Fig. 5.10. It is seen that the normal stress σ_{zz} stays basically compressive, and no significant tensile normal stress is produced by the impact. Thus, for impact of plates with a small contact area, stress waves would propagate as flexural waves away from the impact point. Hence, the danger of damage caused by reflected tensile waves from the back surface does not exist. Therefore, as far as wave motion is concerned, 3-D analysis is not necessary.

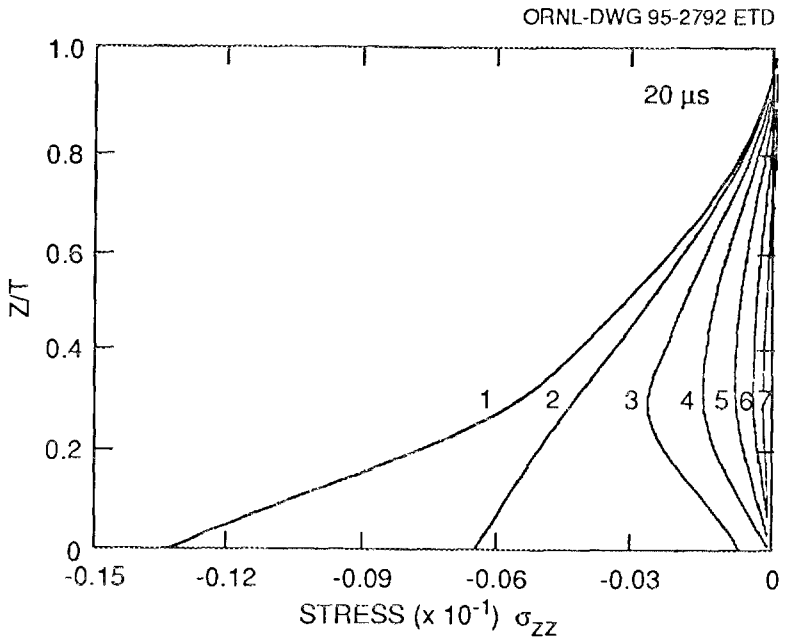

Fig. 5.11. Transverse normal stress distribution in $[0_5/90_5/0_5]$ layup.

5.4.2 2-D Analysis of Impact Response

The discussion in Sect. 5.4.1 helps to justify the use of plate (or beam or shell) theory to analyze impact response. Although wave propagation in the thickness-direction is neglected, plate theory is capable of describing flexural wave propagation very well.

To account for transverse shear deformation in composite plates, Mindlin/Reissner plate theory is usually used for impact analysis. If the finite element method is used, the equations of motion for the plate are given by

$$[M]\left\{\ddot{\Delta}\right\} + [k]\{\Delta\} = \{F\} \ , \tag{5.10}$$

where [M] is the mass matrix, [k] is the stiffness matrix, $\{\Delta\}$ is the nodal displacement vector, and $\{F\}$ is the force vector that contains the contact force F_c. The contact force should also satisfy the equation of motion of the impactor; that is,

$$M_s \ddot{w}_s + F_c = 0 \ , \tag{5.11}$$

where M_s and w_s are the mass and displacement of the impactor, respectively. In addition, the contact force F_c is related to the displacements of the plate and the impactor with a chosen contact model in which indentation α is calculated from

$$\alpha = w_s - \Delta \ , \tag{5.12}$$

where Δ is the nodal displacement of the target at the impact point.

The effects of geometrical nonlinearities have also been included in the finite element formulation (Chen and Sun, 1985; Obst and Kapania, 1992).

Figure 5.12 shows a comparison of the contact forces from a finite element analysis and from a low-velocity impact experiment obtained by Tan and Sun (1985). The target was 102- by 152-mm graphite-epoxy composite laminate subjected to the impact of a small mass at 2.92 m/s. The finite element prediction of the contact force history appears to be quite accurate. Also noted from Fig. 5.12 is the possibility of multiple contacts. This was also found by many authors (e.g., Cairns and Lagace, 1989).

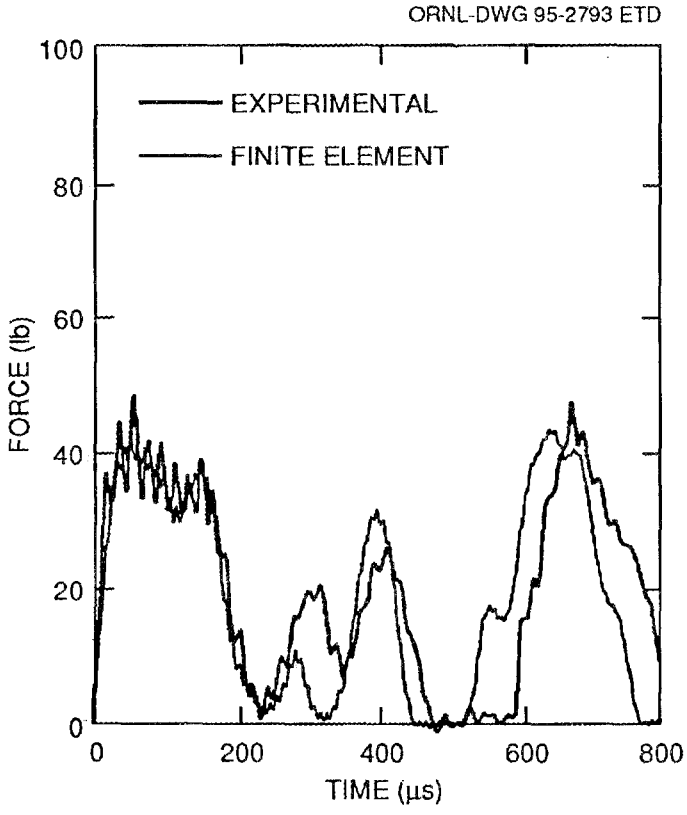

Fig. 5.12. Transducer response histories from experimental and finite element results up to 800 μs.

It is of interest to know the effects of impact velocity, impactor mass and shape, prestress and material system in the target plate on impact response. The following is a summary of numerical studies performed by Sun and Chen (1985), and Cairns and Lagace (1989).

- Effect of impact velocity—For a given impactor mass, the peak contact force is approximately proportional to the impact velocity. The contact duration is not affected by variations of impact velocity.
- Effect of impactor mass—For the same velocity, a larger mass would produce higher contact force and longer contact time. However, the increases are not proportional to the increase of the impactor mass. An impactor of smaller mass is more likely to experience multiple contacts.
- Effect of contact area (or Contact Rigidity)—Larger contact areas lead to higher contact rigidities. Impact responses such as contact force and deflection of the plate after impact are not affected appreciably by contact rigidity.
- Effect of prestress—It is well known that pretension in a plate has a stiffening effect, and precompression has a softening effect in plate bending. However, the first contact force (in the case of multiple contacts in a single impact event) is not influenced by prestress. In other words, the momentum transferred from the impactor to the plate is not influenced by prestress. As expected, pretension would reduce the deflection response, while precompression would increase the deflection response.

- Material systems—Most of the effects due to change of material systems in the plate can be related to the changes in contact rigidity and bending stiffness of the plate. The mass density of the plate is important. Lighter materials tend to lower the peak contact force and produce more multiple contacts and more oscillatory contact force history.

5.4.3 Spring-Mass Models of Impact

Of particular interest to practical engineers is the class of impact problems involving a large impactor mass impacting a light target at low velocities. The main characteristic of such impact is that the contact duration is much longer than the period of the fundamental mode of vibration of the target structure, and the resulting deflection of the target is similar to that produced by a static load. Such deformation is called quasi-static deformation. Quasi-static deformation has a unique shape except for the amplitude. Thus, to the impactor, the target acts more or less like a spring. The effective spring constant k_p can be approximated by the static stiffness of the target at the impact point or by considering the stiffness associated with the fundamental mode of free vibration.

Many spring-mass models have been introduced by various authors (Lee, 1940; McQuillen et al., 1976; Lal, 1983; Caprino, 1984; Shivakumar et al., 1985; Sjoblom et al., 1988; Sun and Jih, 1992). The most popular one is depicted in Fig. 5.13. This model has two degrees of freedom. The lower spring k_p represents the stiffness of the target, and the upper spring k_c accounts for the contact rigidity. The effective mass m_p of the target is derived from requiring the equivalence of kinetic energy between the spring-mass model and the original target based on the quasi-static deformation.

ORNL-DWG 95-2794 ETD

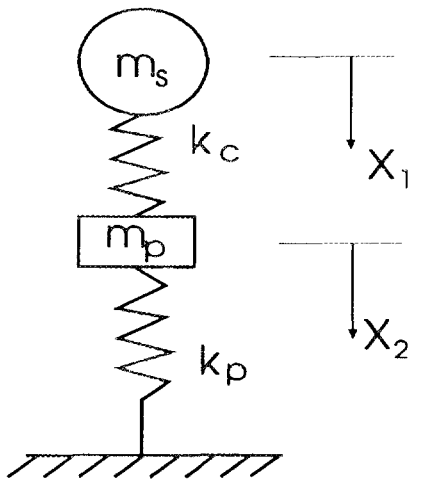

Fig. 5.13. Two-degrees-of-freedom spring-mass model for impact.

The equations of motion for the two-degrees-of-freedom system are given by

$$k_c\left(x_2 - x_1\right)^n = m_s \ddot{X}_1 \quad , \tag{5.13}$$

$$k_c\left(x_2 - x_1\right)^n + k_p x_2 = -m_p \ddot{x}_2 \, , \tag{5.14}$$

where n is to be the same as in the contact model, see Eq. (5.4).

Recognizing the indentation to be $\alpha = x_2 - x_1$, the contact force F is

$$F = k_c \alpha^n = k_c \left(x_2 - x_1\right)^n \quad . \tag{5.15}$$

Using the energy balance concept that the total kinetic energy of the impactor is equal to the maximum deformation energy stored in the springs, we have

$$\begin{aligned} \frac{1}{2} m_s V_0^2 &= \int_0^{\delta_{max}} k_p x_1 dx_1 + \int_0^{\alpha_{max}} F d\alpha \\ &= \frac{1}{2} k_p \left(\delta_{max}\right)^2 + k_c \frac{1}{n+1} \left(\alpha_{max}\right)^{n+1} , \end{aligned} \tag{5.16}$$

where V_0 is the initial impactor velocity. At $\delta = \delta_{max}$ and $\alpha = \alpha_{max}$, $F = F_{max}$ and

$$\delta_{max} = \frac{F_{max}}{k_p} , \text{ and } \left(\alpha_{max}\right)^n = \frac{F_{max}}{k_c} \quad . \tag{5.17}$$

Substituting Eq. (5.17) into Eq. (5.16), we obtain

$$\frac{1}{2} m_s V_0^2 = \frac{1}{2} \frac{F_{max}^2}{k_p} + \frac{1}{n+1} \frac{F_{max}^{(n+1)/n}}{k_c^{1/n}} \quad . \tag{5.18}$$

For a Hertzian type contact law, n = 1.5, and Eq. (5.18) reduces to

$$\frac{1}{2} m_s V_0^2 = \frac{1}{2} \frac{F_{max}^2}{k_p} + \frac{2}{5} \frac{F_{max}^{5/3}}{k_c^{2/3}} , \tag{5.19}$$

which was obtained by Greszczuk (1982).

In general, the contact spring constant k_c is much larger than the effective target stiffness k_p. Thus, the relation of Eq. (5.19) can be simplified to

$$k_p m_s V_0^2 = F_{max}^2 \quad . \tag{5.20}$$

This can easily be verified to be the solution of a single-degree-of-freedom system with a mass m, impacting a spring of stiffness k_p, at velocity V_0. For the single-degree-of-freedom spring-mass model, the contact duration is

$$T = \pi \sqrt{\frac{m}{k_p}} \quad . \tag{5.21}$$

5.4.4 Scaling

Impact response of composite plates involves a large number of variables. It is desirable to reduce the independent variables to a minimum. Such scaling rules have been investigated by a number of authors (Morton, 1988; Qian et al., 1990; and Sankar, 1992). Sankar (1992) employed a dimensionless impact model for systematic laminates for which the governing equations were expressed in terms of some

dimensionless parameters. He normalized the mass, length, and time dimensions by the plate mass m_p, length a, and the fundamental frequency of vibration ω_0 of the plate. He showed that the impact problem could be described in terms of five dimensionless parameters defined as

$$c = \frac{2(D_{12} + 2D_{66})a^2}{D_{11}b^2}, \quad D = \frac{D_{22}a^2}{D_{11}b^4},$$
$$\overline{m}_s = \frac{m_s}{m_p}, \quad \overline{V}_0 = \frac{V_0}{a\omega_0}, \quad \overline{k}_c = \frac{k_c\sqrt{a}}{m_p\omega_0^2}, \tag{5.22}$$

where $\overline{m}_s$, $\overline{V}_0$, $\overline{k}_c$ are the dimensionless impactor mass, impact velocity, and contact rigidity, respectively, and D_{ij} are bending stiffnesses of the laminated plate.

The scaling rules developed so far apply only to elastic response, not to impact damage.

5.5 LOW-VELOCITY IMPACT DAMAGE

Damage in composites inflicted by impact takes many different forms, depending on the material systems, material textures, impactor's mass and shape, impact velocity, and rigidity of impactor. In general, damage results either from direct contact stresses or from global deformation of the target, such as bending. For low-velocity impact, damage may occur beneath the surface of the composite structure, which may not be visible to the natural eye. At the high-velocity end, impact may cause complete penetration. In this section, attention will be focused on low-velocity impact damage.

5.5.1 Damage Inspection Methods

Many existing flaw detection methods can be employed for inspecting impact damage in composites. Some methods such as ultrasonic scanning are nondestructive, and some are destructive. For some composite structures such as laminated composite plates, the damage modes are well defined. Many existing methods (X-ray radiography and ultrasonic scanning) work very well. For SMC composites, in which impact damage is in the form of numerous small cracks, only an averaged damage area can be determined by these conventional methods.

1. Visual inspection—Some composites such as glass-epoxy, kevlar-epoxy, and SMC composites are translucent. Impact damage would change the degree of translucency. Using strong backlighting, the damage area can be determined by visual inspection (Malvern et al., 1978; Takeda et al., 1981; Chaturvedi and Sierakowski, 1985). Visual inspection methods are usually crude and can be used only in cases with large damage areas, such as delamination in composites.

2. Optical microscopy—Using an optical microscope to observe damage directly or to photograph the surface is also very popular among researchers. Except for the original surface of the specimen, to expose the internal damage, the specimen must be sectioned to perform the examination. Thus, it is a destructive method. The main advantage of this method is that details of the damage modes can be captured. The location of matrix cracks and delamination can be determined without ambiguity. The main disadvantages, besides being destructive, are that one can inspect only a finite number of sections and that the process is very labor intensive.

3. Ultrasonic scanning technique—Stress waves propagating through a solid can be distorted by the presence of a flaw (such as a crack or an inclusion) in the path of propagation. The stress wave can be reflected, partially transmitted, or diffracted by the flaw. By analyzing the reflected and/or the transmitted wave, and comparing with the original wave, information about the size and location of the flaw can be obtained.

Ultrasonic C-Scan is the most frequently used ultrasonic scanning technique in composites. It provides ultrasonic information in a plane normal to the ultrasonic beam (stress wave). It is basically 2-D

scanning and is very effective in determining sizable delamination. It usually cannot determine the precise location of the delamination crack.

4. X-Ray radiography—When a penetrant such as diodobutane (DDB) or S-Tetrabromethane (TBE) is injected into cracks in a damaged composite, the damaged region would absorb more X-rays. As a result, the damaged and undamaged regions would display different shades in the radiograph.

X-ray radiography is simple to use. It is very effective in displaying matrix and delamination cracks in laminates of unidirectional composites.

5. Deply technique—A quite novel technique was developed by Freeman (1982) for separating a cured graphite-epoxy laminate into its individual laminae while maintaining the integrity of each lamina. It was demonstrated that this deply technique was excellent for observing fiber breakage on a lamina-by-lamina basis. A combination of the deply technique and a marker technique (using a gold chloride solution to penetrate matrix cracks) can be used to identify the location and area of delamination.

5.5.2 Damage Modes and Mechanisms

Failure in a composite, regardless of load, is the result of excessive stresses. For transverse impact with a solid impactor, two types of deformation would take place, that is, local indentation and global flexural deformation of the target. The indentation produces a state of 3-D contact stresses near the impact site, and the global deformation produces bending, transverse shear, and membrane stresses. Among the components of the contact stresses, the transverse shear stress component is of particular importance because it may cause matrix cracking in the composite. Local contact stresses and global stresses may interact in the formation of impact damage. For example, the matrix cracks produced initially by the contact stresses may be forced into delamination crack propagation by the global stresses.

Impact damage modes depend on the construction or texture of the composite of the target. In general, they can be classified as matrix cracking, delamination, and fiber breakage. In the following, three types of composites are discussed separately.

5.5.2.1 Laminates of unidirectional composites

Laminates consisting of laminae of unidirectionally reinforced composite materials offer good multidirectional in-plane properties. They have been used in military as well as commercial airplanes. Impact response and damage of composite laminates have been extensively studied by many authors in the past 30 years. Because of the simple construction of composite laminates, the damage modes in this type of composite plate have been relatively well understood.

Figure 5.14 depicts typical major impact damage modes in composites laminates. They are classified as follows:

1. Matrix cracking—There are two types of matrix cracks. Transverse shear cracks are produced by high transverse shear stress associated with the concentrated contact force. They appear slanted against the plane of lamina and are concentrated in the neighborhood of the impact location. Another type of matrix crack is the bending crack produced by high bending stresses. Bending cracks usually appear on the opposite side of the impact site. They are parallel to the fiber direction and are perpendicular to the interface in the thickness direction.
2. Delamination—As discussed in Sect. 5.4.1, if the impact contact area is small and the contact duration is long as compared with the time for wave propagation over the thickness of the plate, the compressive wave produced by the dynamic contact cannot be reflected as a tensile wave of significant magnitude. In other words, delamination in a composite plate cannot be induced by through-the-thickness stress waves.

   The actual mechanism that gives rise to delamination in composites is branching of matrix cracks. A matrix crack (transverse shear or bending) appears first in a lamina; when it reaches the interface of the adjacent lamina, the crack turns into a delamination crack along the interface. This phenomenon has been discussed by many authors (Joshi and Sun, 1985; Sun and Rechak, 1988; to cite a few). Figure 5.15 shows delamination in the $[0_3/A/90_6/0_3]$ (Zheng and Sun, 1994). Symbol A in the layup indicates a thin adhesive film added to the laminate to suppress the transverse-shear-crack-induced

ORNL-DWG 95-2795 ETD

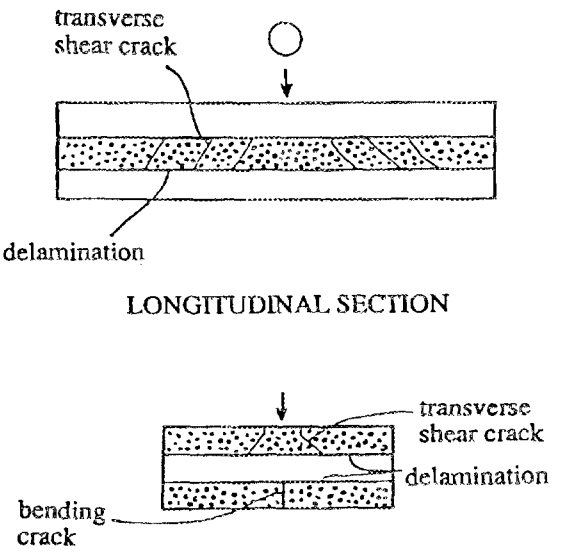

Fig. 5.14. Nomenclature of damage modes.

ORNL-DWG 95-2796 ETD

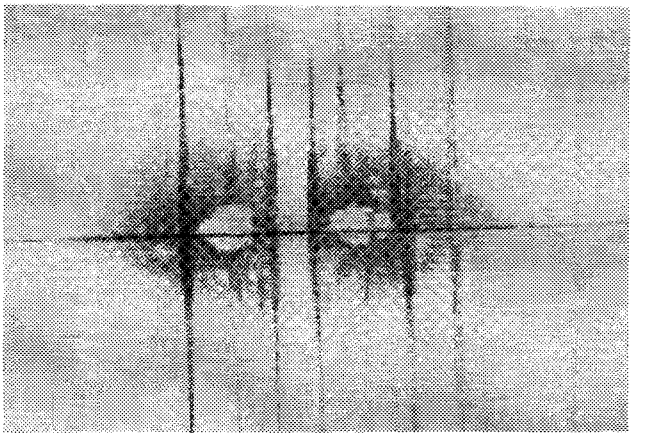

Fig. 5.15. X-ray radiograph of impact damage in $[0_3/A/90_6/0_3]$ graphite-epoxy laminate.

delamination. The horizontal line indicates the bending crack in the bottom 0° lamina. The vertical lines are transverse shear cracks in the 90° lamina. Note that the two delaminated regions may not be necessarily connected.

Additional X-ray radiographs of delamination for other stacking sequences of composite laminates were provided by Finn and Springer (1991).

Transverse-shear-induced delamination is usually smaller in size as compared with that of bending-induced delamination. These delamination cracks in different interfaces may eventually connect through transverse matrix cracks in the laminae and form a spiraling staircase damage pattern as observed by Gosse and Mori (1988).

3. Fiber breakage—Fiber breakage may occur in low-velocity impact if the impactor mass is large enough. Local contact stresses may be high enough to crush the fiber. Another possible mechanism causing fiber breakage is fiber microbuckling on the compression side of the composite plate during impact. This situation is particularly severe for curved panels or shell structures.

5.5.2.2 SMC composites

SMC composites are a polyester matrix reinforced with chopped-glass fibers about 1 in. long. The chopped fibers are randomly distributed in the plane of the panel. Thus, its mechanical properties can be regarded as transversely isotropic.

SMC composites have been used in automobile parts because of their relatively low cost, light weight, good moldability, dimensional stability, and good resistance to corrosive environments. The fiber content in an SMC composite can be varied. If the fiber is 50% by weight, then this SMC composite is labeled as SMC-R50.

Visible impact damage in an SMC includes numerous small cracks. Unlike laminates of unidirectional composites, SMC composites do not allow clear definition of delamination cracks. To determine the impact damage zone, some researchers have used the semitransparency of this material. When exposing the impacted specimen against a high-intensity light source, different shades in the damaged area (which tends to allow more transmission of light) can be approximately determined (Chaturvedi and Sierakowski, 1985).

Khetan and Chang (1983) investigated several methods for measuring impact damage in SMC-R35 panels. They concluded that the X-ray radiograph is not a reliable method for assessing impact damage in SMC panels for low-impact velocities because, at these velocities, internal cracks are generally not connected. As a result, the dye penetrant could not be absorbed properly by the panel to produce good radiographs. The ultrasonic C-Scan was also found inadequate due to the inherent material nonhomogeneity in SMC composites. They found a crack enhancement method (by coating the damaged SMC panel with a black dye) very capable of defining the surface damage area on the front and back sides of the impact panel.

Determination of the impact damage area in an SMC composite does not lead to an assessment of residual strength. Gu and Sun (1983) and Chaturvedi and Sierakowski (1985) pointed out that in general impact conditions, the size of an impact damage zone does not correlate to the reduction of strength. The degree of damage (degradation in mechanical properties) over the thickness of the panel as well as within the damage zone needs to be quantified.

To achieve this end, Gu and Sun (1983) proposed to use the change of thickness in the SMC panel after impact as a measurement of degradation in mechanical properties. They demonstrated that impact could induce thickness changes significant enough to allow accurate measurement. Relations between thickness change and reductions in the tensile modulus and strength were then established experimentally. Figures 5.16 and 5.17, respectively, present the residual Young's modulus and UTS vs thickness change obtained by Gu and Sun (1983) using SMC-R50 composite panels. Later, Gu and Sun (1987*a*) used the same approach to model the reduction of bending properties as a function of thickness change.

5.5.3 Quasi-Static Failure

In general, failure processes in composites are strain-rate dependent; that is, dynamic failure mechanisms and failure modes may be different from those of the static case. However, as in impact response, for low-velocity impact with a heavy impactor mass, the failure process has been found to be basically the same as under static loading.

Norman (1989) performed a comparison of delamination cracks produced by drop-weight impact and by static three-point bending. He used a beamlike $[90_5/0_5/90_5]$ AS4/3501-6 graphite-epoxy laminate clamped at both ends leaving a 10-cm span. The impactor mass ranged up to 3 kg. The drop heights were from 5 to 76 cm. Figure 5.18 presents the relation between the maximum contact force (measured by a transducer) and the resulting delamination crack length a. Comparing with statically produced delamination, the quasi-static nature of impact-induced delamination is evident.

Additional verifications of the quasi-static delamination in a laminated composite beam induced by low-velocity impact were provided by Jih and Sun (1993) and Sun and Jih (1992). Recently, Kwon and Sankar (1993) tested the load-deflection and impact damage behavior of some 32-ply quasi-isotropic and cross-ply composite laminated plates impacted with masses ranging from 1 to 15 kg and velocity up to 3 m/s. They concluded that under these impact conditions, both the load-deflection relation and impact damage were similar to those of static loading.

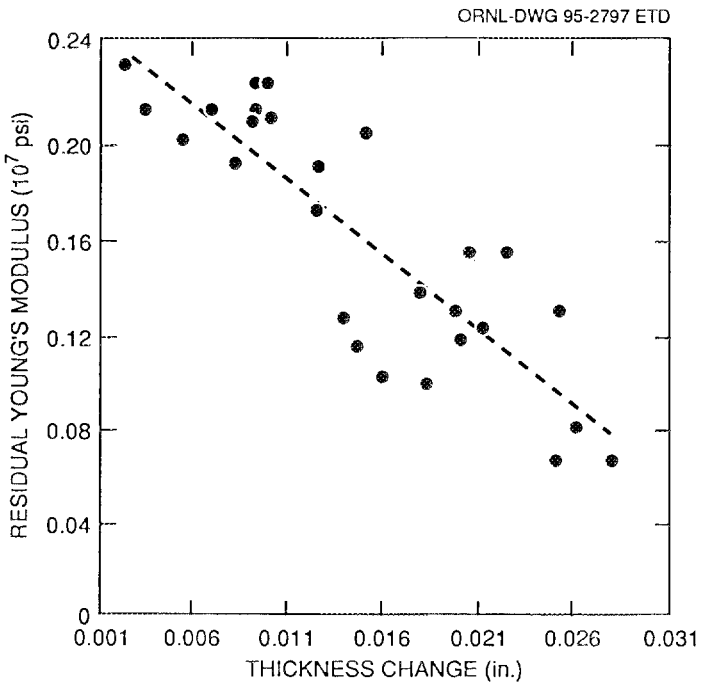

Fig. 5.16. Young's modulus vs thickness change after impact in SMC-R50 composite.

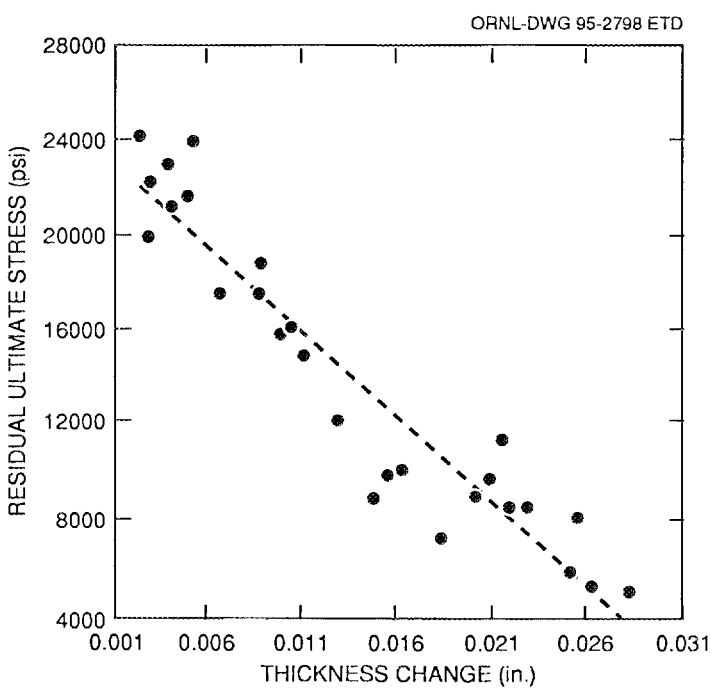

Fig. 5.17. Residual ultimate stress vs thickness change after impact in SMC-1250 composite.

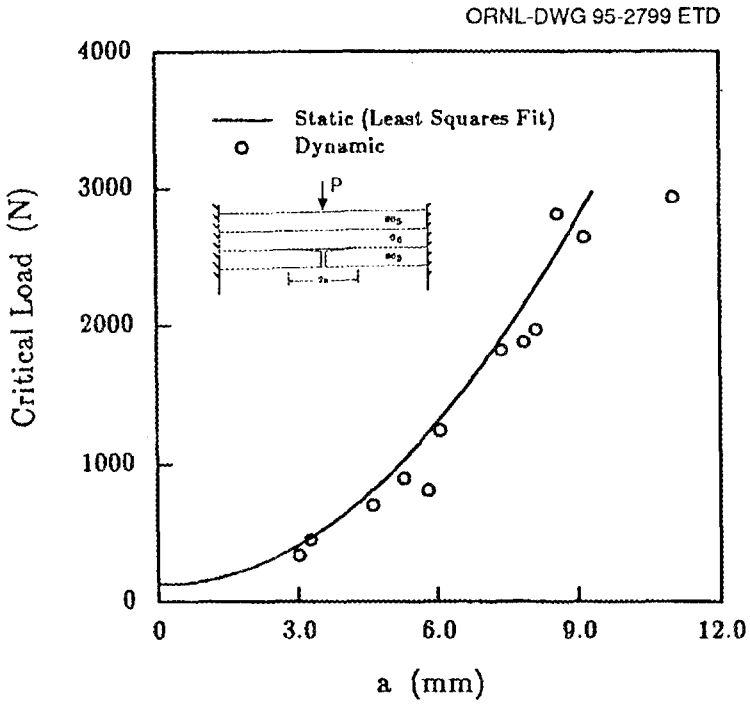

Fig. 5.18. Comparison of delamination caused by impact load and static load; a is delamination size, and critical load is peak impact force.

5.5.4 Prediction of Impact of Damage

An impact damage prediction consists of two parts: damage initiation and damage propagation. The prediction of damage initiation examines a damage-free structure and predicts the conditions under which damage is initiated. The prediction of damage propagation examines a structure with initial damage and predicts the conditions under which the initial damage would propagate.

In order to predict damage initiation and damage propagation, suitable failure criteria are needed. Since different damage modes result from different failure mechanisms, it is expected that different failure criteria must be used for the prediction of different damage modes. Thus, different composite systems may require different failure analysis methods.

5.5.4.1 Laminates of unidirectional composites

As discussed in Sect. 5.5.2.1, laminates of unidirectional composites have very clear failure modes: namely, intraply matrix cracking, delamination, and fiber breakage. For low-velocity impact, matrix cracking and delamination are of particular importance. The following failure criteria are for matrix failure and delamination failure.

1. Matrix cracking—Many failure criteria have been proposed for predicting failure in a composite lamina (Nahas, 1986). The most commonly used failure criteria for matrix cracking in impact dynamics are the maximum stress failure criterion, the maximum strain failure criterion, and the Hashin failure criterion.

   A composite lamina is usually treated as a transversely isotropic material in plane stress. Let x_1 be the fiber orientation and x_2 and x_3 be the transverse directions. The three failure criteria are stated as follows:

- Maximum stress

Matrix tensile mode $\sigma_{22} \geq Y$, (5.23)

Matrix compressive mode $\sigma_{22} \leq Y'$, (5.24)

where Y and Y′ are UTS and compressive strength for the lamina in the transverse direction.

- Maximum strain

Matrix tensile mode: $\varepsilon_{22} \geq Y_\varepsilon$, (5.25)

Matrix compressive mode: $\varepsilon_{22} \leq Y'_\varepsilon$, (5.26)

where Y_ε and Y'_ε are the ultimate tensile strain and compressive strains for the lamina in the transverse direction.

- Hashin

The 3-D Hashin failure criterion is stated as follows:

Matrix tensile mode ($\sigma_{22} + \sigma_{33} > 0$):

$$\frac{1}{Y}\left(\sigma_{22}+\sigma_{33}\right)^2 + \frac{1}{S_t^2}\left(\sigma_{23}^2 - \sigma_{22}\sigma_{33}\right) + \frac{1}{S_a^2}\left(\sigma_{12}^2 + \sigma_{13}^2\right) \geq 1 \ . \tag{5.27}$$

Matrix compressive mode $\left(\sigma_{22}+\sigma_{33} < 0\right)$:

$$\frac{1}{Y}\left(\left[\frac{Y}{2S_t}\right]^2 - 1\right)\left(\sigma_{22} + \sigma_{33}\right) + \frac{1}{4S_t^2}\left(\sigma_{22} + \sigma_{33}\right)^2 + \frac{1}{S_t^2}\left(\sigma_{32}^2 - \sigma_{22}\sigma_{33}\right) + \frac{1}{S_a^2}\left(\sigma_{12}^2 + \sigma_{13}^2\right) \geq 1 \ , \tag{5.28}$$

where S_t is the shear strength in the plane perpendicular to the fiber orientation, and S_a is the shear strength in the fiber plane.

For the plane stress case, the Hashin failure criterion reduces to the following:

Matrix tensile mode ($\sigma_{22} > 0$):

$$\left(\frac{\sigma_{22}}{Y}\right)^2 + \left(\frac{\sigma_{12}}{S_a}\right)^2 \geq 1 \ . \tag{5.29}$$

Matrix compressive mode ($\sigma_{22} < 0$):

$$\left(\frac{\sigma_{22}}{2S_t}\right)^2 + \left[\left(\frac{Y'}{2S_t}\right)^2 - 1\right]\frac{\sigma_{22}}{Y'} + \left(\frac{\sigma_{12}}{S_a}\right)^2 \geq 1 \ . \tag{5.30}$$

Hashin's failure criterion has been extensively used in the prediction of matrix cracking in composite structures subjected to impact loading. Choi et al. (1991, 1992) used this failure criterion to predict matrix cracking in a composite laminate subjected to a line impact load and point impact load. In their application, the ultimate strengths of the lamina Y, Y′, S_t, and S_a were chosen

to be the in situ strength of the considered lamina, and the stress components used were the average values along the thickness of the lamina. Wang and Yew (1990) also adopted the Hashin failure criterion in their prediction of matrix cracking.

2. Delamination—Prediction of delamination growth in composite laminates is the most important impact damage analysis. The occurrence of matrix cracks usually does not reduce the load-carrying capacity of the composite structure. However, the presence of delamination is a threat to the structural integrity of the composite laminate, especially under compression. Hence, a great deal of effort has been directed to predicting delamination in composite laminates.

   At present, there are two major approaches in predicting impact-induced delamination: the strength approach and the fracture mechanics approach.

   - Strength approach

     In the strength approach, the stress field in the impacted composite is first calculated. Based on the strength of material theory, those stress components that would contribute to the growth of delamination are identified. Then a failure criterion including all these stress components is used to check the initiation and propagation of delamination. Choi and Chang (1992) used this approach to predict delamination. The failure criterion used by them is expressed as

$$D_a \left\{ \left(\frac{{}^{n}\overline{\sigma_{23}}}{{}^{n}S_i} \right)^2 + \left(\frac{{}^{n}\overline{\sigma_{13}}}{{}^{n+1}S_i} \right)^2 + \left(\frac{{}^{n+1}\overline{\sigma_{22}}}{{}^{n+1}Y^*} \right)^2 \right\} \geq 1 , \tag{5.31}$$

     where D_a is an empirical constant that must be determined by experiment. The superscript n indicates the ply below the delamination and n + 1 is the ply above. In Eq. (5.31), the average stresses in the (n+1)th ply are defined as

$${}^{n+1}\overline{\sigma_{ij}} = \frac{1}{h_{n+1}} \int_{z_n}^{z_{n+1}} \sigma_{ij} dz \ ;$$

     $Y^* = Y$ if $\sigma_{22} \geq 0$, and $Y^* = Y'$ if $\sigma_{22} < 0$.

     This approach is simple to use because the failure criterion contains only the stress components that are directly obtainable through the finite element analysis. However, in order to successfully apply this kind of failure criterion, stresses must be calculated accurately, which often prompts the use of 3-D finite elements as in Choi and Chang (1992). Moreover, the fact that stresses are singular at the delamination front also poses difficulties.

   - Fracture mechanics approach

     A more rigorous and formal approach for delamination is the fracture mechanics approach. Strain energy release rate is used as a failure criterion that states that a delamination would grow if

$$G \geq G_c \ . \tag{5.32}$$

     If mixed modes are to be accounted for, some researchers have proposed the following fracture criterion

$$\left(\frac{G_I}{G_{Ic}} \right)^m + \left(\frac{G_{II}}{G_{IIc}} \right)^p \geq 1 , \tag{5.33}$$

     where G_I and G_{II} are strain energy release rates for Mode I and Mode II, respectively, and the indices m and p are usually chosen equal to 1. It should be noted that delamination cracks are often

interfacial cracks between different materials (because of different fiber orientation); G_I and G_{II} do not exist, as shown by Sun and Jih (1987). In using the finite element analysis to calculate G_I and G_{II}, a finite crack extension is usually assumed.

Liu (1993) used Eq. (5.33) with a 3-D finite element analysis to predict delamination. Salpekar (1993) also used the fracture mechanics approach in his investigation of impact-induced delamination.

Two-dimensional models have been employed to predict delamination growth due to low-velocity impact. Jih and Sun (1993) used a beam model to predict delamination growth in a composite laminate subjected to low-velocity impacts with a cylindrical impactor. The delamination crack length vs the impact velocity from their prediction matched very well with the experimental results. Figure 5.19 shows the comparison in a $[90_5/0_5/90_5]$ graphite-epoxy composite laminate obtained by Jih and Sun (1993). Sankar and Sonik (1994) proposed using plate theory to calculate strain energy release rate at the delamination front. Zheng and Sun (1994) used a double-plate finite element model to predict the delamination growth in a composite laminate subjected to low-velocity impact. In their double-plate model, they derived an expression for calculating the total strain energy release rate at the delamination front and used Eq. (5.32) to predict delamination growth. The calculation of strain energy release rate for using the double-plate model is as follows.

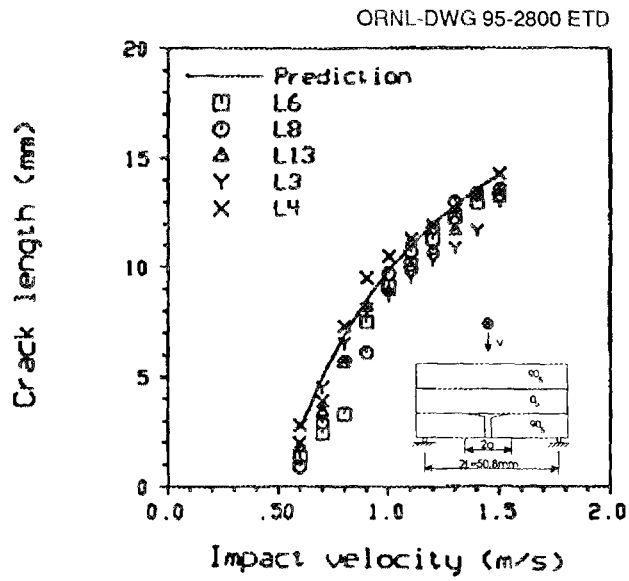

Fig. 5.19. Crack length vs impact velocity for $[90_5/0_5/90_5]$ laminate (Type Ia specimen) under drop-weight impact.

Consider the delamination front $c_1c_2c_3$ in Fig. 5.20. The energy released for a pair of nodes $c_2c'_2$ over a crack extension Δa is

$$W_{c_1c'_2} = \frac{1}{2}\sum_{i=1}^{5}\left(F_i u_i + F'_i u'_i\right) , \tag{5.34}$$

where i represents degree of freedom, and F_i, u_i, and F'_i, u'_i are generalized forces and displacements at the bottom and top plates, respectively.

ORNL-DWG 95-2801 ETD

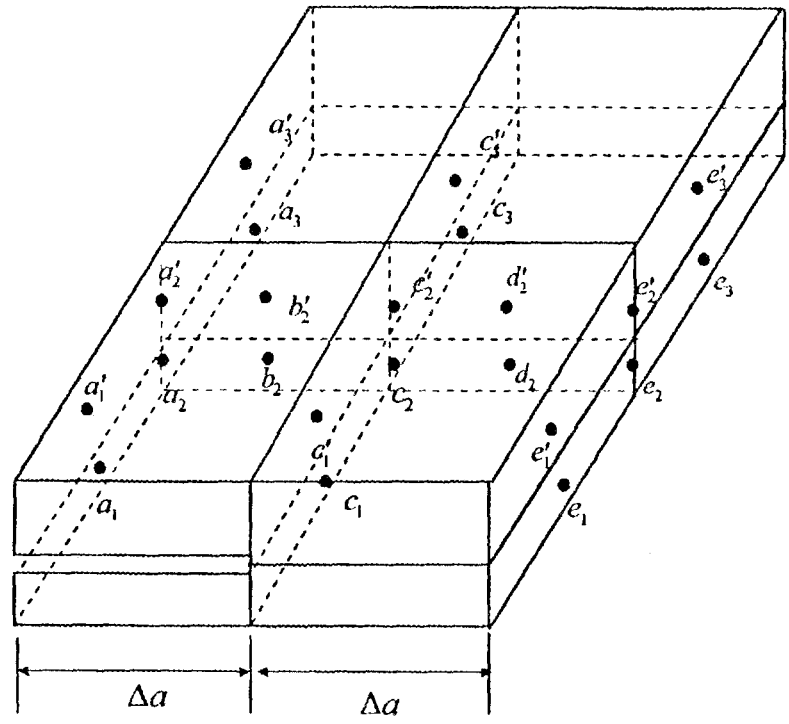

Fig. 5.20. Schematic double-plate model for delaminated plate.

The total energy released for the delamination front extended from $c_1c_2c_3$ (and $c_1'c_2'c_3'$) to $e_1e_2e_3$ (and $e_1'e_2'e_3'$) is

$$W_{total} = W_{c_2c_2'} + W_{d_2d_2'} + \frac{1}{2}\left(W_{c_1c_1'} + W_{c_cc_3'}\right) . \tag{5.35}$$

The corresponding area for this energy released is $A = \Delta a \times \overline{c_1c_3}$; thus, the strain energy release rate at the crack front c_1c_3 is

$$G = \frac{W_{total}}{A} . \tag{5.36}$$

Using Eqs. (5.32) and (5.36), Zheng and Sun (1994) predicted the delamination front in a composite laminate subjected to impact loading. The comparison between the experimental result and the prediction is presented in Fig. 5.21.

Besides the two aforementioned approaches, Finn and Springer (1993) used the available strain energy density concept for delamination prediction. The available strain energy density is contributed to by only those stress components that would affect the development of delamination.

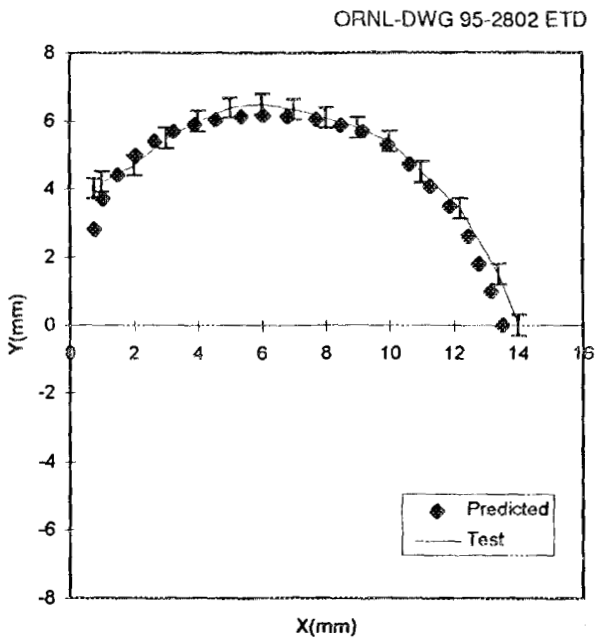

Fig. 5.21. Prediction of delamination front for $[0_3/A/90_6/0_3]$ for maximum impact force of 1000 N (A-FM1000 adhesive film). Test data are plotted with error bar.

5.5.4.2 SMC composites

Impact damage in SMC composites consists of numerous small cracks with no preferred orientations. In the damage zone, the residual material properties may vary [Gu and Sun (1983)]. Nevertheless, it is of interest to be able to predict the damage region for a given impact condition.

Gu and Sun (1987*b*) proposed the use of strain energy density to predict impact damage in SMC composites. They assumed that SMC composites might fail because of excessive deformation induced by impact. Further, they assumed that the dilatational strain energy U_v and distortional strain energy U_s make different contributions toward impact damage. If the Mindlin plate theory is used for the impact analysis, then

$$U = U_v + \beta U_s \ , \tag{5.37}$$

where β is a weighting coefficient; and

$$U_v = \frac{1-2\nu}{6E}\left(\sigma_{xx} + \sigma_{yy}\right)^2 \ ; \tag{5.38}$$

and

$$U_s = \frac{2(1+\nu)}{6E}\left(\sigma_{xx}^2 + \sigma_{xx}\sigma_{yy} + \sigma_{yy}^2\right) + \frac{1+\nu}{E}\left(\sigma_{xy}^2 + \sigma_{yz}^2 + \sigma_{xz}^2\right) . \tag{5.39}$$

Note that in the original paper by Gu and Sun (1987*a,b*), the expressions of U_v and U_s were misprinted.

Failure was assumed to occur when U reached a critical value U_{cr}. For an SMC-R50 composite, they found that $U_{cr} = 66$ in.-lb/in.^{3} and $\beta = 0.3$. This indicates that the dilatational energy is more destructive than the distortional energy.

5.5.5 Parameters Affecting Damage

Kinetic energy of the impactor cannot be used as a sole parameter to gauge impact damage (Husman et al., 1975). Impactor velocity and mass cannot be used as independent impact parameters either, although they are still subjects of study (Robinson and Davies, 1992). Recently, contact force has been proposed as an impact response and damage parameter by Jackson and Poe (1992) and Lagace et al. (1992). As reported by Jackson and Poe (1992), for large mass impacts at a given kinetic energy, impact force can be used as a sole parameter to predict the maximum size of delamination. For small-mass (high-velocity) impacts, this conclusion is not valid.

As far as delamination in composite laminates of unidirectional composites is concerned, fracture mechanics can be used to predict the size of delamination. The effects of stacking sequence, geometry, boundary conditions of the target structure, and contact force can be evaluated by using the fracture mechanics models discussed in Sect. 5.5.4.

5.5.5.1 Effect of matrix properties

Matrix cracking and delamination are governed by the toughness of the matrix material. It is conceptually obvious that composites with tougher matrices would suffer less matrix cracking and delamination for the same impact condition. This subject has been investigated by many researchers. For example, Teh and Morton (1993) investigated nine composite material systems and found that brittle material systems have lower threshold velocities and higher damage area growth rates than toughened material systems. Dan-Jumbo et al. (1989) investigated four composites, including AS4/PEEK and AS4/BMI 24-ply $\pi/4$ quasi-isotropic laminates. The impactor was a 7/8-in. steel ball. Figure 5.22 shows the longitudinal section of the AS4/BMI specimen impacted at 21 m/s. Figure 5.23 shows the longitudinal section of the AS4/PEEK specimen impacted at 29 m/s. Although impacted at a lower velocity, the brittle AS4/BMI composite exhibited much more extensive matrix cracking and delamination than AS4/PEEK.

ORNL-PHOTO 8093-95

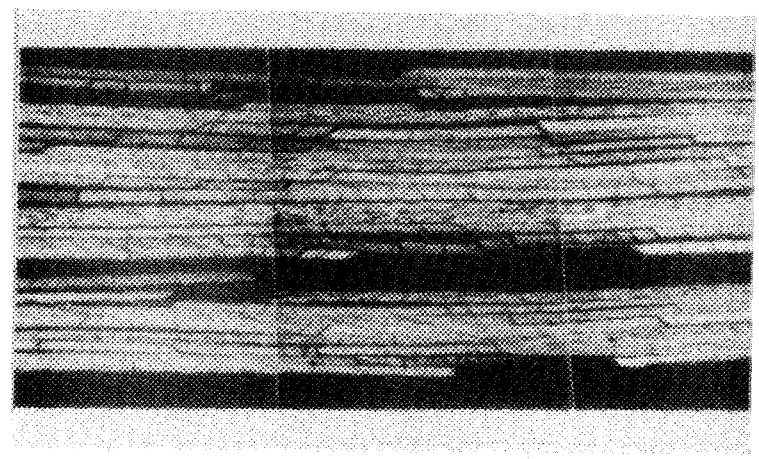

Fig. 5.22. Damage in 24-ply AS4/BMI quasi-isotropic laminate subjected to impact of 7/8-in. steel ball at 21 m/s.

Tough matrices have the ability to delay the initiation of matrix cracking and delamination. In other words, they have a higher threshold velocity below which little impact damage (and then little reduction in strength) would occur. However, Dan-Jumbo et al. (1989) found that at velocities greater than the threshold velocity, the composite with a tough matrix would suffer matrix cracking, delamination, and even fiber breakage. As a result, such a composite tends to lose its strength quickly as impact velocity increases. This behavior was also observed by Sun and Rechak (1988), who used thin adhesive films placed along the

ORNL-PHOTO 8092-95

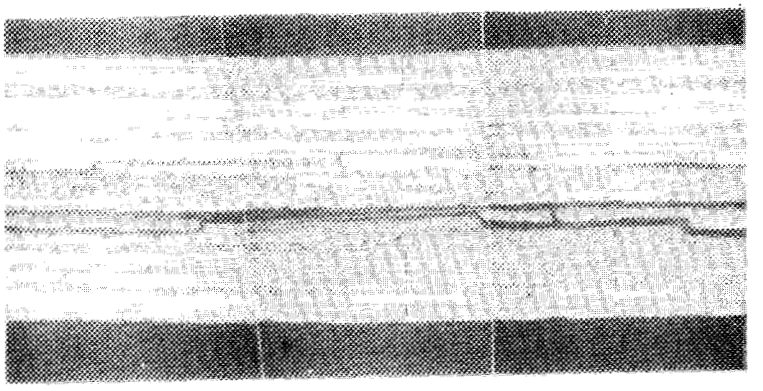

Fig. 5.23. Damage in 24-ply AS4/PEEK quasi-isotropic laminate subjected to impact of 7/8-in. steel ball at 29 m/s.

interfaces of composite laminates. Adhesive films were found to be effective in suppressing delamination. However, at higher impact velocities, the toughened laminates suffered a greater drop in both tensile and flexural strengths due to more severe fiber breakage.

5.5.5.2 Reinforcement architecture

The distinct layered construction of laminates of unidirectional composites allows extensive intraply matrix cracking along the fiber direction and delamination along the interfaces. Changing the reinforcement architecture would modify this behavior.

Woven fabrics of high-performance fibers are used as reinforcements to form composite laminates. Because of the intermingling of fibers, matrix cracks and delamination cracks are usually small. However, at higher impact velocities, woven fabric composite laminates tend to suffer more extensive fiber breakage than laminates of unidirectional composites. Figure 5.24 (by Dan-Jumbo et al., 1989) shows the impact damage in a composite with Amoco's Torlon matrix reinforced with AS4 woven carbon fabric. It is seen that the composite suffered massive fiber breakage, while matrix cracking and delamination were highly localized.

ORNL-PHOTO 8094-95

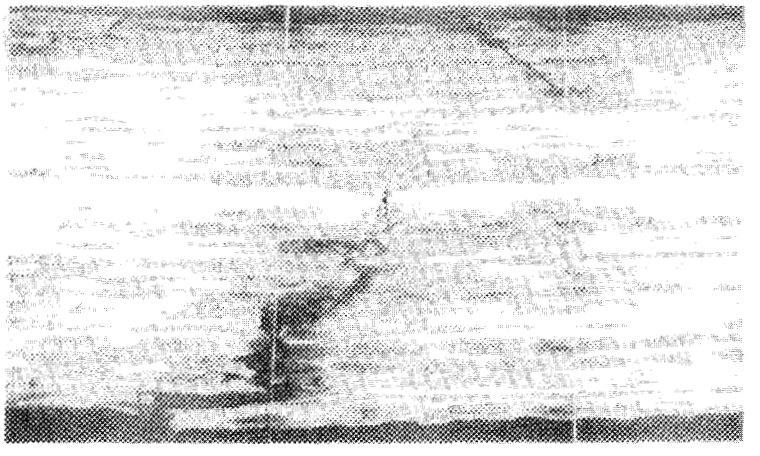

Fig. 5.24. Fiber breakage in fabric composite.

Textile (including stitched) composites with other 2- or 3-D reinforcement architecture exhibit basically behavior similar to that of fabric composites (Gause and Alper, 1987; Ko and Hartman, 1986; and Gong and Sankar, 1989). These types of composites are more capable of containing the spreading of impact damage, especially delamination. Their ability to retain compressive strength after impact is good. However, since the energy dissipation mechanisms in matrix cracking and delamination are significantly suppressed, fiber failure may become more severe than in unidirectional laminates. This is usually displayed as a steep drop in residual strength vs impact energy (Gong and Sankar, 1989).

5.5.5.3 Rigidity of impactor

Rigidity of the impactor affects the contact property and then the contact force response during impact, in particular, the contact area. Kumar and Rai (1993) found that for a given impactor kinetic energy, a steel impactor produced more damage than an aluminum impactor.

In order to drastically enhance the effects of contact rigidity, Cox (1987) used an impactor consisting of a 0.5-in.-diam by 0.5-in.-long solid steel cylinder capped with a 0.5-in.-diam. silicon rubber hemisphere. A 0.5-in. steel ball was also used as an impactor for the purpose of comparison. The mass of the silicon-rubber-capped impactor was about 1.5 times that of the steel ball. Beamlike $[0_5/90_5/0_5]$ graphite-epoxy laminate specimens were impacted to determine the threshold impact velocities at which major matrix failure modes occurred. The test results indicate that the threshold impact velocity for inducing bending cracks, transverse cracks, and delamination was about four times higher with the silicon-rubber-capped impactor than that with the steel ball even though the former had a larger mass.

5.6 RESIDUAL PROPERTIES AFTER IMPACT DAMAGE

Early attempts at predicting residual properties after impact damage included correlating impact kinetic energy with residual properties. Figure 5.25 shows the relation between residual tensile strength and impactor kinetic energy for different specimen sizes based on the test data obtained by Husman et al. (1975). It is easy to see that for the same impact kinetic energy, residual tensile strength varies with specimen size. Thus, impactor kinetic energy alone is not the controlling parameter for residual strength. Test data on SMC by Chaturvedi and Sierakowski (1985) also indicated that overall impact damage area should not be taken as the only controlling parameter for residual tensile strength because the size (mass) of the impactor also affected the residual tensile strength (Fig. 5.26).

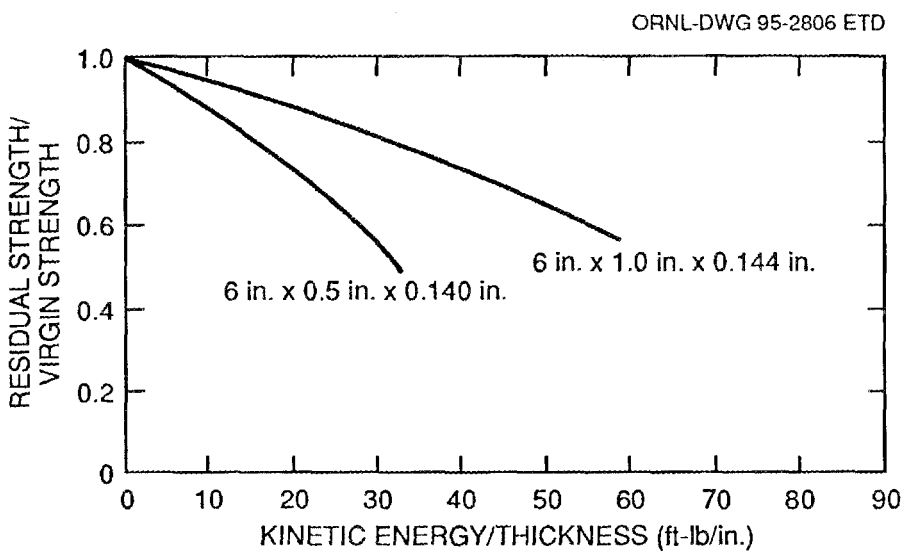

Fig. 5.25. Effect of specimen size on impact residual strength (A-S/4617 composite).

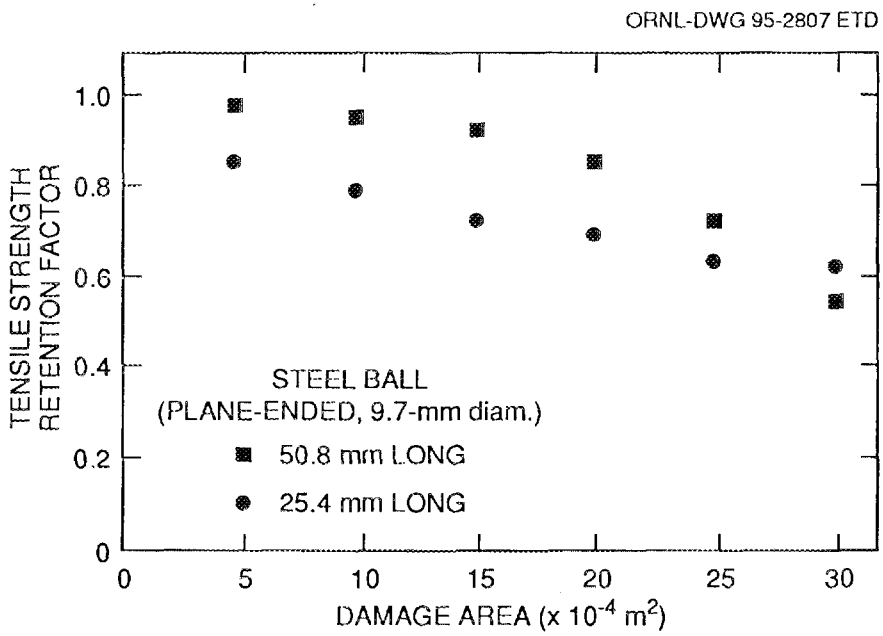

Fig. 5.26. Effect of impactor size on degree of damage at constant damage area.

Impact damage usually reduces the load-carrying capacity of the composite structure. However, reductions in load-carrying capacity are different for different loading cases. In this section, residual properties after impact are addressed through the discussion of residual tensile strength and residual compression strength.

5.6.1 Residual Tensile Strength

To estimate the residual tensile strength of a laminate after impact, it was generally assumed that impact-induced damage introduces the same strength reduction as an equivalent hole or slit of a certain size (Husman et al., 1975; Lal, 1982). Since this approach does not usually consider the effect of delamination and its interaction with fiber breakage, a more rigorous approach is desirable.

Recently Tian and Swanson (1992) used a 3-D finite element analysis to predict residual tensile strength after impact damage. In their model, both the surface crack and delamination were considered, while matrix cracks were assumed to be of negligible effect. The role of delamination in the overall tensile process was found to be important. Delamination reduced the ability of interlaminar shear stresses to transfer the load from plies with broken fibers to adjacent plies and decreased the laminate residual strength up to 45% (as compared with the result in which the effect of delamination is not considered).

5.6.2 Residual Compression Strength

Under in-plane compression, strength reductions are greatest for specimens with impact damage. Much effort has been directed toward understanding the behavior of impact damage specimens under compressive loading. It was found that compression-after-impact (CAI) strength can be significantly affected by the particular design of the test fixture (Prandy et al., 1991). For the same impact energy, damage is less extensive if the holding fixture is more flexible. Since the damage modes for CAI tests are local buckling (buckling of the sublaminates formed by impact damage), delamination growth, and global buckling (final failure), it was observed that stitching through the thickness can improve CAI strength (Pelstring, 1989).

Research in predicting residual compressive strength after impact damage has been conducted for years. Because of the aforementioned damage modes under compression, much attention has been focused

on delamination growth and instability under compression. Analyses were often performed with an embedded delamination. Whitcomb (1981 and 1992) used a 3-D finite element method to analyze the stability of a laminate with an embedded delamination. Strain energy release rate was used to predict delamination growth. Nilsson et al. (1993) used a 2-D plate finite element analysis to investigate the growth of circular delaminations for an isotropic and cross-ply laminate under compressive loading. Klug et al. (1994) also used a plate finite element to analyze delamination growth. Strain energy release rate along an embedded elliptic delamination front was calculated. Delamination growth was simulated when its strain energy release rate reached a critical value. Figure 5.27 shows the delamination growth contours obtained by Klug et al. (1994) for $[(0/90)_s/D/90_{14}/0_{14}]$ graphite-epoxy composite under uniform unidirectional compression. (D indicates the location of the embedded delamination.)

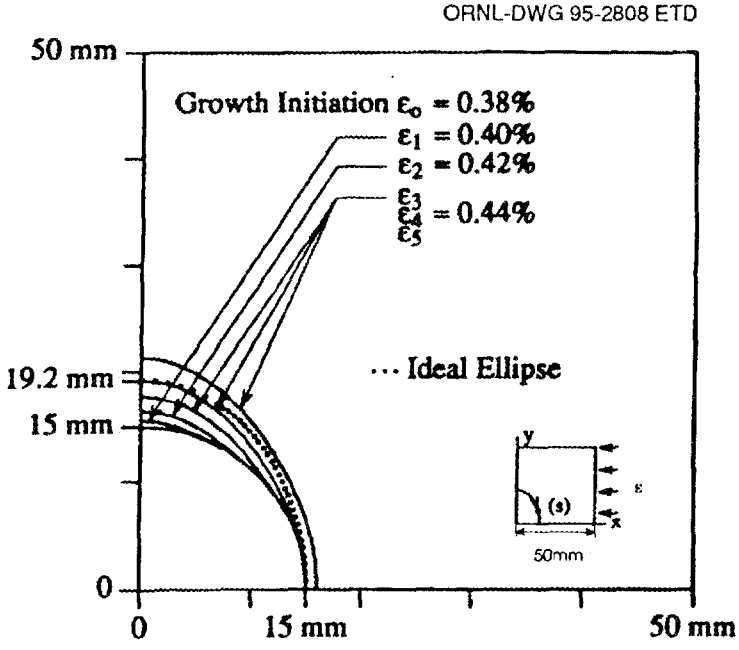

Fig. 5.27. Delamination growth contours for $[(0/90)_s/D/90_{14}/0_{14}]$ cross-ply. D represents location of delamination.

REFERENCES

Abrate, S. 1991. "Impact on Laminated Composite Materials," *Appl. Mech. Rev.* **44**(4), 155–89.

Bogdanovich, A. E., and Yarve, E. V. 1990. "Numerical Analysis of the Impact Deformation of Plates Made of Composites," *Mechanics of Composite Materials* **25**(5), 586–99.

Cairns, D. S., and Lagace, P. A. 1989. "Transient Response of Graphite/Epoxy and Kevlar/Epoxy Laminates Subjected to Impact," *AIAA Journal* **27**(11), 1590–96.

Caprino, G. 1984. "Residual Strength Prediction of Impacted Composite Laminates," *J. Comp. Mater.* **18**, 508–18.

Chang, C., and Sun, C. T. December 1989. "Determining Transverse Impact Force on a Composite Laminate by Signal Deconvolution," *Exp. Mech.*, 414–19.

Chaturvedi, S. K., and Sierakowski, R. L. 1985. "Effects of Impactor Size on Impact Damage-Growth and Residual Properties in an SMC-R50 Composites," *J. Comp. Mater.* **19**(2), 100–13.

Chen, J. K., and Sun, C. T. 1985*a*. "Analysis of Impact Response of Buckled Composite Laminates," *Composite Structures* **3**, 97–118.

Chen, J. K., and Sun, C. T. 1985*b*. "Nonlinear Transient Responses of Initially Stressed Composite Plates," *Comput. Struct.* **21**(3), 391–410.

Choi, H. Y., Wang, H. S., and Chang, F. K. 1992. "Effect of Laminate Configuration and Impactor's Mass on the Initial Impact Damage of Graphite-Epoxy Composite Plates Due to Line Loading Impact," *J. Comp. Mater.* **26**(6), 804–27.

Choi, H. Y., Wu, H. T., and Chang, F. K. 1991. "A New Approach Toward Understanding Damage Mechanisms and Mechanics of Laminated Composites Due to Low-Velocity Impact: Part II—Analysis," *J. Comp. Mater.* **25**, 1012–38.

Choi, H. Y., and Chang, F. K. 1992. "A Model for Predicting Damage in Graphite-Epoxy Laminated Composites Resulting from Low-Velocity Point Impact," *J. Comp. Mater.* **26**(14), 2134–69.

Cox, D. E. 1987. *Effect of Adhesive Layers on Impact Damage Using a Rubber Capped Impactor*, M. S. Thesis, School of Aeronautics and Astronautics, Purdue University, West Lafayette, Indiana.

Dan-Jumbo, E., Leewood, A. R., and Sun, C. T. 1989. "Impact Damage Characteristics of Bismaleimides and Theoplastic Composite Laminates," pp. 356–72 in *Composite Materials: Fatigue and Fracture of Composites*, ASTM STP **1012**, American Society for Testing and Materials, Philadelphia.

Doyle, J. F. 1984. "An Experimental Method for Determining the Dynamic Contact Law," *Exper. Mech.* **24**, 10–16.

Finn, S. R., and Springer, G. S. 1993. "Delaminations in Composite Plates Under Transverse Static of Impact Loads—A Model," *Composite Structures* **23**, 177–190.

Finn, S. R., and Springer, G. S. 1991. *Composite Plates Impact Damage: An Atlas*, Technomic Publishing Company, Lancaster, Pennsylvania.

Freeman, S. M. 1982. "Characterization of Lamina and Interlaminar Damage in Graphite/Epoxy Composite by the Deply Technique," pp. 50–62 in *Composite Materials: Testing and Design (Sixth Conference)*, ASTM STD **787**, ed. I. M. David, American Society for Testing and Materials, Philadelphia.

Gause, L. W., and Alper, J. M. 1987. "Structural Properties of Braided Graphite/Epoxy Composites," *Journal of Composites Technology & Research* **9**(4), 141–50.

Goldsmith, W. 1960. *Impact*, Edward Arnold, London.

Gong, J. C., and Sankar, B. V. 1989. "Impact Response and Damage of Braided Graphite/Epoxy Composites," pp. 915–24 in *Proceedings of the 4th Technical Conference, American Society for Composites, Blacksburg, Virginia, October 3–5*, Technomic Publishing Company, Lancaster, Pennsylvania.

Gosse, J. H., and Mori, P. B. Y. 1988. "Impact Damage Characterization of Graphite/Epoxy Laminates," pp. 344–53 in *Proceedings of the American Society for Composites, 3rd Technical Conference, Seattle, Washington, September 25–29*, Technomic Publishing Company, Lancaster, Pennsylvania.

Greszczuk, L. B., 1982. "Damage in Composite Materials due to Low Velocity Impact," pp. 55–94 in *Impact Dynamics*, John Wiley & Sons, New York.

Gu, Z. L., and Sun, C. T. 1983. Characterization of Impact Damage in an SMC-R50 Composite," *J. Comp. Mater.* **17**(2), 182–94.

Gu, Z. L., and Sun, C. T. January 1987*a*. "Reduction of Flexural Properties in an SMC Composite Due to Impact," *Journal of Reinforced Plastics and Composites* **6**, 13–25.

Gu, Z. L., and Sun, C. T. 1987*b*. "Prediction of Impact Damage Region in SMC Composites," *Composite Structures* **7**, 179–90.

Hodgkinson, J., et al. 1982. "Drop-Weight Impact Tests with the Use of Laser-Doppler Velocimetry," pp. 133–44 in *Proceedings Royal Society London Ser. A. Mat. Phys. Sciences* **379** (1776).

Husman, G. E., Whitney, J. M., and Halpin, J. C. 1975. "Residual Strength Characterization of Laminated Composite Subjected to Impact Loading," pp. 92–113 in *Foreign Object Impact Damage to Composites*, ASTM STP **568**, American Society for Testing and Materials, Philadelphia.

Jackson, W. C., and Poe, Jr., C. C. 1992. *The Use of Impact Force as a Scale Parameter for the Impact Response of Composite Laminates*, NASA TM 104189, January 1992, and also *Journal of Composite Technology & Research* **15**(4), 282–89.

Jih, C. J., and Sun, C. T. 1993. "Prediction of Delamination in Composite Laminates Subjected to Low Velocity Impact," *J. Comp. Mater.* **27**(7), 684–701.

Johnson, K. L. 1987. *Contact Mechanics*, Cambridge University Press.

Joshi, S. P., and Sun, C. T. 1985. "Impact Induced Fracture in a Laminated Composite," *J. Comp. Mater.* **19**, 51–66.

Keer, L. M., and Miller, G. R. 1983. "Smooth Indentation of a Finite Layer," *Journal of Engineering Mechanics* **109**(3), 706–17.

Keer, L. M., and Schonberg, W. P. 1986. "Smooth Indentation of a Transversely Isotropic Cantilever Beam," *Int. J. Solids Struct.* **22**(9), 1033–53.

Khetan, R. P., and Chang, D. C. 1983. "Surface Damage of Sheet Molding Compound Panels Subjected to a Point Impact Loading," *J. Comp. Mater.* **17**(2), 182–94.

Klug, J., Wu, X. X., and Sun, C. T. 1994. "Efficient Modeling of Delamination Growth in Composite Laminates Using Plate Elements," *Proceedings of ASME Winter Meeting, Chicago, Illinois, November 7–11*, American Society for Testing and Materials, Philadelphia.

Ko, F. K., and Hartman, D. July/August 1986. "Impact Behavior of 2-D and 3-D Glass/Epoxy Composites," *SAMPE Journal*, 26–30.

Kumar, P., and Rai, B. 1993. "Delamination of Barely Visible Impact Damage in CFRP Laminates," *Composite Structures* **23**, 313–18.

Kwon, Y. S., and Sankar, B. V. 1993. "Indentation Flexure and Low-Velocity Impact Damage in Graphite/Epoxy Laminates," *Journal of Composite Technology & Research* **15**(2), 101–11.

Lagace, P. A., et al. 1992. "The Use of Force as a (Impact) Damage Resistance Parameter," pp. 991–1000 in *Proceedings of the 7th Technical Conference on Composite Materials, American Society for Composites, Pennsylvania State University, October 13–15*, American Society of Composites.

Lal, K. M. 1982. "Prediction of Residual Tensile Strength of Transversely Impacted Composite Laminates," pp. 97–112 in *Research in Structural and Solid Mechanics*, ed. J. M. Housner and A. K. Noor, NASA CP 2245.

Lal, K. M. 1983. "Low Velocity Transverse Impact Behavior of 8-Ply, Graphite-Epoxy Laminates," *Journal of Reinforced Plastics and Composites* **2**, 226–38.

Lee, E. H. 1940. "Impact of Mass Striking a Beam," *J. Appl. Mech., Trans. ASME* **62**, A129–38.

Liu, S. 1993. "Delamination and Matrix Cracking of Cross-Ply Laminates due to Spherical Indentor," *Composite Structures* **25**, 257–65.

Malvern, L. E., et al. 1978. "Impact Failure Mechanics in Fiber-Reinforced Composite Plates," pp. 120–30 in *High Velocity Deformation of Solids*, Springer-Verlag, Berlin.

McQuillen, E. J., Gause, L. W., and Llorens, R. E. 1976. "Low Velocity Transverse Normal Impact of Graphite/Epoxy Composite Laminates," *J. Comp. Mater.* **10**, 79–91.

Morton, J. 1988. "Scaling of Impact-Loaded Carbon-Fiber Composites," *AIAA Journal* **8**(26), 989–94.

Nahas, M. N. 1986. "Survey of Failure and Post-Failure Theories of Laminated Fiber-Reinforced Composites," *Journal of Composite Technology & Research* **8**(4), 138–53.

Nilsson, K. F., et al. 1993. "A Theoretical and Experimental Investigation of Buckling Induced Delamination Growth," *J. Mech. Phys. Solids* **41**(4), 749–82.

Norman, T. L. 1989. *A Controlled-Damage Concept in Design of Laminate Composites*, Ph.D. Thesis, Purdue University, School of Aeronautics and Astronautics, West Lafayette, Indiana.

Obst, A. W., and Kapania, R. K. 1992. "Nonlinear Static and Transient Finite Element Analysis of Laminated Beams," *Composites Engineering* **2**, 375–89.

Pelstring, R. M. 1989. "Stitching to Improve Damage Tolerance of Composites," pp. 1519–28 in *Proceedings of 34th International SAMPE Symposium, Reno, Nevada, May 5–11*, Society for the Advancement of Material and Process Engineering, Corvina, California.

Prandy, J., et al. 1991. "Effect of Absorbed Energy on the CAI Performance for Composite Materials," *International SAMPE Symposium and Exhibition* **36**, Part I, 901–11, Society for the Advancement of Material and Process Engineering, Corvina, California.

Qian, Y., and Swanson, S. R. 1990. "A Comparison of Solution Techniques for Impact Response of Composite Plates," *Composite Structures* **14**, 117–92.

Qian, Y., et al. 1990. "An Experimental Study of Scaling Rules for Impact Damage in Fiber Composites," *J. Comp. Mater.* **24**, 559–70.

Robinson, P., and Davies, G. A. O. 1992. "Impact Mass and Specimen Geometry Effects in Low Velocity Impact of Laminated Composites," *International Journal of Impact Engineering* **12**(2), 189–207.

Salpekar, S. A. Summer 1993. "Analysis of Delamination in Cross-Ply Laminates Initiating from Impact Induced Matrix Cracking," *Journal of Composites Technology & Research* **15**(2), 88–94.

Sankar, B. V. 1987. "An Approximate Green's Function for Beams and Application to Contact Problems," *J. Appl. Mech.* **53**(3), 735–37.

Sankar, B. V. 1989. "Smooth Indentation of Orthotropic Beams," *Composites Science and Technology* **34**(2), 95–111.

Sankar, B. V. 1992. "Scaling of Low-Velocity Impact for Symmetric Composite Laminates," *Journal of Reinforced Plastics and Composites* **11**(3), 296–309.

Sankar, B. V., and Sonik, V. 1994. "Strain Energy Release Rate Distribution along a Delamination Front Using Plate Theory," pp. 765–74 in *Proceedings of the 35th AIAA/ASME/ASCE/AHS/ASC Structures, Structural Dynamics and Materials Conference, Hilton Head, South Carolina, April 18–20,* American Institute of Aeronautics and Astronautics, Washington, DC.

Shivakumar, K. N., Elber, W., and Illg, W. 1985. "Predication of Impact Force and Duration Due to Low Velocity Impact on Circular Composite Laminates," *J. Appl. Mech.* **52**, 674–80.

Sjoblom, P., Hartness, J., and Cordell, T. 1988. "On Low-Velocity Impact Testing of Composite Materials," *J. Comp. Mater.* **22**(1), 30–52.

Sun, C. T. 1977. "An Analytical Method for Evaluation of Impact Damage Energy of Laminated Composites," pp. 427–40 in *Composite Materials: Testing and Design (Fourth Conference),* ASTM STP **617**, American Society for Testing and Materials, Philadelphia.

Sun, C. T., and Chen, J. K. 1985. "On the Impact of Initially Stressed Composite Laminates," *J. Comp. Mater.* **19**, 490–505.

Sun, C. T., and Jih, C. J. 1987. "On the Strain Energy Release Rates for Interfacial Cracks in Bi-Material Media," *Eng. Fract. Mech.* **28**(1), 13–20.

Sun, C. T., and Jih, C. J. 1992. "A Quasi-Static Treatment of Delamination Crack Propagation in Laminates Subjected to Low Velocity Impact," pp. 949–61 in *Proceedings of the 7th Technical Conference on Composite Materials, American Society for Composites, Pennsylvania State University, October 13–15,* Technomic Publishing Company, Lancaster, Pennsylvania.

Sun, C. T., and Liou, W. J. 1989. "Investigation of Laminated Composite Plates Under Impact Dynamic Loading Using a Three-Dimensional Hybrid Stress Finite Element Method," *Comput. Struct.* **33**(3), 879–84.

Sun, C. T. and Sankar, B. V. 1985. "Smooth Indentation of an Initially Stressed Orthotropic Beam," *Int. J. Solids Struct.* **21**, 161–76.

Sun, C. T., and Rechak, S. 1988. "Effect of Adhesive Layers on Impact Damage in Composite Laminates," ASTM STP **972**, 97–123, American Society for Testing and Materials, Philadelphia.

Tan, T. M., and Sun, C. T. 1985. "Use of Statical Indentation Laws in the Impact Analysis of Laminated Composite Plates," *J. Appl. Mech.* **52**(1), 6–12.

Takeda, N., Sierakowski, R. L., and Malvern, L. E. 1981. "Studies of Impacted Glass Fiber Reinforced Laminates," *SAMPE Quarterly* **12**(2), 9–17.

Teh, K. T., and Morton, J. 1993. "Impact Damage Development and Residual Compression Performance of Advanced Composite Material Systems," pp. 877–86 in *Proceedings of the 34th AIAA SDM Conference Part 2, La Jolla, California*, American Institute of Aeronautics and Astronautics, Washington, DC.

Tian, Z., and Swanson, S. R. 1992. "Residual Tensile Strength Prediction on a Ply-by-Ply Basis for Laminates Containing Impact Damage," *J. Comp. Mater.* **26**(8), 1193–1206.

Wang, C. Y., and Yew, C. H. 1990. "Impact Damage in Composite Laminates," *Comput. Struct.* **37**(6), 967–82.

Whitcomb, J. D. 1992. "Analysis of a Laminate with a Postbuckled Embedded Delamination, Including Contact Effects," *J. Comp. Mater.* **26**(10), 1523–52.

Whitcomb, J. D. 1981. "Finite Element Analysis of Instability Related Delamination Growth," *J. Comp. Mater.* **15**(9), 403–26.

Wu, E., and Yen, C. S. 1994. "The Contact Behavior Between Laminated Composite Plates and Rigid Sphere," *J. Appl. Mech.* **61**(1), 60–66.

Wu, H. T., and Chang, F. K. 1989. "Transient Dynamic Analysis of Laminated Composite Plates Subjected to Transverse Impact," *Comput. Struct.* **31**, 453–66.

Yang, S. H., and Sun, C. T. 1983. "Indentation Law for Composite Laminates," pp. 425–49 in *Composite Materials: Testing and Design (Sixth Conference)*, ASTM STP **787**, ed. I. M. Daniel, American Society for Testing and Materials, Philadelphia.

Zheng, S., and Sun, C. T. 1994. "Prediction of Impact Induced Delamination in Composite Laminates by Using Plate Finite Elements," *Proceedings of ASME Winter Meeting, November 7–11, Chicago, Illinois*, American Society for Testing and Materials, Philadelphia.

6. ENVIRONMENTAL EFFECTS IN POLYMERIC COMPOSITES

Y. Jack Weitsman

6.1 INTRODUCTION

The sorption of fluids in polymeric composites and their effects on composites' performance are highly complex issues. Their study involves, in the least, the disciplines of polymer science and applied mechanics, because the former focuses on molecular-level interactions and the latter is concerned with mechanical response. A comprehensive review of this subject is a formidable task that may require an interdisciplinary team effort rather than an individual undertaking. The current review is based upon information gleaned from several hundred articles, while it is safe to assume that the total number of papers related to the current subject runs into the thousands.

What strikes the reader of articles related to fluid sorption and fluid effects in polymeric composites is the immense variety of materials and circumstances associated with these subjects. To begin with, polymers are highly complex materials that vary in structure and physicochemical properties, and polymeric composites adjoin an assortment of fibers with extremely intricate fiber/matrix interphases and interfacial bonding to an already knotty situation. The complexity is further compounded by the ingress of fluids of many kinds, which interact differently with the polymer, the fiber, and the interphase matters within the composite.

The main issues associated with the mechanical performance of composites in the presence of fluid environments concern their dimensional stability, strength, fatigue response, and impact resistance. To a large degree these issues are only partially resolved at the present time even in the absence of fluids. Consequently, the best that can be expected from this review is the gaining of a certain insight into the various phenomena associated with fluids in composites and the derivation of some guidelines toward evaluating their effects.

The kinetics of fluid sorption in polymers has been studied for about 150 years, perhaps beginning with Fick (1855). Among the review articles on the subject, one may cite several references (Rogers, 1965, 1985; Crank and Park, 1968; Stannett and Hopfenberg, 1972; Frisch and Stern, 1983) as well as several books (Crank, 1975; Ghez, 1988; Shewmon, 1983).

The effects of fluid environments on the creep response of polymers were studied intensively by several Russian researchers in the early 1970s. These studies are noted in a review article (Maksimov and Urzhumstev, 1977).

The interest in fluid sorption and fluid effects in polymers received a new impetus in the West during the mid-1970s with the advent of polymeric composites. Information regarding these investigations can be found in review articles (Delasi and Whiteside, 1978; Komorowski, 1983*a*, 1983*b*, 1983*c*, 1983*d*; Marom, 1989) as well as in three volumes of collected works (Springer, 1981, 1984*b*, 1988). Nevertheless, until recently the issue of fluid effects on composites has been considered of only secondary importance for the following reasons: at the "low-tech" end, glass fiber composites were utilized in the boating industry. While such composites exhibit substantial sensitivity to fluid environments, these effects were overcome rather simply by overdesign, with little concern for any possible waste in weight or performance. On the other hand, at the "high-tech" end, carbon fibers formed the mainstay component of polymeric composites that were utilized for aerospace applications. While tight performance and design requirements were imposed in this case, carbon fibers are largely immune to solvents, and the environmental exposures of practical concern were much less severe than those in the boating industry.

It appears that the interest in environmental effects on composites may be rekindled due to new applications contemplated for these materials, which combine severe exposures and tighter design requirements. These new applications occur in the offshore oil industry, in naval submersibles, and in the automotive industry. Since this overview focuses on concerns related to automotive applications, it is somewhat biased in that direction. For instance, it contains aspects of the corrosion stress cracking of glass and lists

information regarding the effects of fuels and motor oils but omits reference to kevlar composites or to the detrimental effects of thermal spiking, which are characteristic to other applications.

6.2 SORPTION PROCESSES

6.2.1 Basic Considerations: Linear, One-Dimensional, Fickian Diffusion

The simplest model for the diffusion of a solvent into a solid is given by the linear Fick's Law (1855). Accordingly, the flux of the solvent, F, is proportional to the (negative of the mass) concentration gradient ∇m. In the one-dimensional (1-D) case we have

$$F = -D \frac{\partial m}{\partial x} , \tag{6.1}$$

where D is the diffusion coefficient.

The negative sign in Eq. (6.1) indicates that the flux is directed from high-concentration to low-concentration regions.

Conservation of mass states that

$$\frac{\partial m}{\partial t} = - \frac{\partial F}{\partial x} . \tag{6.2}$$

Combining Eqs. (6.1) and (6.2), we obtain the well-known 1-D version of Fick's law:

$$\frac{\partial m}{\partial t} = D \frac{\partial^2 m}{\partial x^2} . \tag{6.3}$$

It should be noted that the above equations can be derived from the statistics of a random walk process (Ghez, 1988).

The field equation (6.3) is accompanied by initial and boundary conditions, the simplest of which are

$$m(x, 0) = m_0 \qquad -L < x < L , \tag{6.4}$$

and

$$m(\pm L, t) = m_b \qquad 0 < t < \infty , \tag{6.5}$$

which correspond to a constant initial concentration and a fixed boundary concentration, respectively, in a plate of thickness 2L.

The solution of Eq. (6.3) with Eqs. (6.4) and (6.5) is well known (Crank, 1975) and is expressible in two well-known alternate forms (Crank, 1975), which can be written compactly. Accordingly (Weitsman, 1981, 1991), the distribution m(x, t) is given by

$$m(x, t) - m_0 f_0(x, t) = m_b f(x, t) , \tag{6.6}$$

where

$$f_0(x,t)) = \begin{cases} C(x,t) \\ \text{or} \\ 1 - E(x,t) \end{cases} \text{and } f(x,t) = \begin{cases} 1 - C(x,t) \\ \text{or} \\ E(x,t) \end{cases} . \tag{6.7}$$

In Eqs. (6.6) and (6.7)

$$C(x,t) = 2 \sum_{n=1}^{\infty} \frac{(-1)^{n+1}}{P_n} \cos\left(\frac{P_n x}{L}\right) \exp\left(-P_n^2 t^*\right) , \tag{6.8}$$

$$E(x,t) = \sum_{n=1}^{\infty} (-1)^{n+1} \left\{ \operatorname{erfc}\left[\frac{2n - 1 - x/L}{(t^*)^{1/2}}\right] + \operatorname{erfc}\left[\frac{2n - 1 + x/L}{(t^*)^{1/2}}\right] \right\} , \tag{6.9}$$

where $P_n = (2n - 1)\pi/2$, $\operatorname{erfc}(z) = \frac{2}{\pi^{1/2}} \int_z^{\infty} - \exp(s^2)ds$, and $t^* = Dt/L^2$ is nondimensional time.

The version that employs cosines, C(x, t), converges rapidly for long times, while the series containing complementary error functions, E(x, t), converges rapidly for short times.

For an initially dry plate exposed to a constant ambient boundary condition $m_b(\pm L, t) = 1$, the distribution m(x, t) vs the nondimensional distance x/L at various nondimensional times, $t^* = Dt/L^2$, is shown in Fig. 6.1.

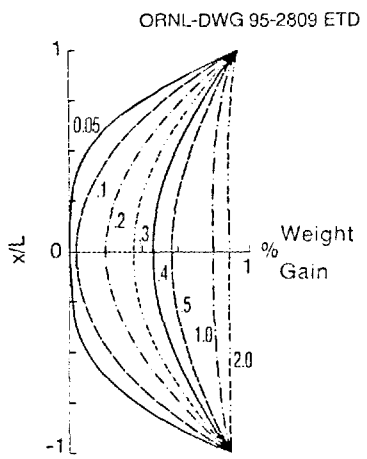

Fig. 6.1. Moisture distribution profiles predicted by Fick's Law at various values of nondimensional time t*.

Extensions to the time-varying diffusion coefficient D, which occur due to fluctuating temperatures, and for time-varying boundary conditions can be constructed by straightforward superposition on the basis of Eqs. (6.6) and (6.7) due to the linearity of the problem (Weitsman, 1991).

The total weight gain M(t) is given by

$$M(t) = \int_{-L}^{L} m(x,t)dx \cdot \tag{6.10}$$

The detailed expression (Crank, 1975) is omitted for the sake of brevity. The magnitude of M(t) is amenable to direct experimental measurement.

For initially dry plates with constant ambient conditions, the plot of relative weight gain $M(t^*)/M(\bullet)$ vs $\sqrt{t^*}$ is shown in Fig. 6.2 [$t^* = Dt/L^2$ is the nondimensional time in Eqs. (6.8) and (6.9)]. The above plot serves as a "baseline" for comparison with actual data.

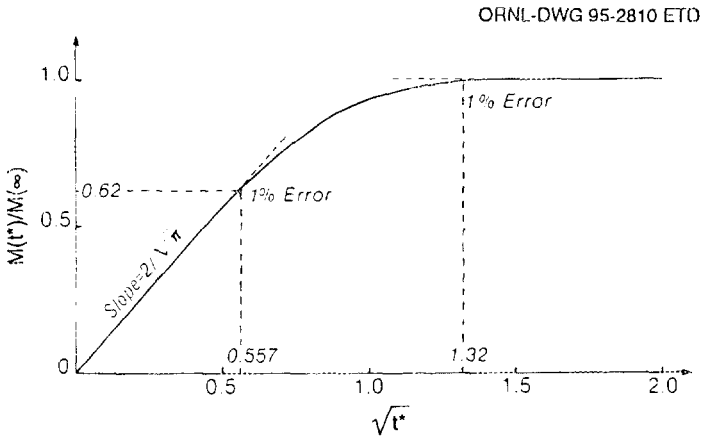

Fig. 6.2. Total weight gain $M(t)/M(\infty)$ vs $\sqrt{t^*}$ according to Fick's Law, with locations where departures from straight lines exceed 1%.

6.2.2 Weight-Gain and Diffusion Data for Polymers and Polymeric Composites

It was noted that in many circumstances weight-gain data for the sorption and desorption of fluids by polymers do not concur with the predictions of linear Fickian diffusion shown in Fig. 6.2. Such "anomalies" are exhibited in Fig. 6.3 (Rogers, 1965). Some of the anomalies noted in Fig. 6.3 can be attributed to the inherent time-dependent response of polymers (Weitsman, 1990). On the other hand, moisture weight-gain data in polymeric composites exhibit departures from linear Fickian behavior (the curve denoted LF in Fig. 6.4, which reproduces the plot shown in Fig. 6.2) that are much more striking than those in Fig. 6.3. Such severe departures correspond to weight-gain data sketched by curves 3 and 4 in Fig. 6.4.

Curve 1 in Fig. 6.4 resembles the "pseudo-Fickian" category in Fig. 6.3, and corresponds to the often encountered circumstance of a continuous gradual increase in weight gain—never attaining equilibrium (e.g., Grayson and Wolf, 1985). Curve 2 in Fig. 6.4 resembles the curve for "two-stage" diffusion in Fig. 6.3. However, curve 3 corresponds to a rapidly increasing moisture content within the composite, which is usually accompanied by large deformations, damage growth, material breakdown, and/or mechanical failure.

Curve 4 accords with weight loss that is attributable to chemical or physical breakdown of a material. Most commonly, weight losses occur in conjunction with hydrolysis the separation of side groups from the polymeric chains, or the dissociation of matter located at the vicinities of fiber/matrix interfaces.

Because of the wide variety of polymeric molecular structures and the large diversity in the polymeric composite material systems, it is impossible to suggest specific causes for the disparate sorption processes typified by the five weight-gain plots shown in Fig. 6.4. However, a comprehensive review of many data suggests that curves 3 and 4 in Fig. 6.4 correspond most frequently to sorption processes that occur under severe circumstances, such as elevated temperatures, high external stresses, or exposure to high levels of ambient solvent concentrations. These types of weight-gain data are encountered much more frequently in composites than with "neat" polymers, except when the latter are undercured or contain nonstoichiometic amounts of curing agents. As noted earlier, weight-gain data that correspond to curve 3 in Fig. 6.4 are associated with substantial degradations in material properties (Springer et al., 1981). They also portend shortened lives and impending failure of the material system. Loss of material integrity is associated with curve 4 in Fig. 6.4.

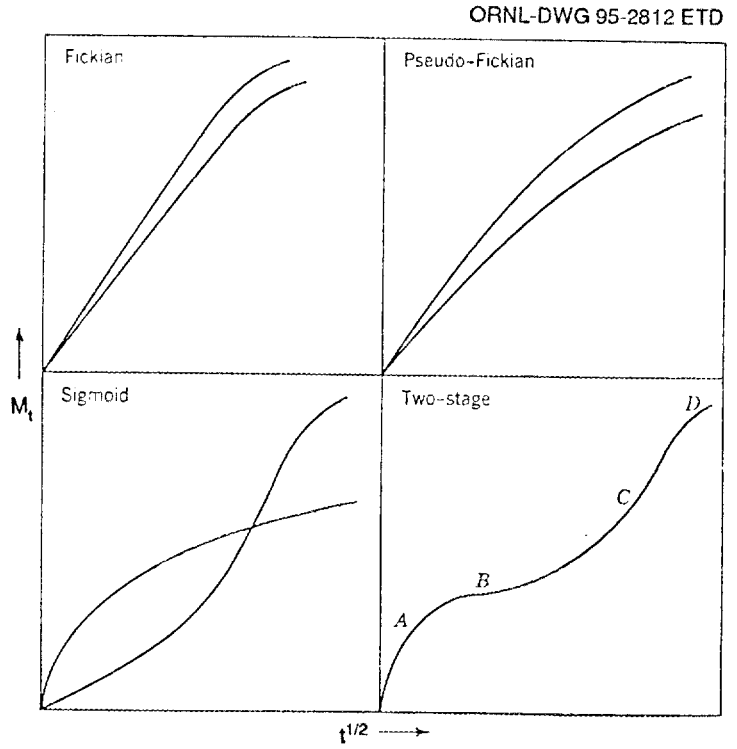

Fig. 6.3. "Non-Fickian" or "anomalous" sorption and desorption curves compared with Fickian type curves. *Source*: Rogers, 1965. Reprinted with permission of John Wiley & Sons, Inc.

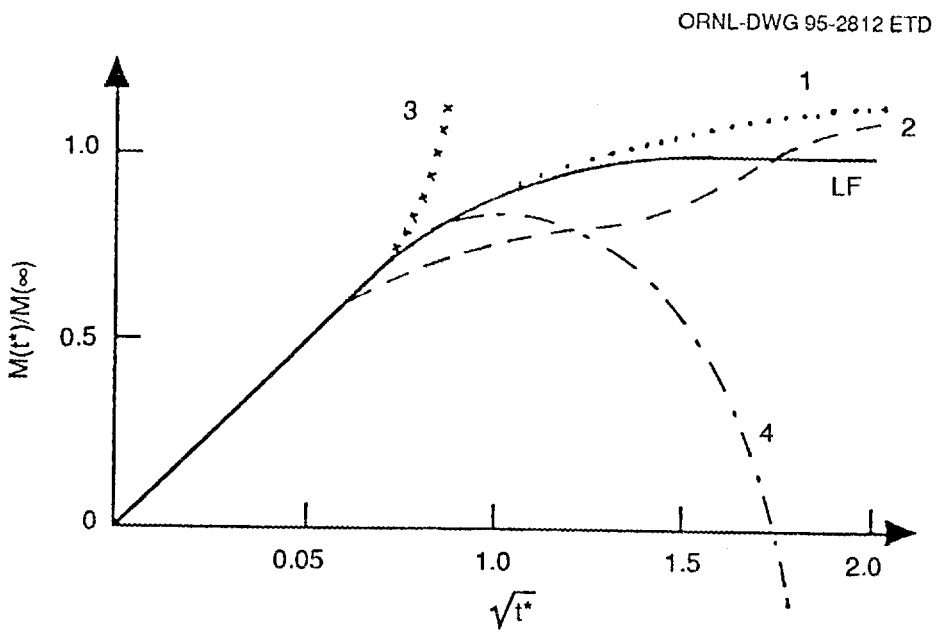

Fig. 6.4. Schematic curves representing four categories of recorded non-Fickian weight-gain sorption data in polymers and polymeric composites. The solid line, designated by LF, corresponds to linear Fickian diffusion.

Circumstances that correspond to weight-gain data categorized by curves 1–4 and LF in Fig. 6.4 are listed in Table 6.1.

Table 6.1. Types of sorption data for various materials and exposures

Type of weight gain data sketched in Fig. 6.4	Material system	Exposure	Reference
LF	T300/5208 graphite-epoxy	T < 60°C	C. D. Shirrell, 1978
1	T300/5208 graphite-epoxy	T > 60°C	C. D. Shirrell, 1978
1 and/or 2	Epoxy and AS/3501-5 graphite-epoxy	Distilled water at 22°C–70°C; humid air and water immersion	J. M. Whitney and C. E. Browning (1978)
LF	T300/1034 (graphite/polymer)	Distilled water at 22°C–70°C; humid air and water immersion	C. H. Shen and G. S. Springer, 1981b; and T. Mohlin, 1988
3	T300/1034 (graphite/polymer)	Distilled water at 90°C	T. Mohlin, 1988
1 or 2	SMC-25, SMC-65, SMC-30 EA glass/polyester	100% RH, 32°C	A. C. Loos, G. S. Springer, B. A. Sanders and R. W. Tung, 1981
LF	SMC-25	100% RH, 50°C	A. C. Loos, G. S. Springer, B. A. Sanders and R. W. Tung, 1981
LF	SMC-25, SMC-65, SMC-30 EA	40% RH, 65°C	A. C. Loos, G. S. Springer, B. A. Sanders and R. W. Tung, 1981
2	SMC-25	60% RH, 65°C	A. C. Loos, G. S. Springer, B. A. Sanders and R. W. Tung, 1981
4	SMC-25	100% RH, 65°C	A. C. Loos, G. S. Springer, B. A. Sanders and R. W. Tung, 1981
4	SMC-65	100% RH, 50°C and 65°C and 60% RH at 65°C	A. C. Loos, G. S. Springer, B. A. Sanders and R. W. Tung, 1981
4	SMC-30 EA	100% RH, 50°C and 65°C and 60% RH at 65°C	A. C. Loos, G. S. Springer, B. A. Sanders and R. W. Tung, 1981
1	SMC-25, SMC-65, SMC-30 EA	Distilled water at 23°C	A. C. Loos, G. S. Springer, B. A. Sanders and R. W. Tung, 1981

Table 6.1. continued

Type of weight gain data sketched in Fig. 6.4	Material system	Exposure	
LF	SMC-25, SMC-65, SMC-30 EA	Saltwater at 23°C	A. C. Loos, G. S. Springer, B. A. Sanders and R. W. Tung, 1981
4	SMC-25, SMC-65, SMC-30 EA	Distilled water at 50°C	A. C. Loos, G. S. Springer, B. A. Sanders and R. W. Tung, 1981
2	SMC-25, SMC-65, SMC-30 EA	Saltwater at 50°C	A. C. Loos, G. S. Springer, B. A. Sanders and R. W. Tung, 1981
1	SMC-25, SMC-65, SMC-30 EA	Diesel fuel at 23°C and 50°C	A. C. Loos, G. S. Springer, B. A. Sanders and R. W. Tung, 1981
1 or 2	SMC-25, SMC-65, SMC-30 EA	Jet fuel at 23°C and 50°C	A. C. Loos, G. S. Springer, B. A. Sanders and R. W. Tung, 1981
1	SMC-25, SMC-65, SMC-30 EA	Gasoline at 23°C	A. C. Loos, G. S. Springer, B. A. Sanders and R. W. Tung, 1981
1	SMC-25, SMC-65, SMC-30 EA	Aviation oil at 23°C and 50°C	A. C. Loos, G. S. Springer, B. A. Sanders and R. W. Tung, 1981
LF	SMC-R25	100% RH and saltwater at 23°C	G. S. Springer, B. A. Sanders, and R. W. Tung, 1981
4	SMC-R25	100% RH at 93°C	G. S. Springer, B. A. Sanders, and R. W. Tung, 1981
LF	SMC-R25	Diesel fuel at 23°C and at 93°C; lubricating oil at 23°C; antifreeze at 23°C and at 93°C	G. S. Springer, B. A. Sanders, and R. W. Tung, 1981
2	SMC-R25	Lubricating oil at 93°C	G. S. Springer, B. A. Sanders, and R. W. Tung, 1981
LF	SMC-R50	50% RH at 23°C and at 93°C and 100% RH at 23°C	G. S. Springer, B. A. Sanders, and R. W. Tung, 1981
4	SMC-R50	100% RH at 93°C	G. S. Springer, B. A. Sanders, and R. W. Tung, 1981

Table 6.1. continued

Type of weight gain data sketched in Fig. 6.4	Material system	Exposure	Reference
1	SMC-R50	Saltwater at 23°C	G. S. Springer, B. A. Sanders, and R. W. Tung, 1981
4	SMC-R50	Saltwater at 93°C	G. S. Springer, B. A. Sanders, and R. W. Tung, 1981
LF	SMC-R50	Diesel fuel at 23°C; lubricating oil at 23°C and 93°C	G. S. Springer, B. A. Sanders, and R. W. Tung, 1981
1 or 2	SMC-R50	Diesel fuel at 93°C; antifreeze at 23°C	G. S. Springer, B. A. Sanders, and R. W. Tung, 1981
4	SMC-R50	Antifreeze at 93°C	G. S. Springer, B. A. Sanders, and R. W. Tung, 1981
LF	Glass/epoxy diamine hardener	12–100% RH, 25–90°C	P. Bonniau and A. R. Bunsell, 1984
1	Glass/epoxy dicyandiamide hardener	28–100% RH, 25–90°C	P. Bonniau and A. R. Bunsell, 1984
4	Glass/epoxy anhydride hardener	52–100% RH, 90°C	P. Bonniau and A. R. Bunsell, 1984
LF (?)	XMC-3 adhesive	50% RH, water and saltwater at 23°C	G. S. Springer, 1981
4	XMC-3 adhesive	Water at 93°C	G. S. Springer, 1981
2	T300/914	70–98% RH at 50–70°C	M. Blikstad, O. W. Sjoblom, and T. R. Johannesson, 1988
LF	Cured or undercured epoxy	Water vapor at "low" temperatures	V. B. Gupta, L. T. Drzal, and M. J. Rich, 1985
1	Cured or undercured epoxy	Water vapor at "intermediate" temperatures	V. B. Gupta, L. T. Drzal, and M. J. Rich, 1985
3	Cured or undercured epoxy	Water vapor at "high" temperatures	V. B. Gupta, L. T. Drzal, and M. J. Rich, 1985
1	S-glass-epoxy	Distilled water at 30–780°C	A. Chateauminois, B. Chabert, J. P. Soulier, and L. Vincent, 1991

Table 6.1. continued

Type of weight gain data sketched in Fig. 6.4	Material system	Exposure	Reference
3	S-glass-epoxy	Distilled water at 90°C	A. Chateauminois, B. Chabert, J. P. Soulier, and L. Vincent, 1991
LF	E-glass-epoxy	Water at 22°C	B. Dewimille, J. Thoris, R. Mailfert, and A. R. Bunsell, 1980
4	E-glass-epoxy	Water at 80–100°C	B. Dewimille, J. Thoris, R. Mailfert, and A. R. Bunsell, 1980
1	Epoxy	Water at 22–100°C	B. Dewimille, J. Thoris, R. Mailfert, and A. R. Bunsell, 1980
4	Glass-epoxy and hybrid glass-carbon epoxy	Water at 80°C	H. Fukuda, 1986
1	Vinylester	Water	H. Hojo, K. Tsuda, K. Ogasawara, and K. Mishima, 1982
4	Vinylester	Saltwater	H. Hojo, K. Tsuda, K. Ogasawara, and K. Mishima, 1982
1	S2 glass-epoxy	75% RH at 75°C—first exposure	S. Y. Lo, H. T. Hahn, and T. T. Chiao, 1982
2	S2 glass-epoxy	75% RH at 75°C—second and third exposures	S. Y. Lo, H. T. Hahn, and T. T. Chiao, 1982
4	Swirl mat glass/PPS	Hot water	A. Y. Lou and T. P. Murtha, 1987
1	Graphite/PPS	Nonimpacted and pre-impacted exposed to jet fuel	C.-C. M. Ma, Y. H. Huang, and M. J. Chang, 1991
LF	APC-2 (graphite/PEEK)	Nonimpacted and pre-impacted exposed to jet fuel	C.-C. M. Ma, Y. H. Huang, and M. J. Chang, 1991
1	CF/epoxy	Sea water	L. M. Manocha, O. P. Bahl, and R. K. Jain, 1982
1	Hybrid CF/kevlar-epoxy	Sea water	L. M. Manocha, O. P. Bahl, and R. K. Jain, 1982

Table 6.1. continued

Type of weight gain data sketched in Fig. 6.4	Material system	Exposure	Reference
LF	Glass/UP	Distilled water at 23°C	G. Menges and H.-W. Gitschner, 1980
3	Glass/UP	Distilled water at 40°C and 60°C[a]	G. Menges and H.-W. Gitschner, 1980
1	CF/epoxy	Water and saltwater at 60°C	Y. Nakanishi and A. Shindo, 1982
1	Glass/polyester	Water immersion at 60°C with s < 0.3 UTS	R. J. White and M. G. Phillips, 1985
3	Glass/polyester	Water immersion at 60°C with s = 0.6 UTS	R. J. White and M. G. Phillips, 1985
LF	Epoxy	97% RH, RT with s < 0.45 UTS	M. C. Henson and Y. Weitsman, 1986
1	AS4/3502 graphite-epoxy	97% RH, RT with s < 0.45 UTS	M. C. Henson and Y. Weitsman, 1986
1	AF126-2 adhesive bond line	75–90% RH, 10–40°C	W. Althof, 1979
1	FM73 adhesive bond line	75–90% RH, 10–40°C	W. Althof, 1979
1	Graphite/F155	95% RH at 49°C	D. L. Clark, 1983
LF	Graphite/F185	95% RH at 49°C	D. L. Clark, 1983
1	Graphite/F155–graphite/F185 lay-up	95% RH at 49°C	D. L. Clark, 1983

[a]Damage observed.

Very few data are available regarding moisture distribution within polymers or polymeric composites. Profiles were inferred from weight-gain measurements accompanying specimen sectionings (Althof, 1979). Alternately, profiles of water within AS/3501-5 graphite-epoxy composites were recorded by radioactive measurements of D_2O at several times during the diffusion process (Whiteside et al., 1984). Typical results of the latter technique are shown in Fig. 6.5, where recorded distributions are compared with predictions of linear Fickian diffusion. In spite of the scatter in the results shown in Fig. 6.5, they tend to corroborate predictions that correspond to weight-gain data that follow curves 1 or 2 in Fig. 6.4 (Cai and Weitsman, 1994).

6.2.3 Causes and Models for Non-Fickian Diffusion

There is a host of possible reasons for non-Fickian diffusion in polymers and yet additional probable causes when considering polymeric composites.

The fact that glassy polymers, with their highly complex molecular configurations, exist in a non-equilibrium thermodynamic state accounts for their inherent time-dependent behavior. The time dependence is compounded by additional temporal phenomena such as aging (Struik, 1978; Adamson, 1980), ongoing chemical reactions (Maksimov and Urzhumstev, 1977), and advancing cure. The time dependence is accelerated by the fact that fluids tend to increase the free volume of polymers, thereby lowering their

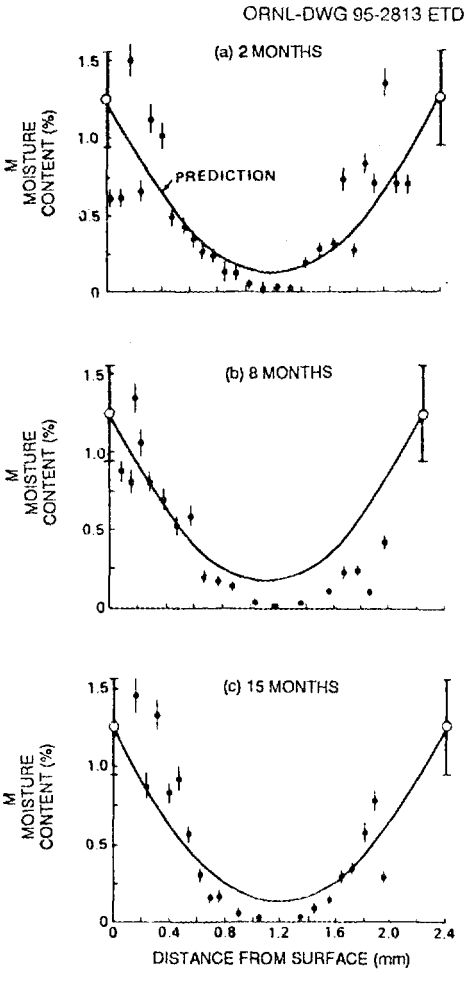

Fig. 6.5. Recorded concentration values with distribution profiles predicted by Fick's Law. *Source*: Whiteside, et al., 1984. Adapted with permission of American Society for Testing and Materials. Dots show average recorded concentrations of heavy water (D_2O) after 56-d exposure to a 70% RH of D_2O at 305 K (90°F), with vertical lines indicating statistical error. Cases (*a*), (*b*) and (*c*) refer to pre-exposure to hygrothermal cycles, after which all specimens were completely redried.

glass transition temperature (DeIasi and Whiteside, 1978; McKague, 1978; Browning, 1978) (typically by 10°C for each 1% solvent weight gained in the polymer). The increased mobility of the molecular chains and side groups is denoted as "plasticization." This is an essentially reversible phenomenon that can be accounted for by means of the time-dependent diffusion model discussed later.

Many of these above considerations, which fall within the realm of polymer science, are discussed in several review articles (Rogers, 1965, 1985; Stannett and Hopfenberg, 1972; Hopfenberg and Stannett, 1973; Frisch and Stern, 1983; Windle, 1985) and texts (such as Crank, 1975, Chaps. 7 and 11).

Consequently, the time-dependent diffusion process occurs conjointly with the time-dependent mechanical response of polymers, namely creep and relaxation. Accordingly, the polymer requires time to approach its new equilibrium state commensurate with externally imposed boundary conditions (Crank, 1953; Long and Richman, 1960; Frisch, 1964, 1966; Crank and Park, 1968; Apicella et al., 1981). More recently, the foregoing circumstance was modeled on the basis of fundamental principles of irreversible thermodynamics and continuum mechanics (Weitsman, 1990) to account for coupled moisture, thermal, and mechanical time-dependent behavior.

Essentially, the source of the non-Fickian sorption noted in curves 1 and 2 in Fig. 6.4 was traced to a time-dependent boundary condition

$$m(\pm L, t) = m_0 + \sum_i m_i \left(1 - e^{-t/t_i}\right) , \tag{6.11}$$

which holds even under exposure to constant ambient conditions since the polymer cannot adapt instantaneously to the imposed external environment.

It has been shown (Weitsman, 1990; Cai and Weitsman, 1994) that solutions of Eq. (6.3) with initial condition [Eq. (6.4)] and boundary condition [Eq. (6.11)] [instead of [Eq. (6.5)] can account for non-Fickian weight-gain data represented by curves 1 and 2 in Fig. 6.4 and correspond to non-Fickian distributions such as those shown in Fig. 6.5.

Another approach to account for non-Fickian behavior is offered by the "two-phase diffusion" model (Gurtin and Yatomi, 1979; Carter and Kibler, 1978; Bonniau and Bunsell, 1984; Weitsman, 1990). Accordingly, a portion n of the diffusing substance is entrapped within the polymeric molecules and becomes immobile, while a remaining part, m, remains mobile and continues to diffuse into the polymer. In analogy with the flux concentration gradient and conservation of mass Eqs. (6.1) and (6.2), one obtains

$$D \frac{\partial^2 m}{\partial x^2} = \frac{\partial}{\partial t} (m + n) , \tag{6.12}$$

with the initial condition [Eq. (6.4)] imposed on (m + n) and the boundary condition [Eq. (6.5)] applying to the mobile portion m only.

In addition, the rate of change of the immobile portion n is assumed to be governed by

$$\frac{\partial n}{\partial t} = \gamma m - \beta n . \tag{6.13}$$

It has been shown (Carter and Kibler, 1978; Bonniau and Bunsell, 1984) that the two-phase diffusion model predicts weight gains that correspond to curve 1 in Fig. 6.4.

Another cause for non-Fickian diffusion is due to concentration-dependent diffusivity D = D(m), which would render Eq. (6.3) to be nonlinear.

All three foregoing circumstances predict the occurrence of hysteresis loops when weight gain of initially dry plates and weight loss of saturated specimens subjected to drying are plotted vs time (or $\sqrt{\text{time}}$). Such hysteresis loops were noted for absorption and desorption data of graphite-epoxy composites (Whitney and Browning, 1978; Shirrel, 1978; Henson and Weitsman, 1986) and to a lesser extent in "neat" epoxy (Henson and Weitsman, 1986). The hystereses loops become more pronounced as diffusion occurs under increasing amplitudes of applied loads. Usually, these loops indicate a desorption process that is initially faster and subsequently slower than the absorption process—a circumstance that is conceptually consistent with the time-dependent response model (Weitsman, 1990). It may be worth noting that analogous hysteresis loops were noted in the transverse strain of glass-epoxy composites subjected to cyclic environment (Lo et al., 1982).

A much more intricate sorption process occurs when diffusion is accompanied by a chemical reaction. The chemical reaction can introduce an inert substance into the host material, in which case solvent absorption is accompanied by an enhanced weight gain. On the other hand, the chemical reaction may involve dissociation of matter; thereby diffusion induces weight losses (Crank, 1975).

A model for diffusion and chemical reaction that occurs at a moving front is represented by the thermal oxidation of silicon (Ghez, 1988) expressed by

$$S_i + O_2 \rightarrow S_i O_2 . \tag{6.14}$$

The distribution C(x, t) of the excess of O_2, when the moving oxidation front is located at x = L(t) is sketched in Fig. 6.6 (Ghez, 1988). In that figure C_0 and C_L are the concentrations of O_2 at the outer boundary and at the oxide/silicon front, respectively. Also, J_0 denotes the flux of O_2 from the ambient into the oxide, and r is the rate of the reaction in Eq. (6.14).

ORNL-DWG 95-2814 ETD

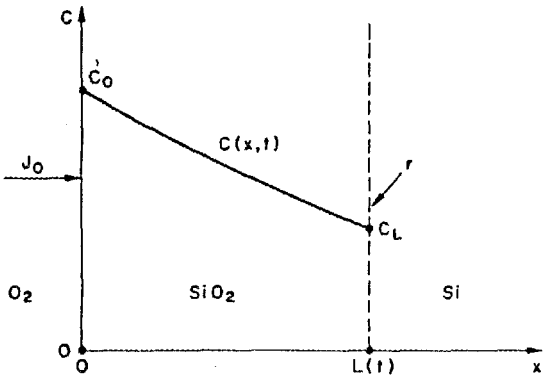

Fig. 6.6. Three-phase oxidation system and excess O_2 distribution in the oxide. *Source*: Ghez, 1988. Reprinted with permission of John Wiley & Sons, Inc.

Conservation of oxygen mass at x = L(t) gives

$$D \left.\frac{\partial C}{\partial x}\right|_{x=L} + r + C_L \dot{L} = 0 . \tag{6.15}$$

Since the concentration of the oxide is evidently constant, say C_i, the reaction rate is

$$r = C_i \dot{L} \cdot \tag{6.16}$$

Assuming that r is linear in the oxygen concentration C_L,

$$r = kC_L \cdot \tag{6.17}$$

One obtains from Eqs. (6.15), (6.16), and (6.17) that

$$\dot{L} = kC_L/C_i , \tag{6.18}$$

and

$$D \left.\frac{\partial C}{\partial x}\right|_{x=L} + kC_L\left(1 + C_L/C_i\right) = 0 . \tag{6.19}$$

If one further assumes linear distribution in x of C(x, t) in Fig. 6.6, then with some additional approximations it follows that for sufficiently long times $L \sim t^{1/2}$ (Ghez, 1988). The above result can explain increasing weight gains for reactions that involve acquisition of matter as well as weight losses if reactions involve dissociation, with time. These weight changes occur in addition to what is attributable to diffusion and predict trends consistent with curves 3 and 4 in Fig. 6.4.

Moving fronts of chemically reacted matter were observed in the case of water-vapor-induced corrosion of glass (Charles, 1958*a*) and also in glass fibers exposed to hydrochloric and sulfuric acids as well as to distilled water (Ehrenstein and Spaude, 1984). The latter observations showed that the rate of etching depended on temperature, as may be expected for thermally activated processes. Similar fronts, which separate reacted and nonreacted matter, were noted in glass-reinforced polyester exposed to sulfur, chlorine, and other substances (Menges and Gitschner, 1980) and in neat APS/epoxy mixtures, with distinct APS (coupling agent)-to-epoxy molar ratios, exposed to water (Hoh et al., 1990).

Although none of the above observations of reaction fronts were accompanied by weight-gain or weight-loss data, such information is reported for the corrosion of glass/vinyl ester composites reacting with NaOH and HCl solutions (Hojo et al., 1982). The foregoing weight-loss data seem to confirm the suggestion that curve 4 in Fig. 6.4 corresponds to a dissociation of matter caused by chemical reactions.

Unlike the reversible "plasticization" phenomenon that may be related to weight gains along curves 1, 2, and LF in Fig. 6.4, chemical reactions may destroy the backbones of polymer chains and dissociate them into separate segments. This phenomenon, denoted as "hydrolysis," is irreversible and would usually result in the leaching of matter and weight loss (curve 4 in Fig. 6.4). Alternately, hydrolysis may have the contrary effect of inducing microcracks within the composite and lead to excessive weight gains (curve 3 in Fig. 6.4).

Though difficult to quantify, the severity of the hydrolysis process increases with temperature and solvent or fluid content (Chateauminois et al., 1993) and depends on the material system (Fukuda, 1986). It seems that the onset of hydrolysis may require some "incubation time" (Maksimov and Urzhumstev, 1977), which also depends on the foregoing parameters.

It is interesting to note that once a weight loss had occurred, the redried material absorbs ever-increasing amounts of solvents upon repeated exposures to ambient environments (Lo et al., 1982). This observation suggests the presence of irreversible damage within the material.

When transport phenomena in composites are considered, it is important to realize that those materials consist not only of fibrous and polymeric phases but also of fiber/matrix interfaces and/or interphase regions. It has been argued (Drzal et al., 1982, 1983, 1985; Gupta et al., 1985; Rich and Drzal, 1988; Hoh et al., 1990) that interphase regions may differ from bulk polymers in their chemical composition as well as in the amount of curing agent that they contain. These differences may lead to substantial discrepancies in the amounts of solvent that are absorbed by the polymer and interphase, with larger absorption within the latter—especially if it is undercured (Gupta et al., 1985; Jones et al., 1986; Hoh et al., 1990).

These observations seem to confirm original, earlier interpretations that viewed the disparate concentrations of solvent in the bulk polymer and interphase matter as caused by an osmosis phenomenon, with the polymer serving as a semipermeable membrane (Ashbee et al., 1967; Ashbee and Wyatt, 1969; Walter and Ashbee, 1982, 1984).

The increased content of fluid in the vicinity of the fiber/matrix interface and the osmotic pressure combine to weaken the interfacial strength and bring about interfacial cracking (Ashbee et al., 1967; Ashbee and Wyatt, 1969; Walter and Ashbee, 1984), which other investigators have observed as well (Menges and Gitschner, 1980; Fang, 1986; Weitsman, 1991). These interfacial cracks are sketched in Fig. 6.7.

The effect of osmotic pressure may be compounded by the microlevel tensile stresses caused by the mismatch in mechanical and expansional properties of the resin and fiber materials (Tsotsis and Weitsman, 1990).

The formation of interfacial cracks, as well as voids, may be the primary cause for an increase in the amount of fluid absorbed by the composites, resulting in a transition from weight gain along curve 1 to weight gain along curve 3 in Fig. 6.4 (Menges and Gitschner, 1980). It is also interesting to note that cyclic exposure to wet/dry environments increased the extent and amount of interfacial fiber/matrix cracks, and drying seemingly contributed more intensively to crack formation (Weitsman, 1991).

ORNL-DWG 95-2815 ETD

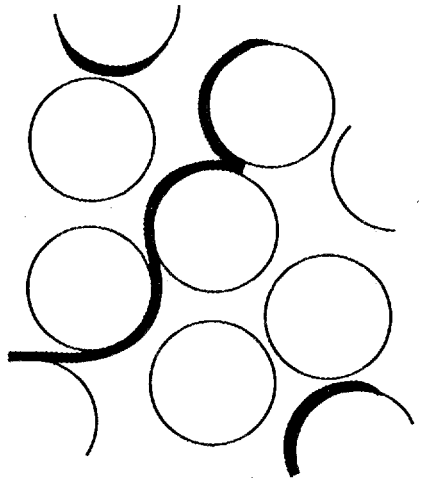

Fig. 6.7. Schematic drawing of moisture-induced fiber/matrix interfacial cracks.

6.3 MOISTURE-INDUCED SWELLING, TEMPERATURE DEPENDENCE, AND TIME SCALES

Upon absorption, fluids induce expansional strains into the polymer that are akin to thermal expansions. Typically, the coefficient of moisture expansion in polymers, b, ranges between 2×10^{-3} and 5×10^{-3} per 1% weight gain (Adamson, 1980; Cairns and Adams, 1984). When it is compared with the coefficient of thermal expansion, of typical value $\alpha \sim 2 \times 10^{-5}$ m/m/°C, we arrive at the rough estimate that the expansional strain due to 1% moisture weight gain is equivalent to the effect of about 100°C of thermal excursion.

In many circumstances fluids induce swelling only upon reaching some threshold value, say m_1. Thus, the expansional strain is given by $\varepsilon^H = \beta(m - m_1)$. Typically $m_1 \simeq 0.1\%$.

The coefficient of moisture diffusion D is extremely sensitive to temperature and may increase by 2 orders of magnitude with a temperature rise of 100°C (Delasi and Whiteside, 1978; Shirrel, 1978; Loos and Springer, 1981; Grayson and Wolf, 1985; Harper and Weitsman, 1985). A typical value of D at room temperature is $D = D_R \sim 10^{-7}$ mm²/s.

Temperature sensitivity can be expressed by an Arrhenius-type relation

$$D(T) = D_0 \exp(-A/T) \ . \tag{6.20}$$

The immediate consequence of the exceedingly small values of D is a very slow diffusion process. In fact, it may require several months to saturate polymeric or polymeric composite plates even as thin as 1 mm. In accordance with Eq. (6.9) the time-to-saturation increases with the square of the thickness, $t_{saturation} \sim L^2$.

On the other hand, for polymeric materials the coefficient of thermal diffusion $k \sim 10^{-3}$ mm²/s. Consequently, heat conduction may be uncoupled from moisture diffusion, but moisture diffusion cannot discard temporal fluctuations in temperature in view of the extreme sensitivity of D to T. Moisture saturation levels depend on the ambient level of fluid (e.g., the relative humidity of water vapor) and to a lesser degree on temperature and mechanical stress.

As will be discussed in more detail in the next section, the viscoelastic behavior of polymers depends on fluid content. Since typical time-spans for creep (which are also extremely sensitive to temperature) may extend up to several days, or even weeks and months, the viscoelastic response of polymers and polymeric composites is strongly coupled with the diffusion process (Weitsman, 1977, 1979, 1987, 1990, 1991; Douglas and Weitsman, 1980; Harper and Weitsman, 1985).

6.4 FLUID EFFECTS ON MECHANICAL RESPONSE AND MECHANICAL PROPERTIES

6.4.1 Elastic Behavior

The expansional strains that accompany the sorption of fluids induce residual stresses within composite materials, analogous to the thermal stresses that arise therein in the presence of geometrical constraints. Essentially, these residual stresses develop on the microscale, due to the mismatch between the properties of the fiber and the matrix, as well as on the ply/laminate level due to the discrepancies between longitudinal and transverse ply properties. The formulation and solution of these stress fields in composite laminates for linear elastic behavior are given in standard texts (Jones, 1975; Agarwal and Boutman, 1980; Hull, 1981; Vinson and Sierakowski, 1986; Gibson, 1994) and will not be reproduced here.

6.4.2 Viscoelastic Response

Fluids accelerate the time-dependent response of polymers and polymeric composites in a manner that is analogous to the influence of temperature. The effect of moisture can be related by a "time-moisture superposition" (Mochalov et al., 1972; Maksimov et al., 1975, 1976*a*, 1976*b*, 1972; Maksimov and Urzhumstev, 1977; Crossman et al., 1978; Renton and Ho, 1978; Ho and Schapery, 1981; Flaggs and Crossman, 1984; Harper and Weitsman, 1985) similar to the well-known time-temperature superposition in thermoviscoelasticity. Accordingly, the effect of moisture can be formulated by means of a moisture-dependent "shift factor" $a_H(m)$, which is coupled with the temperature-dependent shift $a_T(T)$. Though, in principle, the combined effects of moisture and temperature require a shift-factor function of the form $a_{TH}(T,m)$, in many circumstances it was possible to coalesce creep data into a "master curve" by the more convenient product form $a_{TH}(T,m) = a_T(T) \bullet a_H(m)$ (Maksimov et al., 1972; Renton and Ho, 1978; Ho and Schapery, 1981; Harper and Weitsman, 1985).

Typical moisture- and temperature-affected creep data for $[\pm 45°]_{2S}$ AS/3502 graphite-epoxy composites are shown in Fig. 6.8. These data were shifted to form the master curves depicted in Fig. 6.9 with the aid of the shift-factor functions drawn in Fig. 6.10.

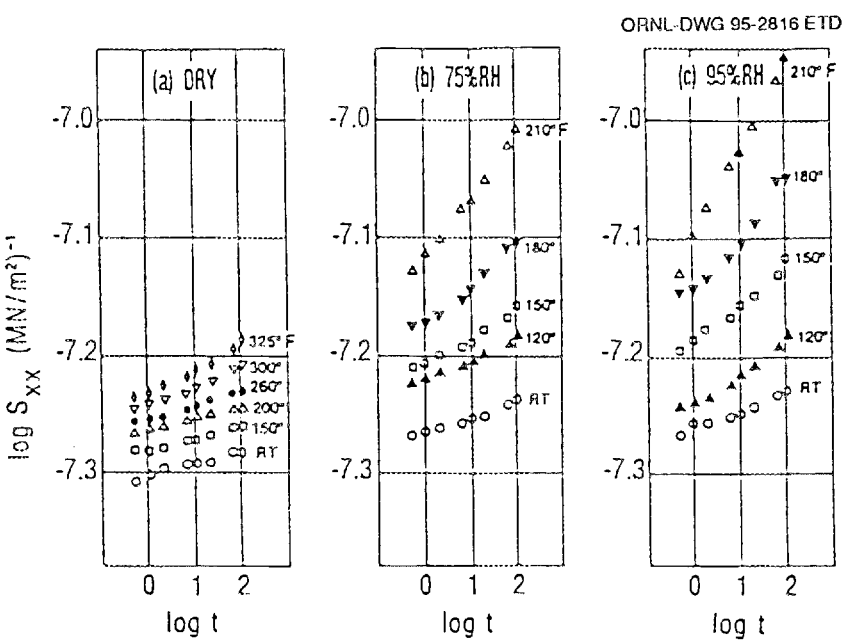

Fig. 6.8. Creep compliance S_{xx}, as recorded at various temperatures and RHs, for $[\pm 45]_{2s}$ AS/3502 composite specimens with (*a*) RH = 0%, (b) RH = 75%, and (*c*) RH = 95%. *Source*: Kibler, 1980.

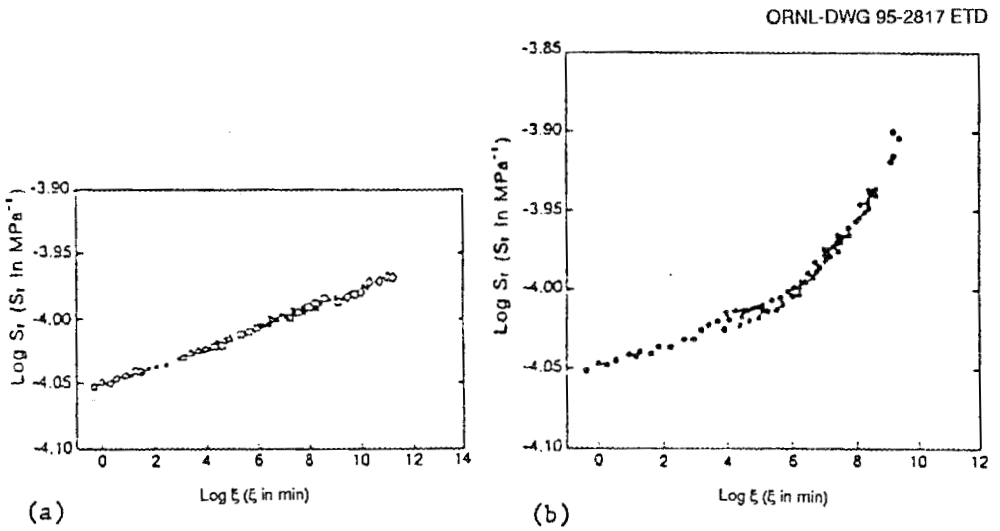

Fig. 6.9. "Master curves" for the transverse compliance S_T, as inferred from data for S_{xx} shown in Fig. 6.8, for AS/3502 composite. Curves obtained by horizontal shifts (parallel to the log t axis) of isothermal data. For (*a*) "dry" and (*b*) "wet" cases. *Source*: Harper, 1983.

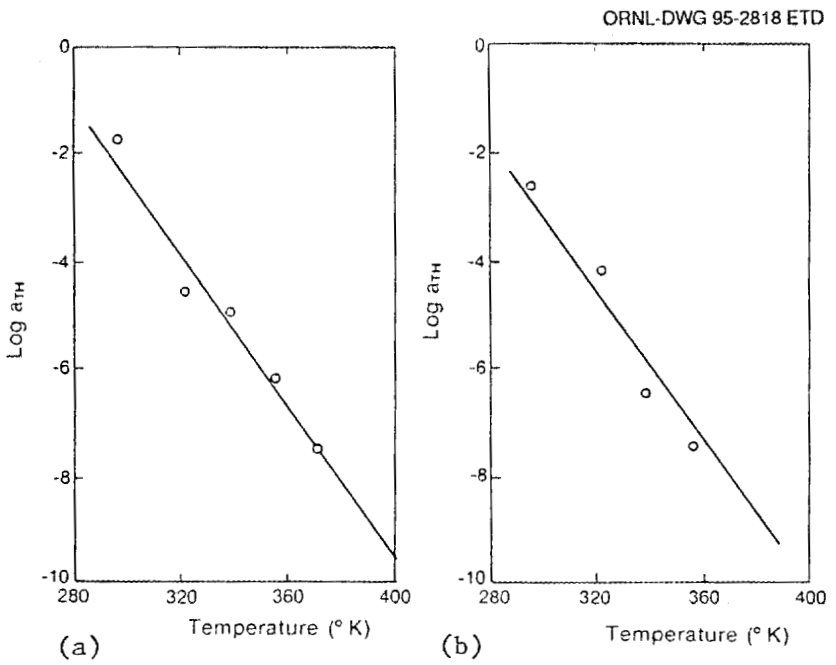

Fig. 6.10. Combined shift factor obtained from samples exposed at various temperatures. Circles indicate data inferred (Komorowski, 1983*a–d*), while full lines are based on $a_{TH} = a_T a_H$. (*a*) RH = 75% and (*b*) RH = 95%. *Source*: Harper, 1983.

For the circumstances shown in Figs. 6.8–6.10 the moisture and temperature shift factors are expressed by $a_T(T) = \exp(B - T/A)$ and $a_H(m) = \exp(-K_0 m + K_1)$ with B = 45.81, A = 6.258, $K_0 = 5.2$, and $K_1 = 0.26$, where T is in degrees Kelvin and m in percent weight gain.

Several viscoelastic solutions that account for moisture and temperature effects (Weitsman, 1977, 1979; Douglas and Weitsman, 1980; Flaggs and Crossman, 1984; Harper and Weitsman, 1985)

demonstrate that viscoelastic relaxation accounts for a behavior that differs qualitatively from an elastically predicted response. Specifically, upon subjecting a viscoelastic material to a humid environment, and subsequently to a dry ambient, the swelling strains introduced during moisture absorption—which tend to induce compression within the polymer—are followed by shrinkage caused by fluid withdrawal during the drying stage and a reversal in the stress amplitudes. However, since shrinkage is superimposed on the relaxed effect of the earlier swelling, the resulting reversal in stresses will overcompensate the relaxed levels of the previously imparted compression and yield a net tensile outcome. Such results explain the emergence of tensile cracks upon drying of previously saturated resins (Browning, 1978) and composites (Jackson, 1984; Fang, 1986; Weitsman, 1991).

The foregoing viscoelastic formulations and solutions are useful for analyzing stresses and, particularly, for determining dimensional changes due to creep in polymeric composites. On the other hand, it is important to recognize that the above methodology is restricted to linear viscoelastic response and applies to a limited range of stresses, temperatures, and moisture content (Maksimov and Urzhumstev, 1977). More significantly, linear hygrothermal viscoelasticity does not apply in circumstances that involve chemical reactions and does not account for damage (Hull and Hogg, 1980). It would therefore be incorrect to utilize that theory in circumstances in which solvent weight-gain data follow curves 3 or 4 in Fig. 6.4.

The latter weight gains are associated with excessive creep and early failures (Chateauminois et al., 1991). This correlation may also be inferred by comparisons of weight-gain data (Springer et al., 1981) and creep data (Springer, 1984*a*).

Another important observation concerns the long-term creep of polymeric composites. It has been noted on several occasions (Jain et al., 1979; Jain and Asthana, 1980; Menges and Gitschner, 1980) that the creep response of wet composites may accord with linear hygrothermal viscoelasticity for a limited duration to be followed by a noticeable upsurge in deformation, as sketched in Fig. 6.11. It seems that the increase in creep strains occurs after certain incubation times required for the inception of additional mechanisms or reactions within the polymeric composite.

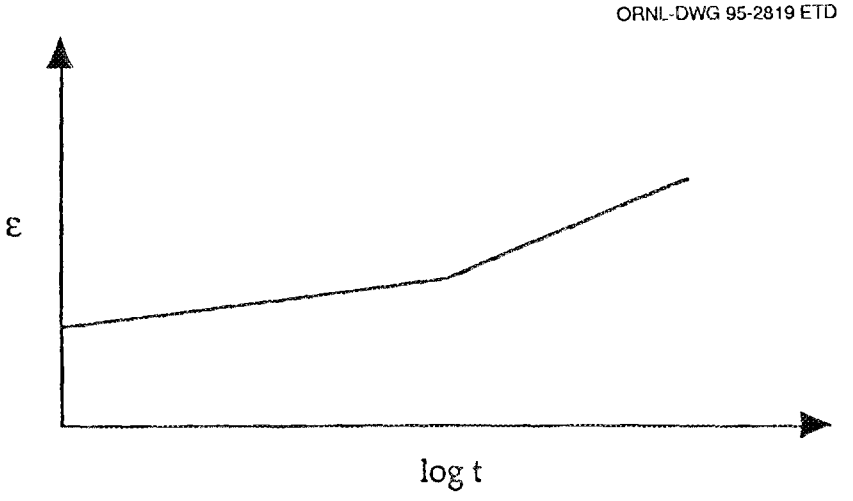

Fig. 6.11. "Two-stage" creep under extended exposure to environment.

6.4.3 Strength and Durability

It was already noted that fluids introduce residual stresses into polymeric composites and affect the mechanical fields by enhancing the creep and relaxation processes. In addition, it was remarked that solvents may degrade polymers and fiber/matrix interfaces by hydrolysis and chemical attack, induce osmotic pressure within interphase regions that contributes to the weakening of the fiber/matrix bond, and chemically decompose the fibers themselves—especially glass fibers.

These effects are reflected in significant reductions in the strength of such polymers as epoxy and in the transverse and shear strengths of unidirectionally reinforced polymeric composites (Hertz, 1973; Kaminski, 1973; Hofer et al., 1974, 1975; Verette, 1975; Browning et al., 1976; Husman, 1976; Dewimille et al., 1980; Shen and Springer, 1981*a*).

Typically, one observes degradations of between 25% and 80% in the strength of epoxies and reductions between 50% and 80% in the transverse strength of fibrous composites attributable to the effects of various fluids. The above range in the reduced values corresponds to an increasing amplitude of temperature.

Lesser reductions were observed in quasi-isotropic laminates, and no diminutions occurred in the longitudinal properties of carbon fiber composites.

It is illuminating to note that in some circumstances strength reductions in E-glass/polyester SMCs (SMC-R50) correlated with moisture weight losses, which accord with curve 4 in Fig. 6.4 (Springer et al., 1981).

Though no information is available about the detailed nature of degradation mechanisms in SMC-R50 caused by water, it is interesting to note that distinct degradation mechanisms were observed in E-glass/polyester SMC composites exposed to chemical solutions. Acids induced stress-corrosion cracking within the fibers (Somiya and Morishita, 1993*a*), while alkalines degraded the fiber/resin interface (Somiya and Morishita, 1993*b*). The latter circumstance resulted in a more severe reduction in the fracture toughness of the composite.

While carbon fibers are largely immune to solvents, glass fibers are highly susceptible to chemical attack by water, acids, and alkaline solutions (Aveston et al., 1980; Bailey et al., 1980; Dewimille et al., 1980; Aveston and Sillwood, 1982; Jones et al., 1982; Hsu and Chou, 1985; Sheard and Jones, 1986). This susceptibility is noted by the formation of pits on the surface of glass fibers immersed in water (Ashbee and Wyatt, 1969) and in sea water (White and Phillips, 1985) and by the progression of stress-corrosion cracking that leads to significant reduction in durability, as reflected by time-to-failure in static fatigue under exposure to water and acids (Charles, 1958*a*, 1958*b*; Aveston et al., 1980, 1982; Bailey et al., 1980; Dewimille et al., 1980; Kelly and McCartney, 1981; Aveston and Sillwood, 1982; Jones et al., 1982; Hsu and Chou, 1985; Sheard and Jones, 1986; Castaing et al., 1993; Chateauminois et al., 1993). As stated earlier, the corrosion of glass fibers is delineated by a sharp front that separates the yet intact core from an outer, corroded, concentrically cylindrical region. Reductions in the strength of glass fibers and their composites can be correlated with the advance of the above corrosion process (Ehrenstein and Spaude, 1984). It is worth noting that times-to-failure under static fatigue of polyester/glass composites immersed in sea water suggest the existence of two-stage mechanisms (White and Phillips, 1985), as depicted in Fig. 6.12,

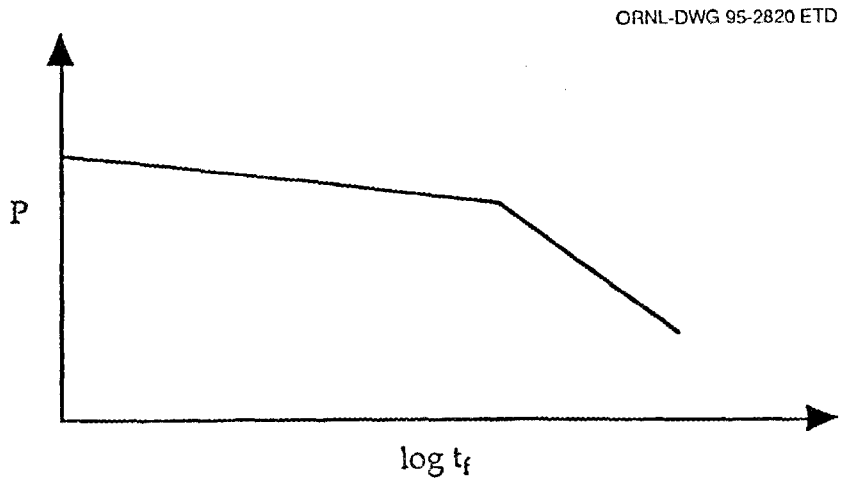

Fig. 6.12. A semilogarithmic plot of load P vs failure time t_f in static fatigue tests of glass/polyester composites in sea water.

which resemble the incubation times required for the stepping-up in creep response (Jain et al., 1979; Jain and Asthana, 1980; Menges and Gitschner, 1980).

The foregoing two-stage mechanisms in the evolution of failure under static fatigue were observed also in R-glass-epoxy specimens exposed to distilled water (Chateauminois et al., 1993). These mechanisms were interpreted in the context of Talreja's (1981) fatigue life diagram, which was shown in Fig. 3.1 of Chap. 3. Accordingly, the shorter lives at elevated stress are due to the incidence of random fiber failures attributed to the statistical distribution of the initial flaw population. The subsequent gradual increase in times to failure under lower levels of external loads is deemed to reflect the progressive failure within the composite as broken fibers transfer their loads to intact neighboring fibers. This interpretation may differ from the aforementioned incubation-time suggestion.

For glass-fiber composites, static fatigue limits correspond to about 50% of their "instantaneous" static strength (Aveston et al., 1980; Chateauminois et al., 1993). Obviously, the durability of polymeric composites exposed to fluids is affected by temperature (Charles, 1958*b*), since it is governed by thermally activated processes.

Swirl mat and chopped mat glass fiber composites exhibit weight losses when exposed to hot water above 90°C. These weight losses correlate with reduction of up to 50% in their strength and stiffness (Lou and Murtha, 1987).

Basic considerations of crack growth at various stages of the stress-corrosion cracking process (Evans, 1972) suggest that chemical reactions control crack growth at low load levels, whereas the diffusion of corrosive substance governs the failure process under higher loads. At yet higher stress levels crack growth is dominated by stress-assisted corrosion.

Upon drying, composites regain a portion or the entire value of their original strength (Phillips et al., 1978; Dewimille et al., 1980; Springer et al., 1981; Manocha et al., 1982; Drzal et al., 1985). The amount of recovery depends on the extent and kind of irreversible damage caused by the prior exposure to solvents.

Prestressing of composites prior to their exposure to solvents may accelerate the solvent-induced corrosion (Sandifer, 1982; Fujii et al., 1993). This enhancement is most likely due to mechanical damage caused by prestressing, which facilitates the subsequent penetration of solvent through capillary action (Ehrenstein and Spaude, 1984).

Though generalizations are risky and unreliable, it seems that in many circumstances water (distilled or salty) causes more significant reductions in the strength of composites than fuels or motor oils (Sandifer, 1982; Blicblau et al., 1993). In some cases an increase in water salinity tends to intensify the losses in composites' properties (Nakanishi and Shindo, 1982).

6.4.4 Solvent Effects on the Fracture Toughness, Fatigue Response, and Impact Resistance of Polymeric Composites

The fracture toughness of composite materials depends on the combined interplay of energy-absorbing micromechanisms in the vicinity of a crack tip (Jordan, 1985). These mechanisms include the ductilities of the resin and the interphase material and the fiber/matrix interfacial bond. It is important to recognize that the capacity of the resin and the interphase matter to undergo ductile deformation is restricted by the confining effects of the stiffer and more brittle fibers.

Fluids enhance the ductility of polymers through plasticization, which should increase the toughness of composites. However, solvents tend to weaken the fiber/matrix interfacial bond and induce osmotic pressures that may assist in the activation of crack growth, thereby diminishing the toughness of composites. The interplay among the foregoing competing effects is difficult to quantify. These contradictory effects may cancel each other, as evidenced by the insensitivity of the extent of edge delaminations in cross-ply glass-epoxy laminates to the presence or absence of water (Yang et al., 1992). Similar insensitivity was observed in the growth of edge delamination in cross-ply graphite-epoxy laminates immersed in sea water, in spite of some differences in detail when compared with dry circumstances (Chiou and Bradley, 1993).

However, in some specific circumstances the presence of fluids may dramatically increase the fracture toughness of composites, as occurs for mode I delamination of unidirectionally reinforced graphite-epoxy double-cantilever beam specimens immersed in sea water (Sloan and Seymour, 1992). The reason

for this seemingly surprising result is that the extended weakening of the fiber/matrix interfaces caused by sea water activated a phenomenon of fiber bridging across the crack surfaces.

Fatigue of composite materials is the subject of much ongoing research (Sendeckyj, 1990). The fatigue response is characterized by the familiar S-N diagrams, except that composites exhibit larger data scatter than metals. The S-N data are described by empirical expressions, and attempted predictions and reliability assessments are based on statistical consideration (Sendeckyj, 1990; Talreja, 1990).

A rational, though still qualitative, approach to fatigue in composites was proposed by Talreja (1981), where S-N data were converted from stress space to strain space, namely into ε vs N diagrams, as was shown in Fig. 3.1. The selection of ε ranging over $\varepsilon_m < \varepsilon < \varepsilon_c$ (where ε_m and ε_c denote the fatigue limit strain and static failure strain of the composite, respectively) was motivated by the fact that during fatigue the various phases (and plies) within a composite are subjected to common strains but to disparate stresses. If failure of a composite can be prescribed by means of a strain criterion, then $\varepsilon - N$ diagrams would account more closely for its fatigue response. The foregoing selection seems natural in accounting for environmental effects in cases in which the major role of the fluid is confined to enhancing the resin's ductility by plasticization. In addition, it is reasonable to expect that, in the least, the fatigue limit corresponds to a physically meaningful value of ε_m.

The horizontal band about ε_c in Fig. 3.1 represents failure strains that are independent of the number of fatigue cycles N. These failures are attributable to the random distribution of initial flaw sizes within the composite. At lower strain levels, the sloping band of failure strains ε vs N corresponds to a progressive failure process within the composite where the weakening caused by localized failures is taken up by intact regions until the interaction and coalescence of growing cracks reach critical levels that result in failure after N fatigue cycles. The lower horizontal band about $\varepsilon = \varepsilon_m$ in Fig. 3.1 corresponds to a sufficiently low strain level, possibly a matrix property, which is commensurate with the fatigue limit.

In a variety of circumstances it was observed that fluids shorten the fatigue life of glass fiber (Phillips et al., 1978; Aveston et al., 1980; Dewimille et al., 1980; Lou and Murtha, 1987; Yang et al., 1992) and carbon fiber (Sumison, 1976; Morton et al., 1988) composites and that the extent of their effects depends on both fluid type and material system (Sandifer, 1982). In addition, the presence of water may affect the failure mechanisms that evolve during the fatigue process (Morton et al., 1988).

It is reasonable to assume that all the aforementioned fluid-induced mechanisms that degrade the strength of composites operate also to shorten the fatigue life of those materials. Nevertheless, there exist two additional degradation mechanisms that are specific to fatigue. The first involves the synergistic interaction between the fluid sorption process and fatigue-induced damage; namely, a profusion of microcracks that opens capillary paths for fluid ingress (Jones et al., 1984). This mode of fluid penetration is order of magnitudes faster than the diffusion process and subjects the composite to accelerated degradation (Kosuri and Weitsman). The second mechanism involves the synergistic destruction of interfacial fiber/matrix bonds caused by their cyclic rubbing under fatigue loading. The introduction of fluids into the composite enhances the above phenomenon, since fluids act as lubricants (Jones et al., 1984). Evidence for the smoothing and polishing of fiber/matrix interfaces due to moisture abound in the literature, but only circumstantial evidence exists at the present time, which implies that the same effect occurs during fatigue (Aveston and Sillwood, 1982; Galea and Saunders, 1993).

All the "wet fatigue" data noted thus far were obtained for specimens with prior, but not concurrent, exposure to solvents. An ongoing study (Kosuri and Weitsman) on the effects of sea water on the fatigue of cross-ply graphite-epoxy composites indicates that significant reductions in fatigue life occur especially under immersed conditions, when capillary action is highly accentuated.

The effects of fluids on the impact resistance of composites contain the contradictory aspects that hold for fracture toughness. In view of the fluid-induced weakening of the fiber/matrix interfacial strength, the impacting object may engage a larger volume of fibers in the absorption of the impact energy, thus resulting in improved impact resistance (Strait et al., 1992; Lin, 1993). In addition, the plasticization and enhanced ductility of the wet polymer may explain the observed reduction in the peak amplitudes of the contact pressures during impact (Strait et al., 1992; Lin, 1993). On the other hand, impact-induced damage may enhance the amounts of absorbed fluids within the composite under subsequent exposures and lead to long-term degradations in residual mechanical properties (Ma et al., 1991).

6.5 CONCLUDING REMARKS

Good basic understandings, accompanied by adequate predictive methodologies, are available to account for sorption mechanisms that are akin to linear Fickian diffusion and for the incorporation of fluid effects within the scope of elastic and linearly viscoelastic material response. Unfortunately, those understandings are inadequate for predicting the more intricate, yet crucially important, matters of durability and strength of composites, since no comprehensive formalism is available to account quantitatively for the multitude of materials and circumstances in a manner that may be applied to a specific case of interest.

What emerges from this review is the realization that practical design considerations must derive from an adequate data base specific to each composite material system. An assessment of the significance of fluid effects can be obtained by recording their weight gain within the composites. Significant departures from linear Fickian predictions portend serious degradation in mechanical properties and should become the subject of detailed study and microscopic examination. Furthermore, careful consideration should be given to circumstances when mechanical loads, temperature, and solvents interact synergistically to degrade properties of the composites. To some extent, such considerations may be guided by fundamental concepts of polymer science and applied mechanics. They may also benefit from familiarity with existing knowledge that, at least to a limited extent, was summarized in the present review.

REFERENCES

Adamson, M. J. 1980. *J. Mater. Sci.* **15**, 1736.

Agarwal, B. D., and Boutman, L. J. 1980. *Analysis and Performance of Fiber Composites*, Wiley, New York.

Althof, W. November 1979. "The Diffusion of Water Vapour in Humid Air into the Bondlines of Adhesive Bonded Metal Joints," *Proceedings of the 11th National SAMPE Conference*, Vol. 11, SAMPE, Azusa, pp. 309–32.

Apicella, A., et al. 1981. *Polym. Eng. Sci.* **2191**, 18.

Ashbee, K. H. G., Frank, F. C., and Wyatt, R. C. 1967. "Water Damage in Polyester Resins," *Proc. Roy. Soc. A* **300**, pp. 415–19.

Ashbee, K. H. G., and Wyatt, R. C. 1969. "Water Damage in Glass Fibre/Resin Composites," *Proc. Roy. Soc. A* **312**, pp. 553–64.

Aveston, J., et al. 1982. "Long Term Strength of Glass Reinforced Plastics," *Proceedings of the Fourth International Conference on Composite Materials (ICCM/4), Tokyo, October 25–28, 1982, Progress in Science and Engineering of Composites*, Vol. 2, ed. T. Hayashi, K. Kawata, and S. Umekawa). pp. 947–55.

Aveston, J., Kelly, A., and Sillwood, J. M. 1980. "Long Term Strength of Glass Reinforced Plastics in Wet Environments," *Proceedings of the Third International Conference on Composite Materials (ICCM/3), Paris, August 26–29, 1980, Advances in Composite Materials*, Vol. 1, ed. A. R. Bunsell, C. Bathias, A. Martrenchar, D. Menkes, and G. Verchery, pp. 556–68.

Aveston, J., and Sillwood, J. M. 1982. "Long-Term Strength of Glass-Reinforced Plastics in Dilute Sulphuric Acid," *J. Mater. Sci.* **17**(12), 3491–98.

Bailey, J. E., Fryer, T. M. W., and Jones, F. R. 1980. "Environmental Stress-Corrosion Edge-Cracking of Glass Reinforced Polyesters," *Proceedings of the Third International Conference on Composite*

Materials (ICCM/3), Paris, August 26–29, 1980, Advances in Composite Materials, Vol. 1, ed. A. R. Bunsell, C. Bathias, A. Martrenchar, D. Menkes, and G. Verchery, pp. 513–28.

Blicblau, A. S., Tran, L., and Warden, P. 1993. "Environmental Effects on Carbon Fibre/Epoxy Shear Strength," *Proceedings of the Ninth International Conference on Composite Materials (ICCM/9), Madrid, July 12–16, 1993, Composite Behaviour*, Vol. 5, ed. A. Miravete, pp. 660–64.

Blikstad, M. Sjoblom, O. W., and Johannesson, T. R. 1988. "Long-Term Moisture Absorption in Graphite/Epoxy Angle-Ply Laminates," ed. G. S. Springer, *Environmental Effects of Composite Materials*, Vol. 3, Technomic Publishing Company, Lancaster, Pennsylvania, pp. 107–21.

Bonniau, P., and Bunsell, A. R. 1984. "A Comparative Study of Water Absorption Theories Applied to Glass Epoxy Composites," ed. G. S. Springer, *Environmental Effects of Composite Materials*, Vol. 2, Technomic Publishing Company, Lancaster, Pennsylvania, pp. 209–28.

Browning, C. E. 1978. "The Mechanisms of Elevated Temperature Property Losses in High Performance Structural Epoxy Resin Matrix Materials After Exposure to High Humidity Environments," *ICCM/2 Proceedings of the 1978 International Conference on Composite Materials, Toronto, April 16–20, 1978*, ed. B. Noton, R. Signorelli, K. Street, and L. Phillips, pp. 1527–43.

Browning, C. E., Husman, G. E., and Whitney, J. M. 1976. "Moisture Effects in Epoxy Matrix Composites," *Composite Materials: Testing and Design*, ASTM STP **617**, American Society for Testing and Materials, Philadelphia.

Cai, L., and Weitsman, Y. 1994. "Non-Fickian Moisture Diffusion in Polymeric Composites," *J. Comp. Mater.* **28**(2), 130–54.

Cairns, D. S., and Adams, D. F. 1984. "Moisture and Thermal Expansion Properties of Unidirectional Composite Materials and the Epoxy Matrix," ed. G. S. Springer, *Environmental Effects on Composite Materials*, Vol. 2, Technomic Publishing Company, Lancaster, Pennsylvania, pp. 300–25.

Carter, H. G., and Kibler, K. G. 1978. *J. Comp. Mater.* **12**, 118.

Castaing, Ph., Lemoine, L., and Tsoubalis, N. 1993. "Experimental Study of the Variation in Mechanical Characteristics of Orthotropic Laminates Immersed in Water by a Non Destructive Method," *Proceedings of the Ninth International Conference on Composite Materials (ICCM/9), Madrid, July 12–16, 1993, Composite Behaviour*, Vol. 5, ed. A. Miravete, pp. 577–84.

Charles, R. J. 1958*a*. "Static Fatigue of Glass I," *J. Appl. Phys.* **29**(11), 1549–53.

Charles, R. J. 1958*b*. "Static Fatigue of Glass. II," *J. Appl. Phys.* **29**(11), 1554–60.

Chateauminois, A., et al. 1991. "Hydrothermal Ageing Effects on Viscoelastic and Fatigue Behavior of Glass/Epoxy Composites," *Proceedings of the Eighth International Conference on Composite Materials (ICCM/8), Honolulu, July 15–19, 1991, Composites Design, Manufacture, and Application*, Section 12-21, ed. S. W. Tsai and G. S. Springer, pp. 16-E-1–16-E-12.

Chateauminois, A., et al. 1993. "Effects of Hygrothermal Aging on the Durability of Glass/Epoxy Composites. Physico-Chemical Analysis and Damage Mapping in Static Fatigue," *Proceedings of the Ninth International Conference on Composite Materials (ICCM/9), Madrid, July 12–16, 1993, Composite Behaviour*, Vol. 5, ed. A. Miravete, pp. 593–600.

Chiou, P., and Bradley, W. L. 1993. "The Effect of Seawater Exposure on the Fatigue Edge Delamination Growth of a Carbon/Epoxy Composite," *Proceedings of the Ninth International Conference on Composite Materials (ICCM/9), Madrid, July 12–16, 1993, Composite Behaviour*, Vol. 5, ed. A. Miravete, pp. 516–23.

Clark, D. L. December 1983. "Moisture Absorption in Hybrid Composites," Texas A&M University Report MM 4665-83-16.

Crank, J. 1953. *Journal of Polymer Science* **11**(2), 151–68.

Crank, J. 1975. *The Mathematical Theory of Diffusion*, Oxford University Press, Oxford, 2d ed.

Crank, J., and Park, G. S. ed. 1968. *Diffusion in Polymers*, Academic Press, New York.

Crossman, F. W., Mauri, R. E., and Warren, N. T. 1978. ed. J. R. Vinson, "Advanced Composite Materials-Environmental Effects," ASTM STP **658**, American Society for Testing and Materials, Philadelphia, pp. 2–20.

DeIasi, R., and Whiteside, J. B. 1978. "Effects of Moisture on Epoxy Resins and Composites," ASTM STP **658**, American Society for Testing and Materials, Philadelphia, pp. 2–20.

Dewimille, B., et al. 1980. "Hydrothermal Aging of an Unidirectional Glass-Fibre Epoxy Composite During Water Immersion," *Proceedings of the Third International Conference on Composite Materials (ICCM/3), Paris, August 26–29, 1980, Advances in Composite Materials*, Vol. 1, ed. A. R. Bunsell, C. Bathias, A. Martrenchar, D. Menkes, and G. Verchery, pp. 597–612.

Douglas, D. A., and Weitsman, Y. 1980. "Stresses Due to Environmental Conditioning of Cross-Ply Graphite/Epoxy Laminates," *Proceedings of the Third International Conference on Composite Materials (ICCM/3), Paris, August 26–29, 1980, Advances in Composite Materials*, Vol. 1, ed. A. R. Bunsell, C. Bathias, A. Martrenchar, D. Menkes, and G. Verchery, pp. 529–42.

Drzal, L. T., Rich, M. J., and Koenig, M. F. 1985. "Adhesion of Graphite Fibers to Epoxy Matrices. III. The Effect of Hygrothermal Exposure" *J. Adhesion* **18**, 49–72.

Drzal, L. T., et al. 1983. "Adhesion of Graphite Fibers to Epoxy Matrices: II. The Effect of Fiber Finish," *J. Adhesion* **16**, 133–52.

Drzal, L. T., Rich, M. J., and Lloyd, P. F. 1982. "Adhesion of Graphite Fibers to Epoxy Matrices: I. The Role of Fiber Surface Treatment," *J. Adhesion* **16**, 1–30.

Ehrenstein, G. W., and Spaude, R. 1984. "A Study of the Corrosion Resistance of Glass Fibre Reinforced Polymers," in *Comp. Struct. 2*, Elsevier Applied Science Publishers, Ltd., England, pp. 191–200.

Evans, A. G. 1972. "A Method for Evaluating the Time-Dependent Failure Characteristics of Brittle Materials—and its Application to Polycrystalline Alumina," *J. Mater. Sci.* (7), 1137–46.

Fang, G.-P. November 1986. *Moisture and Temperature Effects in Composite Materials*, Texas A&M University Report MM 5022-86-21.

Fick, A. 1855. "Uber Diffusion," *Ann. Der. Phys.* **94**, 59–86.

Flaggs, D. L., and Crossman, F. W. 1984. "Analysis of the Viscoelastic Response of Composite Laminates During Hygrothermal Exposure," ed. G. S. Springer, *Environmental Effects of Composite Materials*, Vol. 2, Technomic Publishing Company, Lancaster, Pennsylvania, pp. 363–79.

Frisch, H. L. 1964. "Isothermal Diffusion in Systems with Glasslike Transitions," *J. Chem. Phys.* **41**(12), 3679–83.

Frisch, H. L. 1966. "Irreversible Thermodynamics of Internally Relaxing Systems in the Vicinity of the Glass Transition," ed. R. J. Dennelly, R. Herman, and I. Prigogine, *Non-Equilibrium Thermodynamics, Variational Techniques and Stability*," University of Chicago Press, pp. 277–80.

Frisch, H. L., and Stern, S. A. 1983. *CRC Crit. Rev. Solid State Mater. Sci.* **11**(2), 123.

Fujii, Y., et al. 1993. "Evaluation of Initial Damage and Stress Corrosion of GFRP," *Proceedings of the Ninth International Conference on Composite Materials (ICCM/9), Madrid, July 12–16, 1993, Composite Behaviour*, Vol. 5, ed. A. Miravete, pp. 562–68.

Fukuda, H. 1986. "Effect of Moisture Absorption on the Mechanical Properties of Advanced Composites," *Proceedings of the International Symposium on Composite Materials and Structures, Beijing, June 10–13, 1986*, ed. T. T. Loo and C. T. Sun, pp. 50–55.

Galea, S. C., and Saunders, D. S. 1993. "Effects of Hot/Wet Environments on the Fatigue Behaviour of Composite-to-Metal Mechanically Fastened Joints," *Proceedings of the International Conference on Advanced Composite Materials (ICACM), Wollongong, Australia, February 15–19, 1993*, ed. T. Chandra and A. K. Dhingra, pp. 525–31.

Ghez, R. 1988. *A Primer of Diffusion Problems*, J. Wiley, New York.

Gibson, R. F. 1994. *Principles of Composite Materials*, McGraw Hill, New York.

Grayson, M. A., and Wolf, C. J. 1985. "Diffusion of Water in Carbon Epoxy Composites," *Proceedings of the Fifth International Conference on Composite Materials (ICCM/5), San Diego, July 29–August 1, 1985*, ed. W. C. Harrigan, Jr., J. Strife, and A. K. Dhingra, pp. 1463–73.

Gupta, V. B., Drzal, L. T., and Rich, M. J. 1985. *J. Appl. Polym. Sci.* **30**, 4467.

Gurtin, M., and Yatomi, C. 1979. "On a Model for Two Phase Diffusion in Composite Materials," *J. Comp. Mater.* **13**, 126–30.

Harper, B. D. August 1983. *On the Effects of Post Cure Cool Down and Environmental Conditioning on Residual Stresses in Composite Laminates*, Texas A&M University Report MM-4665-83-11.

Harper, B. D., and Weitsman, Y. 1985. "On the Effects of Environmental Conditioning on Residual Stresses in Composite Laminates," *International Journal of Solids and Structures* **21**(8), 907–26.

Henson, M. C., and Weitsman, Y. 1986 "Stress Effects on Moisture Transport in an Epoxy Resin and Its Composite," *Proc. 3rd Japan-U.S. Conference on Composite Materials, Tokyo, June 1986*, Japan Society of Composite Materials, Tokyo.

Hertz, J. June 1973. *Investigation into the High-Temperature Strength Degradation of Fiber-Reinforced Resin Composite During Ambient Aging*, Convair Aerospace Division, General Dynamics Corporation, Report GDCA-DBG73-005, Contract NAS8-27435.

Ho, T., and Schapery, R. A. January 1981. *The Effect of Environment on the Mechanical Behavior of AS/3501-6 Graphite/Epoxy Material*, Phase III, Vought Corporation, ATC Report No. R-92100/1CR-5, Final Report to the Department of the Navy, Contract No. N00019-79-C-0580, NASC.

Hofer Jr., K. E., Larsen, D., and Humphreys, V. E. February 1975. *Development of Engineering Data on the Mechanical and Physical Properties of Advanced Composites Materials*, Technical Report AFML-TR-74-266, Air Force Materials Laboratory, Air Force Systems Command, Wright-Patterson Air Force Base, Dayton, Ohio.

Hofer Jr., K. E., Rao, N., and Larsen, D. February 1974. *Development of Engineering Data on the Mechanical and Physical Properties of Advanced Composite Materials*, Technical Report AFML-TR-72-205, Part II, Air Force Materials Laboratory, Air Force Systems Command, Wright-Patterson Air Force Base, Dayton, Ohio.

Hoh, K.-P., Ishida, H., and Koenig, J. L. 1990. "Multi-Nuclear NMR Spectroscopic and Proton NMR Imaging Studies on the Effect of Water on the Silane Coupling Agent/Matrix Resin Interface in Glass Fiber-Reinforced Composites," *Polymer Composites* **11**(3), 192–99.

Hojo, H., et al. 1982. "The Effects of Stress and Flow Velocity on Corrosion Behavior of Vinyl Ester Resin and Glass Composites," *Proceedings of the Fourth International Conference on Composite Materials (ICCM/4), Tokyo, October 25–28, Progress in Science and Engineering of Composites*, Vol. 2, ed. T. Hayashi, K. Kawata, and S. Umekawa, pp. 1017–24.

Hopfenberg, H. B., and Stannett, V. 1973. "The Diffusion and Sorption of Gases and Vapours in Glassy Polymers," ed. R. N. Howard, *The Physics of Glassy Polymers*, Applied Science, New York, pp. 504–47.

Hsu, P-L., and Chou, T.-W. 1985. "Corrosion Effects on E-Glass Filaments, Bundles, and their Aligned Short-Fiber Composites," *Proceedings of the Fifth International Conference on Composite Materials (ICCM/5), San Diego, July 29–August 1, 1985*, ed. W. C. Harrigan, Jr., J. Strife, and A. K. Dhingra, pp. 1475–90.

Hull, D. 1981. *Introduction to Composite Materials*, University Press, Cambridge.

Hull, D., and Hogg, P. J. 1980. "Nucleation and Propagation of Cracks During Strain Corrosion of GRP," *Proceedings of the Third International Conference on Composite Materials (ICCM/3), Paris, August 26–29, 1980, Advances in Composite Materials*, Vol. 1, ed. A. R. Bunsell, C. Bathias, A. Martrenchar, D. Menkes, and G. Verchery, pp. 543–55.

Husman, G. E. 1976. "Characterization of Wet Composite Materials," presented at the Mechanics of Composites Review, Bergamo Center, Dayton, Ohio, January 28–29, 1976.

Jackson, S. P. May 1984. *Hygrothermal Effects in an Anti-Symmetric Cross-Ply Graphite/Epoxy Material*, Texas A&M University Report MM 4665-84-7.

Jain, R. K., and Asthana, K. K. 1980. "Effect of Natural Weathering on the Creep Behaviour of GRP Laminates in Tropical Climates," *Proceedings of the Third International Conference on Composite Materials (ICCM/3), Paris, August 26–29, 1980, Advances in Composite Materials*, Vol. 1, ed. A. R. Bunsell, C. Bathias, A. Martrenchar, D. Menkes, and G. Verchery, pp. 613–23.

Jain, R. K., Goswamy, S. K., and Asthana, K. K. 1979. "A Study of the Effect of Natural Weathering on the Creep Behaviour of Glass Fibre-Reinforced Polyester Laminates," *Composites* **10**(1), 39–43.

Jones, C. J., et al. 1984. "The Environmental Fatigue Behaviour of Reinforced Plastics," *Proceedings of the Royal Society of London, Series A* **396**(1811), 315–38.

Jones, F. R., et al. 1982. "The Environmental Stress Corrosion Cracking of Glass Fibre Reinforced Polyester and Epoxy Composites," *Proceedings of the Fourth International Conference on Composite Materials (ICCM/4), Tokyo, October 25–28, Progress in Science and Engineering of Composites,* Vol. 2, ed. T. Hayashi, K. Kawata, and S. Umekawa, pp. 929–36.

Jones, F. R., Shah, M. A., and Bader, M. G. 1986. "The Effect of Curing Conditions on the Equilibrium Moisture Levels and Residual Dicyandiamide (DICY) in GRP Laminates," *Proceedings of the International Symposium on Composite Materials and Structures, Beijing, June 10–13*, ed. T. T. Loo and C. T. Sun, Technomic Publishing Company, Lancaster, Pennsylvania, pp. 87–93.

Jones, R. M. 1975. *Mechanics of Composite Materials*, McGraw Hill, New York.

Jordan, W. M. December 1985. *The Effect of Resin Toughness on the Delamination Fracture Behaviour of Graphite/Epoxy Composites*, Ph.D. Dissertation, Interdisciplinary Engineering, Texas A&M University.

Kaminski, B. E. 1973. "Effects of Specimen Geometry on the Strength of Composite Materials," *Analysis of the Test Methods for High Modulus Fibers and Composites*, ASTM STP **521**, p. 181, American Society for Testing and Materials, Philadelphia.

Kelly, A., and McCartney, L. N. 1981. "Failure by Stress Corrosion of Bundles of Fibres," *Proceedings of the Royal Society of London, Series A* **374**(1758), 475–89.

Kibler, K. F. February 1980. *Time-Dependent Environmental Behavior of Graphite/Epoxy Composites*, Final Report, General Dynamics Corporation, Fort Worth, TX, Contract F33 615-77-C-5109, Report AFWAL-TR-80-4052.

Komorowski, J. P. January 1983*a*. *Hygrothermal Effects in Continuous Fibre Reinforced Composites. Part I: Thermal and Moisture Diffusion in Composite Materials*, National Aeronautical Establishment, National Research Council Canada, Aeronautical Note NAE-AN-4, NRC No. 20974.

Komorowski, J. P. September 1983*b*. *Hygrothermal Effects in Continuous Fibre Reinforced Composites. Part II: Physical Properties*, National Aeronautical Establishment, National Research Council Canada, Aeronautical Note NAE-AN-10, NRC No. 22700.

Komorowski, J. P. September 1983*c*. *Hygrothermal Effects in Continuous Fibre Reinforced Composites. Part III: Mechanical Properties 1 Static Tests*, National Aeronautical Establishment, National Research Council Canada, Aeronautical Note NAE-AN-11, NRC No. 21299.

Komorowski, J. P. September 1983*d*. *Hygrothermal Effects in Continuous Fibre Reinforced Composites. Part IV: Mechanical Properties 2 Fatigue and Time-Dependent Properties*, National Aeronautical Establishment, National Research Council Canada, Aeronautical Note NSE-AN-12, NRC No. 21300.

Kosuri, R., and Weitsman, Y., to be published.

Lin, C-W. 1993. "Effect of Moisture Absorption on the Impact Behavior of Unidirectional Carbon Fiber Reinforced Nylon 6 Composite," *Proceedings of the International Conference on Advanced Composite Materials (ICACM), Wollongong, Australia, February 15–19, 1993*, ed. T. Chandra and A. K. Dhingra, pp. 597–602.

Lo, S. Y., Hahn, H. T., and Chiao, T. T. 1982. "Swelling of KEVLAR 49/Epoxy and S2-Glass/Epoxy Composites," *Proceedings of the Fourth International Conference on Composite Materials (ICCM/4), Tokyo, October 25–28, 1982, Progress in Science and Engineering of Composites,* Vol. 2, ed. T. Hayashi, K. Kawata, and S. Umekawa, pp. 987–1000.

Long, F. A., and Richman, D. 1960. "Concentration Gradients for Diffusion of Vapors in Glassy Polymers and their Relation to Time Dependent Diffusion Phenomena," *J. Am. Chem. Soc.* **82**, 513–19.

Loos, A. C., and Springer, G. S. 1981. "Moisture Absorption of Graphite-Epoxy Composition Immersed in Liquids and in Humid Air," ed. G. S. Springer, *Environmental Effects of Composite Materials,* Technomic Publishing Company, Lancaster, Pennsylvania, pp. 34–49.

Loos, A. C., Springer, G. S., Sanders, B. A., and Tung, R. W. 1981. "Moisture Absorption of Polyester-E Glass Composites," ed. G. S. Springer, *Environmental Effects of Composite Materials,* Technomic Publishing Company, Lancaster, Pennsylvania, pp. 51–63.

Lou, A. Y., and Murtha, T. P. 1987. "Environmental Effects on Glass Fiber Reinforced PPS Stampable Composites," *J. Comp. Mater.* **21**(10), 910–24.

Ma, Chen-Chi M., Huang, Y. H., and Chang, M. J. 1991. "Effect of Jet Fuel on the Mechanical Properties of PPS/C. F. and Peek/C. F. After Impact Loading," *Proceedings of the Eighth International Conference on Composite Materials (ICCM/8), Honolulu, July 15–19, 1991, Composites Design, Manufacture, and Application,* Section 12-21, ed. S. W. Tsai and G. S. Springer, pp. 16-M-1–16-M-10.

Maksimov, R. D., Mochalov, V. P., and Sokolov, E. A. 1975. "Effect of Temperature and Humidity on Creep on Polymeric Materials," *Journal of Polymer Mechanics* **3**, 393–99.

Maksimov, R. D., Mochalov, V. P., and Sokolov, E. A. 1976*a*. "Influence of Temperature and Humidity on the Creep of Polymeric Materials. 3. Shear, and Shear and Tensile Strain Acting Together," *Journal of Polymer Mechanics* **4**, 627–32.

Maksimov, R. D., Mochalov, V. P., and Sokolov, E. A. 1976*b*. "Influence of Temperature and Humidity on the Creep of Polymeric Materials. 4. Prediction on the Basis of Field Test Results," *Journal of Polymer Mechanics* **6**, 982–87.

Maksimov, R. D., Mochalov, V. P., and Urzhumtsev, Yu. S. 1972. "Time-Moisture Superposition," *Journal of Polymer Mechanics* **5**, 780–86.

Maksimov, R. D., and Urzhumstev, Yu. S. July–August 1977. "Prediction of the Long-Term Durability of Polymer Materials. A Review," *Mekh. Polimerov* (4), 631–45.

Manocha, L. M., Bahl, O. P., and Jain, R. K. 1982. "Performance of Carbon Fibre Reinforced Epoxy Composites under Different Environments," *Proceedings of the Fourth International Conference on Composite Materials (ICCM/4), Tokyo, October 25–28, 1982, Progress in Science and Engineering of Composites,* Vol. 2, ed. T. Hayashi, K. Kawata, and S. Umekawa, pp. 957–64.

Marom, G. 1989. "Environmental Effects on Fracture Mechanical Properties of Polymer Composites," ed. K. Friedrich, *Application of Fracture Mechanics to Composite Materials,* Elsevier Science Publishers B. V., New York, p. 397.

McKague, L. 1978. "Environmental Synergism and Simulation in Resin Matrix Composites," ASTM STP **658**, 193–204.

Menges, G., and Gitschner, H.-W. 1980. "Sorption Behaviour of Glass-Fibre Reinforced Composites and the Influence of Diffusing Media on Deformation and Failure Behaviour," *Proceedings of the Third International Conference on Composite Materials (ICCM/3), Paris, August 26–29, 1980, Advances in Composite Materials*, Vol. 1, ed. A. R. Bunsell, C. Bathias, A. Martrenchar, D. Menkes, and G. Verchery, pp. 25–48.

Mochalov, V. P., Aniskevich, N. I., and Maksimov, R. D. 1972. "Creep of Polymer Resin PN-3 Under Moisture-Absorption Conditions," *Polymer Mechanics* **4**, 579–84.

Mohlin, T. 1988. "Deterioration in Compressive Performance of a Graphite/Epoxy Laminate as a Consequence of Environmental Exposure and Fatigue Loading," ed. G. S. Springer, *Environmental Effects of Composite Materials*, Vol. 3, Technomic Publishing Company, Lancaster, Pennsylvania, pp. 163–70.

Morton, J., Kellas, S., and Bishop, S. M. 1988. "Damage Characteristics in Notched Carbon Fiber Composites Subjected to Fatigue Loading—Environmental Effects," *J. Comp. Mater.* **22**(7), 657–73.

Nakanishi, Y., and Shindo, A. 1982. "Deterioration of CFRP and GFRP in Salt Water," *Proceedings of the Fourth International Conference on Composite Materials (ICCM/4), Tokyo, October 25–28, 1982, Progress in Science and Engineering of Composites*, Vol. 2, ed. T. Hayashi, K. Kawata, and S. Umekawa, pp. 1009–16.

Phillips, D. C., Scott, J. M., and Buckley, N. 1978. "The Effects of Moisture on the Shear Fatigue of Fibre Composites," *ICCM/2 Proceedings of the 1978 International Conference on Composite Materials, Toronto, April 16–20, 1978*, ed. B. Noton, R. Signorelli, K. Street, and L. Phillips, pp. 1544–59.

Renton, W. J., and Ho, T. August 1978. "The Effect of Environment on the Mechanical Response of AS/3501-6 Graphite/Epoxy Materials," Final Report to the Department of the Navy, Contract No. N000019-77-C-0369, NASC, for the period June 1977–June 1978.

Rich, M. J., and Drzal, L. T. 1988. "Interfacial Properties of Some High-Strain Carbon Fibers in an Epoxy Matrix," *J. Reinf. Plast. and Comp.* **7**, 145–54.

Rogers, C. E. 1965. "Solubility and Diffusivity," ed. D. Fox, M. M. Labes, and A. Weissberger, *Physics and Chemistry of the Organic Solid State*, Vol. 2, Interscience Pub., New York, pp. 509–635.

Rogers, C. E. 1985. "Permeation of Gases and Vapours in Polymers," ed. J. Comyn, *Polymer Permeability*, Elsevier Applied Science, New York, pp. 11–73.

Sandifer, J. P. 1982. "Effects of Corrosive Environments on Graphite/Epoxy Composites," *Proceedings of the Fourth International Conference on Composite Materials (ICCM/4), Tokyo, October 25–28, 1982, Progress in Science and Engineering of Composites*, Vol. 2, ed. T. Hayashi, K. Kawats, and S. Umekawa, pp. 979–86.

Sendeckyj, G. P. 1990. "Life-Prediction for Resin Matrix Composite Materials," ed. K. L. Reifsnider, *Fatigue of Composite Materials*, Elsevier, New York, pp. 431–83.

Sheard, P. A., and Jones, F. R. 1986. "The Stress Corrosion of Glass Fibres and Epoxy Composites in Aqueous Environments," *Proceedings of the International Symposium on Composite Materials and Structures, Beijing, June 10–13, 1986*, ed. T. T. Loo and C. T. Sun, pp. 118–23.

Shen, C. H., and Springer, G. S. 1981*a*. "Effects of Moisture and Temperature on the Tensile Strength of Composite Materials," ed. G. S. Springer, *Environmental Effects of Composite Materials*, Technomic Publishing Company, Lancaster, Pennsylvania, pp. 79–92.

Shen, C. H., and Springer, G. S. 1981*b*. "Moisture Absorption and Desorption of Composite Materials," ed. G. S. Springer, *Environmental Effects of Composite Materials*, Technomic Publishing Company, Lancaster, Pennsylvania, pp. 15–33.

Shewmon, P. G. 1983. *Diffusion in Solids*, J. Williams Book Company, Jenks, Oklahoma.

Shirrel, C. D. 1978. "Diffusion of Water Vapor in Graphite/Epoxy Composites," ASTM STP **658**, 21–42, American Society for Testing and Materials, Philadelphia.

Sloan, F. E., and Seymour, R. J. 1992. "The Effect of Seawater Exposure on Mode I Interlaminar Fracture and Crack Growth in Graphite/Epoxy," *J. Comp. Mater.* **26**(18), 2655–73.

Somiya, S., and Morishita, T. 1993*a*. "Degradation Phenomenon of Fracture Toughness of SMC Immersed in Acid Condition," *Proceedings of the International Conference on Advanced Composite Materials (ICACM), Wollongong, Australia, February 15–19, 1993*, ed. T. Chandra and A. K. Dhingra, pp. 637–42.

Somiya, S., and Morishita, T. 1993*b*. "Study on the Degradation Phenomena of SMC in Alkali Condition by Acoustic Emission Method," *Proceedings of the Ninth International Conference on Composite Materials (ICCM/9), Madrid, July 12–16, 1993, Composite Behaviour*, Vol. 5, ed. A. Miravete, pp. 585–92.

Springer, G. S. ed. 1981. *Environmental Effects on Composite Materials*, Technomic Publishing Company, Lancaster, Pennsylvania.

Springer, G. S. ed. 1984*a*. "Effects of Temperature and Moisture on Sheet Molding Compounds," *Environmental Effects of Composite Materials*, Vol. 2, Technomic Publishing Company, Lancaster, Pennsylvania, pp. 59–77.

Springer, G. S. ed. 1984*b*. *Environmental Effects on Composite Materials*, Vol. 2, Technomic Publishing Company, Lancaster, Pennsylvania.

Springer, G. S. ed. 1988. *Environmental Effects on Composite Materials*, Vol. 3, Technomic Publishing Company, Lancaster, Pennsylvania.

Springer, G. S., Sanders, B. A., and Tung, R. W. 1981. "Environmental Effects on Glass Fiber Reinforced Polyester and Vinylester Composites," ed. G. S. Springer, *Environmental Effects of Composite Materials*, Technomic Publishing Company, Lancaster, Pennsylvania, pp. 126–44.

Stanett, V., and Hopfenberg, H. B. 1972. "Diffusion in Polymers," ed. C. E. H. Bawn, *MTP International Review of Sciences*, Vol. 8, *Macromolecular Science*, London, pp. 329–69.

Strait, L. H., Karasek, M. L., and Amatean, M. F. 1992. "Effects of Seawater Immersion on the Impact Resistance of Glass Fiber Reinforced Epoxy Composites," *J. Comp. Mater.* **26**(14), 2118–33.

Struik, L. C. E. 1978. *Physical Aging in Amorphous Polymers and Other Materials*, Elsevier, New York.

Sumsion, H. T. 1976. "Environmental Effects on Graphite-Epoxy Fatigue Properties," *Journal of Spacecrafts and Rockets* **13**(1), 150–55.

Talreja, R. 1981. "Fatigue of Composite Materials: Damage Mechanisms and Fatigue-Life Diagrams," *Proc. Roy. Soc. London A* **378**, 461–75.

Talreja, R. 1990. "Statistical Considerations," ed. K. L. Reifsnider, *Fatigue of Composite Materials*, Elsevier, pp. 485–501.

Tsotsis, T. K., and Weitsman, Y. 1990. "Energy Release Rates for Cracks Caused by Moisture Absorption in Graphite/Epoxy Composites," *J. Comp. Mater.* **24**(5), 483–96.

Verette, R. M. 1975. "Temperature/Humidity Effects on the Strength of Graphite/Epoxy Laminates," AIAA Paper No. 75-1011, AIAA 1975 Aircraft Systems and Technology Meeting, Los Angeles, California, August 4–7, 1975.

Vinson, J. R., and Sierakowski, R. L. 1986. "The Behavior of Structures Composed of Composite Materials," Nijhoff.

Walter, E., and Ashbee, K. H. G. 1982. "Osmosis in Composite Materials," *Composites*, 365–68.

Walter, E., and Ashbee, K. H. G. 1984. "Osmosis and Failure Mechanism in Fiber Reinforced Composites," *Can. Metall. Q.* **23**(1), 71.

Weitsman, Y. 1977. "Effects of Fluctuating Moisture and Temperature on the Mechanical Response of Resin-Plates," *J. Appl. Mech. ASME* **44**(4), 571–76.

Weitsman, Y. 1979. "Interfacial Stresses in Viscoelastic Adhesive Layers Due to Moisture Sorption," *Int. J. Solids Struct.* **15**(9), 701–14.

Weitsman, Y. 1981. "A Rapidly Convergent Scheme to Compute Moisture Profiles in Composite Materials Under Fluctuating Ambient Conditions," *J. Comp. Mater.* **15**, 349–58.

Weitsman, Y. 1987. "Stress Assisted Diffusion in Elastic and Viscoelastic Materials," *J. Mech. Phys. Solids* **35**(1), 73–97.

Weitsman, Y. 1990. "A Continuum Diffusion Model for Viscoelastic Materials," *The Journal of Physical Chemistry* **94**(2), 961–68.

Weitsman, Y. 1991. "Moisture in Composites: Sorption and Damage," ed. K. L. Reifsnider, *Fatigue of Composite Materials*, Elsevier Science Pub., New York, pp. 385–429.

White, R. J., and Phillips, M. G. 1985. "Environmental Stress-Rupture Mechanisms in Glass Fiber/Polyester Laminates," *Proceedings of the Fifth International Conference on Composite Materials (ICCM/5), San Diego, July 29–August 1, 1985*, ed. W. C. Harrigan, Jr., J. Strife, and A. K. Dhingra, pp. 1089–99.

Whiteside, J. B., DeIasi, R. J., and Schulte, R. L. 1984. "Distribution of Absorbed Moisture in Graphite/Epoxy Laminates After Real-Time Environmental Cycling," ASTM STP **813**, 192–205.

Whitney, J. M., and Browning, C. E. 1978. "Some Anomalies Associated with Moisture Diffusion in Epoxy Matrix Composite Materials," ASTM STP **658**, 43–60.

Windle, A. H. 1985. "Case II Sorption," ed. J. Comyn, *Polymer Premeability*, Elsevier Applied Science, New York, pp. 75–118.

Yang, B.-X., Kasamori, M., and Yamamto, T. 1992. "The Effect of Water on the Interlamina Delamination Growth of Composite Laminates," *Proceedings of the Second International Symposium on Composite Materials and Structures, Beijing, August 3–7, 1992*, ed. C. T. Sun and T. T. Loo, pp. 334–39.

7. ULTRASONIC TECHNIQUES FOR THE NONDESTRUCTIVE EVALUATION OF SWIRL MAT COMPOSITES

W. A. Simpson, Jr.

7.1 INTRODUCTION

Advanced composite structures, because of their superior strength-to-weight ratios and resistance to corrosion, are finding application in many structural areas traditionally reserved for metals. Unlike their metallic counterparts, however, the fracture properties, modes of failure, etc., of composite materials are much less well known; this promotes overly conservative design by structural engineers and partly offsets the weight advantages enjoyed by composites. One striking example of the differing response of metals and composites to the presence of flaws is that, for the latter, there is generally no critical flaw size that, if present, will lead to catastrophic failure of the part. Indeed, failure in composites often occurs in regions for which no demonstrable initiating flaw can be found, while areas with known discontinuities may survive. Thus, the definition of what constitutes a flaw may be radically different for the two materials, and the fracture mechanics models that have been so successful in predicting service life for structural metals are not applicable to composites. To offset this disadvantage of the latter materials, phenomenological models, often based on observed correlations between composite behavior under stress and some measurable property of the structure, have been developed.

In quantifying the failure predictions for metals, NDE techniques have been the primary tools by which such critical parameters as flaw size and shape, crack-opening displacement, and the stress intensity factor have been determined. To gain more insight into the possibility of assessing the integrity of composite structures, therefore, several NDE techniques have been applied to various fiber-reinforced matrices. Unfortunately, the applicability of traditional NDE techniques to such materials depends very strongly on the design of the particular composite, as well as on the fiber and matrix selected. For example, whisker-reinforced ceramics tend to behave like isotropic, homogeneous materials for ultrasonic evaluation when the wavelength of the interrogating energy is large compared to the whisker diameter. Even at high frequencies, when the ultrasonic wavelength becomes comparable to whisker size, such materials tend to appear locally inhomogeneous but isotropic. A more common design for composites, however, is the structure consisting of one or more plies of a matrix into which have been dispersed unidirectionally or randomly oriented reinforcing fibers. Early designs consisting of single plies of unidirectionally oriented fibers, which generally exhibit poor cross-fiber strength, have been largely supplanted by various types of layups consisting of stacks of plies having some prescribed rotation of the fiber orientation from ply to ply or by designs containing randomly oriented fibers, as in swirl mat composites. These arrangements typically yield a transversely isotropic structure whose plane of isotropy is the plane in which the anticipated stress will act. Unfortunately, the intentional misalignment of structures whose intrinsic elastic symmetry is typically orthotropic, or even of structures whose symmetry is transversely isotropic, produces a product that, from the standpoint of an elastic wave used to probe the composite, is horribly inhomogeneous. This, in turn, means that traditional methods of NDE cannot generally be applied with reasonable success to the evaluation of composite materials.

Fortunately, for discrete but uniform variations in the elastic properties of a medium on a scale small with respect to the wavelength of the probing elastic wave, the material can be adequately represented as anisotropic rather than inhomogeneous, and the former characteristic can be treated rather easily. The low frequencies required to ensure the elastic conditions described above, however, lead once again to numerous problems, chief among them resolution, when traditional methods of NDE are employed.

Because of the unique problems presented by the NDE of composites, mitigated by the recognition of their enormous potential and many advantages in lightweight, high-strength applications, there has been intense effort in the last decade to develop new and more promising methods of assessing the integrity of these advanced materials nondestructively. It has quickly become apparent that no panacea will be

universally applicable to all composite designs. The literature already reflects a schism between techniques for "thick" (i.e., on the scale of a wavelength) composites and those for which the ply—or total—thickness is comparable to or smaller than a wavelength. Within each subdivision, the development of new composite materials generally demands new research to ascertain, or develop, the most effective nondestructive technique for assuring the integrity of the structure.

For virtually all types of advanced composites, it has been recognized that the properties of the fiber-matrix interface are critical in determining the response of the structure to applied stress or in predicting remnant life. Paradoxically, perfect bonding between fiber and matrix may not represent the most desirable material state. In brittle matrix composites (e.g., whisker-toughened ceramics), the strength of the material will fall if the reinforcing fiber becomes perfectly bonded to the matrix. An excellent example is that of SiC-SiC (silicon carbide whiskers dispersed in a silicon carbide matrix) composites. The reason for this counterintuitive anomaly is that, when perfectly bonded, the fiber is broken quickly by the energy released during crack growth in the matrix. On the other hand, if the fiber is totally disbonded from the matrix, then the former absorbs no crack propagation energy and the strength falls to that of the matrix alone. Maximum strength is reached when part of the crack propagation energy is dissipated in breaking the fiber-matrix bond. For these materials, therefore, the ultimate strength of the composite is very strongly dependent on the properties of the fiber-matrix interface. On the other hand, total separation of the fiber content from the matrix will clearly prejudice the strength of all types of composites. Nondestructive techniques developed to monitor or assess the state of the fiber-matrix bond will thus have two goals. In order of increasing difficulty of implementation, they are to (1) indicate, either through appropriate modeling techniques or through empirically developed relationships, the correlation between fiber disbond fraction and some measurable response of the material to NDE and (2) demonstrate the ability to assess—and perhaps predict—strength and remnant life nondestructively by detecting changes in the fiber-matrix bond conditions, including changes that do not necessarily include complete separation of the fiber. The latter condition is particularly challenging since weak, but continuous, bonding between fiber and matrix is difficult to distinguish from strong bonding by conventional nondestructive techniques. Which of the two goals just described is most important, or adequate, for a given composite depends on the nature of the structure. For typical fiber-resin composites, determination of the fiber disbond fraction may be sufficient. In brittle matrix composites, on the other hand, the ultimate goal should be to determine nondestructively the strength of the fiber-matrix bond, not just the presence or absence of bonding.

Of concern in all types of composites is the detection and quantification of damage. Like many other aspects of composites, damage can assume several forms. In some applications, impact damage may be the primary method of material degradation. In others, chemical or environmental damage may predominate. In still others, for example, in the case of composites used as the external covering for aircraft, heat damage is the method of attack that is of principle concern. Each of these types of damage produces a characteristic alteration in the properties of the composite and may be most amenable to detection by a particular NDE technique. For example, impact damage is usually localized in area but often distributed throughout the thickness of a composite. Consequently, it may often be detected by fairly conventional NDE approaches, namely, C-scans. Chemical and environmental damage may be distributed in area but be either confined to the surface or penetrate very little into the structure. Since such damage is not sharply differentiated from the surrounding undamaged material and because the effect of such damage may involve only subtle changes in the properties of the composite, detection is usually more difficult and often intractable to conventional methods of NDE. Heat damage, particularly in the early stages before delamination occurs, is confined to the surface and characteristically produces little change in the elastic behavior of the composite, though the strength is compromised. Finally, if the damage occurs principally through cyclic fatigue or creep, then the changes in the composite are manifested through matrix cracking and fiber-matrix debonding, which may or may not be readily detectable by conventional NDE techniques but which typically produces a demonstrable change in the elastic wave attenuation or scattering behavior. For all of these reasons, the investigator must have a panoply of tools available to intelligently and effectively assess the integrity of advanced composite materials.

Not surprisingly, the development of NDE techniques for composite materials has concentrated primarily on reliable methods for detection of damage. The vast body of work has been concerned with development or adaptation of linear techniques for composite evaluation, but recent efforts have begun to

establish the potential of the nonlinear response of the sample as a sensitive indicator of the global state of the fiber-matrix bond integrity. This later work has begun to change the role of NDE in composite evaluation from that of a tool merely to detect and image internal damage to one that is much more quantitative and that can provide valuable input to models of composite failure designed to predict failure and/or remnant life. A review of the work that has been done in achieving this goal, including a description of the various techniques that have been used or developed for composites, is in order.

7.2 LINEAR TECHNIQUES

Elastic waves propagating in a composite structure will interact with changes or discontinuities in the local elastic properties, thereby revealing the latter. This interaction can be described to a high degree of accuracy by linear theory, and a great deal of work has been performed to develop techniques for applying elastic wave propagation to the evaluation of materials. These techniques range from simple, purely empirical approaches to complex techniques requiring considerable computational power before the information sought can be extracted. In addition to the interaction with discontinuities in the elastic properties, it should be noted that the propagation behavior of elastic waves in any material can yield, nondestructively, information about the elastic properties of the medium that could be attained only with difficulty, or not at all, by conventional mechanical properties testing. As an example, the thin nature of many composites means that only the in-plane moduli can be obtained by tensile testing. On the other hand, the propagation of an elastic wave through the thickness of such a sample yields directly the out-of-plane or through-thickness values, thus complementing the tensile test results very nicely. In addition, techniques now exist to determine all of the elastic properties, in-plane as well as out-of-plane, from nondestructive measurements performed from a single surface of the sample or from both surfaces*. These techniques, which arise from linear theory, often involve generation of types of ultrasonic waves [e.g., surface acoustic and Lamb waves (to be described shortly)] other than the familiar bulk waves.

As a very simple example of the utility of nondestructive techniques to complement conventional mechanical property testing, consider the case of the urethane swirl mat composites described above. Tensile testing has provided estimates of the in-plane elastic constants, but no estimate of the through-thickness properties can be obtained in this manner. On the other hand, ultrasonic waves can be propagated in the through-thickness direction with ease. Both compressional and transversely polarized shear waves can be generated in the sample. In the case of an isotropic medium, there is a very simple relationship connecting the velocities of these two types of waves and the engineering constants (Krauträmer and Krauträmer, 1990):

$$V_t = \sqrt{\frac{\mu}{\rho}} \ , \qquad V_l = \sqrt{\frac{\lambda + 2\mu}{\rho}} \ , \qquad \sigma = \frac{1 - 2\gamma^2}{2 - 2\gamma^2} \ ,$$

$$E = 2\mu(1 + \sigma) \ ,$$

where V_t is the measured shear wave velocity, V_l is the compressional wave velocity, ρ is the material density, μ is the first Lamé constant (also known as the shear modulus), λ is the second Lamé constant, σ is Poisson's ratio, γ is the ratio of shear wave to compressional wave velocities, and E is the Young's modulus. If one measures the two wave velocities V_t and V_l, the complete elastic behavior of the material is known, provided the material density is also available.

The swirl mat composite is not isotropic, however, and the simple model just described will not suffice to characterize its elastic properties. Assuming that the fiber orientation is essentially random, the

---

*Bar-Cohen and Mal (1990), Chu and Rohklin (1994), Chu et al. (1994), Dayal and Kinra (1989), Fitting et al. (1989), Hosten (1991), Hosten and Castaings (1993), Karim et al. (1990), Kline and Chen (1988), Kline et al. (1991), Kline and Sahay (1992), Mal et al. (1992, 1993, 1994), Nayfeh and Chimenti (1988*b*), Rohklin and Wang (1989), Rohklin et al. (1990), Rohklin and Chimenti (1990), Rose et al. (1987), Thompson et al. (1975), Wooh and Daniel (1991).

material should exhibit transversely isotropic behavior, with the plane of isotropy corresponding to the sample plane. This assumption can also be checked nondestructively. For such symmetry, the velocity of the shear wave along the symmetry axis (through-thickness) is independent of wave polarization. Hence, rotation of the transducer while observing the transit time of the wave will reveal no change with polarization. For orthotropic (or other) symmetry, however, the wave velocity will vary as the transducer is rotated. For all of the samples available to us, no variation in the wave velocity with polarization was noted. Hence, the assumption of transverse isotropy seems justified. For this symmetry, five constants are necessary to characterize the elastic behavior fully. The full elastic stiffness matrix with the relationships for the engineering constants follows:

$$\begin{matrix} C_{11} & C_{12} & C_{13} & 0 & 0 & 0 \\ C_{12} & C_{11} & C_{13} & 0 & 0 & 0 \\ C_{13} & C_{13} & C_{33} & 0 & 0 & 0 \\ 0 & 0 & 0 & C_{44} & 0 & 0 \\ 0 & 0 & 0 & 0 & C_{44} & 0 \\ 0 & 0 & 0 & 0 & 0 & 1/2(C_{11}-C_{12}) \end{matrix}$$

$$E_1 = 1/S_{11};\ E_2 = 1/S_{22};\ E_3 = 1/S_{33};\ n_{31} = -S_{13}/S_{11};\ n_{31} = -S_{13}/S_{11};\ n_{21} = -S_{12}/S_{11}$$

$$S_{33} = \frac{C_{11} + C_{12}}{C_{33}(C_{11} + C_{12}) - 2C_{13}^2},$$

where S_{ij} is the compliance matrix, the inverse of the stiffness matrix, C_{ij}. The through-thickness Young's modulus, E_3, thus requires S_{33}, which in turn requires C_{11}, C_{12}, C_{13}, and C_{33}. In measuring the ultrasonic velocities in the through-thickness direction, we obtain C_{33} (and C_{44}) directly. At this point two options exist: (1) measure nondestructively the remaining constants, including the in-plane values, using the techniques described in the group of references cited earlier or (2) use the in-plane values determined by tensile testing to provide the other stiffnesses needed to determine S_{33}, and thus E_3. In the present case, C_{11} was available but not the off-diagonal terms. If we simply employ the isotropic model described earlier, that is, if we neglect the anisotropy of the sample, we can determine an approximate value for the through-plane Young's modulus. Table 7.1 shows the results obtained on two samples.

Table 7.1. Elastic constant results

V_l (km/s)	V_t (km/s)	ρ (g/cm^3)	Shear modulus (GPa)	Poisson's ratio	Young's modulus (GPa)
2.49	1.21	1.51	2.22	0.34	5.96
2.51	1.43	1.48	3.02	0.26	7.61

The values for the first sample should be considered more accurate than the second because of the methods employed to measure velocity. Nevertheless, the variation in Young's modulus between these two samples amounts to almost 28%, although part of this difference is undoubtedly attributable to errors in measuring the shear wave velocity in the second sample. (Note that the variation in this quantity is about 18%.) We then measured the other samples using the more accurate technique, and the results yielded an average Young's modulus of about 6 GPa. This is comparable to, but slightly lower than, the values obtained from tensile testing for the in-plane modulus.

7.2.1 C-Scan

Probably the simplest NDE technique for examining composite structures is the ultrasonic C-scan. In this approach, elastic waves are propagated through the sample under investigation, and the amplitude of the transmitted signal is digitized and recorded as a given gray-scale level or color. One advantage of this approach is that the resulting display produces an actual image of the composite, which requires minimal training to interpret. Regions of localized changes in the elastic properties will appear well differentiated from the surrounding areas, and damaged regions can be seen directly. In its original concept, C-scanning was strictly an amplitude-based technique. In recent years, however, it has been recognized that changes in the modulus of the sample will affect the velocity of the elastic wave more strongly than the amplitude, and the presence of damage at different depths within a composite can be distinguished if time-sensitive rather than amplitude-sensitive techniques are applied. Hence, it is becoming commonplace to acquire and digitize the time-of-flight of the transmitted signal as well as its amplitude. Interestingly, composites are one class of material for which the presence of damage may often produce a change in modulus. In metals, "damage" is most often associated with cracking, which has no effect on elastic wave velocity (neglecting the stress fields produced, which do affect the velocity, albeit very weakly). For many composites, therefore, a map of velocity vs position produces a more noticeable indication of damage than the conventional map of amplitude vs position.

The use of ultrasonic C-scan technology has a long and extensive history. Many of the more recent examples of this approach utilize computer control of the scan process and analysis of the resulting data to extract the maximum amount of information from the acquired signal.* To illustrate this approach, we examined several samples of isocyanurate swirl mat composite. In evaluating these samples, we used a two-transducer, through-transmission arrangement in which one transducer acts as transmitter and the second, positioned on the other side of the sample, as receiver. The elastic wave thus makes a single pass through the specimen. Figure 7.1 shows the results obtained acquiring the amplitude of the signal. (Note: the original data were depicted in color, which enhances the differentiation between regions of differing attenuation or velocity. For this report, this and all other figures are depicted in gray scale.) The sample is about 33 mm wide by 150 mm long, and the bright, circular area near the left is a manufacturing mark, apparently a mold mark. This area appears brighter (greater transmission) for two reasons: the sample thickness is slightly less in this region, which means that less material must be traversed by the elastic wave, and the surface is smoother here, which reduces the scattering losses from the surface. The variations seen throughout the length of the sample are typical of composites, which are notoriously heterogeneous.

Figure 7.2 shows the results obtained when time-of-flight (velocity) is acquired rather than amplitude. The mold mark is seen much more readily, and the sample appears much more homogeneous than when amplitude is acquired. This is also typical; small variations in the fiber-resin ratio will have much less effect on velocity than on attenuation, which is strongly dependent on the fiber fraction encountered.

Figure 7.3 shows an amplitude map of a second specimen. Here the most notable feature is a very bright strip running along the bottom edge of the sample. Visual examination revealed that there was a noticeable reduction in the fiber content of this region; hence, the amplitude of the elastic wave was much greater here. On the other hand, while the velocity map did detect the resin-rich area, the results were far less dramatic. The percentage change in velocity in the anomalous region was considerably less than was the percentage change in transmission amplitude.

The examples given previously did not involve actual damage to the specimen. The molding mark was detectable simply because it was a region that was slightly thinner and much smoother than the adjacent, as-fabricated areas, and the resin-rich area, while probably prejudicial to the integrity of the specimen, did not represent damage. We had available, however, another specimen that had been damaged by impact with a ball-peen hammer. The damage produced was detectable visually, but it was not great. No demonstrable change in the specimen thickness in the impact area was noted, but some broken fibers could be

---

*Bar-Cohen et al. (1993), Bashyam (1990), Blodgett and Ruddell (1992), Buynak and Moran (1987), Buynak et al. (1989), Daniel et al. (1987), Daniel and Wooh (1989, 1990), Frock et al. (1988), Ruber et al. (1988), Martin and Chimenti (1990), Michaels et al. (1993), Murphy et al. (1990), Murri et al. (1987), Rogovsky (1991), Simpson and McClung (1984), Steiner and Lindsay (1994), Thomas and Odegard (1988), Wooh and Daniel (1990).

PHOTO YP20694

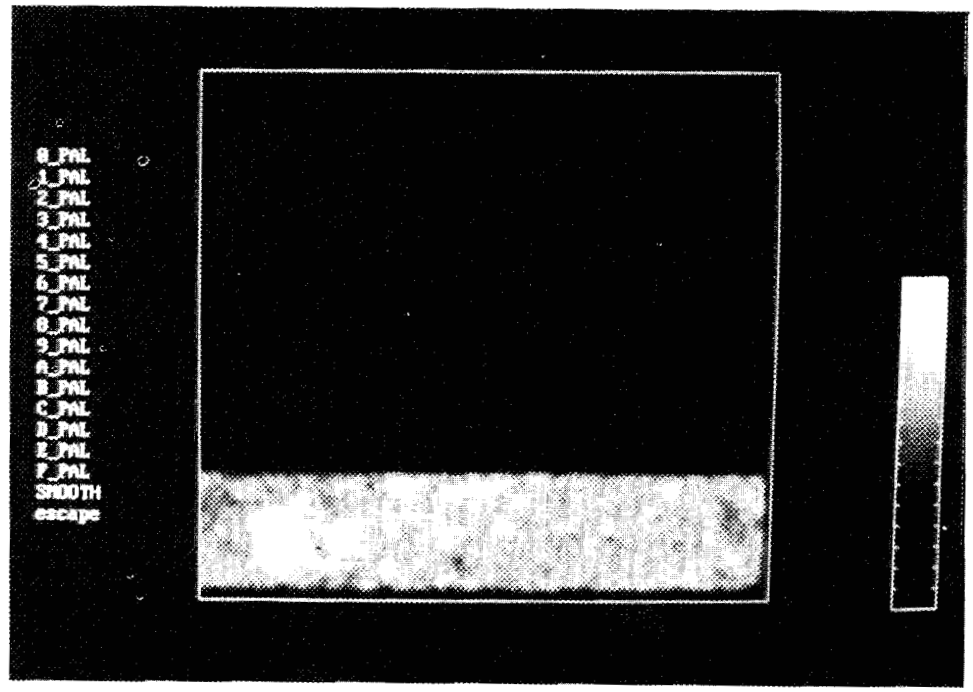

Fig. 7.1. Through-transmission ultrasonic C-scan image (amplitude) of piece of urethane swirl mat composite showing molding mark (bright circle at left of image).

PHOTO YP20698

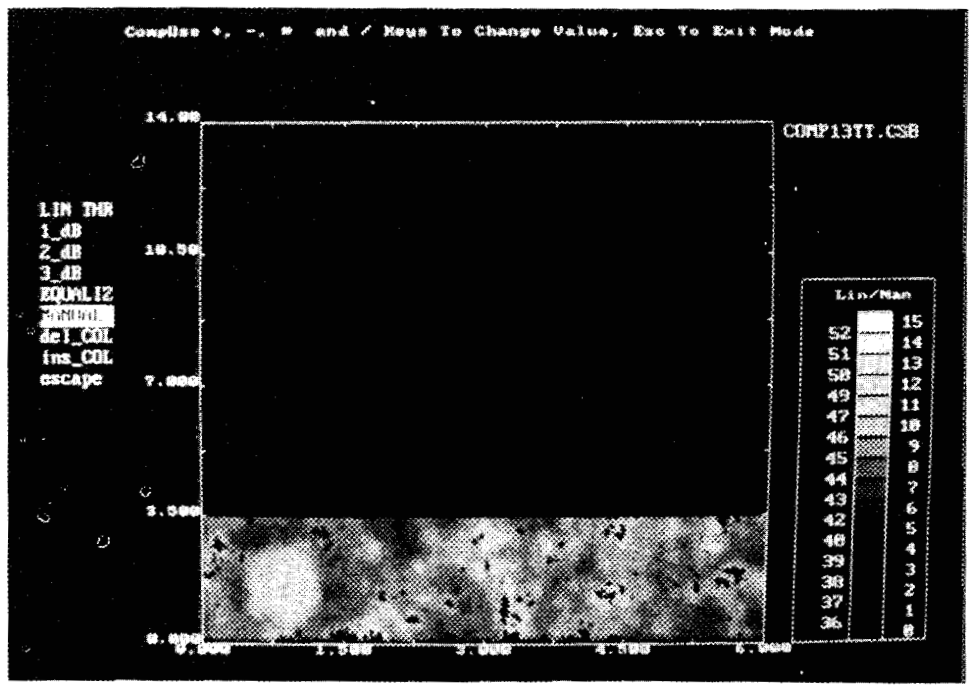

Fig. 7.2. Through-transmission ultrasonic C-scan image (velocity) of piece of urethane swirl mat composite showing molding mark (brighter circular area at left of image).

PHOTO YP20695

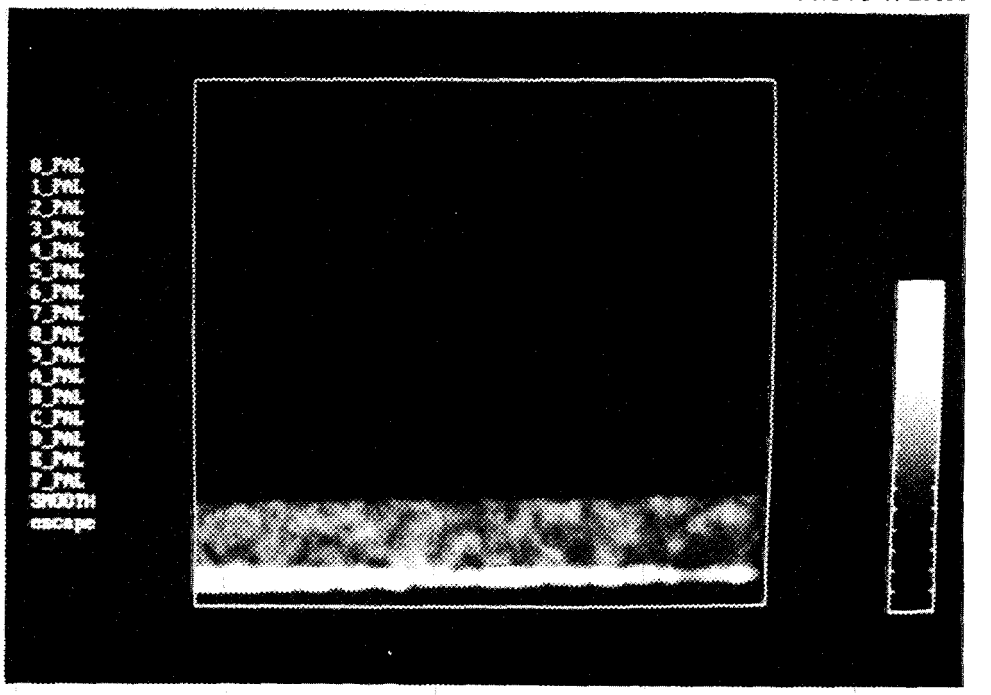

Fig. 7.3. Through-transmission ultrasonic C-scan image (amplitude) of piece of urethane swirl mat composite showing fiber-poor region (bright strip along bottom edge of sample).

seen. Because this material is sufficiently thin (~3 mm) to transmit some light, holding the specimen up to a strong light revealed more extensive internal damage that was not visible in reflection.

The specimen was first examined ultrasonically in through-transmission mode, and the damaged area was located, although the resulting image contained other indications that were very nearly as large in amplitude as the damage. In other words, the discrimination between damage and normal material heterogeneity was poor. We therefore switched to a pulse-echo mode of examination in which a single transducer was used to insonify the specimen and to detect the energy reflected from the back surface of the sample. In this configuration, the elastic wave passes twice through the damaged region, thereby enhancing the effect of the damage on transmission. Because the acoustic impedance of this particular swirl mat composite is only about 2.5 times larger than that of water, more than 80% of the incident energy would pass through the sample and be lost if the examination were conducted with the specimen immersed in water, which is the most convenient and common arrangement for ultrasonic C-scans. Hence, we sealed a portion of one surface of the sample, in effect backing the sample with air. This ensures that 100% of the energy striking the back surface of the sample will be reflected back toward the receiving transducer. This arrangement also simulates the type of inspection that would be required in-service; that is, access to only one side of the sample is available. In addition, we found that damping of the broadband ultrasonic transducer, which enhances the higher-frequency content of the spectrum at the expense of lower frequencies, increased the discrimination between damage and normal heterogeneity, as was expected. With these changes, we scanned the impact sample a second time, and Fig. 7.4 shows the results when the transmitted signal amplitude was acquired. The circular area is the region that was sealed to provide air-backing, and the damage is the dark indication near the center of the sample. The dark circle near the 10 o'clock position in the image is another sprue or molding mark.

The discrimination between damage and sample heterogeneity was quite good in this examination, but the amplitude image did not reveal the true extent of the subsurface damage. Accordingly, we also acquired the velocity data on this sample, and the result is shown in Fig. 7.5. The full extent of the damaged area, corresponding well to what could be seen visually when the specimen was illuminated from behind by

PHOTO YP21001

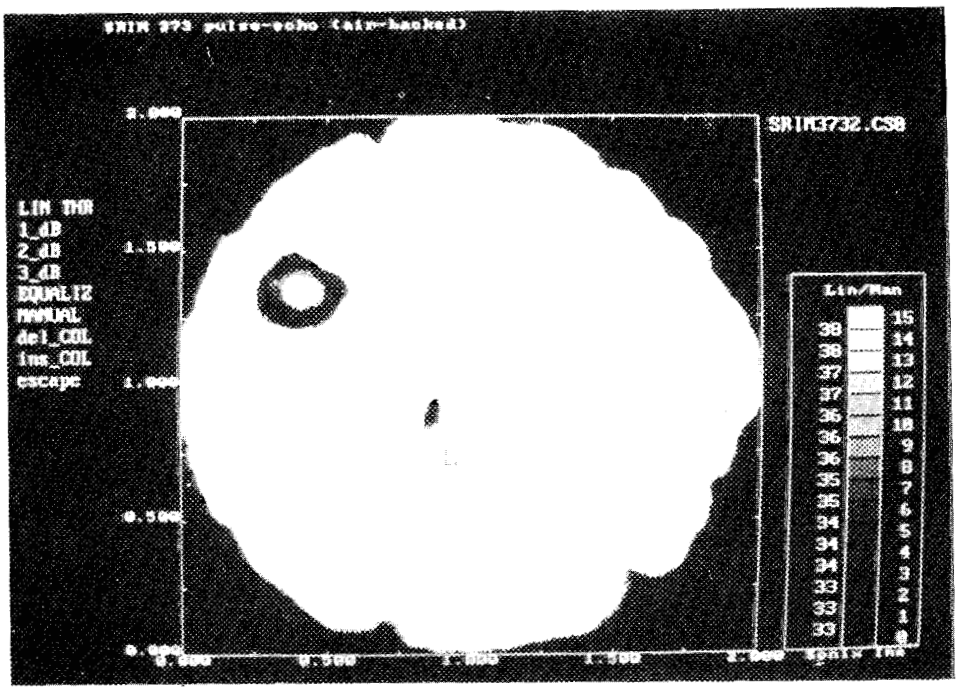

Fig. 7.4. Pulse-echo ultrasonic C-scan image (amplitude) of piece of urethane swirl mat composite showing detection of impact damage (near center) and mold mark (10 o'clock position).

PHOTO YP21000

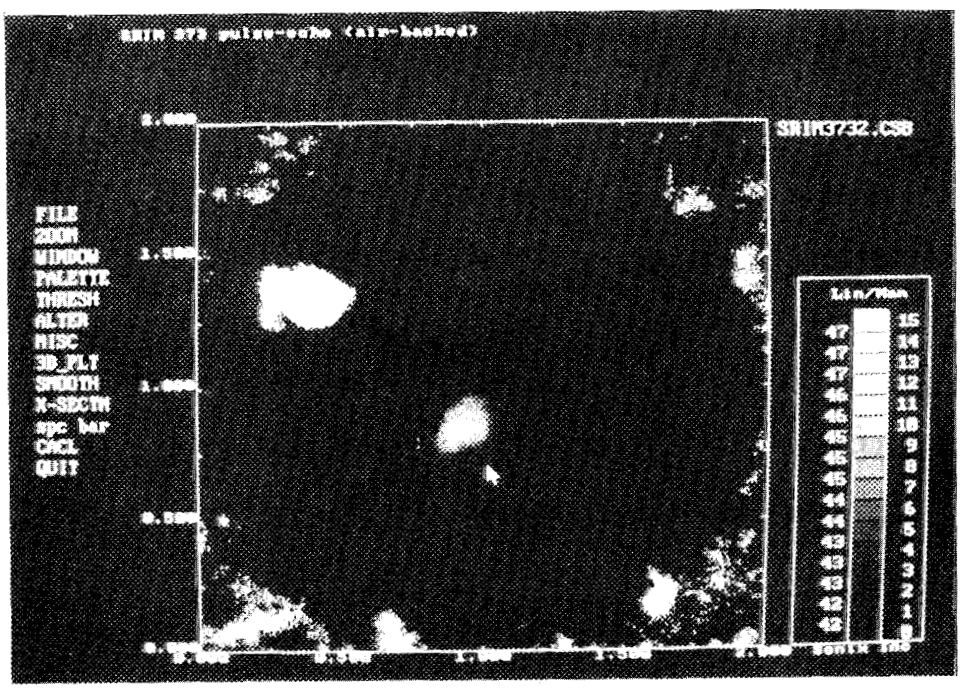

Fig. 7.5 Pulse-echo ultrasonic C-scan image (velocity) of piece of urethane swirl mat composite showing detection of impact damage (arrow, near center) and mold mark (brightest indication, near 10 o'clock position).

strong lighting, is revealed. (Indications outside the circular air-backed area arise from a different source than damage and are not significant.) Since the sample thickness did not appear to change in the impact region, a reasonable conclusion is that the varying depth of the damage produces a greater contrast in the velocity map than in the amplitude map or that the effective modulus of the sample (and therefore the elastic wave velocity) is altered by impact. The first of these conclusions is supported by observation of the behavior of the transmitted signal in the affected area. When the transducer was passing over the damaged region, the signal was seen to shift in time as well as distort in form, due both to the distribution of damage with depth and to multiple scattering from matrix cracks formed at the impact site. In this material, as in many composites, velocity mapping appears to yield better results than conventional amplitude maps.

7.2.2 Frequency-Dependent Attenuation or Velocity

As a composite material undergoes fatigue, more and more fiber-matrix bonds will be broken. Depending on the ultrasonic frequency and the properties of the composite, a probing elastic wave may interact strongly with these broken bonds, undergoing more severe attenuation as damage accumulates. In this manner the effect of increasing damage may be monitored. In addition, the velocity of the wave may undergo change as well because of multiple scattering (Varadan, 1985) or because of actual changes in the modulus of the material. By monitoring both velocity and attenuation, it may be possible to establish a correlation between fatigue damage and a measurable property of the composite.

Simpson (1984) has described such a correlation for an S2 glass-epoxy composite. The material was developed for use in an energy-storage flywheel for alternate power automobiles. The flywheel was composed of layers of staggered orthotropic plies in an alpha-ply arrangement, which yielded a structure that was transversely isotropic macroscopically. The flywheels were subjected to high-speed (up to 43,000-rpm) rotation in a staged sequence for which the maximum rotational rate was slowly increased. After each increase, the wheels were evaluated nondestructively, and the velocity and attenuation of elastic waves were determined at numerous points on the wheel.

For an unconstrained rotating disk, it can be easily shown that the stress varies quadratically with radius. This was confirmed by the ultrasonic results. Figure 7.6 shows the variation in longitudinal wave velocity as a function of radius after fatigue testing. The solid curve is a least-squares fit to the data and

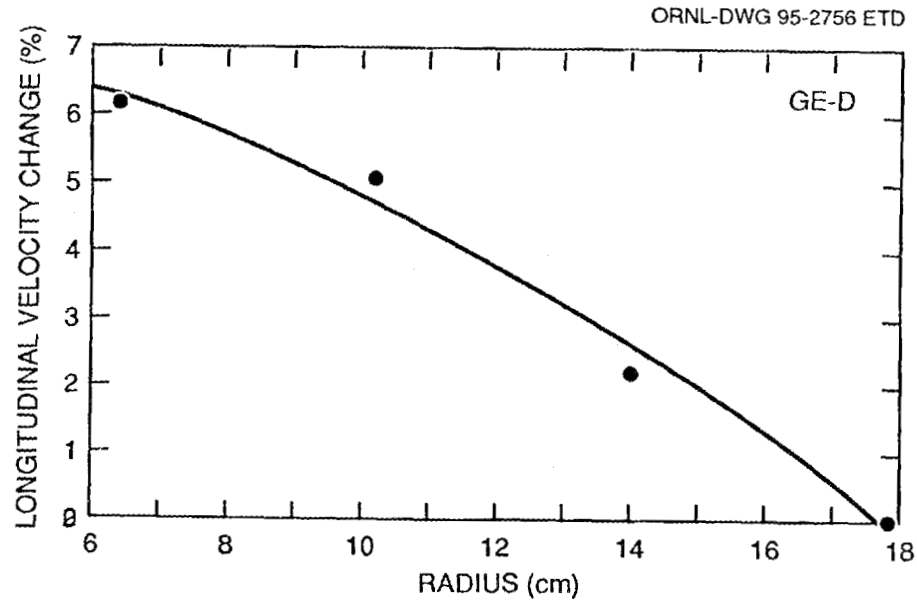

Fig. 7.6. Variation in longitudinal wave velocity as function of radius in S2 glass-epoxy flywheel subject to spin-induced fatigue.

agrees well with the predicted quadratic distribution of stress along the radius. The ordinate gives the percentage change in ultrasonic velocity referenced to the zero-stress values measured before spin testing began. Note that the velocity changed by almost 6.5% near the hub of the wheel, where the stress is highest.

The single-frequency attenuation data, acquired at a relatively low frequency of 1.5 MHz, also reflected the accumulation of damage radially. Table 7.2 shows the results obtained at each of the four radial measurement positions (averaged over 12 circumferential positions for each radius) as a function of test cycles. A cycle included a spin-up from zero to some lower rotational rate, a holding time at that lower rate followed by spin-up to a higher rotation rate, another holding time at maximum revolutions per minute, then return to the lower rate. The cycle numbers given in the table are the total number of such acceleration/deceleration cycles. The maximum rotational rate was held constant throughout the tests so that the flywheel saw an unvarying maximum stress.

Table 7.2. Attenuation (dB)

	Average values for each ring			
Cycles	1	2	3	4
0	44.7 ± 1.1	44.8 ± 1.0	45.5 ± 0.8	46.2 ± 1.6
909	48.5 ± 1.2	48.0 ± 1.0	47.3 ± 0.8	46.8 ± 2.7
2,500	48.8 ± 1.6	48.4 ± 1.6	47.9 ± 1.2	47.2 ± 2.7
5,000	51.7 ± 2.5	50.6 ± 1.4	49.3 ± 1.5	48.9 ± 5.0
7,235	53.7 ± 3.1	51.8 ± 2.0	53.5 ± 1.9	48.2 ± 6.1
10,000	53.9 ± 3.3	50.2 ± 1.9	49.6 ± 1.7	49.3 ± 4.1

In ring 1, the ring closest to the hub and therefore subject to the greatest stress, the single-frequency attenuation increased by 9 dB as the testing progressed, while the outermost ring experienced only a 3-dB increase in elastic wave attenuation.

At the relatively low frequency of 1.5 MHz, the attenuation essentially mirrored the results obtained with ultrasonic velocity. At higher frequencies, however, an entirely different phenomenon was noted. According to theory, there is a critical radius outside of which the stress is too low to initiate cracking in the epoxy matrix (however, some damage will still occur even in low stress areas because of flaws and irregularities present during fabrication). When the flywheels were examined with higher frequency waves, the sharp delineation between lower and higher regions of attenuation became much more pronounced. This is attributable to the higher-frequency components, which are much more strongly affected by matrix cracking, in the spectrum of the wideband ultrasonic transducer. Figure 7.7 shows the results. The dark area at the upper edge of the figure was traced to a resin-rich area in this flywheel. The radius at which the attenuation changes from a relatively lower attenuation regime to a much higher one agreed well with the design calculations for the critical radius to initiate matrix cracking.

These results just described were illustrative but not very quantitative. A more useful result is obtained if absolute attenuation is measured. Unfortunately, this is difficult in ultrasonics because many things that contribute to the total attenuation are not related to the sample. For example, diffraction, or beamspread, causes an apparent frequency-dependent attenuation of the beam even in the absence of a sample. Another source of error is the loss on entry to, and exit from, the sample due to acoustic impedance differences between the sample and the water medium in which the sample is immersed. Another loss is absorption in the coupling fluid itself. Thanks to a closed-form solution for transducer diffraction losses (Rogers and Van Buren, 1974), all of these losses can now be handled analytically, and it has become possible to eliminate the sample-independent sources of attenuation, thereby obtaining a true material signature (Simpson and McClung, 1991), which is the frequency-dependent attenuation characteristic (or transfer curve) of that material. This signature is independent of sample length and depends only on the internal state (microstructure, bonded fiber fraction, etc.) of the specimen. It can be very useful for detecting subtle changes in discontinuities in a material or in revealing damage.

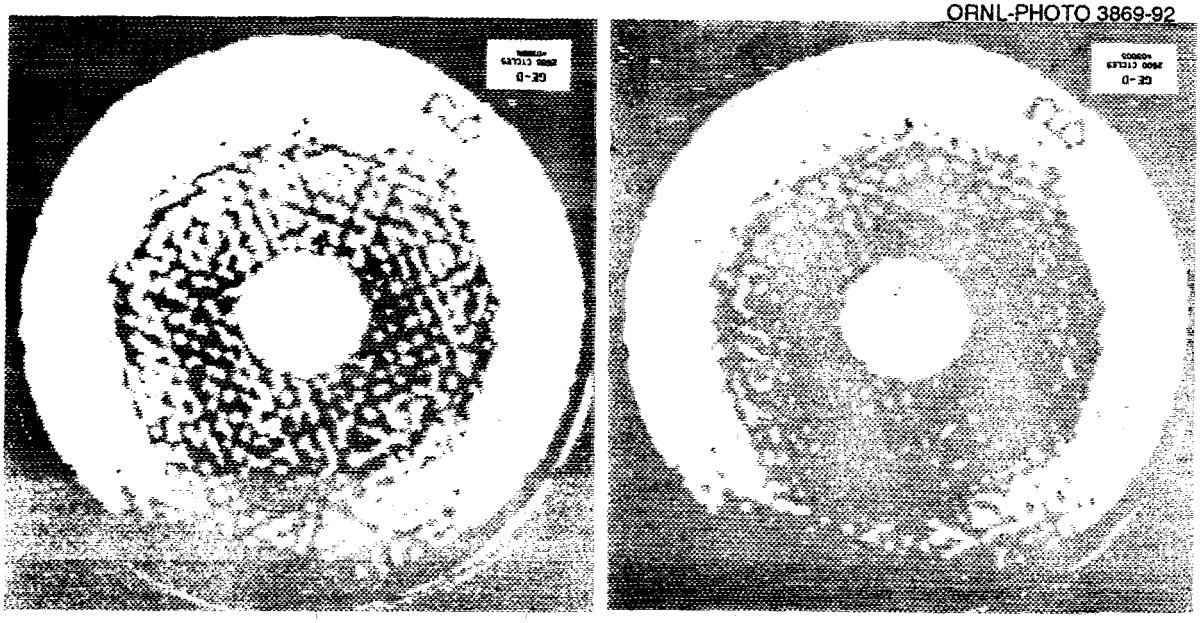

Fig. 7.7. C-scan results at two different gains on S2 glass-epoxy flywheel showing detection of critical radius for matrix cracking.

This quantitative technique was applied to the S2 glass-epoxy composite described above. A broadband source of ultrasonic energy was used to insonify a sample, and the frequency-dependent attenuation was determined after application of all necessary corrections. This process is carried out by computer in the frequency domain. For example, if the impulse response of the transducer and system electronics is denoted by h(t), then the measured response obtained from the sample is (Papoulis, 1962)

$$y(t) = \int_0^t x(t)h(t - \tau)d\tau \quad ,$$

where x(t) is the true material response that we wish to determine. In other words, the measured output is just the convolution of the material response with the system impulse response. Inversion of this integral equation can be accomplished easily in the frequency domain (Papoulis, 1962). If we denote the Fourier transform of each quantity by upper-case letters, then the desired response can be obtained by simple division in the frequency domain:

$$X(\omega) = Y(\omega)/H(\omega) \ .$$

We thus acquire and compute the Fourier transforms of the input and output signals [H(w) and Y(w)], then divide these records in the frequency domain. All corrections are then applied automatically by the computer to yield the true transfer curve, $X(\omega)$, of the specimen.

The results for the S2 glass-epoxy composite before and after strain are shown in Fig. 7.8. The quantity of interest is the slope of the transfer curve, and it can be seen that the attenuation increases dramatically after strain. At intermediate values of strain (not shown), the slope lay between the extremes depicted in the figure, establishing a good correlation between the slope of the transfer curve and the maximum strain to which the material had been subjected. The strain of 2.1% was the last data point obtained before failure.

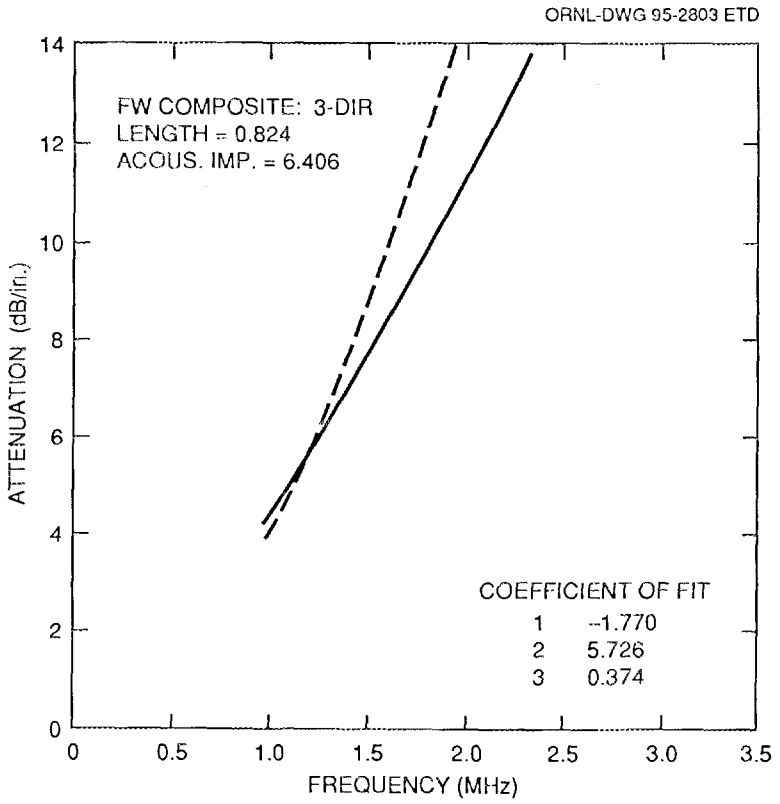

Fig. 7.8. Transfer curve of S2 glass-epoxy composite before (solid curve) and after (dashed curve) application of 2.1% uniaxial strain.

These results show that both the frequency-dependent attenuation and change in velocity are useful for assessing the state of damage in composites. Neither appears to be a predictor of incipient failure, but both correlate well with damage and/or strain history, information which is not obtainable from simple C-scans.

7.2.3 Backscattering

In traditional ultrasonic testing, the incident energy is introduced into the sample at normal incidence. When non-normal angles of incidence were used, it was typically done to excite a mode-converted shear wave, which would then interact with internal defects—voids, cracks, etc.—at normal incidence. However, because discrete flaws or a distribution of flaws scatter energy in all directions, it was recognized many years ago that introducing acoustic energy to a specimen at non-normal angles of incidence (to reduce the very large specular reflection from the surface at normal incidence) and investigating the small signal originating from scattering from ensembles of voids could yield information about the void fraction of the sample. Because a single transducer is most often used, this technique has come to be known as backscattering, and it has proved to be very useful for determining quantitatively the void fraction in metals and other generally homogeneous media.

In the case of composites, the presence of layers and of aligned fiber bundles creates angularly distributed peaks in the backscattering response that complicate the analysis but that provide considerable information about fiber orientation (or misorientation) and fiber-matrix interface conditions. Depending on the nature of the composite and the frequency of the incident energy, Bragg diffraction and Brillouin scattering have been observed in composites.

Perhaps the first systematic study of the backscattering from fiber-reinforced composites was conducted by Bar-Cohen and Crane (1982). By observing the backscattered energy from various unidirectional and quasi-isotropic specimens of glass-epoxy and graphite-epoxy composites, Bar-Cohen was able to detect both fiber misalignment and oriented cracking in these samples. These results were quickly noted by others and applied to additional composite materials, leading to a fairly extensive body of reference material on backscattering in advanced materials.*

The results revealed by polar backscattering can be seen in Fig. 7.9. The material under test is a 0°, ±45°, 90° glass-epoxy composite. The "spokes" are indications obtained when the fibers in a given layer are perpendicular to the propagation direction of the elastic wave. The eight-fold symmetry of the pattern is typical of this type of layup, and the intensity of the indications increases as the material undergoes fatigue damage, providing a quantitative technique for determining the degree of fiber-matrix bond breaking. Note also the indication just to the right of the vertical "spoke" near the bottom of the figure. This feature was present in all the scans on this sample and was probably caused by localized porosity in the matrix. The high contrast of this image shows that backscattering results may reveal local anomalies in the composite without responding to the high degree of material inhomogeneity that is so strongly detected by conventional ultrasonic testing.

*Achenbach and Qu (1986); Blodgett, Miller, and Freeman (1986); Blodgett, Thomas, and Miller (1986); Hsu (1984); Johnston et al. (1994); Martin and Andrews (1986); Qu and Achenbach (1988); Roberts (1987, 1988, 1989); Simpson and McClung (1984); Sullivan et al. (1994); Thomas et al. (1982); Yuhas et al. (1986).

ORNL-PHOTO 0574-83

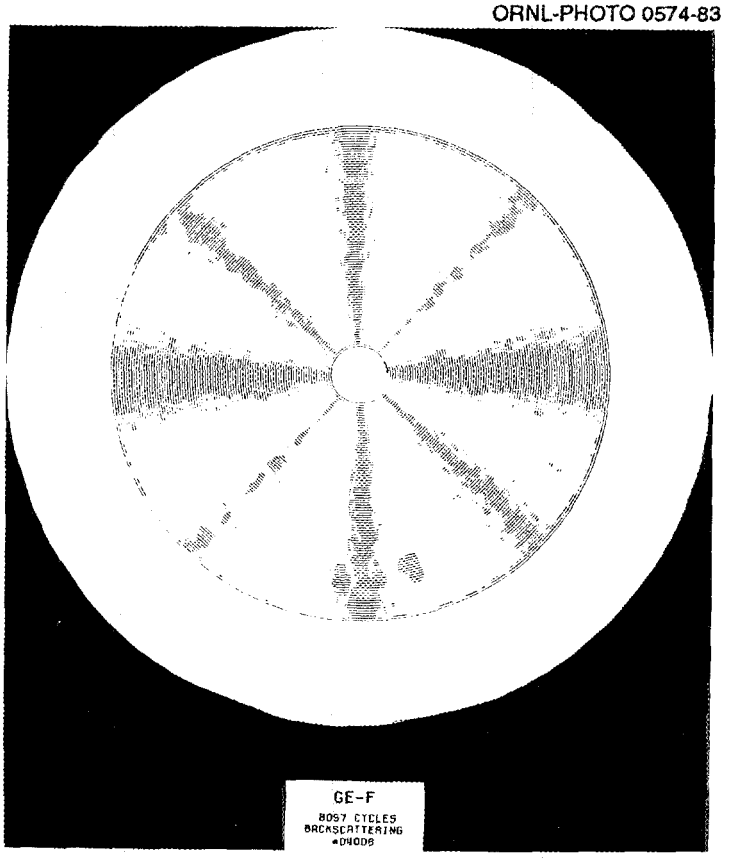

Fig. 7.9. Polar backscattering results on quasi-isotropic (transversely isotropic) glass-epoxy composite that has been subjected to fatigue.

In swirl mat composites, for which the fiber orientation is not uniform, polar backscattering would probably be of little use in revealing fiber-matrix debonding. However, the integrated direction-independent backscattered intensity would very likely correlate with the degree of fiber-matrix separation and microcracking within the matrix.

7.2.4 Lamb Waves

When elastic waves propagate in a material that is thin (i.e., comparable to a few wavelengths or less), the waves will interact with both surfaces simultaneously, and the infinite-medium assumption of conventional ultrasonic evaluation is no longer valid. Under these conditions, nondispersive bulk-wave propagation is replaced by a fundamentally different form of elastic guided-wave propagation, that is, by Lamb wave propagation, so named because the behavior of these waves was first elucidated by Lamb (1917). Unlike the familiar bulk waves, Lamb waves are highly dispersive, and the group velocity of the wave may be very different from the phase velocity. This fact, together with the fact that both velocities vary with frequency, complicates the interpretation of Lamb wave inspection results considerably. In many ways the behavior of Lamb waves parallels that of guided electromagnetic waves. Both exhibit a high degree of dispersion, and both display "cutoff" frequencies below which a typical mode cannot propagate.

In thin composite sheets, the severe attenuation of the structure for elastic waves requires that relatively low frequencies be used for evaluation, and this often means that the generation of Lamb waves is unavoidable. Fortunately, however, Lamb waves have recently been shown to provide greater signal-to-noise detection and imaging of defects in composites than bulk waves under certain conditions. For this reason, Lamb wave inspection of composite plates has now become perhaps the most common evaluation of these materials after conventional ultrasonic C-scanning.

A theoretical treatment of Lamb wave generation and propagation is beyond the scope of this review, but Achenbach (1973) has presented such a treatment, and Simpson and McGuire (1994) recently gave a generalized derivation of both group and phase velocities for Lamb waves. Both of these analyses are valid only for isotropic media, however, and the typical composite is strongly anisotropic. Analyses for this class of materials have been given by Chimenti and Nayfeh (1985, 1988*a*, 1990), Datta et al. (1988), Dayal and Kinra (1989), and Nayfeh and Chimenti (1988*a*). With this theoretical base to guide the analysis of data interpretation, many workers have applied Lamb wave inspection to the evaluation of composite materials.*

Strictly speaking, the waves generated when the ultrasonic energy is introduced into the thin composite from water are known as "leaky" Lamb waves because they continually "leak" energy into the fluid and are therefore attenuated continuously as they propagate. When the acoustic impedances of the sample and the surrounding fluid are very different, the distinction between true Lamb waves and leaky Lamb waves is insignificant, but the dispersion curves become increasingly distorted because of the fluid loading when the properties of the sample and the fluid are similar (Chimenti and Rohklin, 1991). For comparison with the theoretical Lamb modes of a composite plate, this effect must be considered. In many cases, however, the leaky Lamb mode behavior can be examined experimentally, particularly in the frequency regime well above the low-frequency asymptotic limit of the mode.

In applying Lamb wave inspection to a material, one begins most conveniently with the dispersion curves for that material. The curves consist of two sets of modes, known as symmetric and antisymmetric because of the distortions produced in the plate as the waves propagate. Figure 7.10 shows the distinction between these two sets of modes. The operating frequency is then chosen to excite a given mode or modes, and this choice fixes the critical angle in the fluid medium for exciting the choice(s). Examples of the dispersion curves for both iridium and alumina have been given by Simpson and McGuire (1994) and Simpson and McClung (1987). Knowledge of the dispersion curve behavior also allows one to predict which modes will be excited when broadband excitation is used. For example, Figs. 7.11 and 7.12 show the theoretical symmetric and antisymmetric dispersion curves for a particular thickness of alumina. The

---

*Balasubramanian and Rose (1990), Bar-Cohen and Chimenti (1984, 1986), Bar-Cohen and Mal (1989, 1991), Bratton and Datta (1991), Chimenti and Nayfeh (1986), de Billy and Adler (1984), Frame et al. (1990), Guo and Crawley (1992), Kundu and Blodgett (1994), Mal and Bar-Cohen (1989), Mal et al. (1991), Martin and Chimenti (1989), Nagy et al. (1988, 1989), Seale et al. (1994), Tang and Henneke (1989).

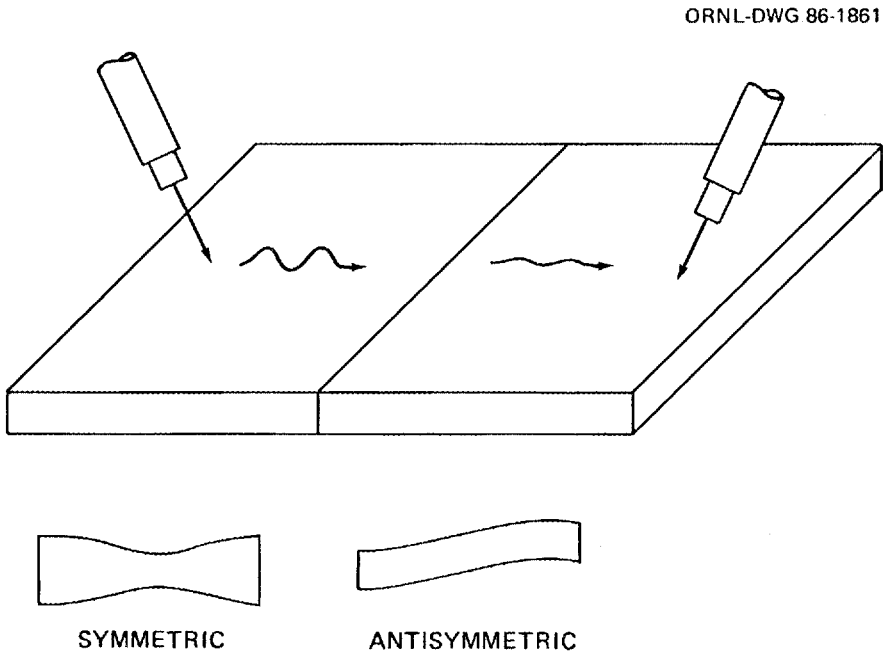

Fig. 7.10. Diagram showing transducer configuration for excitation and detection of Lamb waves and distortions produced in specimen by two classes of waves.

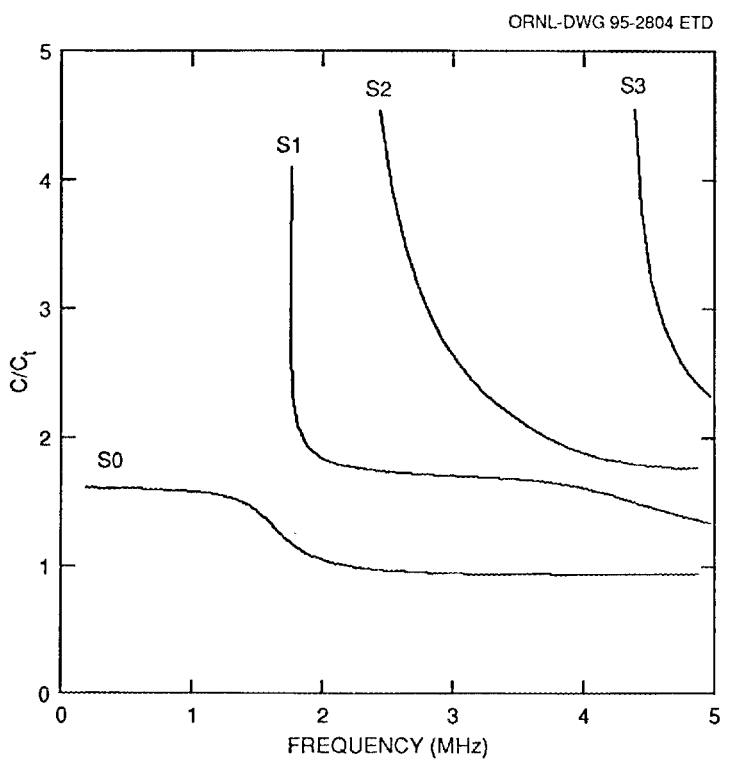

Fig. 7.11. Dispersion curves for symmetric Lamb wave modes in alumina.

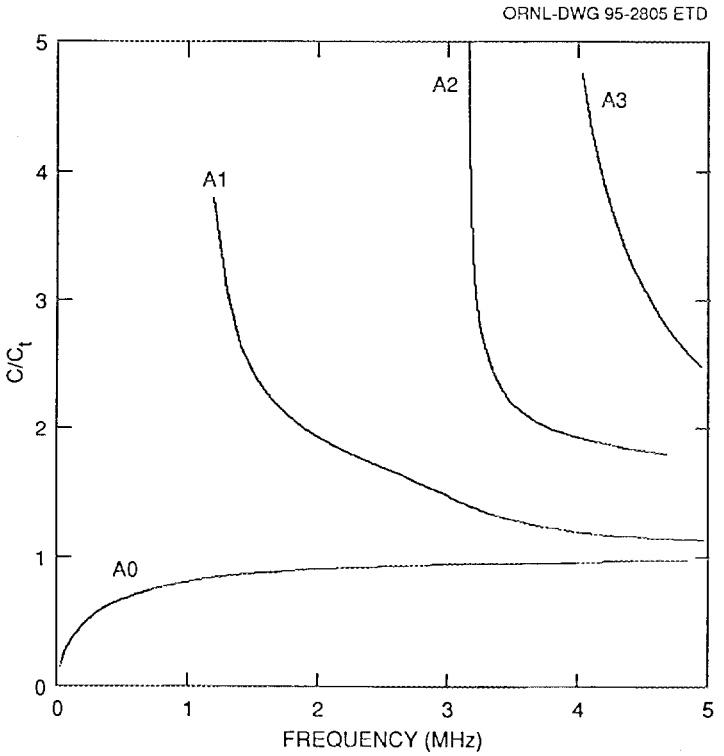

Fig. 7.12. Dispersion curves for antisymmetric Lamb wave modes in alumina.

ordinate gives the phase velocity of the Lamb wave normalized to that of a shear wave in alumina (C_t). If a normalized phase velocity of 1.25 is chosen (corresponding to an excitation angle of about 11° in water) and a broadband 5-MHz ultrasonic transducer is used to excite the spectrum, one can predict the occurrence of five modes. This is confirmed by experiment, where Fig. 7.13 shows the spectrum obtained and the identification of the five modes. The agreement between theory and experiment on the frequency of each mode is quite good.

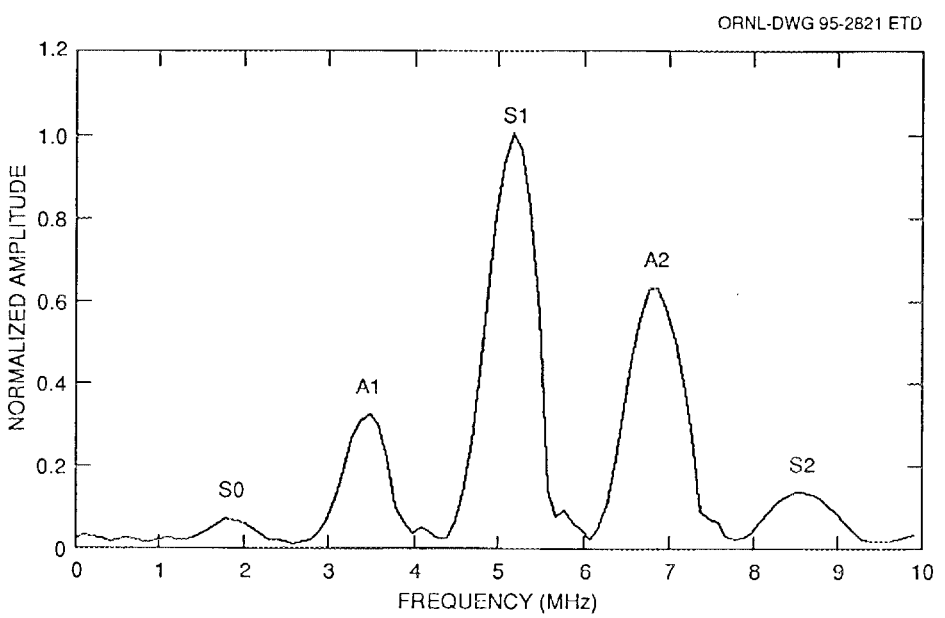

Fig. 7.13. Experimentally obtained spectrum of Lamb wave modes in alumina coupon.

The question naturally arises as to which mode or modes might be more useful in detecting damage in composites. The amplitude distribution for the different modes varies radically throughout the thickness of the specimen (symmetric modes exhibit nodes of vertical particle displacement at the center of the specimen, and antisymmetric modes produce nodes of horizontal particle displacement). It has also been noted that a given defect responds differently to various Lamb modes (Alers and Thompson, 1976; Budenkov et al., 1977; Pilarski et al., 1987). Generally speaking, the selection is most easily effected empirically, that is, by exciting various modes and noting the response of each to a given defect.

When the full elastic matrix of the composite is not known, one has no recourse but to examine the mode structure experimentally. This is efficiently done using the double-transmission arrangement (Nagy et al., 1987) shown in Fig. 7.14. This configuration both simplifies the alignment process and enhances the Lamb mode resonances. In addition, the polar response of the composite structure can be obtained by rotating the sample about any axis normal to the plane of the laminate. If a broadband transducer is used to excite the structure and the resulting echo train is analyzed in the frequency domain, it is possible to detect all Lamb waves excited within the bandpass of the transducer simultaneously. This approach is much simpler and yields a higher signal-to-noise ratio than conventional single-sided evaluation of the composite.

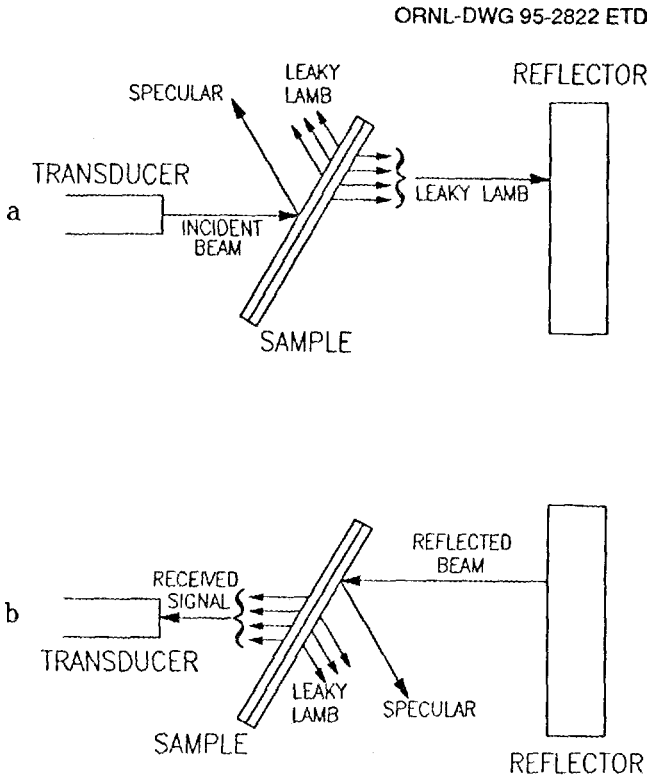

Fig. 7.14. Double-transmission method for generating and detecting Lamb waves in composite laminates.

This technique was used to examine the Lamb wave mode structure of an alpha-ply graphite-epoxy composite (Frame et al., 1990). A strong resonance was found at about 1.5 MHz in the transmitted spectrum. Figure 7.15 shows the spectral content of the double-transmitted signal, while Fig. 7.16 gives the response of the transducer used in the experiments. Note that all spectra are normalized in amplitude; thus, the resonance near 1.5 MHz in Fig. 7.16 actually occurs near the low-frequency limit of the transducer

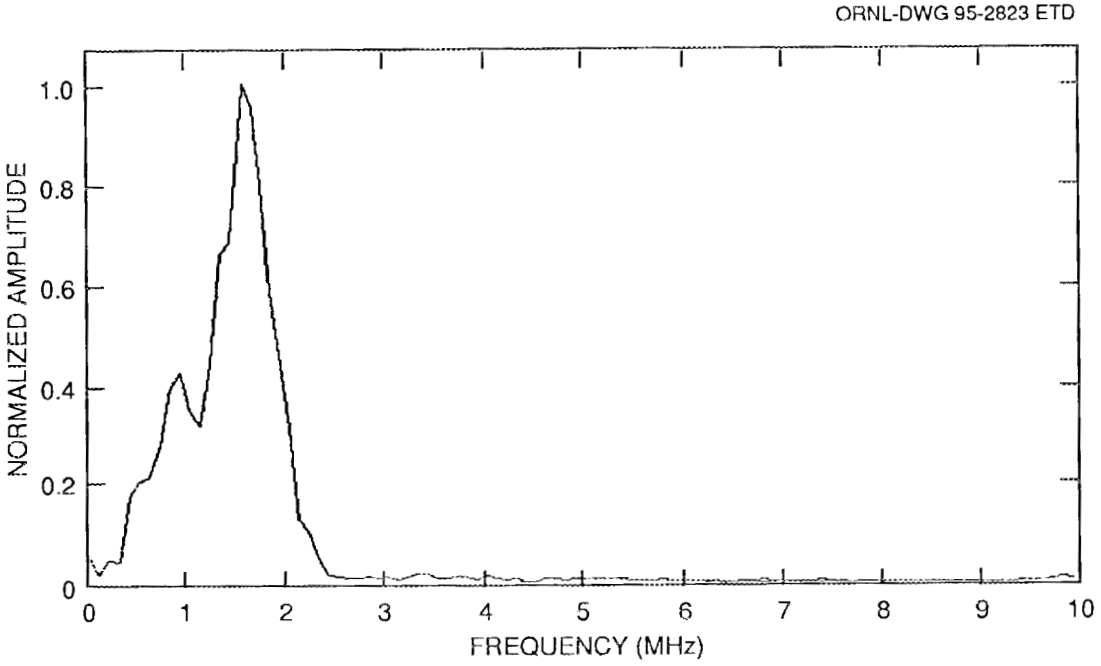

Fig. 7.15. Spectrum of double-transmitted wave in graphite-epoxy composite showing excitation of Lamb wave near 1.5 MHz.

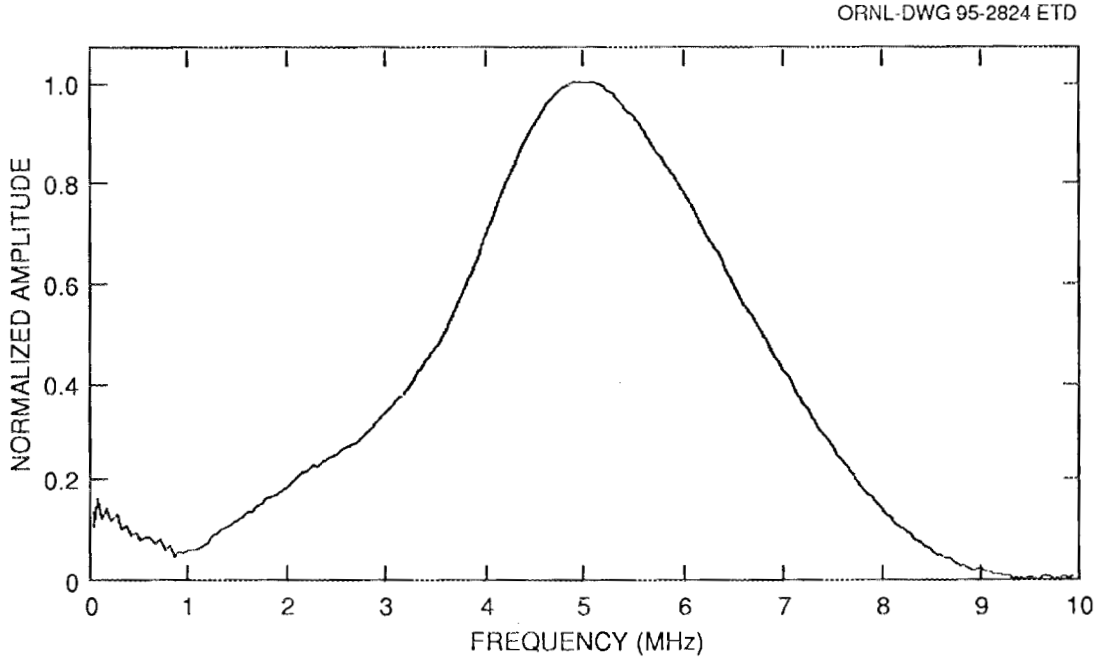

Fig. 7.16. Spectral content of 5-MHz transducer used in Lamb wave studies in graphite-epoxy composite.

shown in Fig. 7.16. The secondary maximum near 0.9 MHz in Fig. 7.15 is caused by random interference from material inhomogeneities; it tended to disappear with a slight displacement of the transducer.

Once the proper angle for generating a Lamb wave resonance in the composite structure was found, it was possible to produce a Lamb wave C-scan map of the structure. Two simulated impact damage defects, one circular and the other square, were placed in the specimen and the sample scanned. Figure 7.17 shows the result obtained. Both simulated defects were detected and imaged easily. Note that neither of these "defects" could be detected using conventional C-scan techniques because of the high degree of material inhomogeneity, which generates many false signals. The relatively noise-free results depicted in Fig. 7.17 show that the Lamb waves were highly sensitive to the simulated defects (which were planar in nature and several wavelengths wide) and almost unresponsive to the material inhomogeneity. It is for this reason that Lamb wave inspection holds great promise for composite evaluation.

ORNL-DWG 89-12940

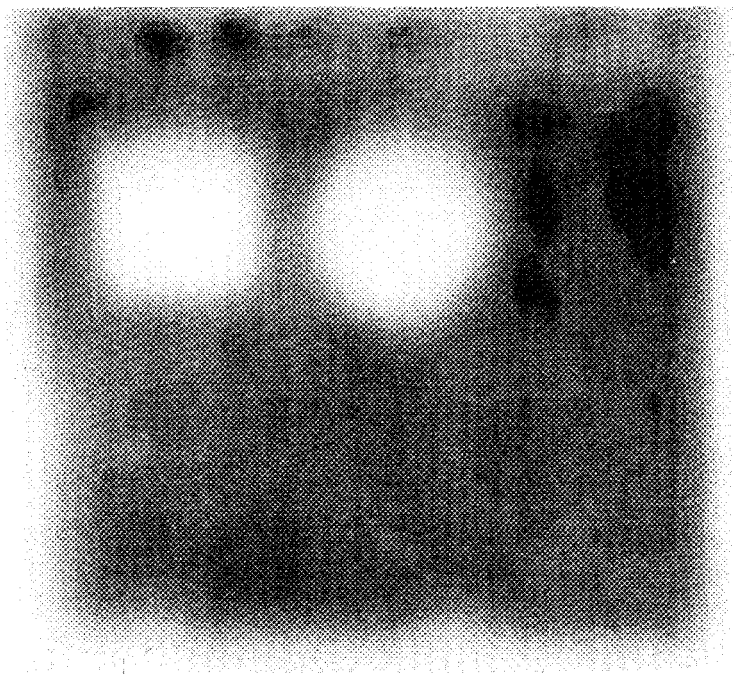

Fig. 7.17. Lamb wave C-scan map of graphite-epoxy composite panel showing image of two simulated impact damage areas.

We also examined a swirl mat composite panel for evidence of Lamb wave excitation using the double-transmission arrangement of Fig. 7.14. However, the transducers initially used were 5-MHz center-frequency broadband units, and this frequency band (~2 to 8 MHz) was too high for the composite. Subsequent examinations using 1-MHz transducers produced an obvious Lamb wave at about 0.8 MHz for all angles of incidence above about 45°. The group velocity of this wave increased as the angle of incidence decreased. At an angle of incidence around 45°, a second mode with a still higher group velocity appeared, then a third as the angle continued to decrease. The waves excited were clearly Lamb modes, and the behavior of the group velocities was at least qualitatively consistent (no theoretical estimates were attempted) with the A_0, S_0, and A_1 Lamb modes.

The above results indicate that Lamb waves can indeed be excited in the isocyanurate swirl mat composite, but no attempt was undertaken to produce images of the impact-damaged specimen using these modes. This remains a promising avenue of investigation, however, and Lamb wave images of this and

other specimens will be pursued. Based on our experience with other composite materials, Lamb wave evaluation may well provide the most useful indication of delaminations and impact damage.

7.2.5 Acousto-Ultrasonics

Occasionally in nondestructive testing a symbiosis of two established techniques is found to provide information that neither approach alone can offer. One such hybridization is acousto-ultrasonics, a marriage of conventional ultrasonic techniques and acoustic emission technology. Introduced by Vary (1976, 1978) and Vary and Bowles (1978), this approach has been extensively developed and applied to a variety of materials, particularly composites. The theory and applications of the acousto-ultrasonic technique have also been reviewed in depth (Duke, 1988). Thus, only a brief overview is given here.

In the implementation of acousto-ultrasonics, a stress wave is generated in the sample under investigation by an ultrasonic transducer. The signals generated by the interaction of this wave with the microstructure of the specimen are then received by a second transducer. What distinguishes the technique from conventional ultrasonic testing is that the receiving transducer is placed in a manner to preclude reception of the direct bulk waves, and the data analysis usually involves monitoring such properties of the received wave as the decay rate of the envelope, number of zero crossings of the waveform, etc., properties that are generally associated with acoustic emission testing. In this case, however, the "emission" signals are generated by the initial stress wave, not by failure mechanisms occurring in the specimen. The technique is thus nondestructive, but many researchers have found good correlation between the acousto-ultrasonic signature, often called the stress-wave factor, and true damage in the sample.

Acousto-ultrasonics has perhaps found its widest application in the evaluation of composites. Duke et al. (1989) have given an excellent treatment of their work. Others have presented results detecting damage in graphite-epoxy composites (Talreja et al., 1984), ceramic composites (Lott and Kunnerth, 1990), and metal matrix composites (Kautz and Lerch, 1991). Particularly for impact damage and fiber-matrix debond degradation, acousto-ultrasonics show considerable potential as a rapid, quantitative evaluation tool for assessing the state of composite integrity.

7.3 NONLINEAR TECHNIQUES

The usual descriptions (Krautkrämer and Krautkrämer, 1990) of elastic wave propagation in materials are based on a linearized theory in which it is assumed that the strain is linearly proportional to the derivative of the material displacement. This approximation arises when higher order terms in the expression for strain are neglected. Specifically, if s is the displacement, then it is easy to show (Simpson, 1969) that

$$\varepsilon_{ij} = \frac{1}{2}\left(\frac{\partial s_j}{\partial x_i} + \frac{\partial s_i}{\partial s_j} + \frac{\partial s_k}{\partial s_i}\frac{\partial s_k}{\partial s_j}\right), \tag{7.1}$$

where ε_{ij} is the strain tensor and x_i is a material coordinate. In the linearized theory, cross terms are neglected, and the strain is usually approximated by

$$\varepsilon_{ij} = \frac{1}{2}\left(\frac{\partial s_j}{\partial x_i} + \frac{\partial s_i}{\partial s_j}\right). \tag{7.2}$$

This simplification leads to the familiar equations for bulk-wave propagation in solids. Likewise the stress tensor σ_{ij} is usually assumed to be linearly related to strain:

$$\sigma_{ij} = C_{ijkl}\varepsilon_{kl}\,, \tag{7.3}$$

where the C_{ijkl} are the familiar second-order elastic constants (simply related to the shear modulus and Young's modulus for an isotropic solid). When the strain energy function is expanded in a Taylor series (Cantrell, 1982), however, higher order terms lead to expressions for the third-order elastic constants, fourth-order, etc. For much of the history of ultrasonic testing, the lowest order (second-order) elastic constants admirably described the measurable properties of the wave behavior, and the nonlinear terms, which introduced considerable complication to the solution of elastic wave propagation, were neglected. In recent years, however, it has been noted that the weak, though detectable, acoustic nonlinearity of materials is amazingly sensitive to very subtle changes in the internal state of the specimen, even to changes very small on the scale of a wavelength. For this reason, evaluation of the anharmonic response of structural materials, particularly composites, holds great promise for the quantitative assessment of damage and material state.

7.3.1 Acousto-Elastic Effect

Because all materials are inherently nonlinear to some degree, the presence of higher order elastic constants means that the elastic wave velocity in the specimen will be a function of stress. The change is slight, but it has been used for several years to gage nondestructively the residual stress in structural materials.* Of more interest than residual stress determination to composite research, however, is the use of acousto-elasticity to monitor the accumulation of damage in materials. Nagy and Adler (1992) have used the second-order acousto-elastic effect to measure the onset and growth of cracking in plastics. In this study the sample was cyclically fatigued and the change in elastic wave velocity monitored. The nonlinear behavior increased smoothly and dramatically prior to failure.

While the acousto-elastic effect appears to have some application to composites for detection and quantification of fatigue damage, the requirement for making measurements under load renders the technique less attractive than other, purely nondestructive measurement techniques. Chief among these is the recognition that acoustic anharmonicity requires that a portion of the energy of a propagating, initially monochromatic wave be converted into second-order and higher order harmonics of the fundamental, and this effect provides an excellent approach for assessing material nonlinearity.

7.3.2 Harmonic Generation

In addition to producing changes in the elastic wave propagation velocity, material nonlinearity also causes harmonics of an initially monochromatic wave to be generated. The degree to which harmonic generation is manifest depends on the material, and it also appears to depend very sensitively on the presence of dislocations, voids, flaws, etc., which may be very small with respect to the acoustic wavelength. The questions then arise as to how one might relate the degree of anharmonicity to the elastic properties of the medium and how the effect of harmonic generation might be maximized. It is possible to proceed in an entirely empirical manner, but a much better approach would be to analyze the problem theoretically and use this result to guide the experiment.

Many people have studied the very difficult problem of nonlinear wave propagation in a generalized anisotropic medium. Two excellent overviews of these developments have been given by Breazeale (1990) and by Cantrell and Yost (1990). Breazeale points out that a perturbation solution of the nonlinear wave equation yields the following form for the particle displacement in a nonlinear medium:

$$\xi = A_1 \sin(kx - \omega t) - \left(\frac{K_3}{K_2} + 3\right)\frac{A_1^2 k^2 x}{8}\cos 2(kx - \omega t) + \ldots , \tag{7.4}$$

where ξ is the particle displacement, k is the wave vector of the disturbance, ω is the angular frequency, x is the propagation distance, and K_2 and K_3 are combinations of the second-order and third-order elastic con-

*Chen and He (1994), Dike et al. (1989), Heyman and Chern (1982), Lee et al. (1986), MacLauchlan and Alers (1987), Mase et al. (1989), Toupin and Bernstein (1961), Wong and Johnson (1988), Yen and Chatterjee (1988).

stants, respectively, of the medium. The term $-(K_3/K_2 + 3)$ is known as the nonlinearity parameter, β, of the medium and is dimensionless. The displacement amplitude thus consists of a fundamental component, the initial wave, and harmonics of all orders.

This equation has several interesting points. First, we note that the amplitude of the second harmonic wave increases quadratically with both fundamental amplitude and frequency and linearly with propagation distance. Second-harmonic generation is thus enhanced by using as high a driving (fundamental) amplitude as possible and as high a frequency as practicable. Second, if we denote the terms in front of the cosine term by A_2, the amplitude of the second harmonic, we can solve for b in terms of the amplitudes of the fundamental and second-harmonic waves:

$$\beta = \frac{8A_2}{A_1^2 k^2 x} \quad . \tag{7.5}$$

The nonlinearity parameter can thus be determined from knowledge of the amplitudes of the fundamental and second-harmonic amplitudes. The utility of this parameter is that it is a pure number associated with a particular material, and with a particular material state. It is extremely sensitive, as several researchers have now established, to the presence of contaminants, precipitates, dislocation density, and aging.*

Once we have settled on the nonlinearity parameter as the figure of merit for acoustic anharmonicity, the problem reduces to one of measuring this parameter. As the equation above shows, we basically must determine the ratio A_2/A_1^2. This can be estimated in the following manner. In the absence of external forces, the stress induced in a piezoelectric transducer by an applied voltage is given by:

$$\overleftrightarrow{S} = D \cdot \vec{E} \ , \tag{7.6}$$

where $\overleftrightarrow{S}$ is the strain dyadic, $\vec{E}$ is the electric field vector, and D is the third-rank piezoelectric strain constant tensor. For a typical piezoelectric transducer material such as $LiNbO_3$, the d_{33} element of D is the quantity of interest and is equal to about 6×10^{-12} coulomb/N. At a frequency of 10 MHz and at an applied voltage of 250 V, the displacement amplitude of the crystal is about 15 Å. Assuming this to be the fundamental wave amplitude in the sample (a liberal estimate; several factors would reduce this value), the second-harmonic amplitude will typically be 2 to 3 orders of magnitude smaller, depending on the material, or 0.015 to 0.15 Å. Clearly, absolute measurement of displacement amplitude in this range is beyond the sensitivity even of optical techniques.

The most commonly used detector for harmonic amplitude measurement is the capacitive detector (Gauster and Breazeale, 1966). The requisite sensitivity is available, but the technology is expensive and requires extremely precise sample surface preparation. However, the sensitivity of piezoelectric sensors is certainly adequate for this task. For example, the voltage produced by the $LiNbO_3$ transducer described above can be estimated from the inverse piezoelectric constitutive relationships. Assuming no external electrical fields, the relationship between applied stress and generated electric field is:

$$\vec{E} = G \cdot \overleftrightarrow{T} \ , \tag{7.7}$$

where G is the third-rank piezoelectric voltage tensor $\overleftrightarrow{T}$ and is the stress dyadic. Again, the salient component of G is G_{33}, whose value is about 0.023 m^2/coulomb for $LiNbO_3$. Now, the relation between particle displacement and acoustic pressure (stress) is given by (Krautkrämer and Krautkrämer, 1990):

$$p = \rho c \omega \xi \ , \tag{7.8}$$

---

*Breazeale and Philip (1984), Cantrell et al. (1986), Cantrell and Yost (1993), Dace et al. (1991, 1992), Li (1985), Mohrbacher et al. (1991), Wu and Prosser (1991), Yost and Cantrell (1990, 1993).

where p is the acoustic pressure, ρ is the material density, c is the compressional wave velocity, ω is the angular frequency, and ξ is the particle displacement. Assuming the larger value of 0.15 Å for ξ and the properties to be those of the swirl mat composite given earlier, the induced second-harmonic voltage in a 10-MHz receiving transducer would be about 28 mV, which is easily detectable with conventional piezoelectrics. These calculations assume no conversion, matching, or material losses, which would further reduce the detected signal, but the voltage available with our newer hardware is also much higher, about 1200 V p-p.

Because it would appear that conventional piezoelectric detection has adequate sensitivity for the detection of harmonics in materials, the question naturally arises regarding why they have not been widely used for this purpose. The reason is that *absolute* measurements of the fundamental and harmonic wave amplitudes are necessary (more precisely, the ratio A_2/A_1^2), and this requires a rather involved calibration procedure as well as assurance that reciprocity holds for the transducer/couplant system. Recently, however, Dace et al. (1991, 1992) have shown that this is indeed the case and have given a procedure for obtaining the necessary calibration. Their work, which involved simple piezoelectric elements and water coupling, has placed the measurement of the nonlinear behavior of materials on a footing comparable to that underpinning conventional ultrasonic testing.

In summary, the measurement of the nonlinear response of materials is in its infancy, but the results already obtained have emphasized the extreme sensitivity of the technique to variations or anomalies that are small on the scale of the acoustic wavelength, even down to the scale of lattice deformations. In addition, the changes induced by defects and fatigue in the nonlinearity of materials are often several hundred percent, in contrast to the fractions of a percent to a few percent typical of changes in the linear response induced by these same material degradations. In particular, the nonlinear response of composite materials seems to be extremely sensitive to changes in the fiber-matrix bond integrity and thereby promises to provide a technique for quantifying globally the debonding induced by fatigue in advanced structural materials.

REFERENCES

Achenbach, J. D., and Qu, J. 1986. "Backscattering From Flaw Distributions in Composite Materials," pp. 1179–88 in *Rev. Prog. in Quant. Nondest. Eval. 5B*, ed. D. O. Thompson and D. E. Chimenti, Plenum Press, New York.

Achenbach, J. D. 1973. *Wave Propagation in Elastic Solids*, North-Holland Publishing Company, New York.

Alers, G. A., and Thompson, R. B. 1976. "Application of Trapped Modes in Layered Media to the Testing of Adhesive Bonds," *1976 IEEE Ultrasonics Symposium Proceedings*, IEEE Cat. 76 CH 1120-5SU, 138–42, Institute for Electrical and Electronics Engineers, New York.

Balasubramanian, K., and Rose, J. L. 1990. "Guided Plate Wave Potential for Damage Analysis of Composite Materials," pp. 1505–12 in *Rev. Prog. in Quant. Nondest. Eval.* **9B**, ed. D. O. Thompson and D. E. Chimenti, Plenum Press, New York.

Bar-Cohen, Y., and Crane, R. L. 1982. "Acoustic-Backscattering Imaging of Subcritical Flaws in Composites," *Mat. Eval.* **40**(9), 970–5.

Bar-Cohen, Y., and Chimenti, D. E. 1984. "Leaky Lamb Waves in Fiber-Reinforced Composite Plates," pp. 1043–9 in *Rev. Prog. in Quant. Nondest. Eval.* **3B**, ed. D. O. Thompson and D. E. Chimenti, Plenum Press, New York.

Bar-Cohen, Y., and Chimenti, D. E. 1986. "Nondestructive Evaluation of Composite Laminates by Leaky Lamb Waves," pp. 1199–1206 in *Rev. Prog. in Quant. Nondest. Eval.* **5B**, ed. D. O. Thompson and D. E. Chimenti, Plenum Press, New York.

Bar-Cohen, Y., and Mal, A. K. 1989. "Leaky Lamb Wave Phenomena in Composites Using Pulses," pp. 1671–7 in *Rev. Prog. in Quant. Nondest. Eval.* **8B**, ed. D. O. Thompson and D. E. Chimenti, Plenum Press, New York.

Bar-Cohen, Y., and Mal, A. K. 1990. "Leaky Lamb Waves (LLW) in Multiorientation Composite Laminates," pp. 1419-23 in *Rev. Prog. in Quant. Nondest. Eval.* **9B**, ed. D. O. Thompson and D. E. Chimenti, Plenum Press.

Bar-Cohen, Y., and Mal, A. K. 1991. "Characterization of Composite Laminates Using Combined LLW and PBS Methods," pp. 1555–60 in *Rev. Prog. in Quant. Nondest. Eval.* **10B**, ed. D. O. Thompson and D. E. Chimenti, Plenum Press, New York.

Bar-Cohen, Y., Mal, A. K., and Lih, S. S. 1993. "NDE of Composite Materials Using Ultrasonic Oblique Insonification," *Mat. Eval.* **51**(11), 1285–95.

Bashyam, M. 1990. "Thickness Compensation Technique for Ultrasonic Evaluation of Composite Materials," *Mat. Eval.* **48**(11), 1360–4.

Blodgett, E. D., Miller, J. G., and Freeman, S. M. 1986. "Correlation of Ultrasonic Polar Backscatter With the Deply Technique for Assessment of Impact Damage in Composite Laminates," pp. 1227–38 in *Rev. Prog. in Quant. Nondest. Eval.* **5B**, ed. D. O. Thompson and D. E. Chimenti, Plenum Press, New York.

Blodgett, E. D., Thomas III, L. J., and Miller, J. G. 1986. "Effects of Porosity on Polar Backscatter From Reinforced Composites," pp. 1267–74 in *Rev. Prog. in Quant. Nondest. Eval.* **5B**, ed. D. O. Thompson and D. E. Chimenti, Plenum Press, New York.

Blodgett, M., and Ruddell, M. 1992. "Ultrasonic Characterization of Woven Composites," pp. 1577–84 in *Rev. Prog. in Quant. Nondest. Eval.* **11B**, ed. D. O. Thompson and D. E. Chimenti, Plenum Press, New York.

Bratton, R., and Datta, S. 1991. "Scattering of Lamb Waves in a Composite Plate," pp. 1507–14 in *Rev. Prog. in Quant. Nondest. Eval.* **10B**, ed. D. O. Thompson and D. E. Chimenti, Plenum Press, New York.

Breazeale, M. A., and Philip, J. 1984. "Determination of Third-Order Elastic Constants from Ultrasonic Harmonic Generation Measurements," *Physical Acoustics*, Vol. 17, ed. W. P. Mason and R. N. Thurston, Academic Press, New York.

Breazeale, M. A. 1990. "Whither Nonlinear Acoustics," pp. 1653–60 in *Rev. Prog. in Quant. Nondest. Eval.* **9B**, ed. D. O. Thompson and D. E. Chimenti, Plenum Press, New York.

Budenkov, G. A., et al. 1977. "Dispersion Relation for Interface Waves in Three-Layered Media," *Sov. J. Nondest. Test.* **13**(4), 272–6.

Buynak, C. F., and Moran, T. J. 1987. "Characterization of Impact Damage in Composites," pp. 1203–11 in *Rev. Prog. in Quant. Nondest. Eval.* **6B**, ed. D. O. Thompson and D. E. Chimenti, Plenum Press, New York.

Buynak, C. F., Moran, T. J., and Martin, R. W. 1989. "Delamination and Crack Imaging in Graphite-Epoxy Composites," *Mat. Eval.* **47**(4), 438–47.

Cantrell, Jr., J. H. 1982. "Anharmonic Properties of Solids From Measurements of the Stress Acoustic Constants," *J. Test. and Eval.* **10**(5), 223–9.

Cantrell, J. H., et al. 1986. "Effective Nonlinearity Parameters of Aluminum Alloys as a Function of Volume Fraction of Second Phase Precipitates," *1986 IEEE Ultrasonics Symposium Proceedings*, p. 1075, Institute for Electrical and Electronics Engineers, New York.

Cantrell, J. H., and Yost, W. T. 1990. "Materials Characterization Using Acoustic Nonlinearity Parameters and Harmonic Generation: Effects of Crystalline and Amorphous Structures," pp. 1661–8 in *Rev. Prog. in Quant. Nondest. Eval.* **9B**, ed. D. O. Thompson and D. E. Chimenti, Plenum Press, New York.

Cantrell, J. H., and Yost, W. T. 1993. "Acoustic Harmonic Generation and Dislocation Dynamics of Fatigued Aluminum Alloys," pp. 2059–66 in *Rev. Prog. in Quant. Nondest. Eval.* **12B**, ed. D. O. Thompson and D. E. Chimenti, Plenum Press, New York.

Chen, H. L., and He, Y. 1994. "Nondestructive Evaluation of Stress in Prestressing Rods of Stressed Timber Bridges," pp. 2055–62 in *Rev. Prog. in Quant. Nondest. Eval.* **13B**, ed. D. O. Thompson and D. E. Chimenti, Plenum Press, New York.

Chimenti, D. E., and Nayfeh, A. H. 1985. "Leaky Lamb Waves in Fibrous Composite Laminates," J. *Appl. Phys.* **58**(12), 4531–8.

Chimenti, D. E., and Nayfeh, A. H. 1986. "Leaky Lamb Waves in Fibrous Composite Laminates," pp. 1083–91 in *Rev. Prog. in Quant. Nondest. Eval.* **5B**, ed. D. O. Thompson and D. E. Chimenti, Plenum Press, New York.

Chimenti, D. E., and Nayfeh, A. H. 1990. "Ultrasonic Reflection and Guided Wave Propagation in Biaxially Laminated Composite Plates," *J. Acoust. Soc. Am.* **87**(4), 1409–15.

Chimenti, D. E., and Rohklin, S. I. 1991. "Influence of Fluid Loading on Reflection Coefficient Zeros and Leaky Lamb Modes for a Composite Plate," pp. 209–24 in *Rev. Prog. in Quant. Nondest. Eval.* **10A**, ed. D. O. Thompson and D. E. Chimenti, Plenum Press, New York.

Chu, Y. C., and Rohklin, S. I. 1994. "Stability of Determination of Composite Moduli From Velocity Data in Planes of Symmetry for Weak and Strong Anisotropies," *J. Acoust. Soc. Amer.* **95**(1), 213–25.

Chu, Y. C., Degtyar, A. D., and Rohklin, S. I. 1994. "On Determination of Orthotropic Material Moduli From Ultrasonic Velocity Data in Nonsymmetry Planes," *J. Acoust. Soc. Am.* **95**(6), 3191–203.

Dace, G. E., et al. 1991. "Nonlinear Acoustics, A Technique to Determine Microstructural Changes in Materials," pp. 1685–92 in *Rev. Prog. in Quant. Nondest. Eval.* **10B**, ed. D. O. Thompson and D. E. Chimenti, Plenum Press, New York.

Dace, G. E., Thompson, R. B., and Buck, O. 1992. "Measurement of the Acoustic Harmonic Generation for Materials Characterization Using Contact Transducers," pp. 2069–76 in *Rev. Prog. in Quant. Nondest. Eval.* **11B**, ed. D. O. Thompson and D. E. Chimenti, Plenum Press, New York.

Daniel, I. M., Wooh, S. C., and Lee, J. W. 1987. "Defect and Damage Characterization in Composite Materials," pp. 1195–1202 in *Rev. Prog. in Quant. Nondest. Eval.* **6B**, ed. D. O. Thompson and D. E. Chimenti, Plenum Press, New York.

Daniel, I. M., and Wooh, S. C. 1989. "Ultrasonic Techniques for Characterization of Manufacturing Defects in Thick Composites," pp. 1605–12 in *Rev. Prog. in Quant. Nondest. Eval.* **8B**, ed. D. O. Thompson and D. E. Chimenti, Plenum Press, New York.

Daniel, I. M., and Wooh, S. C. 1990. "Ultrasonic Characterization of Defects and Damage in Thick Composites," pp. 1489–96 in *Rev. Prog. in Quant. Nondest. Eval.* **9B**, ed. D. O. Thompson and D. E. Chimenti, Plenum Press, New York.

Datta, S. K., Shah, A. H., and Al-Nassar, Y. 1988. "Elastic Wave Dispersion in Laminated Composite Plate," pp. 987–94 in *Rev. Prog. in Quant. Nondest. Eval.* **7B**, ed. D. O. Thompson and D. E. Chimenti, Plenum Press, New York.

Dayal, V., and Kinra, V. K. 1989. "Leaky Lamb Waves in an Anisotropic Plate. I: An Exact Solution and Experiments," *J. Acoust. Soc. Am.* **85**(6), 2268–76.

Dayal, V., and Kinra, V. K. 1989. "Leaky Lamb Waves in an Anisotropic Plate. I: An Exact Solution and Experiments," *J. Acoust. Soc. Am.* **85**(6), 2268–76.

de Billy, M., and Adler, L. 1984. "Measurements of Backscattered Leaky Lamb Waves in Plates," *J. Acoust. Soc. Am.* 75(3), 998–1001.

Dike, J. J., Johnson, G. C., and Fowler, E. C. 1989. "Acoustoelasticity Using Longitudinal Waves for Residual Stress Evaluation," pp. 1847–54 in *Rev. Prog. in Quant. Nondest. Eval.* **8B**, ed. D. O. Thompson and D. E. Chimenti, Plenum Press, New York.

Duke, Jr., J. C. ed. 1988. *Acousto-Ultrasonics: Theory and Applications*, Plenum Press, New York.

Duke, Jr., J. C., et al. 1989. *A Study of the Stress Wave Factor Technique for Evaluation of Composite Materials*, NASA Contractor Report 4195.

Fitting, D. W., Kriz, R. D., and Clark, Jr., A. V. 1989. "Measuring In-Plane Elastic Moduli of Composites With Arrays of Phase-Insensitive Ultrasound Receivers," pp. 1497–1504 in *Rev. Prog. in Quant. Nondest. Eval.* **8B**, ed. D. O. Thompson and D. E. Chimenti, Plenum Press, New York.

Frame, B. J., et al. 1990. *Composite Heat Damage: Part 2. Nondestructive Evaluation Studies of IM6/3501-6 Laminates*, ORNL/ATD-33, May.

Frock, B. G., et al. 1988. "Imaging of Impact Damage in Composite Materials," pp. 1093–9 in *Rev. Prog. in Quant. Nondest. Eval.* **7B**, ed. D. O. Thompson and D. E. Chimenti, Plenum Press, New York.

Gauster, W. B., and Breazeale, M. A. 1966. *Rev. Scient. Instrum.* **37**(11), 1544–8.

Guo, N., and Cawley, P. 1992. "Lamb Waves for the NDE of Composite Laminates," pp. 1443–50 in *Rev. Prog. in Quant. Nondest. Eval.* **11B**, ed. D. O. Thompson and D. E. Chimenti, Plenum Press, New York.

Heyman, J. S., and Chern, E. J. 1982. "Ultrasonic Measurements of Axial Stress," *J. Test. and Eval.* **10**(5), 202–11.

Hosten, B. 1991. "Elastic Characterization of Orthotropic Composite Materials From Ultrasonic Inspection Through Non-Principal Planes," pp. 1437–44 in *Rev. Prog. in Quant. Nondest. Eval.* **10B**, ed. D. O. Thompson and D. E. Chimenti, Plenum Press, New York.

Hosten, B., and Castaings, M. 1993. "An Acoustic Method to Predict Effective Elastic Constants of Orthotropic and Symmetric Laminates," pp. 1201–7 in *Rev. Prog. in Quant. Nondest. Eval.* **12B**, ed. D. O. Thompson and D. E. Chimenti, Plenum Press.

Hsu, D. K. 1984. "Ultrasonic Scattering From a High Symmetry Fiber Composite Model," pp. 965–74 in *Rev. Prog. in Quant. Nondest. Eval.* **3B**, ed. D. O. Thompson and D. E. Chimenti, Plenum Press, New York.

Johnston, P. H., Williams, J. L., and Khanna, G. 1994. "Polar Angle Dependence of Ultrasonic Integrated Backscatter From Graphite-Epoxy Composites With Kevlar Stitching," pp. 1299–1306 in *Rev. Prog. in Quant. Nondest. Eval.* **13B**, ed. D. O. Thompson and D. E. Chimenti, Plenum Press, New York.

Karim, M. R., Mal, A., and Bar-Cohen, Y. 1990. "Inversion of Leaky Lamb Wave Data by Simplex Algorithm," *J. Acoust. Soc. Am.* **88**(1), 482–91.

Kautz, H. E., and Lerch, B. A. 1991. "Preliminary Investigation of Acousto-Ultrasonic Evaluation of Metal-Matrix Composite Specimens," *Mat. Eval.* **49**(5), 607–12.

Kline, R. A., and Chen, Z. T. 1988. "Ultrasonic Technique for Global Anisotropic Property Measurement in Composite Materials," *Mat. Eval.* **46**(7), 986–92.

Kline, R. A., Sahay, S. K., and Madaras, E. I. 1991. "Ultrasonic Modulus Determination in Composite Media," pp. 1491–7 in *Rev. Prog. in Quant. Nondest. Eval.* **10B**, ed. D. O. Thompson and D. E. Chimenti, Plenum Press, New York.

Kline, R. A., and Sahay, S. K. 1992. "Sensitivity Analysis for Elastic Property Reconstruction of Anisotropic Media," pp. 1429–35 in *Rev. Prog. in Quant. Nondest. Eval.* **11B**, ed. D. O. Thompson and D. E. Chimenti, Plenum Press, New York.

Krautkrämer, J., and Krautkrämer, H. 1990. *Ultrasonic Testing of Materials*, 4th ed., Springer-Verlag, Berlin.

Kundu, T., and Blodgett, M. 1994. "Detection of Material Defects in Layered Solids Using Lamb Waves," pp. 1343–50 in *Rev. Prog. in Quant. Nondest. Eval.* **13B**, ed. D. O. Thompson and D. E. Chimenti, Plenum Press, New York.

Lamb, H. 1917. "On Waves in an Elastic Plate," *Proc. Roy. Soc. London* **A 93**, 114–28.

Lee, S. S., Smith, J. F., and Thompson, R. B. 1986. "Absolute Acoustoelastic Measurements of Stress in Textured Plate With Arbitrary Stress Orientations," pp. 1423–30 in *Rev. Prog. in Quant. Nondest. Eval.* **5B**, ed. D. O. Thompson and D. E. Chimenti, Plenum Press, New York.

Lott, L. A., and Kunnerth, D. C. 1990. "Acoustical and Dynamic Mechanical Characterization of Fiber-Matrix Interface Bonds in Ceramic Composites," pp. 1425–31 in *Rev. Prog. in Quant. Nondest. Eval.* **9B**, ed. D. O. Thompson and D. E. Chimenti, Plenum Press, New York.

Li, Y. 1985. "Dependence of Acoustic Nonlinearity Parameters on Second Phase Precipitates," *Proc. IEEE Ultrasonics Symposium Proceedings*, p. 1113, Institute for Electrical and Electronics Engineers, New York.

MacLauchlan, D. T., and Alers, G. A. 1987. "Measurement of Thermal Stress in Railroad Rails Using Ultrasonic SH Waves," pp. 1559–66 in *Rev. Prog. in Quant. Nondest. Eval.* **6B**, ed. D. O. Thompson and D. E. Chimenti, Plenum Press, New York.

Mal, A. K., and Bar-Cohen, Y. 1989. "Ultrasonic NDE of Thick Composite Laminates," pp. 1551–8 in *Rev. Prog. in Quant. Nondest. Eval.* **8B**, ed. D. O. Thompson and D. E. Chimenti, Plenum Press, New York.

Mal, A. K., Yin, C. C., and Bar-Cohen, Y. 1991. "Ultrasonic Nondestructive Evaluation of Cracked Composite Laminates," pp. 1531–8 in *Rev. Prog. in Quant. Nondest. Eval.* **10B**, ed. D. O. Thompson and D. E. Chimenti, Plenum Press, New York.

Mal, A. K., Gorman, M. R., and Prosser, W. H. 1992. "Material Characterization of Composite Laminates Using Low-Frequency Plate Wave Dispersion Data," pp. 1451–8 in *Rev. Prog. in Quant. Nondest. Eval.* **11B**, ed. D. O. Thompson and D. E. Chimenti, Plenum Press, New York.

Mal, A. K., Lih, S., and Bar-Cohen, Y. 1993. "Ultrasonic Determination of the Elastic Properties of Unidirectional Composites," pp. 1233–40 in *Rev. Prog. in Quant. Nondest. Eval.* **12B**, ed. D. O. Thompson and D. E. Chimenti, Plenum Press, New York.

Mal, A. K., Lih, S., and Bar-Cohen, Y. 1994. "Characterization of the Elastic Constants of Unidirectional Laminates Using Oblique-Incidence Pulsed Data," pp. 1149–56 in *Rev. Prog. in Quant. Nondest. Eval.* **13B**, ed. D. O. Thompson and D. E. Chimenti, Plenum Press, New York.

Martin, R. W., and Andrews, R. J. 1986. "Backscatter B-Scan Images of Defects in Composites," pp. 1189–98 in *Rev. Prog. in Quant. Nondest. Eval.* **5B**, ed. D. O. Thompson and D. E. Chimenti, Plenum Press, New York.

Martin, R. W., and Chimenti, D. E. 1989. "Leaky Lamb Wave Inspection of Biaxial Composites," pp. 1663–70 in *Rev. Prog. in Quant. Nondest. Eval.* **8B**, ed. D. O. Thompson and D. E. Chimenti, Plenum Press, New York.

Martin, R. W., and Chimenti, D. E. 1990. "Swept Frequency Ultrasonic Imaging in Composite Plates," pp. 1497–1504 in *Rev. Prog. in Quant. Nondest. Eval.* **9B**, ed. D. O Thompson and D. E. Chimenti, Plenum Press, New York.

Mase, G. T., Wong, T. E., and Johnson, G. C. 1989. "Acoustoelasticity in Fiber Reinforced Composites," pp. 1887–94 in *Rev. Prog. in Quant. Nondest. Eval.* **8B**, ed. D. O. Thompson and D. E. Chimenti, Plenum Press, New York.

Michaels, J. E., Michaels, T. E., and Jönsson, S. 1993. "Ultrasonic Methods for Detection of Micro-Porosity in Composite Materials," pp. 1281–87 in *Rev. Prog. in Quant. Nondest. Eval.* **12B**, ed. D. O. Thompson and D. E. Chimenti, Plenum Press, New York.

Mohrbacher, H., et al. 1991. "Acoustic Nonlinearity in Metal-Matrix Composites," pp. 1821–28 in *Rev. Prog. in Quant. Nondest. Eval.* **10B**, ed. D. O. Thompson and D. E. Chimenti, Plenum Press, New York.

Murphy, R. F., Reed, R. W., and Batzinger, T. J. 1990. "Multiparameter Ultrasonic Evaluation of Thick Composite Materials," pp. 1473–80 in *Rev. Prog. in Quant. Nondest. Eval.* **9B**, ed. D. O. Thompson and D. E. Chimenti, Plenum Press, New York.

Murri, W. J., et al. 1987. "Ultrasonic Techniques to Produce Damage Profiles Through the Thickness of a Sample," pp. 1213–20 in *Rev. Prog. in Quant. Nondest. Eval.* **6B**, ed. D. O. Thompson and D. E. Chimenti, Plenum Press, New York.

Nagy, P. B., Rose, W. R., and Adler, L. 1987. "A Single Transducer Broadband Technique for Leaky Lamb Wave Detection," pp. 483–90 in *Rev. Prog. in Quant. Nondest. Eval.* **6A**, ed. D. O. Thompson and D. E. Chimenti, Plenum Press, New York.

Nagy, P. B., Jungman, A., and Adler, L. 1988. "Measurements of Backscattered Leaky Lamb Waves in Composite Plates," *Mat. Eval.* **46**(1), 97–100.

Nagy, P. B., et al. 1989. "Single Mode Lamb Wave Inspection of Composite Laminates," pp. 1535–42 in *Rev. Prog. in Quant. Nondest. Eval.* **8B**, ed. D. O. Thompson and D. E. Chimenti, Plenum Press, New York.

Nagy, P., and Adler, L. 1992. "Acoustic Nonlinearity in Plastics," pp. 2025–32 in *Rev. Prog. in Quant. Nondest. Eval.* **11B**, ed. D. O. Thompson and D. E. Chimenti, Plenum Press, New York.

Nayfeh, A. H., and Chimenti, D. E. 1988*a*. "Propagation of Guided Waves in Fluid-Coupled Plates of Fiber-Reinforced Composite," *J. Acoust. Soc. Am.* **83**(5), 1736–43.

Nayfeh, A. H., and Chimenti, D. E. 1988*b*. "Ultrasonic Wave Reflection From Liquid-Coupled Orthotropic Plates With Application to Fibrous Composites," *J. Appl. Mech.* **55**, 863–70.

Papoulis, A. 1962. *The Fourier Integral and Its Applications*, McGraw-Hill, New York.

Pilarski, A., Rose, J. L., and Balasubramanian, K. 1987. "On a Plate-Surface Wave Mode Selection Criteria for Ultrasonic Evaluation in Layered Structures," *J. Acoust. Soc. Am.* **82**, S21.

Qu, J., and Achenbach, J. D. 1988. "Backscatter From Porosity in Cross-Ply Laminates," pp. 1029–36 in *Rev. Prog. in Quant. Nondest. Eval.* **7B**, ed. D. O. Thompson and D. E. Chimenti, Plenum Press, New York.

Roberts, R. A. 1987. "Porosity Characterization in Fiber-Reinforced Composites by the Use of Ultrasonic Backscatter," pp. 1147–56 in *Rev. Prog. in Quant. Nondest. Eval.* **6B**, ed. D. O. Thompson and D. E. Chimenti, Plenum Press, New York.

Roberts, R. A. 1988. "Characterization of Porosity in Continuous Fiber-Reinforced Composites With Ultrasonic Backscatter," pp. 1053–62 in *Rev. Prog. in Quant. Nondest. Eval.* **7B**, ed. D. O. Thompson and D. E. Chimenti, Plenum Press, New York.

Roberts, R. A. 1989. "Analysis of Ultrasonic Backscatter for Porosity Characterization in Graphite-Epoxy Composites," pp. 1559–66 in *Rev. Prog. in Quant. Nondest. Eval.* **8B**, ed. D. O. Thompson and D. E. Chimenti, Plenum Press, New York.

Rogers, P. H., and Van Buren, A. L. 1974. "An Exact Expression for the Lommel Diffraction Correction Integral," *J. Acoust. Soc. Am.* **55**(4), 724–8.

Rogovsky, A. J. 1991. "Development and Application of Ultrasonic Dry-Contact and Air-Contact C-Scan Systems for Nondestructive Evaluation of Aerospace Composites," *Mat. Eval.* **49**(12), 1491–7.

Rohklin, S. I., and Wang, W. 1989. "Ultrasonic Evaluation of In-Plane and Out-of-Plane Elastic Properties of Composite Materials," pp. 1489–96 in *Rev. Prog. in Quant. Nondest. Eval.* **8B**, ed. D. O. Thompson and D. E. Chimenti, Plenum Press, New York.

Rohklin, S. I., Wu, C. Y., and Wang, L. 1990. "Application of Coupled Ultrasonic Plate Modes for Elastic Constant Reconstruction of Anisotropic Composites," pp. 1403–10 in *Rev. Prog. in Quant. Nondest. Eval.* **9B**, ed. D. O. Thompson and D. E. Chimenti, Plenum Press, New York.

Rohklin, S. I., and Chimenti, D. E. 1990. "Reconstruction of Elastic Constants From Ultrasonic Reflectivity Data in a Coupled Composite Plate," pp. 1411–8 in *Rev. Prog. in Quant. Nondest. Eval.* **9B**, ed. D. O. Thompson and D. E. Chimenti, Plenum Press, New York.

Rose, W. R., Rohklin, S. I., and Adler, L. 1987. "Evaluation of Anisotropic Properties of Graphite-Epoxy Composites Using Lamb Waves," pp. 1111–8 in *Rev. Prog. in Quant. Nondest. Eval.* **6B**, ed. D. O. Thompson and D. E. Chimenti, Plenum Press, New York.

Ruber, J. J. Smith, J. M., and Brockelman, R. H. 1988. "Ultrasonic C-Scans for Ceramic and Composite Material Characterization," *Mat. Eval.* **46**(1), 90-6.

Seale, M. D., Smith, B. T., Prosser, W. H., and Masters, J. E. 1994. "Lamb Wave Response of Fatigued Composite Samples," pp. 1261–6 in *Rev. Prog. in Quant. Nondest. Eval.* **13B**, ed. D. O. Thompson and D. E. Chimenti, Plenum Press, New York.

Simpson, Jr., W. A. 1969. unpublished notes. For an abbreviated derivation of this relationship, see R. Truell, C. Elbaum, and B. Chick, *Ultrasonic Methods in Solid State Physics*, Academic Press, New York.

Simpson, Jr., W. A., and McClung, R. W. August 1984. *Ultrasonic Characterization of Advanced Composite Flywheels*, ORNL/TM-9046, Martin Marietta Energy Systems, Inc., Oak Ridge Natl. Lab.

Simpson, Jr., W. A., and McClung, R. W. April 1987. *Ultrasonic Techniques for the Evaluation of Ceramic Joints*, ORNL-6350, Martin Marietta Energy Systems, Inc., Oak Ridge Natl. Lab.

Simpson, Jr., W. A., and McClung, R. W. 1991. "Quantitative Attenuation Technique for Materials Characterization," *Mat. Eval.* **49**(11), 1409–13.

Simpson, Jr., W. A., and McGuire, D. J. July 1994. *Phase and Group Velocities for Lamb Waves in DOP-26 Iridium Alloy Sheet*, ORNL/TM-12749, Martin Marietta Energy Systems, Inc. Oak Ridge Natl. Lab.

Steiner, K. V., and Lindsay, T. C. 1994. "Correlation of Full-Waveform Ultrasonic NDE Data and Low-Velocity Impact Damage to Composite Panels," pp. 1283–90 in *Rev. Prog. in Quant. Nondest. Eval.* **13B**, ed. D. O. Thompson and D. E. Chimenti, Plenum Press, New York.

Sullivan, R. 1994. "Experimental Imaging of Fiber Orientation in Multi-Layered Graphite-Epoxy Composite Structures," pp. 1313–20 in *Rev. Prog. in Quant. Nondest. Eval.* **13B**, ed. D. O. Thompson and D. E. Chimenti, Plenum Press, New York.

Talreja, R., Govada, A., and Henneke II, E. G. 1984. "Quantitative Assessment of Damage Growth in Graphite Epoxy Laminates by Acousto-Ultrasonic Measurements," pp. 1099–1106 in *Rev. Prog. in Quant. Nondest. Eval.* **3B**, ed. D. O. Thompson and D. E. Chimenti, Plenum Press, New York.

Tang, B., and Henneke II, E. G. 1989. "Lamb-Wave Monitoring of Axial Stiffness Reduction of Laminated Composite Plates," *Mat. Eval.* **47**(8), 928–34.

Thomas III, L. J., Madaras, E. I., and Miller, J. G. 1982. "Two-Dimensional Imaging of Selected Ply Orientations in Quasi-Isotropic Composite Laminates Using Polar Backscattering," *IEEE Ultrasonics Symposium*, **82** CH 1823-4, pp. 965–70.

Thomas, G., and Odegard, B. C. 1988. "Inspecting Advanced Composite Materials at Ultrasonic Frequencies From 2 MegaHertz to 2 GigaHertz," pp. 1003–10 in *Rev. Prog. in Quant. Nondest. Eval.* **7B**, ed. D. O. Thompson and D. E. Chimenti, Plenum Press, New York.

Thompson, R. B, 1975. "Dispersion of Flexural Elastic Waves in Honeycomb Sandwich Panels," *J. Acoust. Soc. Am.* **57**, 1119–27.

Toupin, R. A., and Bernstein, B. 1961. "Sound Waves in Deformed Perfectly Elastic Materials. Acoustoelastic Effect," *J. Acoust. Soc. Am.* **33**(2), 216–25.

Varadan, V. K., Ma, Y., and Varadan, V. V. 1985. "A Multiple Scattering Theory for Elastic Wave Propagation in Discrete Random Media," *J. Acoust. Soc. Am.* **77**(2), 375–85.

Vary, A. March 1976. "Correlations Among Ultrasonic Propagation Factors and Fracture Toughness Properties of Metallic Materials," NASA Technical Memorandum, NASA TM X-71889.

Vary, A. 1978. "Correlations Among Ultrasonic Propagation Factors and Fracture Toughness Properties of Metallic Materials," *Mat. Eval.* **36**(7), 55–64.

Vary, A., and Bowles, K. J. February 1978. "Use of an Ultrasonic-Acoustic Technique for Nondestructive Evaluation of Fiber Composite Strength," NASA Technical Memorandum, NASA TM-73813.

Wong, T. E., and Johnson, G. C. 1988. "Ultrasonic Evaluation of the Nonlinearity of Metals From a Design Perspective," pp. 1203–10 in *Rev. Prog. in Quant. Nondest. Eval.* **7B**, ed. D. O. Thompson and D. E. Chimenti, Plenum Press, New York.

Wooh, S. C., and Daniel, I. M. 1990. "Three-Dimensional Imaging of Impact Damage in Composite Laminates," pp. 1513–20 in *Rev. Prog. in Quant. Nondest. Eval.* **9B**, ed. D. O. Thompson and D. E. Chimenti, Plenum Press, New York.

Wooh, S. C., and Daniel, I. M. 1991. "Nondestructive Determination of Elastic Constants of Composite Materials," pp. 1445–52 in *Rev. Prog. in Quant. Nondest. Eval.* **10B**, ed. D. O. Thompson and D. E. Chimenti, Plenum Press, New York.

Wu, M. C., and Prosser, W. H. 1991. "Harmonic Generation Measurements in Unidirectional Graphite/Epoxy Composites," pp. 1477–82 in *Rev. Prog. in Quant. Nondest. Eval.* **10B**, ed. D. O. Thompson and D. E. Chimenti, Plenum Press, New York.

Yen, C. F., and Chatterjee, S. N. 1988. "Acoustoelastic Wave Velocity in Metal Matrix Composites," pp. 1357–64 in *Rev. Prog. in Quant. Nondest. Eval.* **7B**, ed. D. O. Thompson and D. E. Chimenti, Plenum Press, New York.

Yost, W. T., and Cantrell, J. H. 1990. "Materials Characterization Using Acoustic Nonlinearity Parameters and Harmonic Generation: Engineering Materials," pp. 1669–76 in *Rev. Prog. in Quant. Nondest. Eval.* **9B**, ed. D. O. Thompson and D. E. Chimenti, Plenum Press, New York.

Yost, W. T., and Cantrell, J. H. 1993. "The Effects of Artificial Aging of Aluminum 2024 on its Nonlinearity Parameter," pp. 1267–73 in *Rev. Prog. in Quant. Nondest. Eval.* **12B**, ed. D. O. Thompson and D. E. Chimenti, Plenum Press, New York.

Yuhas, D. E., Vorres, C. L., and R. Roberts, (1986. "Variations in Ultrasonic Backscatter Attributed to Porosity," pp. 1275–84 in *Rev. Prog. in Quant. Nondest. Eval.* **5B**, ed. D. O. Thompson and D. E. Chimenti, Plenum Press, New York.

8. CONCLUSIONS AND RECOMMENDATIONS

J. M. Corum

8.1 DAMAGE AND FAILURE MECHANISM DETERMINATION

The ability to detect and quantify the initiation and growth of damage, to correlate the damage with loading history and environmental effects, and to understand the events leading to failure are key needs of the Durability of Lightweight Composite Structures Project. Since the determination of damage and failure mechanisms is a crucial part of resolving all of the durability issues—fatigue, creep, impact, and environmental effects—it is addressed first in this chapter.

In general, the approach should be to monitor, at least periodically, damage development and failure-initiating events during the various types of durability tests. This should be augmented by postmortem examinations of the failed specimens by optical microscopy and scanning electron microscopy.* Based on the preliminary ultrasonic C-scan results for the isocyanurate CSM reference material discussed in Chaps. 2 and 7, this method should be initially used for detecting the distribution and magnitude of damage. Following the work of Karger-Kocsis, reported in Chap. 2, the C-scans should be augmented with some simultaneous in-situ acoustic emission, thermography, and optical microscopy monitoring to identify how distributed damage ultimately leads to failure-initiating events and what those events are.

It is likely that an NDE method having higher resolution than the basic ultrasonic C-scan will ultimately be needed to discriminate between types of damage. Based on the discussion in Chap. 7, three NDE techniques appear to be particularly promising. For distributed damage, for example, for the fiber-matrix interface damage occurring as a result of fatigue, the nonlinear and acousto-ultrasonic responses of test specimens would appear to be promising. Both have been demonstrated to correlate well with fatigue damage, and the nonlinear behavior has, in those composites for which it has been studied, increased by several hundred percent with increasing bond damage. Acousto-ultrasonics has the added potential advantage of allowing some degree of continuous monitoring during a test, or even during the life of an actual component. In the case of impact damage, which is a localized phenomenon, both acousto-ultrasonic and Lamb wave techniques hold considerable promise for detecting the subtle changes occurring when CSM composites are subjected to impact. Both techniques are suitable for generating images of the damaged areas, and both have demonstrated the requisite sensitivity in many other types of composites.

8.2 FATIGUE

As reviewed in Chap. 3, the mechanisms of fatigue in polymeric composites are complex, even in the absence of environmental effects. Consequently, modeling of fatigue has met with only limited success, even for materials with oriented microstructures such as laminates. The challenge will be even greater in swirl mat composites. Nonetheless, interpretation and understanding of fatigue test results and mechanisms will be very important to the success of the Durability of Lightweight Composite Structures Project. Such an understanding and interpretation will help first to characterize the synergistic effects of creep, impact, and environment together with fatigue on strength and stiffness. Second, it will aid in characterizing cumulative fatigue damage for design.†

The fatigue life diagram, discussed in Chap. 3, should be used as an aid to sorting out the relative roles of the various mechanistic features and their associated ranges of operation. A key goal should be to answer the following four basic questions raised in Chap. 3.

---

*Since the failure mechanisms in CSM composites act on a relatively large scale, light microscopy will likely be the most revealing. Scanning electron microscopy can provide supplementary information at the very localized level (fiber surfaces, interfaces, etc.).

†It seems unlikely that Miner's rule $\left(\Sigma n/N = 1\right)$ will be valid or usable even as an approximate design rule.

1. What are the microstructural changes in going from the virgin state to the first maximum load in a fatigue test?
2. What are the irreversible changes on unloading?
3. What are the consequences of the irreversible changes (stiffness change, strength change)?
4. What is the critical state of the material causing failure and how do the progressive microstructural changes from cycle to cycle reach this state?

To answer these questions, the issue of the scale at which damage descriptors must be described will have to be answered as well.

As a first step toward characterizing durability under fatigue loadings, a data base (at room temperature in air) should be generated. Some block loading tests should be included to examine cumulative damage. The data base should include both modulus of elasticity and Poisson's ratio degradation with cycles. Both stiffness quantities should be measured because they reflect different degrees of damage. Strain gages or extensometers of different lengths should be used to help identify the minimum representative volume for describing damage. The specimens should be periodically subjected to NDE (i.e., ultrasound, thermography, acoustic emission, light microscopy) to characterize the distributed damage and failure mechanisms, which should then be correlated with stiffness degradation. Particular attention should be paid to the first cycle, so that the failure data can be presented in a fatigue life diagram.

Later, when phenomenological models and an understanding of the damage mechanisms have been developed, the interactive effects of temperature, creep, and fluid environments should be addressed.

In developing and transferring the fatigue findings into design guidance, it will be important to define "failure" with ACC; what constitutes loss of usable life? This definition will help focus the characterization and modeling effort.

8.3 CREEP

In contrast to fatigue failure modeling, efforts to model and predict creep deformation have met with more success. The variety of models that have been used were reviewed in Chap. 4. Thus, it is recommended that an effort be made to develop a damage-based, time-dependent model describing creep, recovery, and modulus degradation. The model will need to be based on a well-conceived data base. Creep-rupture or static fatigue failures are, as in the case of fatigue, likely to be much more random and probably not amenable to basic modeling. Thus, a more phenomenologically based approach is recommended for failure.

Activities of the Durability of Lightweight Composite Structures Project in the creep area should consist of two parts: (1) a test program to characterize the time-dependent deformation and failure response and identify the fundamental behavioral features and (2) a modeling effort. Tests to characterize the material behavior will necessarily be fairly extensive and time-consuming. They should include

- room-temperature creep and creep-rupture tests over a range of stress levels, including the low levels germane to design;
- tests at several temperatures over the range from –40 to 250°F;
- tensile tests (strength and stiffness) of creep-damaged specimens; and
- creep and creep-rupture tests in automotive fluid environments.

Selected creep tests should be monitored for damage development and failure initiation using ultrasonics, light microscopy, acoustic emission, etc. Failed specimens should be examined by both light and scanning electron microscopy.

These basic characterization tests should be augmented with more specialized tests to aid the modeling effort. For example, both short- and long-time creep recovery tests should be performed. Step-load creep tests and cyclic creep tests will shed light on creep hardening or softening, cumulative creep damage, and time-dependent fatigue. Long-term constant strain rate tests should be performed to examine the limits of linear creep, as explained in Chap. 4. Finally, since neat resin properties are important to the modeling effort, these should be studied if they are not available.

The tests and NDE studies recommended previously should reveal the fundamental features of creep behavior and provide a sound basis for model development. Work on the damage-based, time-dependent deformation model should focus first on room-temperature creep and recovery. Temperature effects should be added next, followed by cyclic loading response, and finally the effects of automotive fluid environments.

8.4 IMPACT

The goal of impact studies in the Durability of Lightweight Composite Structures Project should be to (1) identify the impact damage modes in the automotive structural composites of interest and how they interact with the damage produced by fatigue, creep, and environment and (2) characterize property degradation in terms of appropriate impact parameters. Since the focus is on the material response, a single impact specimen geometry should be used. Experimental and analytical techniques should be combined to characterize the contact force vs time and the specimen dynamic structural response. Ultrasonics and other possible nondestructive techniques should be used to characterize the damage zone and, in the case of repeated impacts, its growth. Postmortem tests of specimens containing the damage zone should be used to characterize stiffness and strength degradation. Sectioned parts of the damaged specimens should be examined using both light and scanning electron microscopy to help identify the actual impact damage mechanisms.

For the SRIM CSM reference material, it is recommended that a 9-in.-square plate, clamped along an 8-in.-diam. circle, be used for all tests. This plate diameter should be sufficiently large (in terms of diameter-to-thickness ratio) to allow the effects of impacts to propagate freely through flexure. On the other hand, the plate should be sufficiently stiff to limit the contact area and rigidity between the impactor and plate (these considerations were discussed in Chap. 5).

Since the main impact threats to automotive composite structures are (1) tool drops and other low-velocity impacts during assembly and maintenance and (2) higher velocity kickups of roadway rocks and other debris, two impact test set-ups are recommended: (1) a pendulum device for large masses at low velocity and (2) a gas gun for lower masses at higher velocities. The specimen should be the same in both cases, and the impactor should, at least initially, have a hemispherical face and be made of a hardened steel. In both cases, velocity of the impactor should be measured using an interrupted light beam and photosensors. In the case of the gas gun setup, the force-time history will have to be inferred from specimen strain gages and dynamic structural analyses. For the pendulum, a small load cell can be incorporated into the impactor to measure the force-time history. The measurements should still be correlated with strain gage and structural analysis results. The changing force-time diagrams from repeated impacts should be used to correlate with cumulative impact damage and property degradation.

As input to the structural analyses, the contact behavior must first be modeled. The indentation test method described in Chap. 5 for establishing a load-indentation relation is recommended. The classical Hertzian contact law with a power of 3/2 is usually adequate to describe the experimental data. The test data are then used to determine the remaining parameter, the contact rigidity.

A 2-D thick-plate theory analysis (one that accounts for transverse shear effects) should be adequate. It will provide the contact force history and the stresses and strains outside the contact zone.

In both the low- and high-velocity tests, a range of impact energy levels, velocities, impactor diameters, and masses should be studied. Multiple impacts should also be examined to see how damage effects accumulate. A few specimens should be tested statically to determine if the low-velocity impact tests produce the same failure modes as are produced under static conditions. Eventually, predamaged impact specimens (with damage from prior loadings or environmental exposure) should be tested.

Mechanical property test specimens should be cut from the impacted specimens and subjected to tensile and fatigue testing to establish strength, stiffness, and fatigue life degradation. For this purpose, the impact plate specimens should be square, even though they are clamped on a circle. The square plate will allow a series of side-by-side specimens to be cut from across the plate, thus providing data from the central impact zone outward. These tensile specimens should be as narrow as possible (limited by the size of a representative volume element) in order to capture the expected large property variations. By relating the

property degradation to the appropriate impact damage and failure mode parameters, design guidance to account for the deleterious effects of impacts can be established.

8.5 ENVIRONMENTAL EFFECTS

As described in Chap. 6, the effects of sorption of liquid into polymeric composites can be numerous. In addition to weight gain, swelling can occur beyond some threshold. Osmotic pressures can cause internal residual stresses, as well as microcracking and fiber-matrix debonds, thus degrading strength and stiffness. The presence of fluid within the materials can accelerate time-dependent response. Chemical and physical changes of the constituent composite materials can lead to weight loss. Even distilled water can chemically react with the glass fibers, producing corrosion or etching. Most of these processes are thermally activated, so temperature has a significant effect. The presence of stress and cyclic loadings can also accelerate the processes.

In terms of composite durability, there are two concerns. First, as shown in Chap. 2 for the reference isocyanurate CSM composite, fluid exposure can degrade properties. Second, the various processes and effects described above can interact synergistically with the damage and failure mechanisms of cyclic, long-term, and impact loadings. Thus, the goal of the Durability of Lightweight Composite Structures Project should be (1) to characterize the effects of fluid sorption on composite dimensional stability and tensile property degradation and (2) to understand the mechanisms and damage and how they interact with fatigue, impact, and creep loadings to alter their effects. A significant data base will be required to sort out and characterize these various effects.

The scoping environmental exposure tests described in Chap. 2 for the reference isocyanurate CSM composite should be repeated for much longer exposure periods, the full range of temperatures of interest, and using a more statistically valid number of test specimens. In addition to determining stiffness and strength degradation, weight gain data should be assessed to determine the limits for Fickian behavior and to relate the subsequent departure from Fickian behavior to damage and property degradation.

Likewise, creep and fatigue tests of immersed specimens should be conducted. Damage and weight gain should be monitored with time or cycles and related to property degradation and ultimate creep and fatigue failure.

In addition to the nondestructive and postmortem evaluation methods described in previous sections, failed specimens should be examined for corrosion and other physical changes (reaction products, interfacial damage, etc.). Matrix digestion techniques should be explored for viewing fiber integrity.

Finally, the interaction of fluid sorption with impact damage accumulation should be evaluated. On the one hand, the presence of sorption damage (weakened bonds and interfaces) might serve to spread out the absorption of impact energy, thus making the material more resistant to impact effects. On the other hand, however, the presence of impact damage may enhance sorption. Thus, impact specimens pre-exposed to fluids should be tested, and impact-damaged material samples should be subsequently used in fluid exposure weight gain tests.

ORNL-6869
Dist. Category UC-1425, 1500

INTERNAL DISTRIBUTION

1. R. A. Bradley
2. C. R. Brinkman
3–7. J. M. Corum
8. W. G. Craddick
9. S. A. David
10. R. C. Gwaltney
11. J. G. Hansen
12. H. W. Hayden, Jr.
13. R. G. Gilliland
14. W. J. McAfee
15. H. E. McCoy, Jr.
16. R. N. McGill
17. D. J. Naus
18. R. E. Norris
19. M. B. Ruggles
20. J. T. Shaffer
21–23. W. A. Simpson, Jr.
24. P. A. Sklad
25. L. V. Smith
26. C. C. Southmayd
27. C. D. Warren
28–30. Y. J. Weitsman
31. G. M. Wood
32. G. T. Yahr
33. R. E. Ziegler
34. ORNL Patent Section
35. Central Research Library
36. Document Reference Section
37–38. Laboratory Records
39. Laboratory Records, ORNL-RC

EXTERNAL DISTRIBUTION

40–42. C. T. Sun, School of Aeronautics and Astronautics, Purdue University, 1282 Grissom Hall, West Lafayette, Indiana 47907-1282
43–45. R. Talreja, School of Aerospace Engineering, Georgia Institute of Technology, Atlanta, Georgia 30332-0150
46–75. E. M. Hagerman, Automotive Composite Consortium, General Motors, 30500 Mound Road, Box 9055, Warren, Michigan 48090-9055
76. P. K. Liaw, Department of Materials Science and Engineering, The University of Tennessee, 427-B Dougherty Engineering Building, Knoxville, Tennessee 37996-2200
77. R. S. Benson, Department of Materials Science and Engineering, The University of Tennessee, 427-B Dougherty Engineering Building, Knoxville, Tennessee 37996-2200
78. H. M. Herring, Department of Materials Science and Engineering, The University of Tennessee, 427-B Dougherty Engineering Building, Knoxville, Tennessee 37996-2200
79. D. C. Worley, Department of Materials Science and Engineering, The University of Tennessee, 427-B Dougherty Engineering Building, Knoxville, Tennessee 37996-2200
80. C. R. Schultheisg, National Institute of Standards and Technology, Building 224, Room A209, Gaithersburg, Maryland 20899
81. A. M. Vinogradov, Montana State University, Department of Mechanical Engineering, Bozeman, Montana 59717-0007
82. D. K. Hsu, Center for Nondestructive Evaluation, Iowa State University, Applied Sciences Complex, 1915 Scholl Road, Ames, Iowa 50011
83–85. S. Diamond, U.S. Department of Energy, 1000 Independence Avenue, SW, Washington, DC 20588
86. T. Grobstein, U.S. Department of Energy, 1000 Independence Avenue, SW, Washington, DC 20588

87. J. J. Eberhardt, U.S. Department of Energy, 1000 Independence Avenue, SW, Washington, DC 20588
88. D. Haught, U.S. Department of Energy, 1000 Independence Avenue, SW, Washington, DC 20588
89. M. McMonogle, U.S. Department of Energy, 1000 Independence Avenue, SW, Washington, DC 20588
90. J. Russell, U.S. Department of Energy, 1000 Independence Avenue, SW, Washington, DC 20588
91. R. Peavy, U.S. Department of Energy, 1000 Independence Avenue, SW, Washington, DC 20588
92. M. F. Kanninen, 7322 Ashton Place, San Antonio, Texas 78229
93. W. L. Bradley, Department of Mechanical Engineering, College of Engineering, Texas A&M University, College Station, Texas 77843-3123
94. M. Rowlins, U.S. Department of Energy, Oak Ridge Site Office, Oak Ridge, Tennessee 37831

95–264. DOE, Office of Scientific and Technical Information, P.O. Box 62, Oak Ridge, Tennessee 37831. Given distribution as shown in DOE/OSTI-4500-R75 under categories UC-1425 and -1500

☆U.S. GOVERNMENT PRINTING OFFICE: 1995-650-187-00013